EXPERIMENTAL AND COMPUTATIONAL INVESTIGATION OF STRUCTURE-REACTIVITY RELATIONSHIP OF METHACRYLATES

by

Özlem Karahan

M. S., Chemistry, Marmara University

B. S., Chemistry, Marmara University

Submitted to the Institute for Graduate Studies in
Science and Engineering in partial fulfillment of
the requirements for the degree of
Doctor of Philosophy

Graduate Program in Chemistry

Boğaziçi University

2012

To my Mother

ACKNOWLEDGEMENTS

I would like to express my deepest appreciation to my thesis supervisors Prof. Duygu Avcı Semiz, Prof. Viktorya Aviyente for their encouragement, systematic guidance, and support throughout this study. I gained a lot of experience thanks to their invaluable guidance and attention.

This research project would not have been without the support of many people. My deepest gratitude is also due to the members of the committee, Assoc. Prof. Ersin Acar , Prof. İlknur Doğan and Prof. Safiye Sağ Erdem for generously giving their valuable time for reviewing the final manuscript.

I would like to express my heartful thanks to my experimental and computational labmates and also to my dear friends, Burçin Akgün, Zeynep Saraylı Bilgici, Ayse Altın, Asli Yıldırım, Tuğba Furuncuoğlu Özaltın, Gülsah Çiftci, Berna Doğan, Hasan Huseyin İnce, İlke Uğur, Burcu Çakır Dedeoğlu, Özgül Gök, Pelin Ertürk for their endless help and precious friendships, all funny and happy hours together.

I am grateful to Ayla Türkekul and Burcu Selen Çağlayan for their cooperation in NMR analysis.

I thankfully acknowledge the TUBITAK ULAKBIM High Performance Computing Center which provided the computational resources used in this work.The computational resources used in this work were also provided by the National Center for High Performance Computing of Turkey (UYBHM) under grant number 20792009, the Bogazici University Research Foundation (Projects 03M501 and 05HB501), and the State Planning Organization (DPT-2009K120520). We also thank the Netherlands Organization for Scientific Research (NWO-CW and NWO-NCF) for financial support.

I would like to thank all the former and current members of the Boğaziçi University Experimantal Polymer Group, Computational Chemistry Group and the members of the Chemistry Department in Boğaziçi University.

Finally, my deepest thanks go to my mother and father who have shown endless support during my life. I would also like to thank to my brother and my sisters for their continuous support.

ABSTRACT

EXPERIMENTAL AND COMPUTATIONAL INVESTIGATION OF STRUCTURE-REACTIVITY RELATIONSHIP OF METHACRYLATES

In the first part of this work, a series of alkyl α-hydroxymethacrylates (RHMA) were synthesized and computationally modeled in order to understand the structure-reactivity relationships in their polymerizations. Several factors including H-bonding, π-π interactions and dipole moment were investigated. Experimentally, among the studied monomers, aromatic carbamates containing π-π stacking and H-bonding were found to have highest rate of polymerization. Computationally, the rate constants for propagation k_p mimic the qualitative polymerization trends of the monomers modeled and can be used with confidence in predicting the polymerizability behaviors of alkyl α-hydroxymethacrylates. Finally, these studies are expected to be used for the prediction of RHMA monomers prior to synthesis. In addition, RHMA based polymerizable and polymeric photoinitiators were synthesized and evaluated for UV curable coatings. In the second part of this work, glycidyl methacrylate (GMA) derivatives were synthesized and evaluated with respect to their potential to be used as reactive diluents in dental materials. An explanation was also proposed for the cyclopolymerization of methyl α-[(allyloxy) methyl] acrylate via 5-membered rings, while allyl methacrylate (AMA) and allyl 2-cyanoacrylate (ACA) polymerize without ring formation. It has been pointed out that the presence of carbonyl group at C3 in AMA and ACA inhibits the cyclization because of its incompatibility in hybridization with the other unsaturated carbon next to the oxygen. In the last part of this thesis, the effect of solvent on the propagation rate coefficients of acrylic acid (AA) and methacrylic acid (MAA) have been elucidated. Both for MAA and AA it was experimentally found that the propagation rate constants of the monomers increase by more than one order of magnitude in going from the bulk to a highly dilute system. The reactivities of these two monomers have been explained in the bulk and dilute medium by using quantum chemical methods.

ÖZET

METAKRILATLARIN YAPI-REAKTİVİTE İLİŞKİLERİNİN DENEYSEL VE HESAPSAL İNCELENMESİ

Bu çalışmanın ilk bölümünde, bir dizi alkil α-hidroksimetakrilat (RHMA) sentezlendi ve yapı-reaktivite ilişkilerinin polimerleşmeleri üzerindeki etkisini anlamak için hesapsal modelleme yapıldı. H-bağı, π-π etkileşimleri ve dipol moment gibi çeşitli faktörler incelendi. Deneysel olarak, çalışılan monomerler arasında π-π istiflenmesi ve H-bağı içeren aromatik karbamatların en yüksek polimerleşme hızına sahip oldukları bulundu. Hesapsal olarak, ilerleme hız sabiti k_p, modellenmiş olan monomerlerin polimerleşme özelliklerini kalitatif olarak taklit etmektedir ve alkil α-hidroksimetakrilatların polimerleşme özelliklerinin öngörüsünde güvenle kullanılabilir. Sonuç olarak bu çalışmaların, RHMA monomerlerinin sentezinden önce reaktivite tahmini için kullanılacağı düşünülmektedir. Ek olarak, RHMA bazlı polimerleşebilen ve polimerik fotobaşlatıcılar sentezlendi ve UV ile kürleştirilebilir kaplamalar için değerlendirildi. Bu calışmanın ikinci bölümünde ise, glisidil metakrilat (GMA) türevleri sentezlendi ve dişçilikte kullanılan malzemelerde reaktif seyreltici ajan olarak kullanılma potansiyelleri değerlendirildi. Ayrıca, metil α-[(aliloksi) metil] akrilatın 5-elemanlı halkalarla siklopolimerleşmesine rağmen alil metakrilat (AMA) ve alil 2-siyanoakrilatın (ACA) herhangi bir halka düzenlenmesi olmadan polimerleşmesine bir açıklama getirildi. AMA ve ACA'nın yapısındaki C3 pozisyonundaki karbonil grubunun varlığının, oksijenin yanındaki diğer doymamış karbon ile hibridizasyonundaki uyumsuzluktan dolayı siklizasyonu engellendiği saptandı. Tezin son bölümünde, çözücünün akrilik asit (AA) ve metakrilik asit (MAA) in ilerleme hız sabitlerine etkisi incelendi. Her iki monomer için de, derişik ortamdan seyreltik ortama geçerken monomerlerin ilerleme tepkimesinin hız sabitinin arttığı deneysel olarak gözlemlenmiş, kanıtlanmışdır. Bu iki monomerin reaktivitesi derişik ve seyreltik ortamda kuantum kimyasal methodlar kullanılarak açıklanmıştır.

TABLE OF CONTENTS

LIST OF TABLES

LIST OF FIGURES

LIST OF SYMBOLS

D_j	Dipole moment of the conformation
f	Initiator efficiency
h	Planck's constant
k_B	Boltzmann's constant
k_{ct}	The rate constant of the chain transfer reaction
k_d	The decomposition rate constant of the initiation reaction
K_{ij}	Exchange integral
k_p	The rate constant of the propagation reaction
k_{tc}	The rate constant of the termination by coupling reaction
k_{td}	The rate constant of the termination by disproportionation reaction
Q / s	Heat flow per second
G_{rel}	Relative Gibbs free energies
[*I*]	Concentration of the initiator
[A]	Concentration of absorber
p_j	Probability of finding the monomer in conformation *j*
R	Boltzmann constant
Å	Angstrom
$BO_{C=O}$	Bond order of carbonyl double bond of monomer
Res	Resonance stabilization parameter
R_p	Rate of polymerization
μ	Dipole moment
$\Delta E^{\#}$	Energy of activation
$\Delta G^{\#}$	Activation Gibbs free energy
$\Delta H^{\#}$	Enthalpy of activation
ΔH_0^{theor}	Theoretical heat evolved for complete conversion
ΔH_{teor}	Heat released per mole of double bonds reacted
ΔH_j	Heat of formation of conformation *j*
ΔH_p	Heat released per mole of double bonds reacted
Φ	Number of propagation chains initiated per light photon absorbed

ε	Extinction coefficient
κ	Transmission coefficient
ρ_s	Mulliken atomic spin density
p^{θ}	Standard pressure
υ_i	Rate of initiation
υ_t	Rate of termination
I_a	Intensity of absorbed light

A1	Ethyl 2-((2-morpholinoethoxy)methyl)acrylate
A2	Tert-butyl 2-((2-morpholinoethoxy)methyl)acrylate
A3	Ethyl 2-((2-cyanoethoxy)methyl)acrylate
A4	Tert-butyl 2-((2-cyanoethoxy)methyl)acrylate
A5	Ethyl 2-(((3-methyloxetan-3-yl)methoxy)methyl)acrylate
A6	Ethyl 2-(((2-oxo-1,3-dioxolan-4-yl)methoxy)methyl)acrylate
A7	Ethyl 2-(phenoxymethyl)acrylate
A8	Ethyl 2-((ethoxycarbonyloxy)methyl)acrylate
A9	Tert-butyl 2-((ethoxycarbonyloxy)methyl)acrylate
A10	Ethyl 2-((2-(2-(2-methoxyethoxy)ethoxy)acetoxy)methyl)acrylate
A11	Tert-butyl2-((2-(2-(2 methoxyethoxy)ethoxy)acetoxy)methyl)acrylate
A12	2-(ethoxycarbonyl)allyl benzoate
A13	Ethyl 2-((phenylcarbamoyloxy)methyl)acrylate
A14	Tert-butyl 2-((phenylcarbamoyloxy)methyl)acrylate
A15	Ethyl 2-((butylcarbamoyloxy)methyl)acrylate
A16	Tert-butyl 2-((butylcarbamoyloxy)methyl)acrylate
B1	Methyl 2-(butoxymethyl)acrylate
B2	Methyl 2-(acetoxymethyl)acrylate
B3	2-(ethoxycarbonyl)allyl benzoate
B4	Hexyl acrylate
B5	Benzyl acrylate
B6	Phenyl acrylate
C1	Tert-butyl 2-(((2-oxo-1,3-dioxolan-4-yl)methoxy) methyl)acrylate

C2	Ethyl 2-(hydroxymethyl)acrylate
C3	Tert-butyl 2-(hydroxymethyl)acrylate
C4	Ethyl 2-(acetoxymethyl)acrylate
D1	2-hydroxy-3-(2-(2-methoxyethoxy)acetoxy)propyl methacrylate
D2	13-hydroxy-10-oxo-2,5,8,11-tetraoxatetradecan-14-yl methacrylate
D3	3-(2-cyanoacetoxy)-2-hydroxypropyl methacrylate
D4	2-hydroxy-3-(2-phenylacetoxy)propyl methacrylate
D5	3-((diethoxyphosphoryl)oxy)-2-hydroxypropyl methacrylate
D6	2-hydroxy-3-methoxypropyl methacrylate
E1	Tert-butyl 2-((4-benzoylphenoxy)methyl)acrylate
E2	2-((4-Benzoylphenoxy)methyl)acrylic acid
E3	2-(Ethoxycarbonyl)allyl 4-benzoylbenzoate
F1	Allyl methacrylate
F2	Allyl 2-cyanoacrylate
F3	α(allyloxy)methyl] acrylate

LIST OF ACRONYMS/ABBREVIATIONS

AA	Acrylic Acid
ACA	Allyl 2-cyanoacrylate
AIBN	2,2’-Azobisisobutyronitrile
AMA	Allyl methacrylate
ANN	Artificial neural networks
Bis-GMA	2,2-Bis[4-(2-hydroxy-3-methacryloyloxy propyloxy) phenyl] propane
BHT	2,6-di-tert-butyl-4-methyl phenol
BP	Benzophenone
B3LYP	Becke-3-Lee-Yang-Parr
COSMO-RS	Computing solution phase calculations
DCC	1,3-Dicyclohexylcarbodiimid
DFT	Density functional theory

DMAEMA	N,N-dimethylaminoethyl methacrylate
DMPA	2,2-dimethoxy-2-phenylacetophenone
DSC	Differential Scanning Calorimetry
EA	Electron affinity
EBBr	Ethyl α-bromomethacrylate
EHMA	Ethyl α-hydroxymethacrylate
E_{HOMO}	Energy of the highest occupied molecular orbital
E_{LUMO}	Energy of the lowest unoccupied molecular orbital
FRP	Free radical polymerization
FT-IR	Fourier Transform Infrared Spectroscopy
GDMA	Glycerol dimethacrylate
GMA	Glycidyl methacrylate
GPC	Gel Permeation Chromatography
HA	Hexyl acrylate
HDDA	Hexanedioldiacrylate
HEMA	2-hydroxyethyl methacrylate
HOMO	Highest occupied molecular orbital
IEFPCM	Integral equation formalism polarized continuum model
IE	Ionization energy
LUMO	Lowest unoccupied molecular orbital
MAA	Methacrylic acid
MDEA	N-methyldiethanolamine
MMD	Molar mass distribution
MHMA	Methyl alpha-hydroxymethacrylate
MLRA	Multiple linear regression analysis
MP2	Second order perturbation
NBO	Natural bond orbital
NMR	Nuclear Magnetic Resonance Spectroscopy
PCM	Polarizable continuum model
PES	Potential energy surface
PM3	Parameterization method 3
QSAR	Quantitative structure-activity relationships

RHMA	Alkyl alpha-hydroxymethacrylate
RTIR	Real time infrared
SCF	Self-consistent field
SCRF	Self-consistent reaction field theory
TBBr	Tert-butyl α-bromomethacrylate
TBHMA	Tert-butyl alpha-hydroxymethacrylate
TEA	Triethylamine
TEGDMA	Triethyleneglycol dimethacrylate
T_g	Glass transition temperature
TGA	Thermal Gravimetric Analysis
TS	Transition state
TST	Transition state theory
ZPVE	Zero-point vibration energy

1. INTRODUCTION

1.1 Free Radical Polymerization

Conventional free-radical polymerization (FRP) is a very important commercial process for preparing high molecular weight polymers because it can be employed for polymerization of many vinyl monomers under mild reaction conditions, requiring the absence of oxygen, but tolerant to water, and can be conducted over a large temperature range (-80 to 250°C) [1,2]. The main limitation of FRP is the poor control of some of the key elements of macromolecular structures such as molecular weight (MW), polydispersity, end functionality, chain architecture, and composition.

The free radical polymerization process via chain mechanism, basically consists of four types of reactions involving free radicals: (i) radical generation from non radical species (initiation), (ii) radical addition to a substituted alkene (propagation), (iii) chain transfer reactions, (iv) termination reaction (by combination and by disproportionation) [1].

The initiation step is considered to proceed via two reactions. The first is the production of free radicals by heat or light. The usual case is the homolytic dissociation of an initiator or a catalyst *I* to yield a pair of radicals $R\bullet$

$$I \xrightarrow{k_d} 2R\bullet \tag{1.1}$$

where k_d is the rate constant for the initiator dissociation. The second part of the initiation involves the addition of this radical to the first monomer molecule to produce the chain initiating species $M_1\bullet$

$$R_1\bullet + M \xrightarrow{k_i} M_1\bullet \tag{1.2}$$

where M represents a monomer molecule and k_i is the rate constant for the initiation step (Equation 1.2). For the polymerization of $CH_2{=}CXY$, Equation 1.2 takes the form

$$R\bullet + CH_2 = CXY \longrightarrow R - CH_2 - CXY\bullet$$

(1.3)

Here, the radical $R\bullet$ is often referred to as an initiator radical or a primary radical.

The propagation consists of the growth of $M_1\bullet$ by the successive additions of large numbers of monomer molecules. Each addition creates a new radical which has the same identity as the previous one, except that it is larger by one monomer unit. The successive additions may be represented by

$$M_1\bullet + M \xrightarrow{k_p} M_2\bullet \qquad (1.3)$$

$$M_2\bullet + M \xrightarrow{k_p} M_3\bullet \qquad (1.4)$$

$$M_3\bullet + M \xrightarrow{k_p} M_4\bullet \qquad (1.5)$$

or in general terms

$$M_n\bullet + M \xrightarrow{k_p} M_{n+1}\bullet \qquad (1.6)$$

where k_p is the rate constant for propagation. Propagation with growth of the chain to high polymer proportions takes place very rapidly. The value of k_p for most monomers is in the range 10^2-10^4 liter/mole-sec.

The propagating radical may attack to another monomer by chain transfer and the radical center may be transferred to another chain, so that the molecular weight of the propagating polymer can be controlled.

$$M_n\bullet + R-H \xrightarrow{k_{ct}} M_n - H + R\bullet \tag{1.7}$$

k_{ct} in these reactions is the rate constant for the chain transfer reaction. Depending on the reactivity of the new radical center, a new growing species is generated or propagating and the new radical is terminated.

At some point, the propagating polymer chain stops growing and terminates. The termination with the annihilation of the radical centers occurs by bimolecular reaction between radicals. Two radicals react with each other by *combination* (*coupling* (k_{tc})),

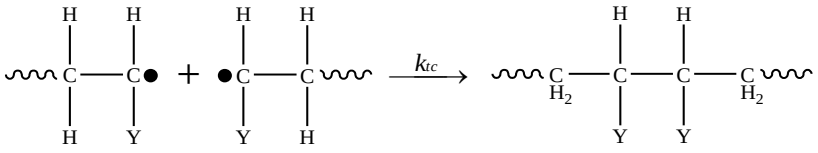

(1.8)

or, more rarely, by *disproportionation* in which a hydrogen radical that is *beta* to a radical center is transferred to another radical center (k_{td}). This results in the formation of two polymer molecules-one saturated and one unsaturated:

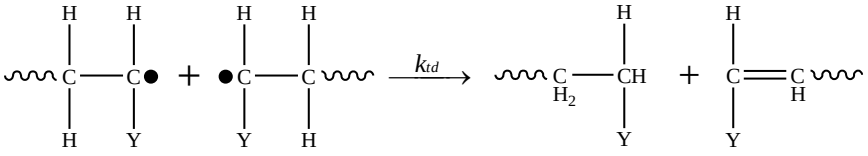

(1.9)

where k_{tc} and k_{td} are the rate constants for termination by coupling and disproportionation, respectively. One can express the termination step by

$$M_n\bullet + M_m\bullet \xrightarrow{k_t} \text{dead polymer} \tag{1.10}$$

where the particular mode of termination is not specified, and

$$k_t = k_{tc} + k_{td} \tag{1.11}$$

The term *dead polymer* signifies the cessation of growth for the propagating radical. Typical termination rate constants are in the range of 10^6-10^8 liter/mole-sec, orders of magnitude greater than the propagation rate constants. The much greater value of k_t (whether k_{tc} or k_{td}) compared to k_p does not prevent propagation because the radical species are present in very low concentrations and because the polymerization rate is dependent on only the one-half power of k_t.

1.2. Free Radical Polymerization Kinetics

When the reaction kinetics is considered, the rate of initiation (υ_i) according to the initiation reaction may be given as

$$\upsilon_i = 2 f k_d [I] \tag{1.12}$$

where f is the initiator efficiency, k_d is the rate constant for the decomposition of the initiator and [I] is the concentration of the initiator. The initiator efficiency factor is used since not all the generated free radicals are able to initiate polymer growth, e.g. sometimes recombination between radicals may take place. Initiator efficiency therefore may take values between zero and one.

Termination is a bimolecular process so that the rate of termination (υ_t) is given by

$$\upsilon_t = 2k_t [M^\bullet]^2 \tag{1.13}$$

where k_t and [M**.**] stand for the termination rate constant and the concentration of the growing radicals respectively. The rate constant $2k_t$ is actually (k_{tc} + k_{td}).

The overall rate of polymerization is calculated with the aid of the steady-state approximation. The steady-state approximation assumes that, after an initial induction period, an interval during which the concentrations of intermediates, rise from zero, and during the major part of the reaction, the rates of change of concentrations of all reaction intermediates are negligibly small [3]. According to the steady state approximation for the FRP, the initiation is relatively small but continuous. The termination speeds up as the active radical concentration builds up and the termination removes (kills) active radicals. Therefore it is an excellent approximation to assume that rate of initiation of radicals is equal to the rate of termination of radicals:

$$\upsilon_i = \upsilon_t \tag{1.14}$$

hence

$$2 f k_d [I] = 2 k_t [M^\bullet]^2 , \tag{1.15}$$

yielding

$$[M^\bullet] = \left(\frac{f k_d [I]}{k_t} \right)^{1/2} \tag{1.16}$$

Thus, rate of propagation (υ_p) may be given as

$$\upsilon_p = k_p [M][M^\bullet] = k_p [M] \left(\frac{f k_d [I]}{k_t} \right)^{1/2} \tag{1.17}$$

where k_p stands for the propagation rate constant. In the derivation of polymerization rate, the propagation (k_p) and termination (k_t) rate coefficients are assumed to be chain length and conversion independent [4].

The overall homopolymerization rate constant, k, is based on the kinetic expression for homopolymerization [5]

$$R_p = k[I]^{1/2}[M] \tag{1.18}$$

Then, the expression for *k* is

$$k = \frac{k_p}{k_t^{1/2}}(fk_d)^{1/2} \tag{1.19}$$

1.3. Photopolymerization

Photopolymerization, the utilization of light as the energy source for polymerization of monomers, oligomers, and polymers, is widely used for a variety of applications that include inks, coatings, adhesives, microcircuits, printing plates, dental restoratives, biomaterials and contact lenses [6-9]. The main advantage of this process lies in the very high polymerization rates. It generally takes place within a fraction of a second. Besides its great speed it has other advantages such as polymerization at room temperature, solventless polymerization, spatial control of polymerization, and energy efficiency [10].

Photopolymerization process involves photoinitiation to produce reactive species that initiates polymerization. Photoinitiated production of a radical will start radical chain polymerization, whereas photoinitiated production of an ionic monomer can be used for ionic chain polymerizations. Photoinitiated radical chain polymerization starts with irradiation of photoinitiators with UV or visible light (250-450 nm). Photoinitiator molecules absorb light energy and fragments into two radicals that attack a monomer, converting it to another radical. The monomer radical attacks a second monomer and this process continues to give high molecular weight polymers until termination of radicals.

The rate of photochemical initiation is given by [11]

$$R_i = 2\,\Phi I_a \tag{1.20}$$

Where I_a is the intensity of absorbed light (called einstein in photochemistry) in moles of light quanta per liter-second and Φ is the number of propagation chains initiated per light

photon absorbed. Φ is referred to as the quantum yield for initiaton. The factor of 2 in Equation 1.20 indicates that two radicals are produced per molecule undergoing photolysis, is not used for those initiating systems that yield only one radical. The maximum value of Φ is 1 for all photoinitiating systems.

$$R_p = k_p[M]\left(\frac{R_i}{2k_t}\right)^{1/2} \tag{1.21}$$

Where R_p is the rate of the polymerization, [M] is the monomer concentration, R_i is the rate of initiation, k_t is the termination rate constant.

Combining Equations 1.20 and 1.21 we get

$$R_p = k_p[M]\left(\frac{\Phi I_a}{k_t}\right)^{1/2} \tag{1.22}$$

The absorbed light intensity I_a is obtained from a consideration of the Beer-Lambert Law in the form

$$I_a = I_0 - I_0 e^{-\varepsilon[A]D} \tag{1.23}$$

Where I_0 is the incident light intensity and I_a is the intensity of light on a layer at a distance D (cm) into the reaction system, ε the extinction coefficient and [A] concentration of absorber. Hence the rate of polymerization in a layer of small thickness at depth b is given by

$$R_p = k_p/k_t^{\frac{1}{2}}[M]\{\Phi I_0\left(1 - e^{\varepsilon[In]b}\right)\}^{1/2} \tag{1.24}$$

where, [In] the photoinitiator concentration. The application of Equation 1.24 was derived on assumptions of steady-state and bimolecular termination, therefore is limited for describing the photopolymerization of multifunctional monomers [12].

1.3.1. Monitoring Photopolymerization Kinetics

Two methods are usually used to study photopolymerization kinetics: the photocalorimetry [13-15] and the real time infrared (RTIR) spectroscopy (16-19). The first

technique is based on measurement of heat flow during photopolymerization as a function of time at a constant temperature. The main advantage of photocalorimetry is good temperature control for reactions having a $t_{1/2}$ (time to reach 50% conversion) higher than 15 s [13]. However this technique gives no information about the chemical reaction. Also due to low thermal conductivity of materials, the increase in sample temperature due to the exothermicity of the photopolymerization is high, preventing the study of very fast photopolymerization kinetics ($t_{1/2}$<15 s).

Conversion is calculated from the overall heat evolved at time t (ΔH_t) as

$$C = \Delta H_t / \Delta H_0^{theor} x100 \tag{1.25}$$

where ΔH_0^{theor} is the theoretical heat evolved for complete conversion. This value is 13.1 kcal/mol for a methacrylate double bond. The rate of polymerization is directly connected to the heat flow according to

$$R_p = dC/dt = \frac{dH}{dt} / \Delta H_0^{theor} \tag{1.26}$$

RTIR spectroscopy is a unique method to study ultrafast photopolymerization reactions quantitatively [16-19]. It can monitor the decrease in the absorbance of the specific functional groups (for example, the C=C stretching vibrations of the (meth)acrylates at 1646 cm^{-1} or 812 cm^{-1}) to determine rate of polymerization and conversion as a function of time. The polymerization profiles are recorded on millisecond time scale, thus allowing a precise evaluation of the reaction rate, the photosensitivity, the polymerization quantum yield, the induction period, and the polymer unsaturation content [13].

Lasers have appeared recently as one of the most powerful tools to transform rapidly a liquid monomer into a solid polymer. Pulsed lasers, which deliver high energy in nanoseconds, have been used, to measure kinetic rate constants for free radical polymerizations [13]. Pulsed-laser polymerizations (PLP) can be followed by RTIR (PLP-NIR), DSC, fluorescence, size exclusion chromatography (PLP-SEC) and electron spin resonance [ESR] (PLP-ESR) techniques. PLP-SEC technique generates radicals at

preselected time intervals and the characteristic pattern of the molecular weight distribution of the polymers enables determination of the propagation rate constants. The fluorescence method follows the changes in the local rigidity of the medium by incorporation of fluorescent probes into the formulations. PLP-ESR technique allows detection of the decay in radical concentration after pulsing and gives the termination rate constant (k_t) from radical concentration versus time plot.

1.3.2. Photoinitiators

Photoinitiators play an important role by controlling both the rate of initiation and the penetration of incident light into the sample, and therefore control the depth of cure. It is essential to select a photoinitiator showing the highest initiation efficiency and undergoing fast photobleaching upon UV exposure in order to achieve a deep-through cure.

Photoinitiators are generally divided into two classes as *Type I* and *Type II* initiators according to the mechanism by which initiating radicals are formed. Photoinitiators which undergo unimolecular bond cleavage upon irradiation are called *Type I* photoinitiators.

$$PI \rightarrow (PI)^{*} \rightarrow R1\bullet + R2\bullet \qquad (1.27)$$

These initiators are usually aromatic ketones with substituents that facilitate direct photofragmentation according to a Norrish-*Type I* mechanism. Examples of this type of initiators include benzoin derivatives such as benzoin ethers, α-aminoalkylphenones, and acylphosphine oxides (Table 1.1). Benzoin ethers readily undergo α-fragmentation on exposure to near-UV light in a process that is not quenched by oxygen, thereby making them suitable for curing in air. The benzoyl radical is the major initiating species (Figure 1.1).

Table 1.1. Structures of typical *Type I* photoinitiators.

Photoinitiators	**Structure**	**λ_{max} (nm)**
Benzoin ethers	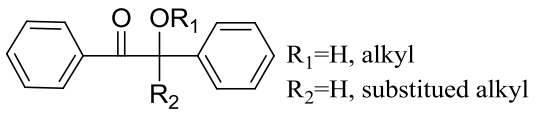	323
Benzil ketals	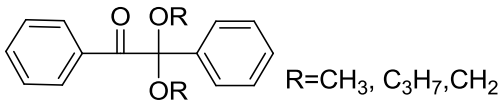	365
Acylphospine oxides	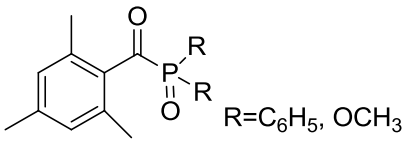	380
Aminoalkyl phenones	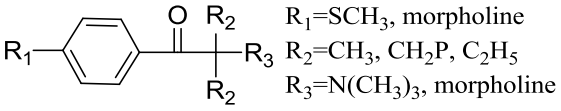	320

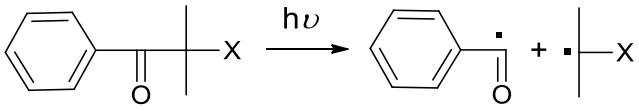

Figure 1.1. The mechanism of photoinitiation by α-cleavage type (*Type I*) photoinitiators.

Type II photoinitiators include aromatic ketones such as benzophenone, thioxanthones, benzyl, and quinones. *Type II* initiators normally generate radicals by abstracting hydrogen from the environment (solvent) or undergoing photoinduced electron and hydrogen transfer with a coinitiator resulting in radical ions that fragment to generate radicals. Because the initiation is based on a bimolecular reaction, generation of radicals from *Type II* photoinitiators and curing rates is generally slower than the generation of free radicals from *Type I* photoinitiators, which are based on unimolecular formation of radicals [20]. The most common coinitiators for aromatic ketones are tertiary amines.

$$PI \xrightarrow{h\upsilon} (PI)^{*} + COI \xrightarrow{k} R1\bullet + R2\bullet \quad (1.28)$$

Table 1.2 Structures of typical *Type II* photoinitiators.

Photoinitiators	**Structure**	**λ_{max} (nm)**
Benzophenone	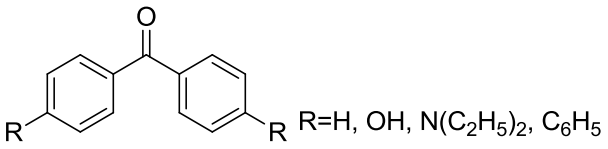	335
Thioxanthones	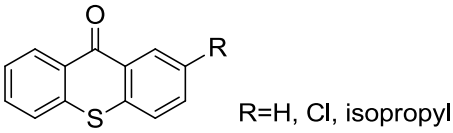	390
Coumarins	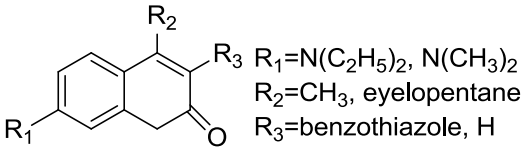	370
Benzils	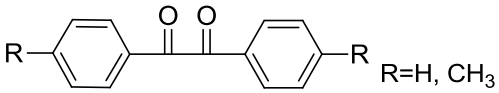	340

The mechanism of the photoinitiation on the example of benzophenone is shown in Figure 1.2. Upon light absorption, a ketyl radical from the carbonyl compound and another radical from the hydrogen donor are generated. The ketyl radical formed from benzophenone is not reactive toward double bonds due to steric hindrance and delocalization of the unpaired electron (Figure 1.2). Moreover, the ketyl radicals may act as chain terminators leading to ketyl groups incorporated into polymer chains and relatively short chains [20]. Therefore the initiation occurs from the radical formed from the H-donor. Tertiary amines are more reactive co-initiators than alcohols or ethers. Thiols are another class of co-initiators in thiol-ene polymerization systems [20].

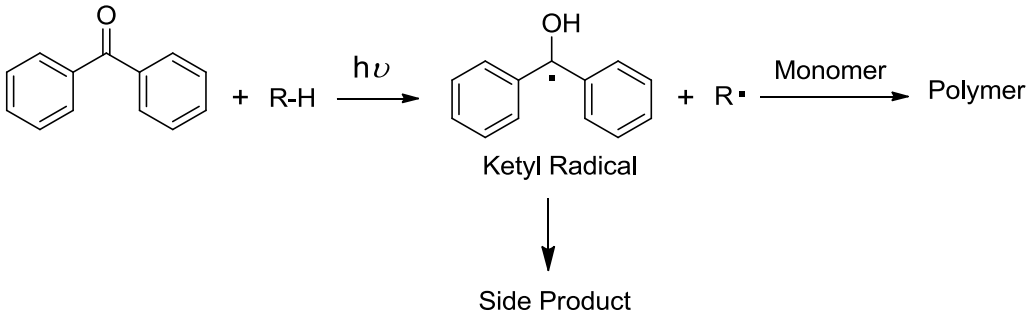

Figure 1.2. The mechanism of photoinitiation by benzophenone.

Polymeric photoinitiators (PP) can be defined as macromolecular systems that contain pendent or in-chain chromophores, which absorb light efficiently and generate radicals capable of initiating polymerization. The importance of polymeric photoinitiators lies in their capability of combining the properties of polymers with those of low-weight photoinitiators [21-27]. The high cost of these initiators can be compensated by their advantages compared to their low molecular weight analogues: Solubility and miscibility problems, often observed with coatings containing low-molecular weight photoinitiators, do not occur with the resin to be cured as well as with the final cured film. Moreover, the low volatility of the large molecules prevents odor and toxicity problems observed with the conventional photoinitiators. The low migration tendency of polymeric photoinitiators and photoproducts means that cured coatings are less prone to yellowing [28-31].

The main advantage of polymeric initiators, however, is photoinitiation efficiency compared to the low molecular weight counterparts. This ‘polymer effect’ can be obtained as a result of energy migration between excited and ground state photosensitive groups along the polymer backbone and/or intramolecular reactions increasing production of more efficient radicals which can be protected similar to cage effect by the polymer chain, thus reducing coupling processes [32]. Also, copolymerization of suitable monomers allows the production of polymeric derivatives having different photosensitive groups in the same molecule, with a synergistic effect on activity [33].

In addition to those above mentioned advantages, polymeric photoinitiators were also investigated to understand the chemistry and reactivity of macromolecular free

radicals; how the reduced mobility of the polymeric radicals affects their reactivity and the shielding of the polymer backbone retards bimolecular reactions [32].

There have been many new developments in the synthesis and photochemical studies of novel polymeric photoinitiators containing the two main types of free radical photoinitiators: photofragmenting (*Type I* photoinitiators) and hydrogen abstraction (*Type II* photoinitiators). Examples for *Type I* photoinitiators are benzoin ether derivatives having the benzoin methyl ether moieties on the side chain of the polymers [34] (Figure 1.3). The photoinitiating activity of polymeric photoinitiator derived from α-methylbenzoin methyl ether acrylate, give rise to the low molecular weight benzoyl radical and the polymer-bound α-alkoxybenzyl radical (Figure 1.4). Benzoyl radicals are more active as initiating species than α-alkoxybenzyl radicals which are involved mainly in the termination reactions. This PP is more reactive than polymeric initiator prepared from 4-acryloyloxy-α-methyl benzoin methyl ether, where benzoyl radical is bound to the polymer (Figure 1.4). This result can be explained by the reduced capability to give termination reactions, due to the steric hindrance by polymer coiling.

Polymeric initiators bearing the 2,6-dimethylbenzoylphosphine oxide group pendant from flexible tetramethylene oxide side chains were found to be less reactive than the low molecular weight analogs due to their high viscosities (Figure 1.4).

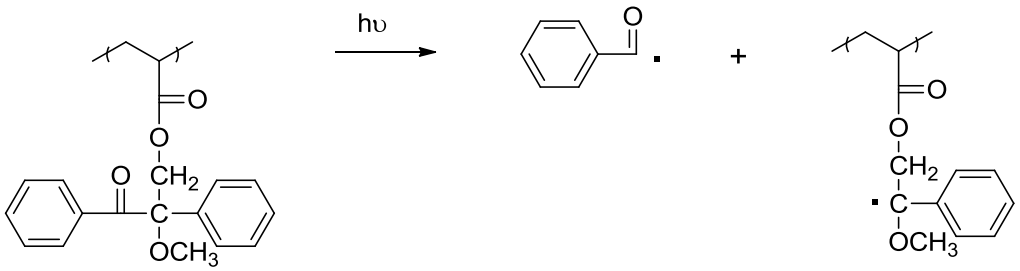

Figure 1.3. Photofragmentation process for a *Type I* polymeric photoinitiator.

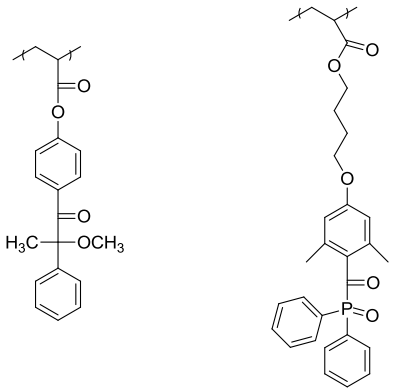

Figure 1.4. Examples of polymeric photoinitiators of *Type I*.

Most of the *Type II* polymeric photoinitiators are based on benzophenone due to their low cost [36-41]. The other initiators include thioxanthone (TX), anthraquinone, camphorquinone or benzyl groups [42,43].

For hydrogen-abstracting photoinitiators, the photoinitiating activity has been investigated in terms of amount and type of substituent in the polymer, and their influence to prevent the recombination of radicals, favoring their reaction with the monomer. Also, copolymers carrying chromophore and amine groups with potential synergistic effects on activity are reported. It has been found that the approach of the tertiary amine to the chromophore to produce the corresponding exciplexes is dependent on both the monomeric and polymeric nature of chromophore and the tertiary amine.

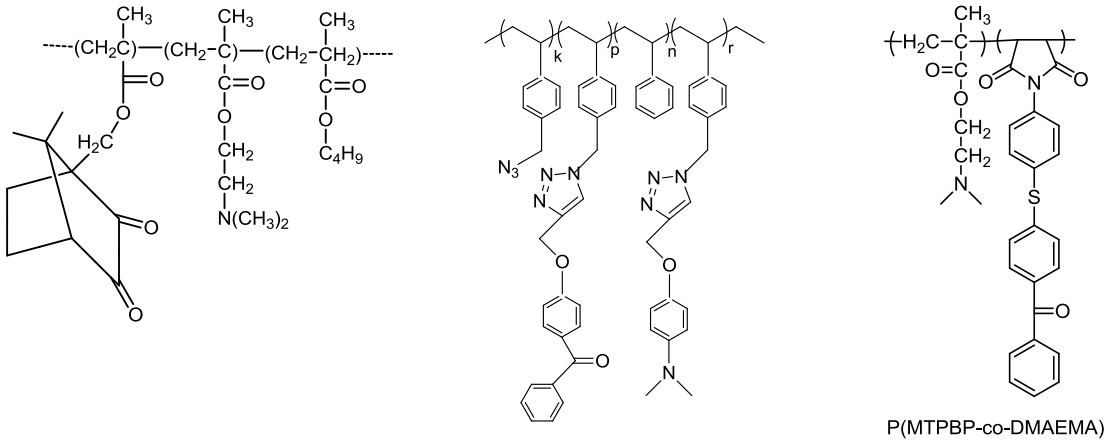

Figure 1.5. Examples of polymeric photoinitiators of *Type II* [24, 26, 27].

Figure 1.5 shows some examples for the polymeric photoinitiators bearing side chain camphorquinone and benzophenone groups. The polymeric initiator containing both camphorquinone and amine groups in the side chain showed lower reactivity compared to those in which only one of the photoreactive moieties is in the polymeric form, particularly the camphorquinone group [24]. Another polymeric photoinitiator, polystyrene-b-dimethylamino benzoate, possessing both light absorbing and hydrogen donating sites as side chain in the structure, shows similar absorption characteristics to benzophenone and is able to polymerize mono and multifunctional acrylate monomers without the requirement of an additional coinitiator [26]. For the last example, a copolymer of a polymerizable benzophenone photoinitiator (MTPBP) and an unsaturated coinitiator amine N,N-dimethylaminoethyl methacrylate (DMAEMA) were found to be the most efficient for the polymerization of hexanedioldiacrylate (HDDA) compared to their low molecular weight analogs, BP/DMAEMA and MTPBP/poly-DMAEMA and poly-MTPBP/DMAEMA (Figure 1.5) [27].

1.3.3. Monomers

Acrylates and methacrylates are the most common monomers in photopolymerizations due to their high reactivities in free radical polymerizations [6-8]. This property together with good chemical, optical and mechanical properties of their polymers account for the great commercial success of acrylates and methacrylates. However, (meth)acrylates are subject to some limitations including polymerization shrinkage, oxygen inhibition, low polymerization rate and residual unsaturation which decreases the polymer lifetime and performance [44]. For example, shrinkage during polymerization of dimethacrylate-based dental restorative materials generates stress, which weakens the performance and longevity of dental composites [45]. Therefore, development of new (meth)acrylates which will overcome these limitations are very important.

UV-curing of acrylate coatings is generally carried out in the presence of air and oxygen inhibition has always been an important problem [46-48]. Indeed, the free radicals formed by the initiator are rapidly scavenged by O_2 molecules to yield peroxyl radicals (Figure 1.6). These species are not reactive towards the acrylate double bonds and can therefore not initiate any polymerization reaction. They usually abstract hydrogen atoms

from the polymer backbone to generate hydroperoxides. Moreover, this chain termination modifies the mechanical properties of the film. An additional amount of photoinitiator (and of UV energy) is therefore needed to consume the dissolved oxygen in the sample, as well as the atmospheric O_2 diffusing into the sample during the UV exposure. Overcoming this unwanted reaction has become a major challenge [46]. Different methods have been considered: addition of amines, conversion of the dissolved oxygen into its excited singlet state by means of a red light irradiation in the presence of a dye sensitizer, an increase of the formulation reactivity to shorten the UV exposure time during which atmospheric oxygen diffuses into the film, performing the radical photopolymerization under inert conditions, wax barrier coats or performing the UV exposure under water.

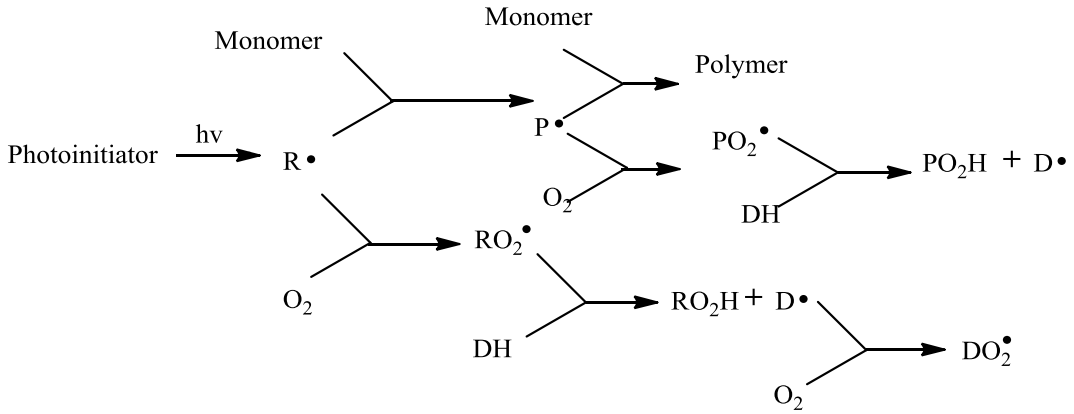

Figure 1.6. Oxygen inhibition in radical-induced polymerization [46].

In order to increase the polymerization rate multifunctional monomers can be used. Increasing monomer functionality results in diffusion limited termination which leads to early autoacceleration and an increase in polymerization rate. Photopolymerization of multifunctional monomers is a commonly used process for producing crosslinked polymer coatings with high mechanical strength. However, an increase in monomer functionality increases residual unsaturation and crosslink density which decreases material properties due to increased brittleness. The residual unsaturation causes toxicity problems due to leakage of monomer. In general, there are trade offs when one is trying to obtain a material with a large storage modulus, high glass transition temperature, and high double bond conversion as well as a rapid rate. Monomer structure, the distance and flexibility between

functional groups and the number of functional groups, affect the relative numbers of crosslinks, primary and secondary cycles that are formed during polymerization [49].

Monofunctional monomers with high rate of polymerization, almost complete conversion and good polymer properties are very important to be used as reactive diluents. Therefore understanding the factors enhancing their reactivities and crosslinking abilities are the subject of many research which enables design of monomers with enhanced reactivity and tailored polymer properties.

1.3.4. Factors that Affect the Monomer Reactivity

Because of the wide range of applications, development of high performance (meth)acrylates has been the focus of interest. The extensive research has been conducted to understand the relationship between the monomer structure and reactivity; and to develop monomers with enhanced reactivity. In recent years, several factors leading to the enhanced reactivity of (meth)acrylates were hypothesized. These are hydrogen abstraction from labile hydrogens in monomers, π-π interactions, hydrogen bonding and electronic effects (dipole moment, secondary functionalities) [50-55].

1.3.4.1. Hydrogen bonding. Monomers containing hydrogens attached to oxygen or nitrogen can engage in intramolecular and/or intermolecular hydrogen bonding with similar groups or with carbonyl, ether and other electronegative acceptor functionality. These interactions can affect the monomer configuration and mobility which results in viscosity differences [47]. Since multifunctional monomers polymerize faster than monofunctional monomers due to the reduction in termination rate the hydrogen-bonded monomers are also expected to have rapid polymerization rates [10].

Also it was proposed that hydrogen bonding facilitates preorganization in acrylates, forcing the acrylate double bonds to be in close proximity to each other [56]. As a consequence, the propagation reaction rate constant (k_p) will be enhanced resulting in higher R_p. The effect of preorganization can be examined further by looking at the tacticity of the resultant polymer [57]. Generally, polyacrylates produced by a free radical

mechanism yield predominantly syndiotactic material. The monomers capable of hydrogen bonding give rise to more isotactic polymer in comparison with non-hydrogen bonding monomers.

It is known that when reactions are performed at higher temperatures, higher rates will be observed; this is the so-called Arrhenius behavior. However, if the high R_p is due to preorganization via hydrogen bonding or via a noncovalent connection, at higher temperatures where the extent of hydrogen bonding is reduced, one can expect lower R_p.

Hoyle *et al*. showed that the degree of hydrogen bonding and the rate of polymerization of hydroxyalkyl acrylates are directly related and both decrease with increasing temperature [35]. The maximum rate of polymerization of 2-hydroxyethyl acrylate (HEA) decreases drastically with increasing temperature while those of 1,6-hexanediol diacrylate (HDDA) increase moderately. Deepak *et al.* also observed a decrease in the extent of the double bond conversion with increasing temperature for hydrogen bonding telechelic urethane methacrylate crosslinkers [58].

One consequence of preorganization is that when the hydrogen-bonding moiety is at a larger distance from the reactive acrylate group, there will be a critical distance beyond which the preorganization due to the hydrogen bonding will have little or no effect on R_p. This is because conformational mobility of the skeletal bonds between the hydrogen-bonding moiety, and the acrylate double bond will reach a level whereby the acrylate double bond can be regarded as isolated from the hydrogen bonding moiety. Verification of this prediction based on the preorganization theory was done by preparing and evaluating several ethyl amide *N*-alkyl acrylates, in which the alkyl chain was varied in length from ethyl to hexyl. The R_p's of the ethyl amide *N*-alkyl acrylates are gradually reduced going from ethyl to pentyl, in line will be reduced at a larger distance from the acrylate group [56].

1.3.4.2. Electronic effects. Jansen and co-workers [56] have claimed that for molecules with a high dipole moment, the more polar medium reduces the activation energy for propagation, leading to acceleration in the propagation reaction rate [56]. Also, in a highly

polar medium there would be a more organized, tightly held solvent cage around the propagating radical, which would lead to a reduction in the termination rate [56]. Radicals may also have a greater partial charge in a polar medium, resulting in further reduced termination, due to electrostatic repulsion between the radicals. Overall these effects would lead to the observed propagation being favored over termination, causing an observed increase in reactivity. Furthermore, it has been claimed that for monomers or polymerizing mixtures where the average dipole moment exceeds 3.5 debye, the reactivity correlates monotonically with the dipole moment, with molecules possessing higher dipole moment having greater reactivity.

This correlation between a monomer molecular structure, its associated polarity, and R_p for acrylate polymerization would facilitate the rational design of new monomers with higher rate of polymerization.

This suggestion opens up two possibilities. The first is that under identical conditions mixtures of acrylates should obey the same correlation. The second is that in case small amounts of highly polar inert solvents are added the rates of polymerization should increase. Therefore in the same work solution studies were conducted to investigate the contribution of a high dipole moment solvent on the reactivity of the novel acrylic monomers. Tetrahydrofurfuryl acrylate (μ_{calc} = 2.05 D) was diluted with a high polar (propylene carbonate, μ = 5 D) and with a low polar (dimethyl carbonate, μ =0.9 D) solvent. The rate enhancements were achieved by the addition of polar inert solvents, which is contradictory to the general belief that dilution with an inert solvent automatically will lead to a reduction of the polymerization rate (due to the reduced monomer concentration).

1.3.4.3. π-π stacking. Other results seem to suggest a higher reactivity for aromatic-containing monomers over those containing branched hydrocarbons over those containing linear alkyl groups. This may be the result of π-π stacking which increases viscosity, suppressing termination and hence improving the polymerization rate [59]. The combination of the carbamate and aromatic substitution increases monomer reactivity to a greater extent.

1.3.4.4. Hydrogen abstraction. In the early 1990s, Decker and coworkers developed a new class of acrylate monomers that incorporated second functionalities such as carbonates, carbamates, cyclic carbonates and oxazolidones [50]. These monomers showed ultrarapid polymerizations and gave crosslinked polymers. The reason for the enhanced reactivity and gelation behavior of these monoacrylates is not fully understood.

One hypothesis is that the reactivity is a result of an efficient chain transfer that involves labile hydrogens from the secondary functional groups. The chain transfer leads to cross-linking and viscosity increase, thereby allowing an earlier onset of autoacceleration (Trommsdorf effect), which would account for high R_p's. However, experimental evidence in the literature, is inconclusive. The fact that the polymerization of glycerol carbonate acrylate can be initiated with benzophenone, a Norrish *Type II* photoinitiator, suggests that under these conditions some of the hydrogens are relatively labile. However, it does not indicate that these hydrogens are abstracted during the radical polymerization. It only demonstrates that they can be abstracted during the initiation (when nothing else can happen).

1.3.4.5. Heteroatom effect. Andrzejewska reported that the presence of the heteroatom in the ester group led to enhanced reactivity due to the CH_2 group attached to the heteroatom donating hydrogen to give a crosslinked network. This reaction also leads to a reduction in oxygen inhibition and faster rates and higher conversions in air [60].

2. RESEARCH OBJECTIVES

Free radical polymerization (FRP) is widely used in industrial fields because of its advantages such as compatibility, convenience, and applicability. Kinetics of FRP have been thoroughly investigated experimentally and computationally. In this work, the general aim is to elucidate experimentally and computationally the structure-reactivity relationship of acrylates and methacrylates.

In Chapter 3, a series of alkyl α-hydroxymethacrylate derivatives with various secondary functionalities (ether, ester, carbonate, and carbamate) and terminal groups (alkyl, cyano, oxetane, cyclic carbonate, phenyl and morpholine) were synthesized to investigate the effect of intermolecular interactions, H-bonding, π–π interactions, and dipole moment on monomer reactivity.

In Chapter 4, the free radical polimerizability behavior of alkyl α-hydroxymethacrylate (RHMA) derivatives has been modeled by considering the propagation of the dimeric units of the compounds of interest. The same type of study has been carried out for hexyl, benzyl, and phenyl acrylate derivatives whose increasing reactivity has been attributed to the presence of C=O…H-C, C=O…H-Φ as well as π-π stabilizing interactions, respectively.

In Chapter 5, the B3LYP/6-31+G* methodology has been used to derive a structure-reactivity relationship for RHMA monomers whose rates of photopolymerization have been experimentally measured. Calculated descriptors such as the ionization energy the electron affinitiy, the atom-atom overlap weighed bond order of carbonyl double bond, the resonance stabilization parameter, the Mulliken atomic spin density (ρ_s) of the monomeric radical were investigated to find a correlation between ther experimental rates and the above descriptors which was then tested on three RHMA monomers whose rates of photopolymerization have also been measured. This study is expected to shed light on predicting the reactivities of RHMA monomers prior to their synthesis and thus to rank their photopolymerization abilities based on their structural properties.

In Chapter 6, six methacrylate monomers have been synthesized for use as reactive diluents in dental composites and evaluated to investigate the relationship between molecular structure and monomer reactivity. The photopolymerization efficiencies and oxygen sensitivity of each monomer was investigated and compared with commercial ones.

In Chapter 7, three novel polymerizable photoinitiators, bearing side-chain benzophenone (BP) groups, were synthesized from RHMA's. These photoinitiators were thermally homopolymerized using free radical polymerization to give the corresponding polymeric photoinitiators. One of the monomeric photoinitiators was also copolymerized with a coinitiator, N,N-dimethylaminoethyl methacrylate, in order to check the effect on the photoinitiation activity of having the coinitiator also on the polymer, hence always in close vicinity to BP group. The UV-vis characterization of synthesized photoinitiators was investigated. The photoefficiencies of each photoinitiator were compared with commercial ones.

In Chapter 8, the density functional theory has been used to model the elementary steps and rationalize the free radical polymerization kinetics in 1,6 heptadienes. The models used in this study have revealed the fact that while methyl α-[(allyloxy) methyl] acrylate cyclopolymerizes via 5-membered rings, allyl methacrylate and allyl 2-cyanoacrylate do not.

In Chapter 9, the relative rate of polymerization of acrylic acid (AA) versus methacrylic acid (MAA) and the effect of water on the polymerization kinetics have been investigated within a combined static and molecular dynamics set of computational tools. Classical Molecular Dynamics calculations have been carried out to determine the location of the solvent molecules in the proximity of the dimeric AA and MAA units. A combined implicit/explicit solvent model was used for the evaluation of the kinetics of the dimeric polymer chains.

The general conclusions of the experimental and computational work conducted in this thesis on free radical polymerization is discussed in Chapter 10.

3. STRUCTURE-REACTIVIY RELATIONSHIPS OF ALKYL α-HYDROXYMETHACRYLATE (RHMA) DERIVATIVES

3.1. Introduction

Acrylates and methacrylates are the most commonly used monomers in photoinitiated polymerizations due to their high reactivities and excellent polymer properties. They are used in dental materials, biomaterials, coatings, adhesives, and photolithography [6-8]. Because of the wide variety of application areas, extensive research has been conducted to understand the relationship between the monomer structure and reactivity and to develop monomers with enhanced reactivity.

In recent years, several factors leading to the enhanced reactivity of (meth)acrylates were hypothesized. These are hydrogen abstraction from labile hydrogens in monomers, hydrogen bonding, and electronic effects (dipole moment, secondary functionalities).

Decker and Bowman formulated new monoacrylate monomers with carbonate, cyclic carbonate, carbamate, and oxazolidone groups that react extremely rapidly despite one vinyl group and form crosslinked polymers. They mentioned that crosslinking due to hydrogen abstraction reactions causes an increase in viscosity, earlier gelation, and autoacceleration, which lead to high rate of polymerization [44, 50-55, 59].

It was observed that the presence of secondary functionalities (carbamates, carbonates, cyclic carbonates, cyclic acetals, morpholine, oxazolidones, hydroxyl, and aromatic rings) enhances the reactivity by reducing the activation energies in both Michael addition and photopolymerizations as indicated by a monotonic correlation between reactivities of monomers with respect to both processes. The cyclic voltammetry experiments also proved a correlation between reduction potential of the monomers and Michael addition and photopolymerization reactivities [51].

Andrzejewska reported that the presence of the heteroatom in the ester group led to enhanced reactivity due to the CH_2 group attached to the heteroatom donating hydrogen to give a crosslinked network. This reaction also leads to a reduction in oxygen inhibition and faster rates and higher conversions in air [60].

Jansen *et al.* investigated the rate of polymerization of different acrylates as a function of hydrogen bonding capability for systems containing amide, urethane, and urea groups and found that the monomers capable of forming hydrogen bonds show three to six times higher polymerization rates compared with their nonhydrogen-bonded analogs possessing ester and carbonate groups [56]. The high reactivities were suggested to be due to preorganization via hydrogen bonding to bring the double bonds close to each other, enhancing propagation, although reduction in termination rate may also be involved or be the cause. Hoyle *et al.* showed that the degree of hydrogen bonding and the rate of polymerization of hydroxyalkyl acrylates are directly related and both decrease with increasing temperature. Although they could not find a quantitative relationship between hydrogen bonding and termination rate constants, they claimed that highly hydrogen-bonded systems behave as multifunctional monomers and have low termination constants [61].

Jansen *et al.* also investigated the effect of monomer polarity on the rate of polymerization and found a direct correlation between the maximum rate of polymerization and the dipole moment for the monomers having dipole moments higher than 3.5 Debye. However, Kilambi *et al.* found no monotonic correlation between monomer reactivity and molecular dipole moment during bulk polymerization of various acrylate monomers [44]. They suggested that a low dipole moment conformation of some monomers may be more reactive due to intermolecular hydrogen bonding than a conformation with a higher dipole moment.

Monomers based on alkyl α-hydroxymethacrylates (RHMA) and their halide derivatives offer great versatility for functionalization. Conversion of the alcohol group to various ester, ether, and other derivatives has been demonstrated by us and others [62-69]. Although these derivatives have smaller k_p values than methyl methacrylate due to the

steric effect of the a-substituent, they have good polymerizability due to their low k_t values, and this type of polymerization has been called ‘‘steric hindrance assisted polymerization’’ by Yamada *et al.* [70]. Studies on the reactivities of several ester derivatives of ethyl α-hydroxymethacrylate indicated that aromatic esters are more reactive than nonaromatic ones, ether derivatives, and methyl methacrylate [63, 70].

In this work, we report the synthesis and photopolymerizations of ester, ether, carbonate, and carbamate derivatives of RHMA to evaluate the role of hydrogen bonding, dipole moment, and π-π interactions on the reactivity.

3.2. Experimental Work

3.2.1. Materials and Apparatus

3.2.1.1. Materials. Ethyl α-hydroxymethacrylate (EHMA), t-butyl α-hydroxymethacrylate (TBHMA), t-butyl α-bromomethacrylate (TBBr), and ethyl α-bromomethacrylate (EBBr) were synthesized according to literature procedures [71, 72]. 2-[2-(2-Methoxyethoxy)ethoxy]- acetic acid, 3-hydroxypropionitrile, 3-hydroxymethyl-3-methyloxetane, ethyl chloroformate, 4-(2-hydroxyethyl)morpholine, 4-(hydroxymethyl)-1,3-dioxolan-2-one, 2,6-di-tert-butyl-4-methyl phenol (BHT), trifluoroacetic acid, triethyl amine (TEA), 2-hydroxyethyl methacrylate (HEMA), butyl isocyanate, and phenyl isocyanate were obtained from Aldrich and Fluka and used as obtained.

3.2.1.2. Apparatus. The monomer characterization involved ^{1}H and ^{13}C nuclear magnetic resonance (NMR) spectroscopy (Varian Gemini 400 MHz) and Fourier transform infrared (FTIR) spectroscopy (T 380). The photopolymerizations were carried out on a TA Instruments (Q100) photodifferential scanning calorimeter (photo-DSC). Elemental analyses were obtained from Thermo Electron SpA FlashEA 1112 elemental analyser (CHNS separation column, PTFE; 2 m; 6 x 5 mm^2).

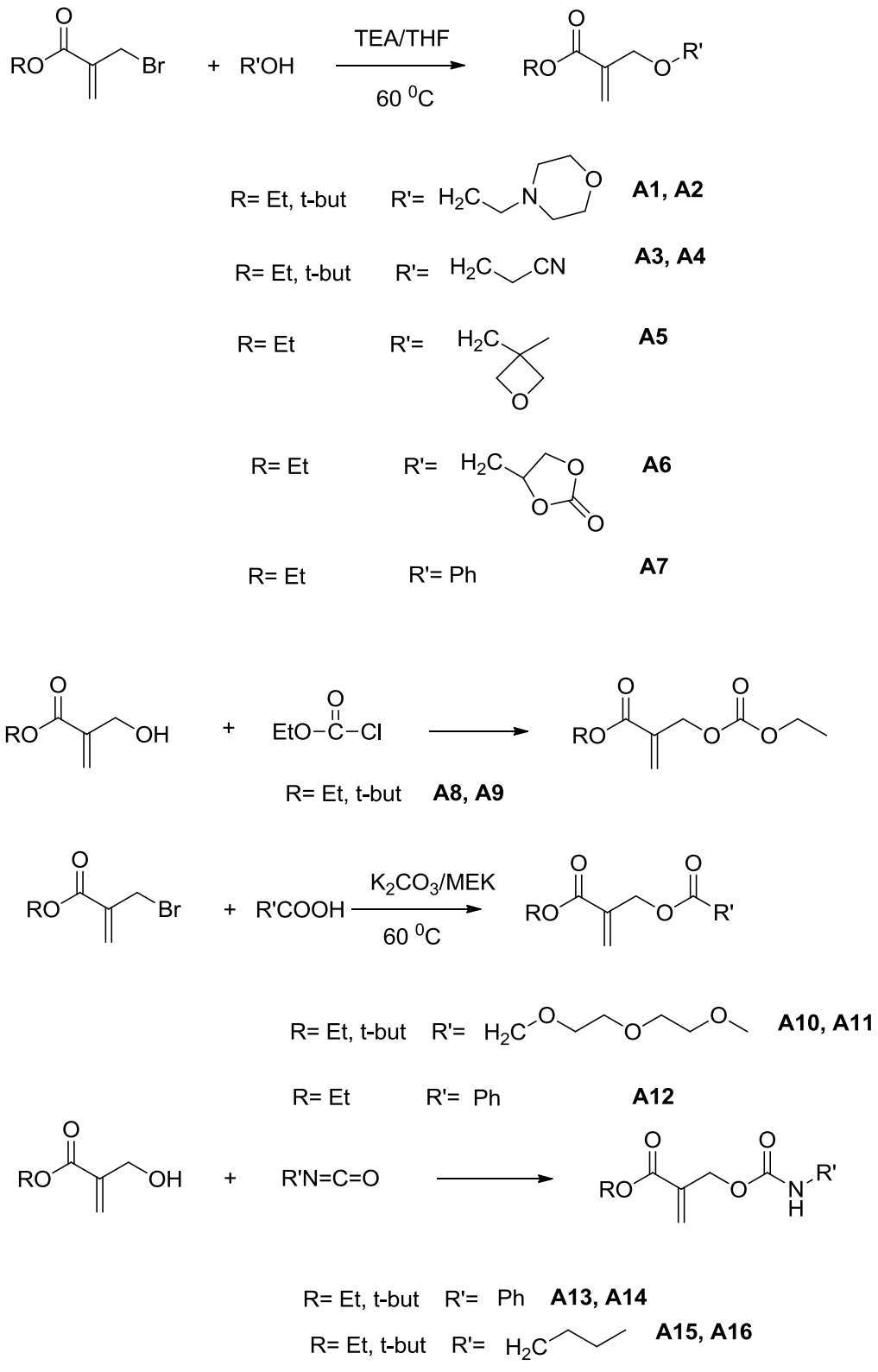

Figure 3.1. Synthesis of monomers.

3.2.2. Synthesis of Monomers

3.2.2.1. General Procedure for the Synthesis of Ether Derivatives (**A1**–**A7**). To a mixture of alcohol (10 mmol) and TEA (3.86 g, 38 mmol) in 5 mL THF in an ice bath, EBBr or TBBr (10 mmol) in 5 mL THF was added dropwise. The mixture was stirred at 60 ^{o}C for 24 h. After removal of the solvent, the mixture was diluted with CH_2Cl_2 and extracted with water (3x5 mL). The organic phase phase was separated, dried with anhydrous sodium sulfate, and evaporated under reduced pressure. The crude products were purified by column chromatography (silica gel 0.063–0.200 mm) using hexane initially and gradually changing to CH_2Cl_2 as eluent.

Ethyl 2-((2-morpholinoethoxy)methyl)acrylate (**A1**) was obtained as a colorless liquid in 62% yield (bp=76–78 ^{0}C/1.2 x 10^{-2} mbar). Viscosity=0.014 Pa s.
^{1}H NMR (400 MHz, $CDCl_3$, δ, ppm): 1.3 (t, 3H, CH_3), 2.5 (t, 4H, CH_2-N), 2.6 (t, 2H, CH_2-N), 3.6 (t, 2H, CH_2-O), 3.7 (t, 4H, CH_2-O), 4.1 (m, 4H, CH_2-CH_3, CH_2-O), 5.8 (s, 1H, CH_2=C), 6.3 (s, 1H, CH_2=C).

^{13}C NMR (400 MHz, $CDCl_3$, δ, ppm): 14.0 (CH_3), 53.9, 58.1 (CH_2-N), 60.5 (CH_2-CH_3), 66.8, 68.3, 69.1 (CH_2-O), 125.3 (CH_2=C), 137.3 (C=CH_2), 165.7 (C=O).

FTIR (cm^{-1}): 2941 (C-H), 1713 (C=O), 1638 (C=C), 1108 (C=O).

ELEM. ANAL., Calcd. for $C_{12}H_{21}NO_4$: C, 59.26%; H, 8.64%; N, 5.76%; O 26.34%. Found: C, 58.98%; H, 9.03%; N, 5.67%; O, 26.32%.

Tert-butyl 2-((2-morpholinoethoxy)methyl)acrylate (**A2**) was obtained as a colorless liquid in 51% yield (bp= 90-92 °C/1.2x10^{-2} mbar). Viscosity= 0.024 Pa s.

^{1}H NMR (400 MHz, $CDCl_3$, δ, ppm): 1.5 (s, 9H, CH_3), 2.5 (t, 4H, CH_2-N), 2.6 (t, 2H, CH_2-N), 3.6 (t, 2H, CH_2-O), 3.7 (t, 4H, CH_2-O), 4.1 (s, 2H, CH_2-O), 5.8 (s, 1H, CH_2=C), 6.2 (s, 1H, CH_2=C).

^{13}C NMR (400 MHz, $CDCl_3$, δ, ppm): 27.9 (CH_3), 53.9 (CH_2-N), 58.1 (CH_2- CH_2), 66.7, 68.2, 69.1 (CH_2-O), 80.6 (*C*-CH_3), 124.3 (*C*H_2=C), 138.6 (*C*=CH_2), 164.9 (C=O).

FTIR (cm^{-1}): 2973 (C-H), 1708 (C=O), 1638 (C=C), 1110 (C-O).

Ethyl 2-((2-cyanoethoxy)methyl)acrylate (**A3**) was obtained as a colorless liquid in 31% yield (bp= 99-100 °C/1.2x10^{-2} mbar). Viscosity= 0.004 Pa s.

^{1}H NMR (400 MHz, $CDCl_3$, δ, ppm): 1.3 (t, 3H, CH_3), 2.6 (t, 2H, CH_2-CN), 3.7 (t, 2H, C*H*$_2$-CH_2), 4.2 (m, 4H, CH_2-O, C*H*$_2$-CH_3), 5.9 (s, 1H, CH_2=C), 6.3 (s, 1H, CH_2=C).

^{13}C NMR (400 MHz, $CDCl_3$, δ, ppm): 14.1 (CH_3), 18.8 (*C*H_2-CN), 60.8 (*C*H_2-CH_3), 65.3, 69.3 (CH_2-O), 117.8 (*C*N-CH_2), 126.2 (*C*H_2=C), 136.6 (*C*=CH_2), 165.6 (C=O).

FTIR (cm^{-1}): 2982 (C-H), 2252 (C-N), 1712 (C=O), 1638 (C=C), 1103 (C-O).

Tert-butyl 2-((2-cyanoethoxy)methyl)acrylate **A4** was obtained as a colorless liquid in 47% yield (bp= 109-111 °C/1.2x10^{-2} mbar). Viscosity= 0.009 Pa s.

^{1}H NMR (400 MHz, $CDCl_3$, δ, ppm): 1.4 (s, 9H, CH_3), 2.6 (t, 2H, CH_2-CN), 3.7 (t, 2H, C*H*$_2$-CH_2), 4.2 (s, 2H, CH_2-O), 5.8 (s, 1H, CH_2=C), 6.2 (s, 1H, CH_2=C).

^{13}C NMR (400 MHz, $CDCl_3$, δ, ppm): 18.8 (*C*H_2-CN), 27.9 (*C*H_3-C), 65.2, 69.4 (CH_2-O), 81.1 (*C*-CH_3), 117.7 (*C*N-CH_2), 125.2 (*C*H_2=C), 137.8 (*C*=CH_2), 164.8 (C=O).

FTIR (cm^{-1}): 2978 (C-H), 1707 (C=O), 1639 (C=C), 1105 (C-O).

Ethyl 2-(((3-methyloxetan-3-yl)methoxy)methyl)acrylate (**A5**) was obtained as a light yellow liquid in 47% yield (bp= 88-89 °C/1.2x10^{-2} mbar). Viscosity= 0.009 Pa s.

^{1}H NMR (400 MHz, $CDCl_3$, δ, ppm): 1.3 (t, 6H, CH_3), 3.6 (s, 2H, CH_2-O), 4.2 (m, 4H, CH_2-O, C*H*$_2$-CH_3), 4.4 (d, 2H, CH_2-C), 4.51 (d, 2H, CH_2-C), 5.8 (s, 1H, CH_2=C), 6.3 (s, 1H, CH_2=C).

^{13}C NMR (400 MHz, $CDCl_3$, δ, ppm): 14.1 (CH_3), 21.3 (*C*H_3-C), 39.9 (*C*-CH_2), 60.7, 69.5, 76 (CH_2-O), 80 (CH_2-*C*), 125.5 (*C*H_2=C), 137.3 (*C*=CH_2), 165.8 (C=O).

FTIR (cm^{-1}): 2932 (C-H), 1714 (C=O), 1637 (C=C), 1098 (C-O).

ELEM. ANAL., Calcd. for $C_{11}H_{18}O_4$: C, 61.68%; H, 8.41%; O, 29.91%. Found: C, 61.82%; H, 8.44%; O, 29.74%.

Ethyl 2-(((2-oxo-1,3-dioxolan-4-yl)methoxy)methyl)acrylate (**A6**) was obtained as a light yellow liquid in 72% yield. Viscosity= 0.026 Pa s.

^{1}H NMR (400 MHz, $CDCl_3$, δ, ppm): 1.3 (t, 3H, CH_3), 3.7 (m, 1H, CH_2-O), 3.8 (m, 1H, CH_2-O), 4.2 (q, 2H, CH_2-CH_3), 4.3 (s, 2H, CH_2-O), 4.4 (t, 1H, CH_2-CH), 4.5 (t, 1H, CH_2-CH), 4.8 (s, 1H, CH-CH_2), 5.8 (s, 1H, CH_2=C), 6.3 (s, 1H, CH_2=C).

^{13}C NMR (400 MHz, $CDCl_3$, δ, ppm): 14.1 (CH_3), 60.8 (*C*H_2-CH_3), 66.1, 69.6 (CH_2-O), 69.8 (CH), 74.9 (CH_2-O), 126.3 (*C*H_2=C), 136.4 (*C*=CH_2), 154.8 (C=O), 165.5 (C=O).

FTIR (cm^{-1}): 2983 (C-H), 1792 (C=O), 1711 (C=O), 1636 (C=C), 1165 (C-O).

ELEM. ANAL., Calcd. for $C_{10}H_{14}O_6$: C, 52.17%; H, 6.09%; O, 41.74%. Found C, 51.75%; H, 6.07%; O, 42.18%.

Ethyl 2-(phenoxymethyl)acrylate (**A7**) was obtained as a light yellow liquid in 66% yield (bp= 93-95 °C/1.2x10^{-2} mbar). Viscosity= 0.008 Pa s.

^{1}H NMR (400 MHz, $CDCl_3$, δ, ppm): 1.3 (t, 3H, CH_3), 4.3 (q, 2H, CH_2-CH_3), 4.8 (s, 2H, CH_2-O), 6.0 (s, 1H, CH_2=C), 6.4 (s, 1H, CH_2=C), 6.8 (d, 2H, CH-CH), 7.0 (t, 1H, CH-CH), 7.3 (t, 2H, CH-CH).

^{13}C NMR (400 MHz, $CDCl_3$, δ, ppm): 14.0 (CH_3), 60.9 (*C*H_2-CH_3), 65.9 (CH_2-O), 114.7, 121.0, 126.3 (Ar-CH), 127.4 (*C*H_2=C), 135.9 (*C*=CH_2), 158.1 (Ar-C), 165.6 (C=O).

FTIR (cm^{-1}): 3434 (Ar-CH), 2981 (C-H), 1710 (C=O), 1640 (C=C).

3.2.2.2. General procedure for the synthesis of Carbonate Derivatives (**A8** and **A9)**. Ethyl chloroformate (5.43 g, 50 mmol) in 10 mL CCl_4 was added dropwise to the mixture of RHMA (38 mmol) and pyridine (3.95 g, 50mmol) in 20 mL CCl_4 under nitrogen. The mixture was stirred at RT for ½ h. After removal of the solvent, the mixture was poored into ice water and neutralized with $NaHCO_3$ (5%). The mixture was extracted with CH_2Cl_2,

dried with anhydrous sodium sulfate, and evaporated under reduced pressure. The crude product was purified by column chromatography (silica gel 0.063-0.200 mm) using hexane initially and gradually changing to CH_2Cl_2 as eluent.

Ethyl 2-((ethoxycarbonyloxy)methyl)acrylate (**A8**) was obtained as a dark red liquid in 40% yield.

^{1}H NMR (400 MHz, $CDCl_3$, δ, ppm): 1.3 (t, 6H, CH_3), 4.2 (m, 4H, C*H*$_2$-CH_3), 4.8 (s, 2H, CH_2-O), 5.8 (s, 1H, CH_2=C), 6.2 (s, 1H, CH_2=C).

^{13}C NMR (400 MHz, $CDCl_3$, δ, ppm): 14.0 (CH_3), 14.1 (CH_3-CH_2), 60.9 (CH_2-O), 64.1 (CH_2-CH_3), 65.4 (CH_2-O), 127.3 (*C*H_2=C), 135.0 (*C*=CH_2), 154.6 (C=O), 164.9 (C=O).

FTIR (cm^{-1}): 2982 (C-H), 1711 (C=O), 1638 (C=C), 1095 (C-O).

Tert-butyl 2-((ethoxycarbonyloxy)methyl)acrylate (**A9**) was obtained as a light yellow liquid in 35% yield (bp=67–68 ^{0}C/1.2x10^{-2} mbar). Viscosity=0.006 Pa s.

^{1}H NMR (400 MHz, $CDCl_3$, δ, ppm): 1.3 (t, 3H, C*H*$_3$-CH_2), 1.5 (s, 9H, CH_3-C), 4.2 (q, 2H, C*H*$_2$-CH_3), 4.8 (s, 2H, CH_2-O), 5.8 (s, 1H, CH_2=C), 6.3 (s, 1H, CH_2=C).

^{13}C NMR (400 MHz, $CDCl_3$, δ, ppm): 14.2 (CH_3), 27.9 (*C*H_3-C), 65.6 (*C*H_2-CH_3), 68.9 (CH_2-O), 81.4 (*C*-CH_3), 126.3 (*C*H_2=C), 136.4 (*C*=CH_2), 154.7 (C=O), 164.1 (C=O).

FTIR (cm^{-1}): 1706 (C=O), 1751 (C=O), 1640 (C=C).

3.2.2.3 General procedure for the synthesis of Ester Derivatives (**A10**-**A12**). The acid (1.78 g, 10 mmol), EBBr or TBBr (10 mmol), K_2CO_3 (1.38 g, 10 mmol) and methyl-ethyl-ketone (MEK; 25 mL) were added to a round bottom flask with a nitrogen inlet. The mixture was stirred at 60 ºC for 24 h. After removal of the solvent, the mixture was diluted with CH_2Cl_2 and extracted with water (3x5 mL). The organic phase was separated, dried with anhydrous sodium sulfate, and evaporated under reduced pressure. The crude products (A**10** and **A12**) were purified by column chromatography (silica gel 0.063-0.200 mm) using hexane initially and gradually changing to CH_2Cl_2 as eluent. Monomer **A12** was purified by distillation.

Ethyl 2-((2-(2-(2-methoxyethoxy)ethoxy)acetoxy)methyl)acrylate (**A10**) was obtained as a colorless liquid in 41% yield. Viscosity=0.010 Pa s.

^{1}H NMR (400 MHz, $CDCl_3$, δ, ppm):1.3 (t, 3H, CH_3), 3.4 (s, 3H, CH_3-O), 3.55 (t, 2H, CH_2-O), 3.65 (t, 2H, CH_2-O), 3.69 (t, 2H, CH_2-O), 3.75 (t, 2H, CH_2-O), 4.2 (m, 4H, CH_2-O, *C*H_2-CH_3), 4.9 (s, 2H, CH_2-O), 5.9 (s, 1H, CH_2=C), 6.4 (s,1H, CH_2=C).

^{13}C NMR (400 MHz, $CDCl_3$, δ, ppm): 14.1 (CH_3), 58.9 (CH_3-O), 60.9 (*C*H_2-CH_3), 62.5, 68.5, 70.4, 70.5, 70.8 (CH_2-O), 127.6 (*C*H_2=C), 135.0 (*C*=CH_2), 164.9 (C=O), 169.8 (C=O).

FTIR (cm^{-1}): 2878 (C-H), 1757 (C=O), 1717 (C=O), 1640 (C=C), 1106 (C-O).

ELEM. ANAL., Calcd. For $C_{13}H_{22}O_7$: C, 53.79%; H, 7.59%; O, 38.62%. Found: C, 53.61%; H, 7.79%; O, 38.60%.

Tert-butyl 2-((2-(2-(2 methoxyethoxy)ethoxy)acetoxy)methyl)acrylate (**A11**) was obtained as a colorless liquid in 52% yield. Viscosity= 0.019 Pa s.

^{1}H NMR (400 MHz, $CDCl_3$, δ, ppm): 1.5 (s, 9H, CH_3), 3.4 (s, 3H, CH_3-O), 3.5 (t, 2H, CH_2-O), 3.6 (t, 2H, CH_2-O), 3.7 (t, 2H, CH_2-O), 3,8 (t, 2H, CH_2-O), 4.2 (s, 2H, CH_2-O), 4.9 (s, 2H, CH_2-O), 5.8 (s, 1H, CH_2=C), 6.3 (s, 1H, CH_2=C).

^{13}C NMR (400 MHz, $CDCl_3$, δ, ppm): 27.4 (CH_3), 58.4 (CH_3-O), 62.2, 68.0, 69.95, 70.09, 70.38, 71.3, 80.9 (CH_2-O), 126.1 (*C*H_2=C), 135.9 (*C*=CH_2), 163.6 (C=O), 169.3 (C=O).

FTIR (cm^{-1}): 2978 (C-H), 1760 (C=O), 1711 (C=O), 1641 (C=C), 1140 (C-O).

2-(ethoxycarbonyl)allyl benzoate (**A12**) was obtained as a colorless liquid in 81% yield (bp= 118-120 °C/1.2x10^{-2} mbar). Viscosity= 0.010 Pa s.

^{1}H NMR (400 MHz, $CDCl_3$, δ, ppm): 1.3 (t, 3H, CH_3), 4.3 (q, 2H, CH_2-CH_3), 5.1 (s, 2H, CH_2-O), 5.9 (s, 1H, CH_2=C), 6.4 (s, 1H, CH_2=C), 7.5 (t, 2H, CH-CH), 7.6 (t, 1H, CH-CH), 8.0 (d, 2H, CH-CH).

^{13}C NMR (400 MHz, $CDCl_3$, δ, ppm): 14.1 (CH_3), 60.9 (*C*H_2-CH_3), 62.8 (CH_2-O), 127.0 (*C*H_2=C), 128.4, 129.6, 130.1, 133.1 (Ar-CH), 129.8 (Ar-C), 135.5 (*C*=CH_2), 165.1 (C=O), 165.9 (C=O).

FTIR (cm^{-1}): 3381 (Ar-CH), 2982 (C-H), 1717 (C=O), 1641 (C=C), 1175 (C-O).

3.2.2.4.General procedure for the synthesis of Carbamate Derivatives (**A13-A16)**. The isocyanate (7.69 mmol) was added dropwise to a mixture of RHMA (7.69 mmol) and BHT (4 mg, 0.018 mmol) in an ice bath. After stirring (1.5 h for monomers **A13** and **A14** and 10 h for monomers **A15** and **A16**) at 60 ^{0}C, the mixture was washed with hexane.

Ethyl 2-((phenylcarbamoyloxy)methyl)acrylate (**A13**) was obtained as a white solid after recrystallization from methanol in 79% yield. M_p=58 °C

^{1}H NMR (400 MHz, $CDCl_3$, δ, ppm): 1.3 (t, 3H, CH_3), 4.3 (q, 2H, C*H*$_2$-CH_3), 4.9 (s, 2H, CH_2-O), 5.9 (s, 1H, CH_2=C), 6.4 (s, 1H, CH_2=C),), 6.7 (s, 1H, NH-C) 7.1 (t, 1H, Ar-CH), 7.3-7.4 (m, 4H, Ar-CH).

^{13}C NMR (400 MHz, $CDCl_3$, δ, ppm): 14.2 (CH_3), 61.0 (*C*H_2-CH_3), 63.2 (CH_2-O), 118.7, 123.6 (Ar-CH), 127.6 (*C*H_2=C), 129.1 (Ar-CH), 135.7 (*C*=CH_2), 137.6 (Ar-C), 152.8 (C=O), 165.3 (C=O).

FTIR (cm^{-1}): 3349 (N-H), 2982 (C-H), 1728 (C=O), 1691 (C=O), 1637 (C=C), 1601 (C=C), 1540 (N-H).

ELEM. ANAL., Calcd. for C13H15NO4: C, 62.65%; H, 6.03%; N, 5.63%; O, 25.69%. Found: C, 62.35%; H, 6.26%; N, 5.81%; O, 25.58%.

Tert-butyl 2-((phenylcarbamoyloxy)methyl)acrylate (**A14**) was obtained as a colorless liquid in 45% yield after purification by column chromatography (using hexane initially and gradually changing to CH_2Cl_2 then gradually changing to 4% ethanol). Viscosity= 0.014 Pa s.

^{1}H NMR (400 MHz, $CDCl_3$, δ, ppm): 1.5 (s, 9H, CH_3), 4.9 (s, 2H, CH_2-O), 5.8 (s, 1H, CH_2=C), 6.3 (s, 1H, CH_2=C), 6.7 (s, 1H, NH), 7.1 (t, 1H, Ar-CH), 7.3-7.4 (m, 4H, Ar-CH).

^{13}C NMR (400 MHz, $CDCl_3$, δ, ppm): 27.9 (CH_3), 63.2 (CH_2-O), 81.4 (*C*-CH_3), 118.7, 123.4 (Ar-CH), 126.4 (*C*H_2=C), 128.9 (Ar-CH), 137.0 (*C*=CH_2), 137.7 (Ar-C), 152.9 (C=O), 164.4 (C=O).

FTIR (cm^{-1}): 3332 (N-H), 2979 (C-H), 1710 (C=O), 1640 (C=C), 1601 (C=C), 1540 (N-H).

ELEM. ANAL., Calcd. for $C_{15}H_{19}NO_4$: C, 64.98%; H, 6.86%; N, 5.05%; O, 23.11%. Found C, 64.88%; H, 6.55%; N, 5.19%; O, 23.38%.

Ethyl 2-((butylcarbamoyloxy)methyl)acrylate (**A15**) was obtained as a colorless liquid in 32% yield. Viscosity= 0.029 Pa s.

^{1}H NMR (400 MHz, $CDCl_3$, δ, ppm): 0.9 (t, 3H, CH_3), 1.3 (m, 5H, C*H*$_3$-CH_2, C*H*$_2$-CH_3), 1.5 (m, 2H, C*H*$_2$-CH_2), 3.2 (t, 2H, C*H*$_2$-NH), 4.2 (q, 2H, O-C*H*$_2$-CH_3), 4.8 (s, 2H, CH_2-O), 5.8 (s, 1H, CH_2=C), 6.3 (s, 1H, CH_2=C).

^{13}C NMR (400 MHz, $CDCl_3$, δ, ppm): 14.0 (CH_3), 14.1 (*C*H_3-CH_2), 20.4 (*C*H_2-CH_3), 29.5, 30.6 (*C*H_2-CH_2), 54.0 (CH_2-NH), 54.6 (CH_2-O), 60.5 (CH_2-O), 125.5 (*C*H_2=C), 138.6 (*C*=CH_2), 167.9 (C=O).

FTIR (cm^{-1}): 2958 (C-H), 1714 (C=O), 1636 (C=C), 1148 (C-O).

Tert-butyl 2-((butylcarbamoyloxy)methyl)acrylate (**A16**) was obtained as a very light yellow liquid in 45% yield after purification by column chromatography (silica gel 0.063-0.200 mm) using hexane initially and gradually changing to CH_2Cl_2 then gradually changing to 4% ethanol). Viscosity= 0.050 Pa s.

^{1}H NMR (400 MHz, $CDCl_3$, δ, ppm): 0.9 (t, 3H, CH_3), 1.3 (m, 2H, C*H*$_2$-CH_3), 1.5 (m, 11H, CH_3-C, C*H*$_2$-CH_2), 3.2 (m, 2H, CH_2-NH), 4.8 (s, 2H, CH_2-O), 5.7 (s, 1H, CH_2=C), 6.2 (s, 1H, CH_2=C).

^{13}C NMR (400 MHz, $CDCl_3$, δ, ppm): 14.0 (*C*H_3-CH_2), 20.5 (*C*H_2-CH_3), 28.0 (*C*H_3-C), 29.7 (*C*H_2-CH_2), 54.1 (CH_2-NH), 54.6 (CH_2-O), 80.4 (*C*-CH_3), 124.5 (*C*H_2=C), 140.0 (*C*=CH_2), 166.3 (C=O).

FTIR (cm^{-1}): 3344 (N-H), 2960 (C-H), 1707 (C=O), 1638 (C=C), 1149 (C-O).

3.2.3. Photopolymerizations

3.2.3.1. Photopolymerization Procedure. Approximately 3.0 or 4.0 mg of sample was placed in an aluminium DSC pan. The photoinitiator which was dissolved in CH_2CI_2 was added with a micro-syringe to give a final concentration in the monomer of 2.0 mol per cent after evaporation of the solvent. The sample and the reference pans were placed in the DSC chamber, the system was purged with nitrogen flow to remove air and CH_2CI_2 for 10 min before polymerization and purging was continued during polymerization. Heats of photoreactions were measured using a DSC equipped with a mercury arc lamp. The samples were irradiated for 10 min at 40 °C with an incident light density of 20 mW/cm^2. The heat flux as a function of reaction time was monitored using DSC under isothermal conditions and both the rate of polymerization (R_p) and conversion were calculated as a function of time. The theoretical values used for the heats of reaction (ΔH_p) were 13.1 kcal/mol for methacrylate double bonds [73, 74]. Rates of polymerization were calculated according to the following formula:

$$\text{Rate} = \frac{(Q/s)\, M}{n\, \Delta H_p\, m} \qquad (3.1)$$

where Q /s is heat flow per second, M the molar mass of the monomer, n the number of double bonds per monomer molecule, ΔH_p is the heat released per mole of double bonds reacted and m the mass of monomer in the sample.

3.2.4. Calculation of Dipole moment

Boltzman-averaged dipole moments were calculated with PM3 for all the monomers. For this purpose, all posible rotations around single bonds were considered for a given acrylate to generate all the conformations corresponding to stationary points. Minimization, followed by the calculation of the Boltzmann-averaged dipole moments for all the conformations was carried out with PM3 by using Spartan ’06 [75]. The unique structures were sorted in the order of increasing energy. The dipole moments of the first 100 conformers are Boltzmann averaged at 298.15 K according to the following formula:

$$\langle \mu_{calc} \rangle = \sum D_j \frac{e^{\Delta H_j / RT}}{\sum_i e^{\Delta H_i / RT}} = \sum_j D_j p_j \qquad (3.2)$$

where D_j is the dipole moment of the conformation j, ΔH_j is the heat of formation of conformation j, T is the absolute temperature, R is the Boltzmann constant and p_j is the probability of finding the monomer in conformation j at the temperature T [56].

3.3. Results and Discussion

3.3.1..Synthesis of the Monomers

The general structure of the synthesized monomers can be given as

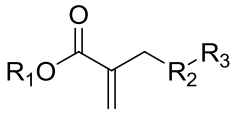

Figure 3.2. General structure of synthesized monomers.

where R1 is ethyl or t-butyl group due to methacrylate, R2 is the secondary functionality which displays the ester, ether, carbonate and carbamate groups and R3 is the terminal group. The terminal groups were varied to incorporate highly polar or cyclic groups (Figure 3.2).

The synthesis of all the monomers is illustrated in Figure 3.1. The ether derivatives (**A1**-**A7**) were synthesized by the reaction of alcohols with EBBr and/or TBBr using TEA as catalyst in THF at 60 ^{o}C for 24 h: 4-(2-hydroxyethyl)morpholine with EBBr and TBBr gave **A1** and **A2**; 3-hydroxypropionitrile with EBBr and TBBr gave **A3** and **A4**; 3-hydroxymethyl-3-methyloxetane with EBBr gave **A5**, 4-(hydroxymethyl)-1,3-dioxolan-2-one with EBBr gave **A6** and phenol with EBBr gave **A7**. Four of these (**A1**, **A2**, **A5**, **A6**) contain cyclic terminal groups, which were found to enhance the reactivities of acrylates and methacrylates [51]. The other two (**A3** and **A4**) contain a cyano group and are designed to assess the electron withdrawing effect of the substituent. Monomer **A7** was

synthesized to evaluate the importance of π–π interactions. The reaction time for monomer **A3** was decreased to 7h due to unexpected polymerization in 24 h. This monomer polymerizes without an initiator to give a polymer with M_n and T_g values of 3200 and 45 ^oC during the synthesis; other indications and possible reasons for the high reactivity of this monomer are discussed later in this work.

The carbonate derivatives (**A8** and **A9**) were prepared from the reactions of EHMA and TBHMA with ethyl chloroformate using pyridine as the catalyst; the aim being to evaluate the enhancement of reactivity due to carbonates, as discussed above. Although the crude products were purified by column chromatography, monomer **A8** quickly turned to dark red color after storage, even refrigerated. In the literature, the use of pyridine and dimethylaniline during the synthesis of (2-oxo-1,3-dioxolan-4-yl)methyl acrylate produced yellow and dark purple colors. [76]. The color change during storage of monomer **A8** may be explained by one of the two following mechanisms: (i) sorption of carbon dioxide released during storage of the monomer to residual pyridine and formation of protonated pyridine bicarbonates in the presence of water [77] and (ii) attack of residual pyridine to double bond of the monomer with the release of carbonate ion and forming a carbonate salt. Because we were not able to solve coloration problem, we did not further investigate this monomer.

The ester derivatives were synthesized from the reactions of EBBr and/or TBBr and 2-[2-(2-methoxyethoxy)ethoxy]acetic acid and benzoic acid to increase the dipole moment in an effort to investigate the electronic effect of high dipole moment (**A1**) and also π–π interactions. Also, the monomers obtained from 2-[2-(2-methoxyethoxy)ethoxy]acetic acid will contain two ether linkages with abstractable hydrogens, which may reduce the oxygen inhibition [47]. The reaction was carried out at 60 ^oC in methyl ethyl ketone in the presence of the catalyst potassium carbonate and gave the ester derivatives **A10**, **A11**, and **A12**.

To investigate the importance of hydrogen bonding and π–π interactions in the polymerization rate, the carbamate derivatives **A13**–**A16** were prepared via a reaction of the isocyanates (phenyl and butyl isocyanates) with EHMA and TBHMA with catalyst

(dibutyltin dilaurate) at room temperature or without catalyst at 60 ^{o}C. The reactions were monitored by following the disappearance of the isocyanate peak in the FTIR spectrum.

The synthesis of monomers gave the crude products in high yields (80–90%). All of the monomers were liquids except monomer **A13**, which was a white solid (m_p=58 ^{o}C) at room temperature. The monomers were purified by column chromatography, distillation, or recrystallization and characterized by using FTIR, ^{13}C NMR, and ^{1}H NMR spectra (Figures 3.3 and 3.4). The ^{1}H NMR of monomer **A1** showed methyl protons at 1.3 ppm, two methylene protons adjacent to nitrogen at 2.5 and 2.6 ppm, four methylene protons adjacent to oxygen at 3.6, 3.7, and 4.1 ppm and double bond protons at 5.8 and 6.3 ppm (Figure 3.3). The ^{13}C NMR spectrum of monomer **A6** showed characteristic peaks for methyl carbon at 14.1 ppm, methylene carbons at 60.8, 66.1, 69.6, and 74.9 ppm, a methine carbon at 69.8 ppm, double bond carbons at 126.3 and 136.4 ppm, and carbonyl carbons at 154.8 and 165.5 ppm (Figure 3.4). The FTIR spectra of monomers **A13** and **A14** are shown in Figure 3.5.

3.3.2. Photopolymerization

The reactivities of the synthesized monomers in photopolymerization were investigated with photodifferential scanning calorimetry and compared with those of EHMA, TBHMA, and HEMA. Photopolymerizations were carried out using 2,2-dimethoxy-2-phenylacetophenone (DMPA; 2 mol %) at 40 ^{o}C.

EHMA, TBHMA, and HEMA polymerizations behave in the same way in which a distinct shoulder at the onset of autoacceleration was observed (Figure 3.6 and Table 3.1). This shoulder was observed earlier for EHMA and HEMA when compared with TBHMA. It is known that intermolecular hydrogen bonding and/or chain transfer reactions leading to an increase in viscosity and a decrease in termination rate cause autoacceleration. The extent of autoacceleration was observed in the following order: HEMA > EHMA > TBHMA, this was also the order of their maximum rates of polymerization. Increasing the size of the ester group from ethyl to t-butyl decreased the polymerization rate due to steric effects. We observed this behavior in all of the synthesized monomers here.

The high reactivity of HEMA compared with EHMA was also observed by Buback *et al* [5]. They reported propagation rate coefficients for bulk polymerizations of EHMA and HEMA at 50 ^{o}C as 944 and 2563 L mol^{-1} s^{-1}.The activation energy of HEMA (21.9 kJ mol^{-1}) is not significantly different from the one of EHMA (20.4 kJ mol^{-1}) but the frequency factor (which reflects the steric effect) for HEMA (8.88 x10^{6} L mol^{-1} s^{-1}) is higher than that of EHMA (1.87x10^{6} L mol^{-1} s^{-1}). Davis et al. also reported the activation energy and the frequency factor for EHMA as 14–17 kJ mol^{-1} and (3-8) x10^{6} L mol^{-1} s^{-1}, respectively [78, 79]. They also found an important solvent effect on k_p of EHMA that changes between 580 L mol^{-1} s^{-1} (THF) and 1860 mol^{-1} s^{-1} (xylene) at 15 ^{o}C. [80].

In general, overall monomer conversion increases for systems that are polymerized at faster rates. As the polymerization rate increases, the volume relaxation is unable to keep pace with conversion, leading to increased free volume formation. The free volume in excess of equilibrium values causes higher mobility, which results in increased conversion. Also, conversion depends on the polymerization temperature and the T_g of the system, which indicates its mobility. The T_g of a polymerization system depends on flexibility of monomers. For example, polar groups are responsible for intramolecular and intermolecular interactions and decrease flexibility of the system, increase T_g and decrease conversion.

The overall conversions were 90, 69, and 51% for HEMA, EHMA, and TBHMA. It was observed that the greater the extent of autoacceleration, the higher the conversion. The T_g values for poly-HEMA, poly-EHMA, and poly-TBHMA are 83–95, 64, and 120 ^{o}C [72]. Low conversion of TBHMA is due to a combination of high T_g of its polymer and low rate of polymerization.

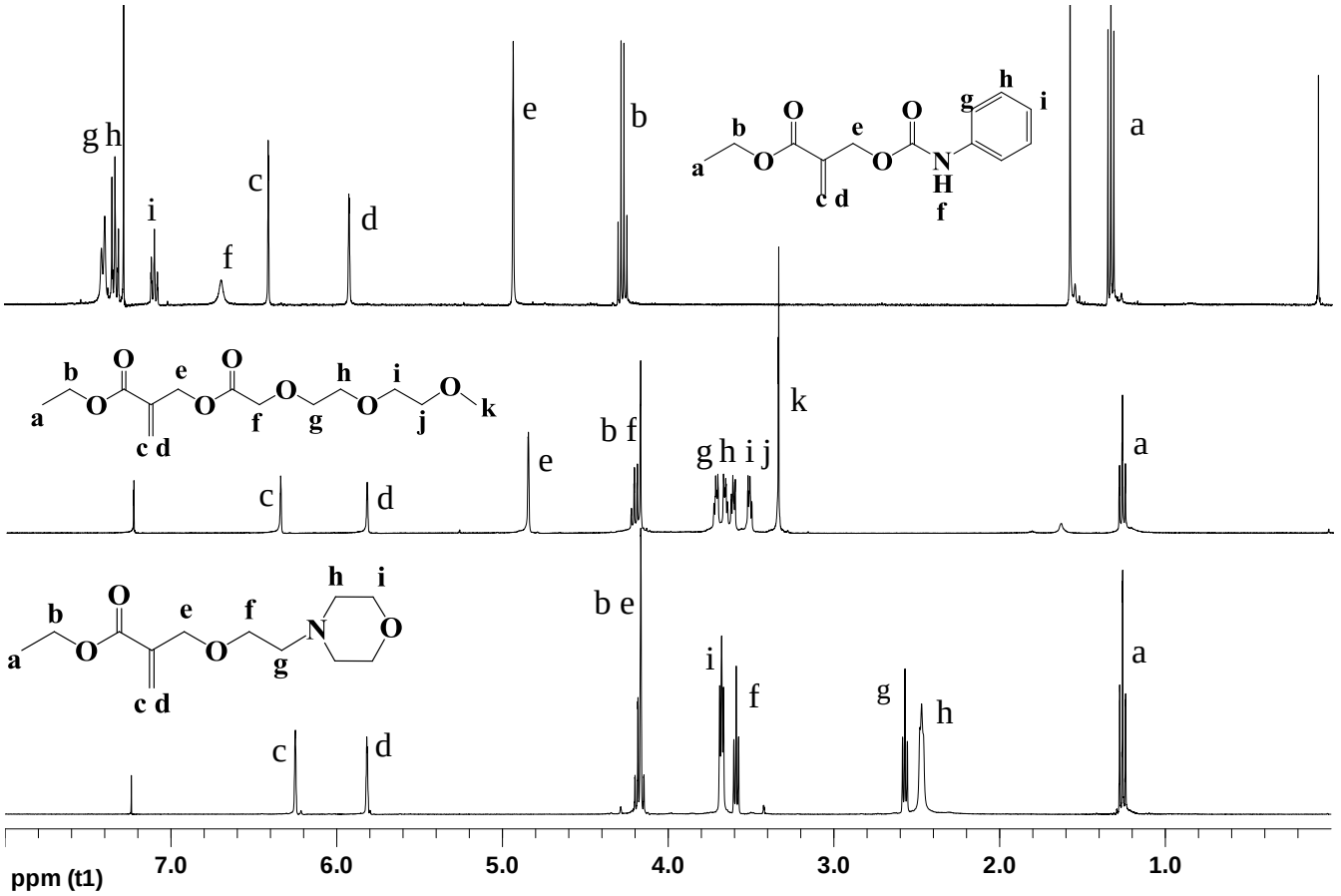

Figure 3.3. ^{1}H NMR spectra of monomers **A1**, **A10** and **A13**.

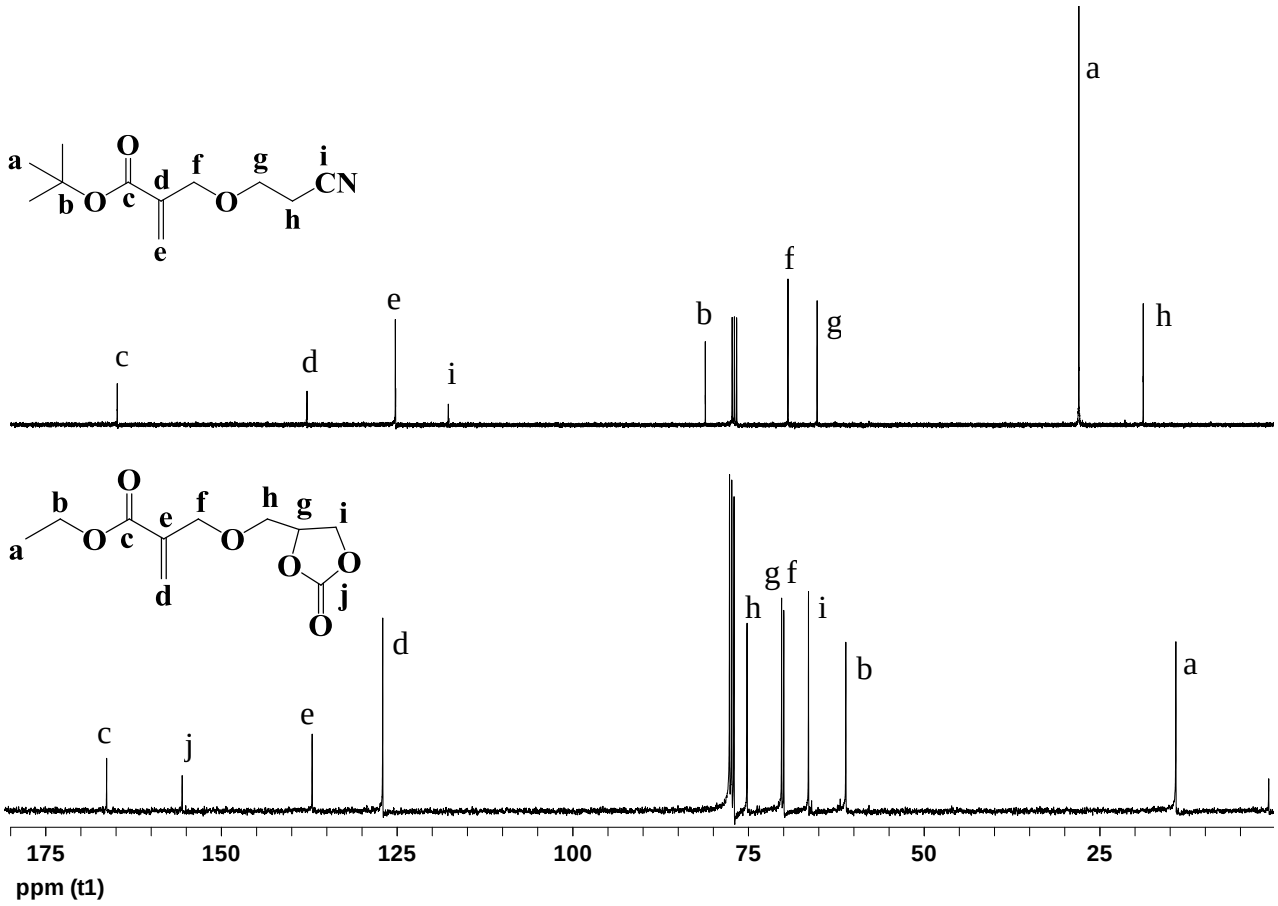

Figure 3.4. ^{13}C NMR spectra of monomers **A4** and **A6**.

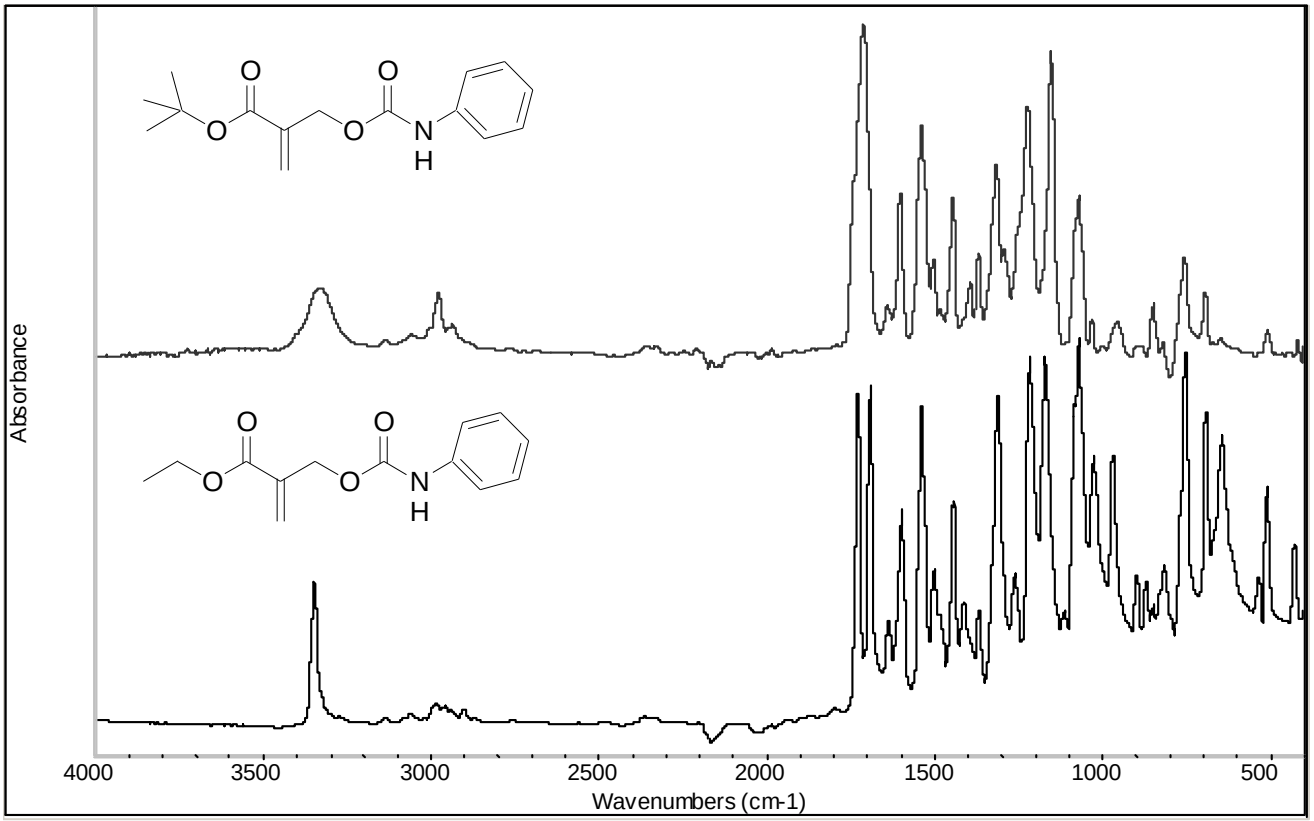

Figure 3.5. FTIR spectra of monomers **A13** and **A14**.

It is known that hydrogen bonding decreases with increasing temperature, which tends to decrease the polymerization rate, whereas chain transfer increases with increasing temperature which tends to increase the polymerization rate. To investigate the effect of temperature change on polymerization rate, the monomers were polymerized at 25, 40, and 70 ^{o}C. We found that rate of polymerizations of these monomers increase roughly with temperature (Table 3.1). This can be explained by competing effects of activation, which occurs by increasing temperature and deactivation, which is due to decreased hydrogen bonding. The FTIR spectrum of HEMA clearly shows two carbonyl peak maxima at 1713 and 1699 cm^{-1} due to a hydrogen-bonded carbonyl and free carbonyl stretching bands. However, FTIR spectrum of EHMA and TBHMA shows one peak at 1704 and 1707 cm^{-1} corresponding more to a hydrogen-bonded carbonyl stretching band (Figure 3.7). Additionally, thermal bulk polymerization of HEMA and EHMA gave crosslinked polymers, indicating the importance of chain transfer reactions.

The rates of polymerization of the phenyl carbamate monomers (monomers **A13** and **A14**) were found to be significantly higher than those of the monomers with other functional groups (Figure 3.8, Table 3.1); even higher than EHMA and TBHMA. The intermolecular interactions due to hydrogen bonding and/or π-π stacking are probably the reason for the high reactivity of monomers **A13** and **A14**.

The different states of monomer **A13** and **A14** (solid vs. liquid) indicate their different extent of hydrogen bonding. The extent of hydrogen bonding was evaluated by NH and C=O stretching modes observed by FTIR spectra of monomers (Figure 3.5). The locations of NH peaks were 3349 and 3331 cm^{-1} (monomers **A13** and **A14**), both correspond to hydrogen bonded NH peaks [10]. The locations of C=O peaks were 1690 (carbamate) and 1728 cm^{-1} (ester) for monomer **A13**. Because monomer **A13** is crystalline and its C=O groups are completely bonded to NH, the peak at 1690 cm^{-1} is due to ordered carbamate C=O. The other C=O peak at 1728 cm^{-1} is due to the free ester C=O. However, monomer **A14** is liquid and both C=O groups (carbamate and ester) can make hydrogen bonding with NH. Therefore, carbamate C=O shifts to higher frequency and overlaps with hydrogen bonded ester C=O at 1710 cm cm^{-1}. No free ester C=O exists. All these results confirm a greater extent of hydrogen bonding in monomer **A13**, which results in high rate

of polymerization. Therefore, photopolymerization of this monomer was investigated in both crystalline (40 ^{o}C) and noncrystalline states (70 ^{o}C; Table 3.1). The results showed that polymerization occurs in both states and the rate increases with temperature. Also, higher conversions were obtained in noncrystalline state, as expected.

To investigate the effect of π-π stacking on monomer reactivity, the aliphatic carbamate monomers (**A15** and **A16**) were polymerized. These monomers were found to be about four or five times less reactive than phenyl carbamate monomers (**A13** and **A14**; Figure 3.8, Table 3.1). They have rates of polymerization comparable with ether derivatives. These monomers were liquids and the locations of NH (3344 cm^{-1}) and overlapping ester and carbamate C=O peaks (1710 cm^{-1}) in their FTIR spectra were similar to those of monomer **A14**. Thus, we can say that the strength of hydrogen bonding of these monomers (**A14**, **A15**, and **A16**) has no discernible effect on the polymerization rate. The relatively low reactivity of monomers **A15** and **A16** despite their ability to still make hydrogen bonding brings out the importance of π-π stacking. We observed a similar behavior in the literature [81]. For example, the maximum rate of polymerization of phenyl carbamate ethyl acrylate was 1.3 s^{-1} whereas n-butyl carbamate ethyl acrylate gave a much lower rate of polymerization of 0.38 s^{-1}. The conversions obtained for monomers **A15** and **A16** were higher than those of monomers **A13** and **A14** despite their lower rates of polymerization, indicating the enhanced mobility of these monomers.

Among the ester-linked monomers (**A10**, **A11**, and **A12**), the aromatic ester monomer (**A12**) capable of π-π interaction exhibited about twice the rate of polymerization of the aliphatic monomer (**A10**), approaching even that of the most reactive carbamate monomer (**A13**; Figure 3.9, Table 3.1). This result was previously indicated with the evaluation of k_p and k_t of the benzoate derivative (990 and $2.9x10^{-6}$ L mol^{-1} s^{-1}) of EHMA and the acetate derivative (k_p= 350, k_t= $2.1x10^{-6}$ L mol^{-1} s^{-1}) of MHMA [70, 82]. Also, Davis et al. indicated that when going from EHMA to its acetate derivative both Eact (12.4 kJ mol^{-1}) and the frequency factor (L mol^{-1} s^{-1}) decrease [78]. Monomer **A10**, due to its very flexible structure and high rate of polymerization exhibits the highest conversion among the monomers studied in this work.

The carbonate derivative (**A9**) was found to be less reactive than ester and aromatic carbamate derivatives, EHMA, TBHMA, and HEMA. It showed similar reactivity with TBHMA-ether and TBHMA-aliphatic carbamate derivatives.

On the average, ether derivatives were found to be less reactive than ester derivatives (Table 1). Yamada et al. previously reported k_p and k_t values for the butyl ether derivative of MHMA as 298 and 8.0 x10^{-6} L mol s^{-1}, respectively [70, 83]. Although this k_p value is similar to that of the acetate derivative, the higher k_t value of the ether derivative is responsible for the lower rate of polymerization. However, we observed that rates of ether derivatives can be increased by modifications of the terminal groups. The maximum rate of polymerizations of EHMA ether derivatives (**A1**–**A7**) with different terminal groups showed the following trend: cyclic carbonate > phenyl > cyano > morpholine > oxetane, where $R_{p,max}$ (monomer **A6**) = 1.08, $R_{p,max}$ (monomer **A7**) = 1.83, $R_{p,max}$ (monomer **A3**) = 2.44, $R_{p,max}$ (monomer **A1**) = 4.4, and $R_{p,max}$ (monomer **A5**; Figure 3.9, Table 3.1). This trend was similar to that observed for acrylate monomers reported by Jansen et al. where $R_{p,max}$ (glycerol carbonate acrylate) =2.16, $R_{p,max}$ (cyano ethyl acrylate)=3.66 and $R_{p,max}$ (oxethane acrylate) [56]. The high reactivity of monomer **A6** may be due to hydrogen abstraction, ring stacking interactions, and relatively high dipole moment. However, monomers that also possess a heterocyclic ring (**A1**, **A2**, and **A5**) did not exhibit such rate enhancement. To check the possibility of hydrogen abstraction, the photopolymerization of monomer **A6** in the presence of benzophenone was tried; no polymerization was observed, indicating that there are no labile hydrogens under our photopolymerization conditions. Additionally, the polymers obtained from this monomer were totally soluble indicating that chain transfer is not important. The effect of temperature on photopolymerization of **A6** was also investigated (Table 3.1). Monomer **A6** exhibited small changes in polymerization rate over the 25–70 ^{o}C range, while the conversion was increased by about 25%. Although monomer **A6** has the highest rate of polymerization among the ether derivatives, its conversion was lower, similar to cyclic carbonate-containing (meth)acrylates reported in the literature [59], which may be attributed to early autoacceleration and/or high T_g of its polymer (85 ^{o}C). Among the ether derivatives, monomer **A3** with a high rate of polymerization and flexible structure exhibited highest conversion.

The rate differences of ether derivatives can be explained by the differences in dipole moment as will discussed in the next section.

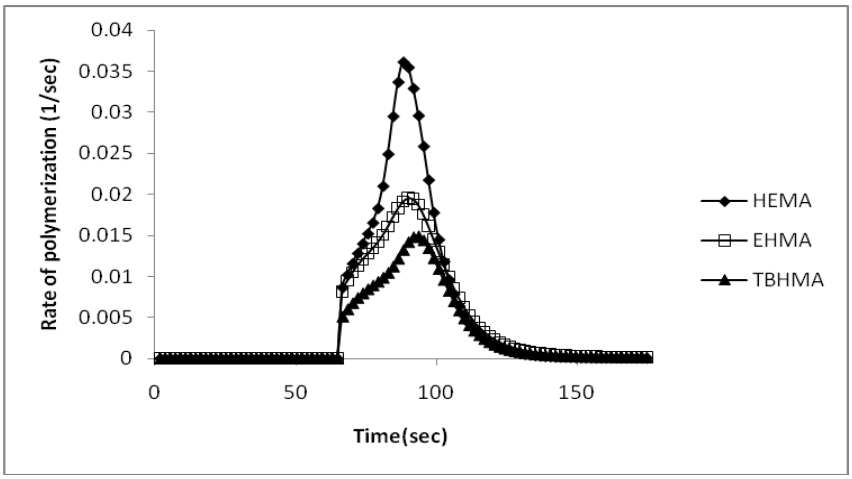

Figure 3.6. Rate of polymerization versus time for HEMA, EHMA and TBHMA.

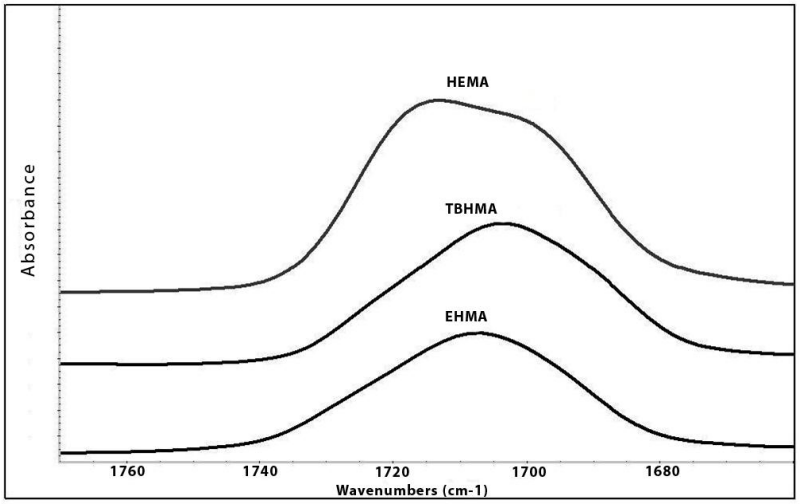

Figure 3.7. FTIR spectra of carbonyl stretching regions of HEMA, EHMA and TBHMA.

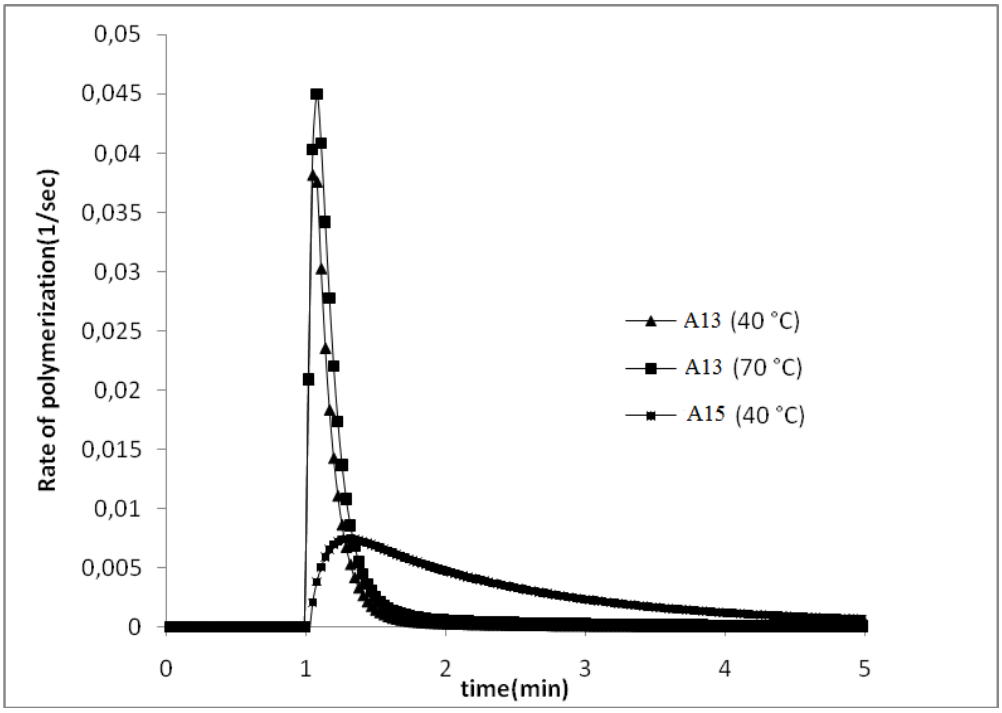

Figure 3.8. Rate of polymerization versus time for monomers **A13** and **A15**.

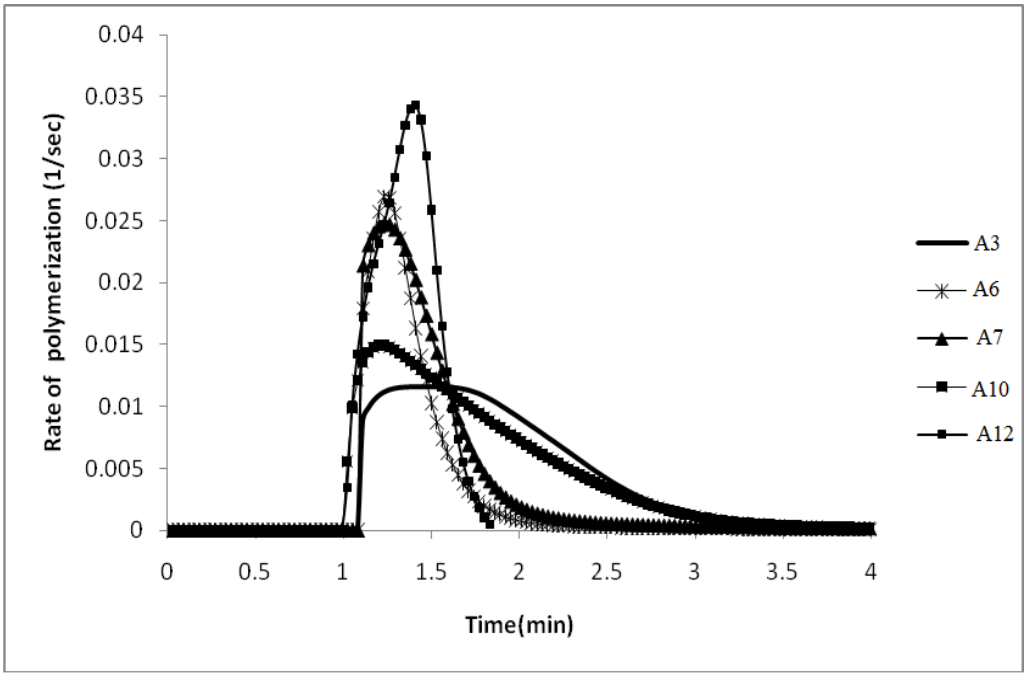

Figure 3.9. Rate of polymerization versus time plots of monomers **A3**, **A6, A7**, **A10** and **A12.**

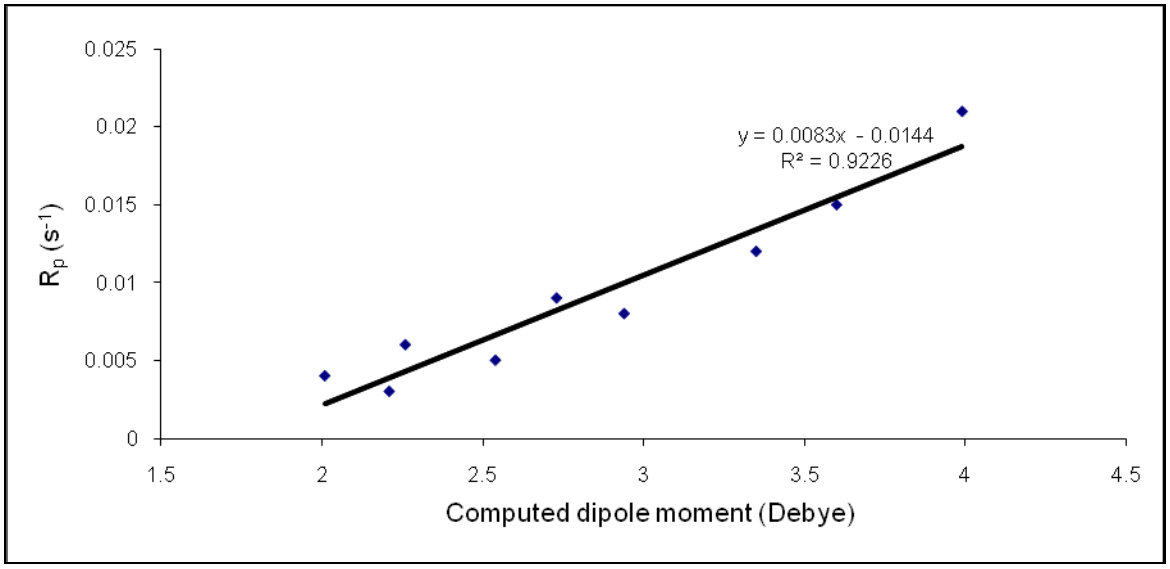

Figure 3. 10. Rate of polymerization versus calculated dipole moment plot for monomers **A1**-**A12** except monomers **A7** and **A12.**

3.3.3. Dipole Moment

The synthesized monomers were evaluated in terms of dipole moment to find a relation between the monomer structure and the reactivity. The Boltzmann-averaged dipole moments of the monomers were calculated for their minimum energy conformers (Table 3.1). When we consider non hydrogen bonding monomers (**A1**–**A12**), there seems to be a correlation except for monomers **A7** and **A12** (Table 3.1, Figure 3.10). This exception may be due to an additional π–π interaction, which increases the rate of polymerization. The high reactivity of monomer **A6** can be explained by its high dipole moment.

When we consider all hydrogen-bonding monomers (**A13**–**A16**, HEMA, EHMA, and TBHMA), it was not possible to find a correlation between monomer reactivity and dipole moment. For example, monomers **A13** and **A15**, both having approximately similar dipole moments (2.99 and 2.93 Debye), showed completely different polymerization rates. Kilambi et al. have also investigated hydrogen-bonding monomers having high reactivity but low dipole moments. They said that a particular conformation with a low dipole moment may be energetically favored due to intermolecular hydrogen bonding [44].

3.3.4. Chemical Shift Values

^{13}C NMR can be used to predict the free radical polymerizability of monomers. Vaidya *et al*. have reported that chemical shifts of the C=C double bonds (($C_\beta H_2$=C_α)) depend on the substituents. δC_β and δC_α shift to lower and higher fields, respectively, with an increase in electron withdrawing power of the substituents [84]. Therefore, $\Delta\delta$ (δC_β-δC_α) shows the effects of substituents on polymerizability. The stronger the electron-withdrawing power of the substituents the smaller the chemical shift difference and the higher the radical polymerizability [84, 85]. Also, bulky substituents may cause differences in chemical shifts and/or lead to lower propagation enthalpy through steric hindrance.

Table 3.1. Rate of polymerizations, conversions, calculated dipole moments and differences in chemical shift values of monomers **A1**-**A16**, HEMA, EHMA, and TBHMA.

Monomer	**Monomer Structure**	**Rate (s^{-1})**	**Converison (%)**	**Dipole Moment (Debye)**	**Δδ (ppm)**
A13	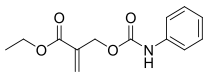	0.038 0.045[b]	44 63	2.99	8.1
HEMA	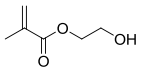	0.031[a] 0.036 0.042[b]	81 90 83	3.55	10.0
A12	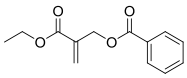	0.033	89	3.18	8.5
A6	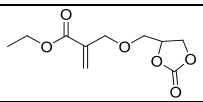	0.023[a] 0.026 0.030[b]	64 56 74	3.99	10.1
A7	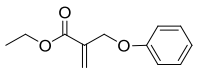	0.024	80	3.66	9.6
A14	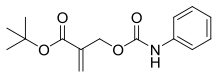	0.022	62	2.67	10.6
EHMA	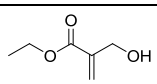	0.016[a] 0.019 0.023[b]	61 69 71	3.19	14.0
A10	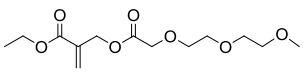	0.015	94	3.60	7.4
TBHMA	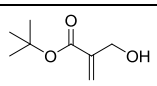	0.012[a] 0.015 0.016[b]	49 51 61	2.76	16.4
A3	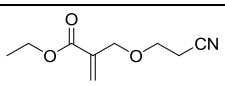	0.012	90	3.35	10.4
A1	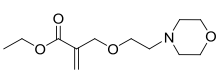	0.009	78	2.73	12.0

Table 3.1. Rate of polymerizations, conversions, calculated dipole moments and differences in chemical shift values of monomers **A1**-**A16**, HEMA, EHMA, and TBHMA (cont.).

A11	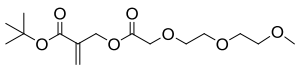	0.008	70	2.94	9.8
A15	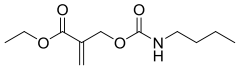	0.007	77	2.93	13.1
A9	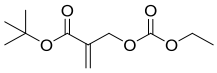	0.006	85	2.26	10.1
A5	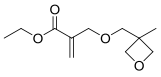	0.005	82	2.54	11.8
A16	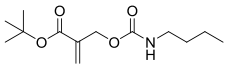	0.005	72	2.35	15.5
A4	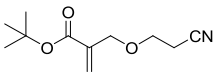	0.004	65	2.01	12.6
A2	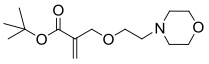	0.003	66	2.21	14.3

[a] 25 ºC, [b] 70 ºC

To see a correlation between polymerizability and differences in chemical shift values ($\Delta\delta$), we evaluated the monomers in three categories. In the first category (HEMA, EHMA, and TBHMA), the reactivity trend was correlated to $\Delta\delta$ values (Table 3.1). As expected, TBHMA was found to be the least reactive monomer due to steric effect. The second category involved ester, ether, and carbonate derivatives (**A1**–**A12**) of RHMA monomers. Here also, the reactivity of ester derivatives, compared with carbonate and ether derivatives was confirmed by low $\Delta\delta$ values. For example, the maximum rates of polymerization of TBHMA derivatives (**A11**, **A9**, **A4**, and **A2**) with the chemical shift values of 9.8, 10.1, 12.6, and 14.3 ppm were found to be 0.008, 0.006, 0.004, and 0.003 s^{-1}. Among the ether derivatives, monomers **A3**, **A6**, and **A7** were expected to have the highest reactivity, comparable with those of the ester derivatives.

The last category involved carbamate derivatives (**A13**–**A16**) of RHMA monomers. The $\Delta\delta$ values were well correlated with the reactivities, indicating the low reactivities of monomers **A15** and **A16**.

3.4. Conclusion

Novel RHMA derivatives were prepared and evaluated using photopolymerization rates to understand the relation between the monomer structure and the reactivity. It was observed that the nature of both secondary functionalities (ester, ether, carbonate, and carbamate) and the terminal groups (phenyl, cyano, morpholine, butyl, etc.) have significant effects on polymerization kinetics. Depending on the type of the secondary functionality, the polymerization rate may increase up to five times by changing terminal groups. The π–π interactions were found to be an important rate enhancing factor. Among the monomers studied here, aromatic carbamates capable of both π–π interactions and hydrogen bonding were found to show highest rate of polymerization. Studies on the other aromatic carbamate derivatives of RHMA monomers are continuing. The high reactivity of cyclic carbonate-containing monomers was shown once more with a new derivative. The relationship between the polymerization and the dipole moment of monomers for non hydrogen-bonded monomers seems to hold.

4. A COMPUTATIONAL STUDY ON THE REACTIVITY ENHANCEMENT IN FREE RADICAL POLYMERIZATION OF ALKYL α-HYDROXYMETHACRYLATE (RHMA) AND ACRYLATE DERIVATIVES

4.1. Introduction

Several potential factors enhancing the reactivities of (meth)acrylates have been mentioned in Chapter 3. Kilambi *et al*. [81] have studied experimentally the intermolecular and intramolecular interactions that affect different monomers differently. These studies have demonstrated that certain functional groups primarily lead to intermolecular interactions (for example hydrogen bonding, π-π stacking etc.) that increase polymerization, while other substituents lead primarily to intramolecular interactions. Acrylate monomers functionalized by an aromatic ring such as phenyl acrylate and benzyl acrylate polymerize much faster than traditional acrylates such as hexyl acrylate. It was hypothesized that increased viscosity effects due to π-π stacking and increase in molecular rigidity contribute to the monomer reactivity to a significant extent.

Here, we focus on the propagation reaction of a series of alkyl α-hydroxymethacrylate (RHMA) and acrylates in order to understand the effect of the nature of the pendant group (linear vs aromatic), the role of long-range stabilizing interactions and π-π stacking on their reactivities. For this purpose, we computationally investigated the polymerizations of three RHMA-derived monomers: methyl 2-(butoxymethyl)acrylate-**B1**, methyl 2-(acetoxymethyl)acrylate-**B2**, 2-(methoxycarbonyl)allyl benzoate-**B3**. This study has been complemented with a modeling study on three representative acrylate derivatives: hexyl acrylate-**B4**, benzyl acrylate-**B5** and phenyl acrylate-**B6** (Figure 4.1).

The kinetics of photopolymerizations are experimentally investigated using photodifferential scanning calorimetry, real-time Fourier transform infrared spectroscopy (RT-FTIR), electron spin resonance spectroscopy (ESR) and pulsed laser polymerization

(PLP) with molar mass distribution (MMD) analysis by size exclusion chromatography [86, 87, 73].

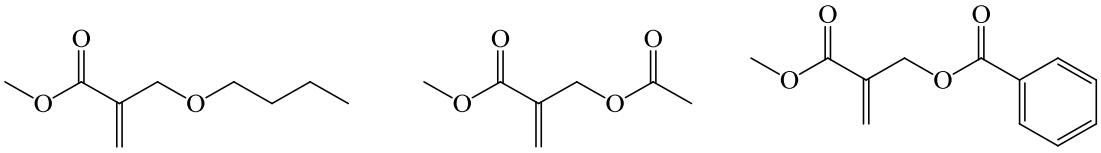

B1 **B2** **B3**

methyl 2-(butoxymethyl)acrylate methyl 2-(acetoxymethyl)acrylate 2-(methoxycarbonyl)allyl benzoate

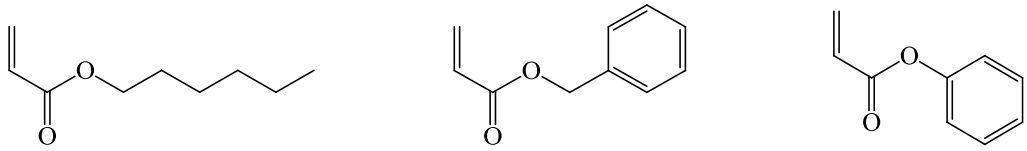

B4 **B5** **B6**

hexyl acrylate benzyl acrylate phenyl acrylate

Figure 4.1. RHMA (**B1-B3**) and acrylate (**B4-B6**) monomers considered in this study.

.

In this work, the k_p values for the free radical polymerization of **B1-B3** obtained by Yamada *et al*. using ESR and the rates of polymerization of **B4-B6** obtained by Kilambi *et al.* using RT-FTIR studies are taken into consideration [81, 88]. The experimentally determined propagation rate constants and rate of polymerizations for **B1-B6** are displayed in Table 4.1.

4.2. Computational Details

The B3LYP methodology combined with the 6-31+G(d) basis set within the Gaussian 03 software package [18] was chosen as a cost effective and accurate method for geometry optimizations. Geometry optimizations have also been carried out with the M06-2X/6-31+G(d) methodology using the Gaussian 09 [90] software package. M06-2X ranks top among the functionals for the study of noncovalent interactions [91] and this method was

chosen because it has proven to be successful for describing thermochemistry, reaction kinetics and hydrogen bonding [91, 92].

Table 4.1. Propagation rate constants (k_p) of **B1-B3** and rates (R_p) of photopolymerization of **B4-B6**.

Monomer	**k_{p*}**	**R_{p**}**
Methyl 2-(butoxymethyl)acrylate – **B1**	298[88]	-
Methyl 2-(acetoxymethyl)acrylate – **B2**	350[88]	-
2-(ethoxycarbonyl)allyl benzoate - ethyl derivative of **B3**	990[88]	-
hexyl acrylate – **B4**	-	0.02[81]
benzyl acrylate – **B5**	-	0.09[81]
phenyl acrylate – **B6**	-	0.23[81]

* Measurements for k_p (L/mol.s) were carried out in benzene.
**The maximum rate of polymerization (s^{-1}) was measured in bulk.

The MPWB1K functional [93] which is successfully used for thermochemistry, thermochemical kinetics, hydrogen bonding, and weak interactions has been used to evaluate the kinetics of the propagation reactions for the dimeric models of **B1-B6** optimized with M062X/6-31+G(d). The kinetics have also been evaluated with the M06-2X/6-31+G(d) and MPWB1K/6-311+G(3df,2p)//M06-2X/6-31+G(d) methodologies in order to take into account long range interactions as well as π-π stacking.

The conventional transition state theory (TST) [94] is used to calculate the rate constant for the bimolecular reaction as follow:

$$k_2 = \kappa \frac{kT}{h} \frac{RT}{p^\theta} e^{-\Delta G^\ddagger / RT}$$

In this equation k represents Boltzmann's constant, T is the temperature, h is Planck's constant, $\Delta G^\ddagger$ represents the Gibbs free energy difference between the activated complex and the reactants, R is the universal gas constant, κ is the transmission coefficient which is assumed to be about 1 and p^θ is the standard pressure 10^5 Pa (1 bar).

Rotational potential energy scans around the forming bond are performed in order to locate the energetically most stable transition states [95]. NBO charges were calculated to rationalize the electrostatic interactions between the various moieties [96].

The reaction kinetics of **B1-B3** have been evaluated in solution by using a dielectric continuum model, the integral equation formalism model (IEF-PCM) [97-100] with the UFF radii. The gas phase geometries were re-optimized in a polarizable continuum medium (PCM) in order to access the effect of the solvent. The calculated free energy of solvation was corrected with the RT ln (24.46) term in order to take into account the unit transformation from 1 mol L^{-1} (g) to 1 mol L^{-1} (soln) [95]. In continuum solvation models, the solvent is represented as a polarizable medium characterized by its static dielectric constant ε (ε = 2.2706 for benzene) and the solute is embedded in a cavity surrounded by this dielectric medium [101]. This methodology was successfully used in understanding the effect of the solvent in the free radical polymerization of AA and MAA [102].

4.3. Results and Discussion

A conformer search of all the monomers and radicals has been carried out with the B3LYP/6-31+G(d) and M06-2X/6-31+G(d) methodologies in vacuum. The models used for the formation of the unimeric radical and the propagation of the chain are depicted in Figure 4.2. The methyl radical adds to the double bond to yield a unimeric radical which then adds to the monomer to generate the propagating polymer chain (propagation reaction). The propagation of the polymer chain has been modeled by taking into account the mode of addition –tacticity– of the radicalic chain to the monomer.

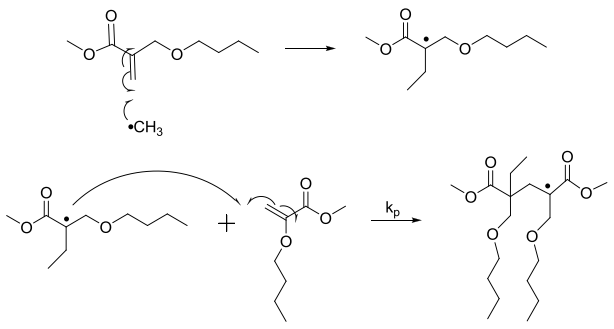

Figure 4.2. Models for the formation of the unimeric radical and the dimeric chain.

Stereoregularity affects many important properties of the polymers, such as solubility, crystallinity, melting point, glass transition temperature, and mechanical strength. The stereoregularity of the polymer main chain is referred to as tacticity and depicts the relationship between two adjacent monomer units consisting of meso (*m*) and racemo (*r*) diads. For obtaining highly stereoregular polymers such as isotactic (*mm*), syndiotactic (*rr*), and heterotactic (*mr*) sequences (Figure 4.3), highly diastereoselective reactions would be necessary, where an asymmetric environment between the pendant groups and the incoming monomer could be created.

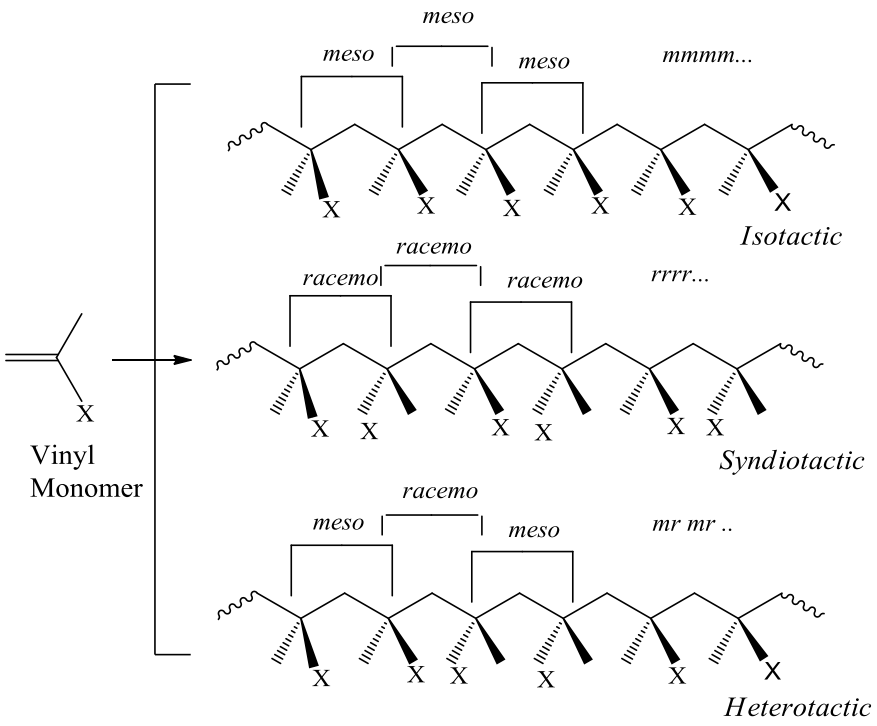

Figure 4.3. Tacticity of vinyl polymer.

In this study, the inherent tendency for the formation of syndiotactic and isotactic monomers has been modeled as displayed in Figure 4.4. Most aliphatic methacrylic polymers formed by a radical polymerization have an excess of syndiotactic over isotatic diads, probably due to the steric repulsion among the R groups of the incoming monomer

and growing radical species. Methacrylates with extremely bulky substituents, give highly isotactic polymers even via free radical solution polymerization.

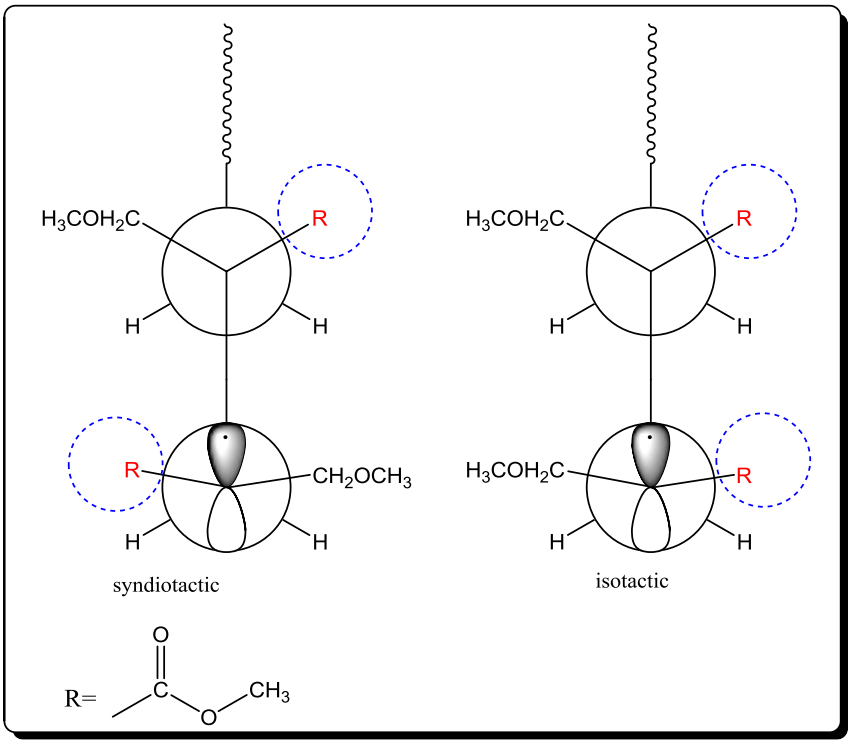

Figure 4.4. Stereoselective growth of the polymer chain.

Transition states for syndiotactic and isotactic propagation reactions for six monomers (**B1-B6**) with different tacticities have been located. The direction of attack of the radical to the monomer is of uttermost importance because it determines the tacticity of the polymer chain: isotactic, syndiotactic or atactic (Figure 4.4). There are four different geometries for the attack of a *syn* radical; and also four such possibilities for the *anti* radical. Therefore, for each transition structure eight different geometries have been considered.

4.3.1. Propagation of RHMA Monomers

In each case, the most stable monomers and radicals are used to calculate the free energy barriers of the propagation steps. Since the same reactants are used for each monomer, the activation energies depict the relative stabilities of the transition structures (Table 4.2).

4.3.1.1. Methyl 2-(butoxymethyl)acrylate (**B1**). The most stable transition state structures for **B1** are shown in Figure 4.5. **TS2-B1** and **TS1-B1** have lower free energy barriers than the others due to stronger long range stabilizing electrostatic interactions between the carbonyl oxygen and alkyl group hydrogens. In **TS2-B1**, both hydrogen-bonding interactions are better oriented (2.478 Å and 2.615 Å) as compared to the ones in **TS1-B1** (2.504 Å and 2.796 Å). Also notice that the critical distance between the radical center and the double bond of the monomer in **TS2-B1** (2.258 Å) is longer than in its counterparts in the other syndiotactic transition structures, **TS2-B1** is earlier and more stable than the others (Figure 4.5, Table 4.2).

4.3.1.2. Methyl 2-(acetoxymethyl)acrylate (**B2**). It is known that ester derivatives of α-hydroxymethacrylates –RHMA's– show fast photopolymerization rates both on their own and in the presence of acrylate or methacrylate crosslinkers [103]. The effect of the ester group on the free radical polymerization of α-hydroxymethacrylates has been investigated theoretically [104, 105] and the rate of free radical polymerization was shown to depend on the steric hindrance caused by the alkyl substituents. Furthermore, a series of alkyl α-hydroxymethacrylate derivatives with various secondary functionalities (ether, ester) were experimentally investigated and it has been found that ester functional monomers show slightly higher reactivity than ether functional monomers [106, 66, 67]. **TS1-B2** and **TS2-B2** have lowest barriers among the others, **TS1-B2** is better stabilized by long range interactions (2.466 Å, 2.503 Å and 2.519 Å) as compared to **TS2-B2** (2.513 Å, 2.633 Å and 3.001 Å) (Figure 4.6, Table 2).

4.3.1.3. 2-(Methoxycarbonyl)allyl benzoate (**B3**). Experimentally, among the monomers possessing the ester functionality, 2-(methoxycarbonyl)allyl benzoate-**B3** with the aromatic ester group capable of π-π interactions was found to polymerize twice as fast as the aliphatic ester monomer [88] and has been modelled in order to demonstrate the effect of the aromaticity on reactivity. Since B3LYP cannot detect dispersion effects, a further investigation of the transition structures with M06-2X has been carried out. Among the optimized transition structures of **B3** with M06-2X/6-31+G(d), **TS3-B3** and **TS2-B3** are found to be the most stable structures (Figure 4.7, Table 4.2) due to a higher number of

stabilizing long range hydrogen interactions (2.319 Å, 2.795 Å) and (2.546 Å, 2.850 Å) respectively.

Non-covalent interactions between aromatic systems have been discussed during the last two decades, by experimentalists [107-109] and theoreticians [110-112]. Benzene dimers have been considered computationally as prototypes for π-π interactions, in which the sandwich (face to face), parallel-displaced and T-shaped dimers were taken into account. Geerlings and coworkers [113] have analyzed the stacking of substituted benzene-pyridine complexes to study the interplay of stacking and hydrogen bonding. In particular, they showed that H-bond capacity of pyridine is closely related to the electron donating/withdrawing character of substituents on the benzene ring, while the stacking energy is less dependent on those properties. Hobza and coworkers have tested *ab initio* methods such as MP2 and CCSD(T) for benzene dimers and extensively applied them to interactions between DNA bases [114]. These authors showed that the deficiencies of MP2 can be suppressed in an empirical fashion by use of a medium-sized basis set with a more diffuse polarization function than normal, a method they termed MP2/6-31G(0.25)* [115, 116]. Truhlar *et al.* claim that M06 functionals give the best performance for π-π stacking interactions in conjugated polyenes [92]. In recent studies, the M06-2X functional has been found to be able to predict stacked and hydrogen-bonded structures of nucleobase and other dimers that are in good agreement with MP2 and CCSD(T)/MP2 reference data [117, 118].

In this study, B3LYP has been used to optimize the transition state structures because it is known to perform reasonably well in many cases, including hydrogen bonding [119]. However, because B3LYP cannot detect π-π interactions [120], all the structures have been re-modeled with M06-2X/6-31+G(d).

4.3.2. Kinetics of RHMA Monomers (B1-B3)

The critical forming bonds (M06-2X/6-31+G(d)) are almost equal in all cases. The rates of polymerization of RHMA monomers (Table 4.1) show that monomer **B3** (aromatic ester functionality) polymerizes faster than **B2** (ester functionality) and **B1** (ether

functionality) (Table 4.3). The rate enhancement of **B3** is due to its lower activation barrier as expected from the long range stabilizing C=O…H-C interactions between the two moieties in **TS3-B3** (the formal charges on O are -0.261, -0.303, -0.305, -0.272 and those on H are 0.137, 0.114, 0.120, 0.139 in Figure 4.8). The calculated values of k_p for **B1** and **B2** are close to each other as their experimental counterparts, with **B2** polymerizing slightly faster than **B1**. **TS1-B2** possesses three long range hydrogen stabilizing interactions as opposed to **TS2-B1** which has only two such stabilizing interactions. Syndiotactic polymer chains are slightly preferred for **B1**, **B2** and **B3** as observed experimentally for aliphatic methacrylic monomers [121]. The MPWB1K/6-311+G(3df,2p)//M06-2X/6-31+G(d) methodology predicts the rate acceleration of **B3** but not that of **B2**. The kinetics in benzene with M06-2X/6-31+G(d) (IEF-PCM) show the same qualitative trend as the results in vacuum.

Table 4.2. Relative Gibbs's free energies of activation ($\Delta \mathbf{G}^{\ddagger}$) (kcal/mol) at 298.15K of the transition states of **B1-B3** (M06-2X/6-31+G*).

	TS1-X	TS2-X	TS3-X	TS4-X	TS5-X	TS6-X	TS7-X	TS8-X
X=B1	12.80	**12.69**	12.86	16.11	13.29	14.10	13.99	15.95
X=B2	**12.66**	13.80	14.46	16.85	16.31	17.68	16.81	18.41
X=B3	12.17	11.17	**10.69**	11.23	12.92	15.93	14.20	16.86

Table 4.3. Propagation rate constants, k_p (L/mol.s) for RHMA (**B1-B3**) monomers at T=298.15 K in vacuum and in benzene (italics). (Relative k_p values are given in parenthesis).

Method	**B1**	**B2**	**B3**
M06-2X/6-31+G(d)	$7.63x10^{+4}$ (1)	$8.12x10^{+4}$(1.06)	$225x10^{+4}$ (29.49)
M06-2X/6-31+G(d)-IEFPCM-opt	*$2.70x10^{+5}$ (1)*	*$8.64x10^{+5}$(3.20)*	*$70.8x10^{+5}$ (26.24)*
MPWB1K/6-311+G(3df,2p)//M06-2X/6-31+G(d)	$1.36x10^{+1}$(1)	$1.18x10^{0}$(0.087)	$3.25x10^{+1}$(2.39)
Experimental k_p	298*(1)	350*(1.17)	990* (3.32)

*Ref88

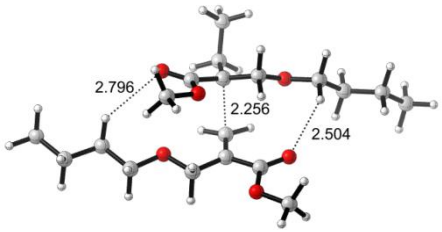

TS1-B1 (mc-rs-syn)

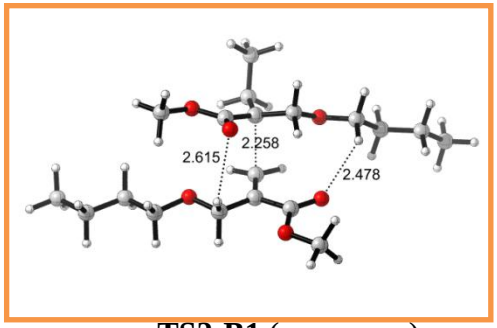

TS2-B1 (mc-ra-syn)

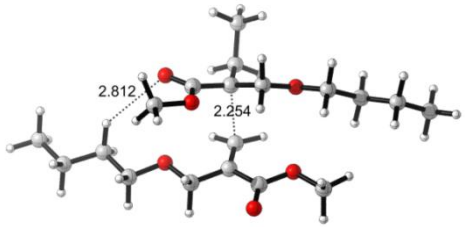

TS3-B1 (mt-rs-syn)

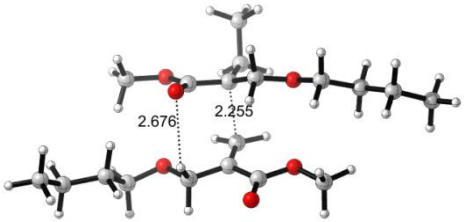

TS4-B1 (mt-ra-syn**)**

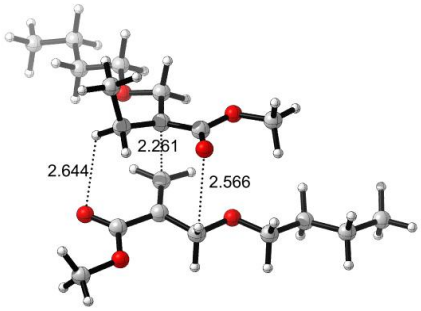

TS5-B1 (mc-rs-iso)

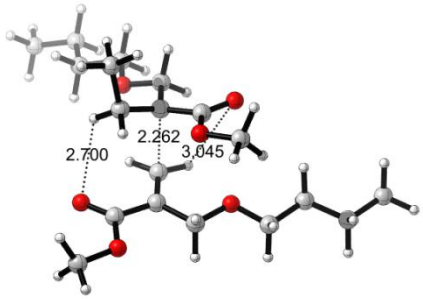

TS6-B1 (mc-ra-iso)

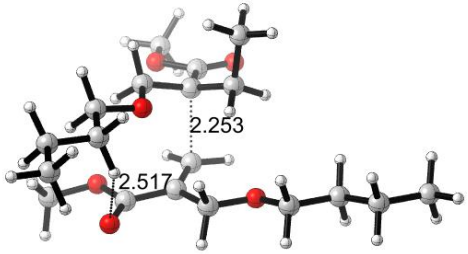

TS7-B1 (mt-rs-iso)

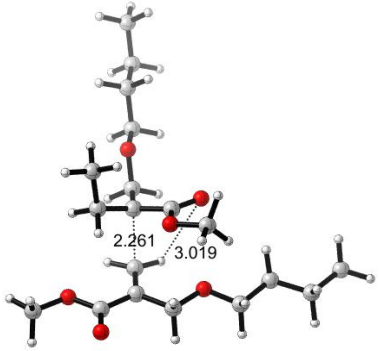

TS8-B1 (mt-ra-iso)

Figure 4.5. Transition state structures of methyl 2-(butoxymethyl)acrylate-**B1** (M06-2X/6-31+G(d)). Structures in the first row are syndiotactic (syn); structures in the second row are isotactic (iso). (mc: *cis* monomer, mt: *trans* monomer, rs: *syn* radical, ra:*anti* radical, syn: syndiotactic, iso: isotactic).

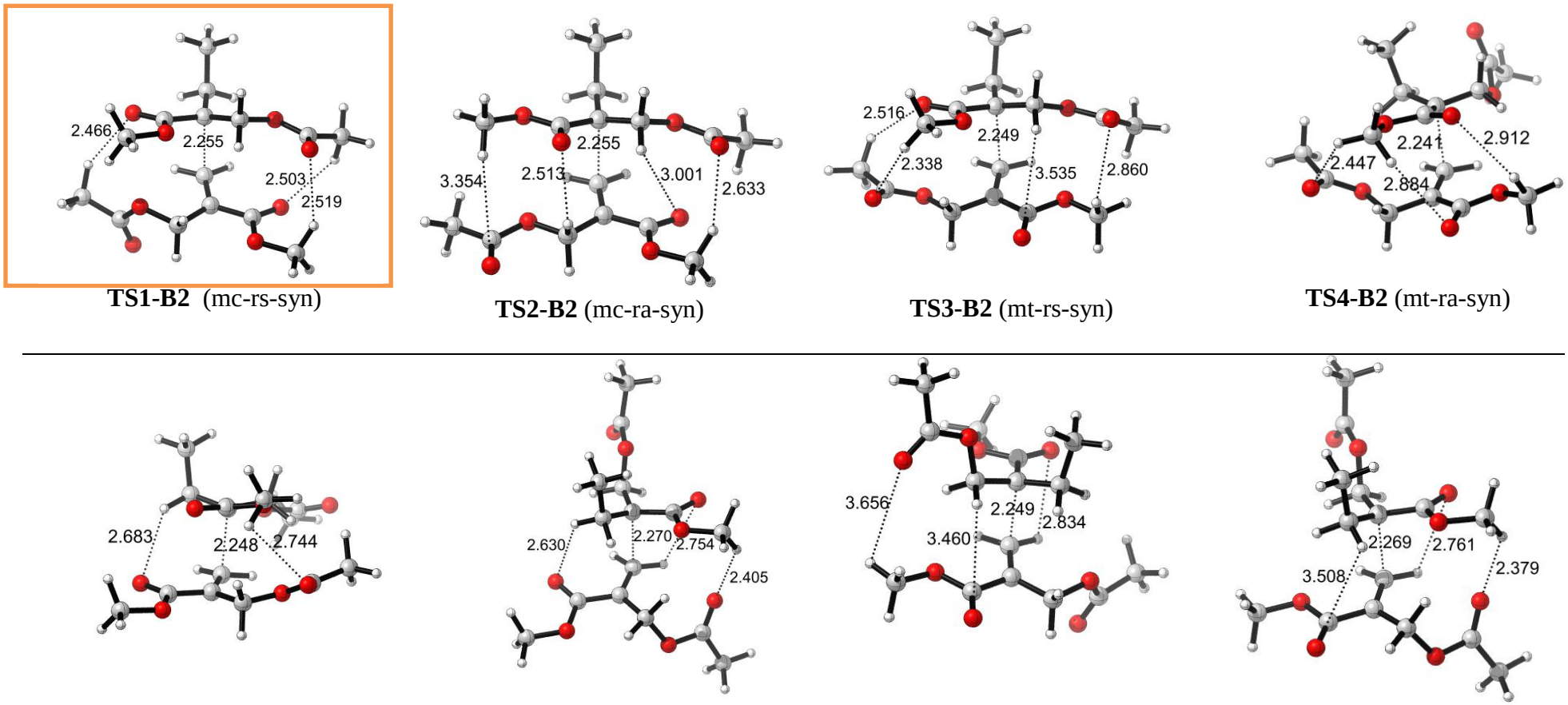

TS1-B2 (mc-rs-syn) **TS2-B2** (mc-ra-syn) **TS3-B2** (mt-rs-syn) **TS4-B2** (mt-ra-syn)

TS5-B2 (mc-rs-iso**)** **TS6-B2** (mc-ra-iso) **TS7-B2** (mt-rs-iso) **TS8-B2.** (mt-ra-iso)

Figure 4.6. Transition state structures of methyl 2-(acetoxymethyl)acrylate-**B2** (M06-2X/6-31+G(d)). Structures in the first row are syndiotactic (syn); structures in the second row are isotactic (iso). (mc: *cis* monomer, mt: *trans* monomer, rs: *syn* radical, ra:*anti* radical, syn: syndiotactic, iso: isotactic).

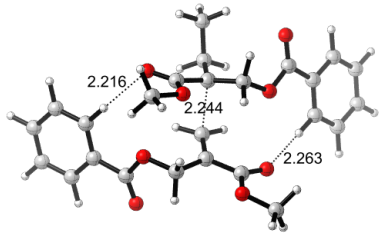

TS1-B3 (mc-rs-syn**)**

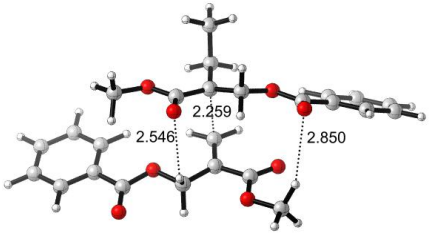

TS2-B3 (mc-ra-syn**)**

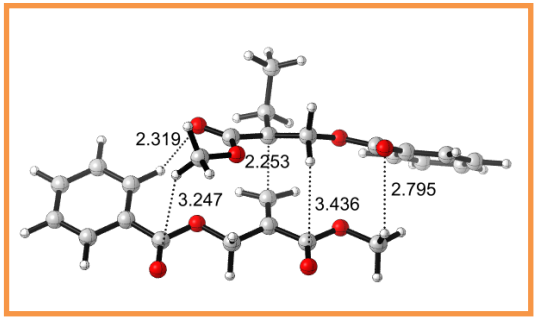

TS3-B3 (mt-rs-syn**)**

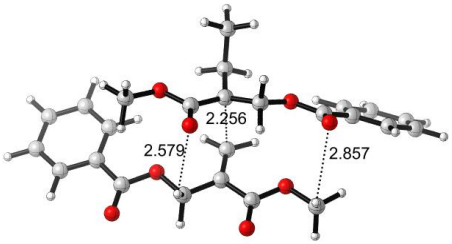

TS4-B3 (mt-rt-syn)

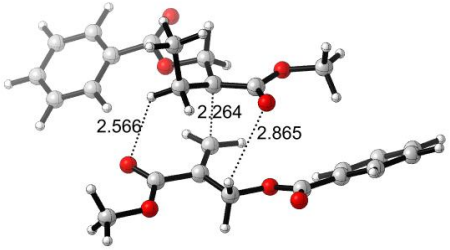

TS5-B3 (mc-rs-iso)

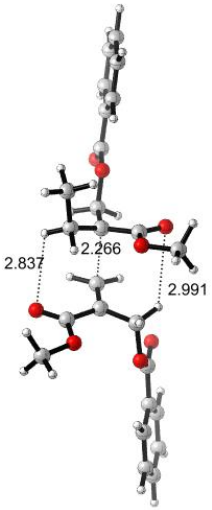

TS6-B3 (mc-ra-iso)

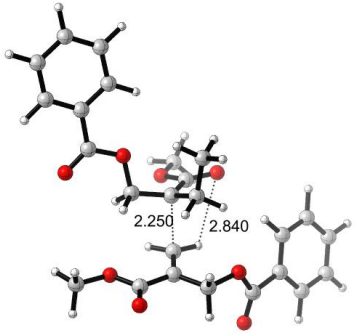

TS7-B3 (mt-rs-iso)

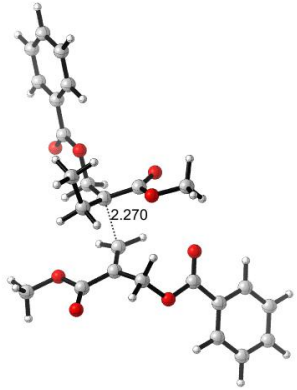

TS8-B3 (mt-ra-iso)

Figure 4.7. Transition state structures of 2-(methoxycarbonyl)allyl benzoate–**B3** (M06-2X/6-31+G(d)). Structures in the first row are syndiotactic (syn); structures in the second row are isotactic (iso). (mc: *cis* monomer, mt: *trans* monomer, rs: *syn* radical, ra:*anti* radical, syn: syndiotactic, iso: isotactic).

TS2-B1 (mc-ra-syn) (12.69)	
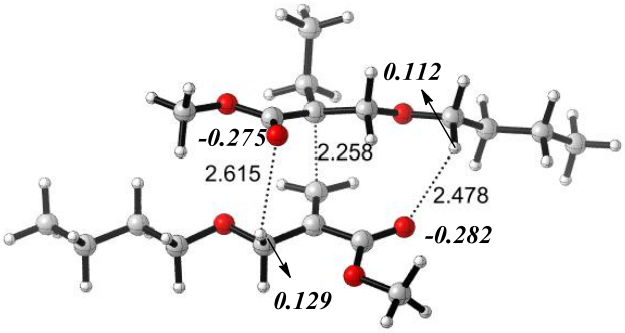	
TS1-B2 (mc-rs-syn) (12.66)	**TS3-B3** (mt-rs-syn) (10.69)
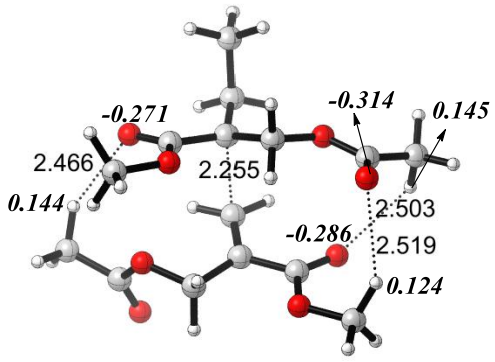	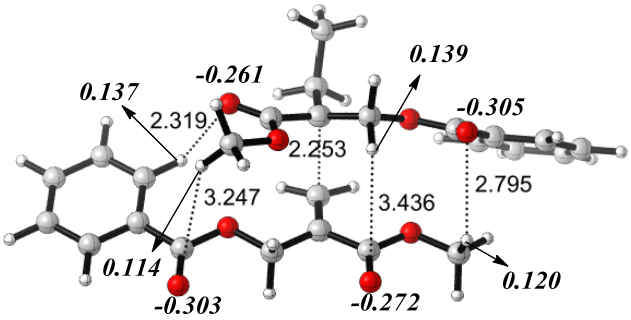

Gibbs free energies of activation are given in parentheses (kcal/mol).
NBO charges are displayed in italics and bold.

Figure 4.8. Most stable transition states of RHMA monomers (**B1-B3)** (M06-2X/6-31+G*).

4.3.3. Propagation of Acrylates

For acrylate derivatives, the most stable monomers and radicals are used to calculate the free energy barriers of the propagation steps based on the transition structures located with M06-2X/6-31+G(d) (Table 4.4).

4.3.3.1. Hexyl acrylate (**B4**). In the transition structures of **B4**, the backbone of hexyl acrylate is extended and the radical approaches the monomer in a way that minimizes steric interactions. Among all possible transition states, **TS6-B4** has the lowest barrier because of strongest C=O…H-C interactions (2.462 Å) (Figure 4.9, Table 4.4)

4.3.3.2. Benzyl acrylate (**B5**). The transition structures **TS7-B5**, **TS5-B5** and **TS2-B5** are stabilized by long-range C=O…H-C electrostatic interactions; furthermore π-π interactions stabilize **TS7-B5** which has lower activation barrier than the others. (Figure 4.10, Table 4.4).

4.3.3.3. Phenyl acrylate (**B6**). **TS6-B6** and **TS1-B6** have lower barriers than the other transition structures. **TS6-6b** is better stabilized by π-π interactions and long range electrostatic interactions (2.166 Å and 2.365 Å) as compared to **TS1-B6** (2.724 Å, 3.437 Å) (Figure 4.11, Table 4.4).

4.3.4. Kinetics of Acrylate Monomers (B4-B6)

The most stable transition state structures (**TS6-B4, TS7-B5** and **TS6-B6)** and their activation barriers are displayed in Figure 4.12. While **TS6-B4** has greater negative charge on the carbonyl oxygen in (-0.269 and -0.294) as compared to **TS7-B5** (-0.251), **TS7-B5** has the π-π stacking (parallel-displaced type interaction with distance of 4.55 Å from center to center). Among the acrylate monomers, **B6** has the highest reactivity, which is consistent with experimental findings (table 5) [81]. **TS6-B6** is mainly stabilized by close and strong C=O…H-Φ interactions as well as by π-π stacking (parallel-displaced type interaction with distance of 5.30 Å from center to center). The aromatic groups are held together by C=O…H-Φ interactions (2.166 Å and 2.365 Å). **TS6-B6** has greater negative charge accumulated on the carbonyl oxygens (-0.257 and -0.279) than **TS7-B5 (**-0.251).

Table 4.4. Relative Gibbs's free energies of activation ($\Delta \mathbf{G}^{\ddagger}$) (kcal/mol) at 298.15K of the transition states of **B4-B6** (M06-2X/6-31+G*).

	TS1-X	TS2-X	TS3-X	TS4-X	TS5-X	TS6-X	TS7-X	TS8-X
X=B4	15.50	16.70	---	15.25	---	**14.88**	15.19	15.93
X=B5	---	14.63	---	15.0	14.59	---	**14.56**	---
X=B6	14.34	15.01	15.71	18.10	14.95	**13.15**	14.93	17.35

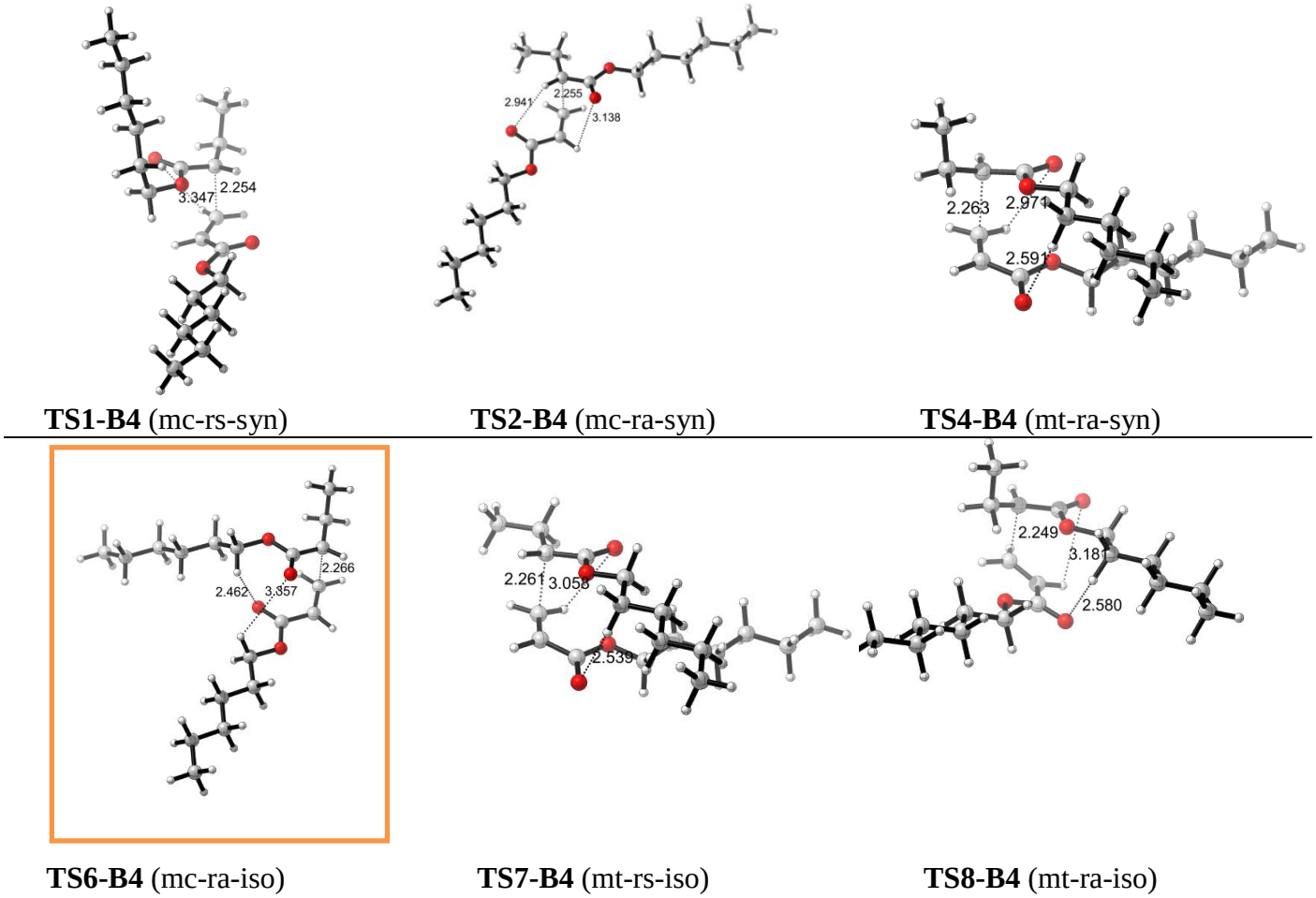

TS1-B4 (mc-rs-syn) **TS2-B4** (mc-ra-syn) **TS4-B4** (mt-ra-syn)

TS6-B4 (mc-ra-iso) **TS7-B4** (mt-rs-iso) **TS8-B4** (mt-ra-iso)

Figure 4.9. Transition state structures of hexyl acrylate-**B4** (M06-2X/6-31+G(d)). Structures in the first row are syndiotactic (syn); structures in the second row are isotactic (iso). (mc: *cis* monomer, mt: *trans* monomer, rs: *syn* radical, ra:*anti* radical, syn: syndiotactic, iso: isotactic).

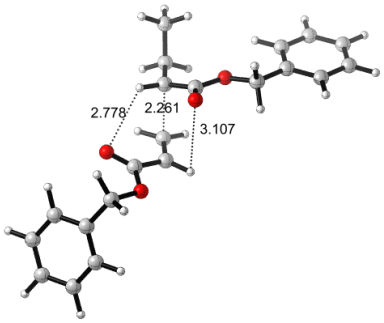

TS2-B5 (mc-ra-syn)

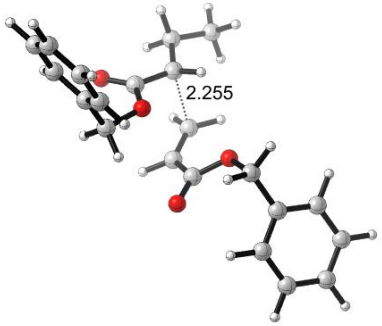

TS4-B5 (mt-ra-syn)

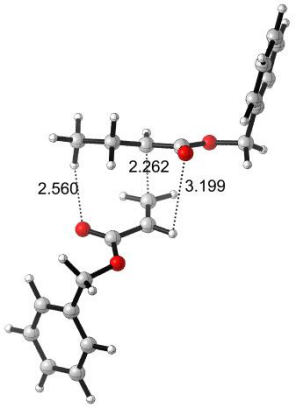

TS5-B5 (mc-rs-iso)

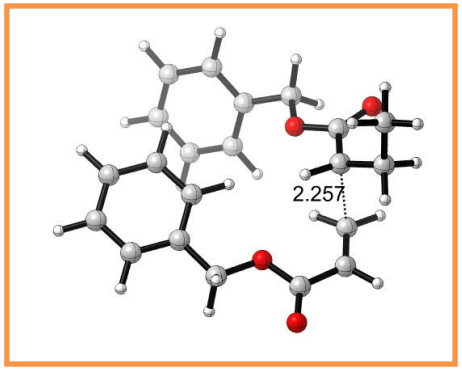

TS7-B5 (mt-rs-iso)

Figure 4.10. Transition state structures of benzyl acrylate-**B5** (M06-2X/6-31+G(d)). Structures in the first row are syndiotactic (syn); structures in the second row are isotactic (iso). (mc: *cis* monomer, mt: *trans* monomer, rs: *syn* radical, ra:*anti* radical, syn: syndiotactic, iso: isotactic).

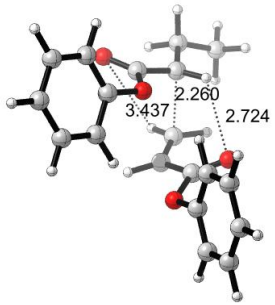

TS1-B6 (mc-rs-syn)

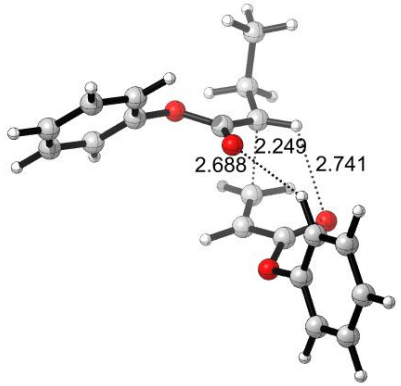

TS2-B6 (mc-ra-syn)

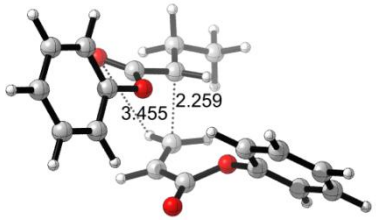

TS3-B6 (mt-rs-syn)

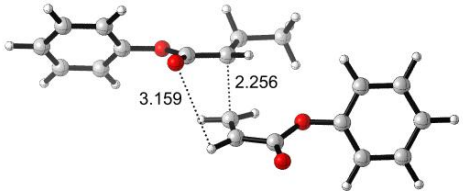

TS4-B6 (mt-ra-syn)

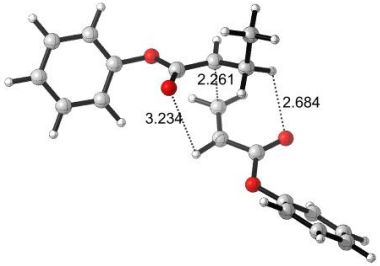

TS5-B6 (mc-rs-iso)

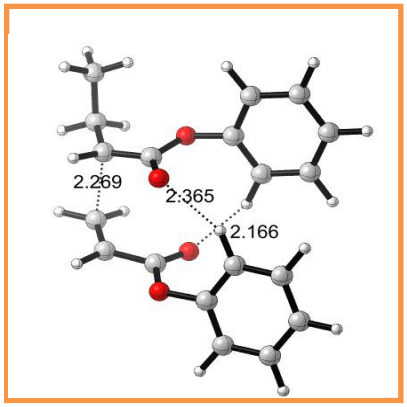

TS6-B6 (mc-ra-iso)

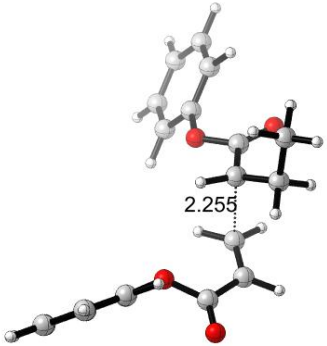

TS7-B6 (mt-rs-iso)

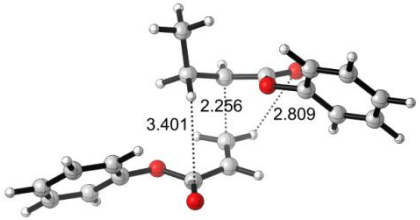

TS8-B6 (mt-ra-iso)

Figure 4.11. Transition state structures of phenyl acrylate-**B6** (M06-2X/6-31+G(d)). Structures in the first row are syndiotactic (syn); structures in the second row are isotactic (iso). (mc: *cis* monomer, mt: *trans* monomer, rs: *syn* radical, ra:*anti* radical, syn: syndiotactic, iso: isotactic).

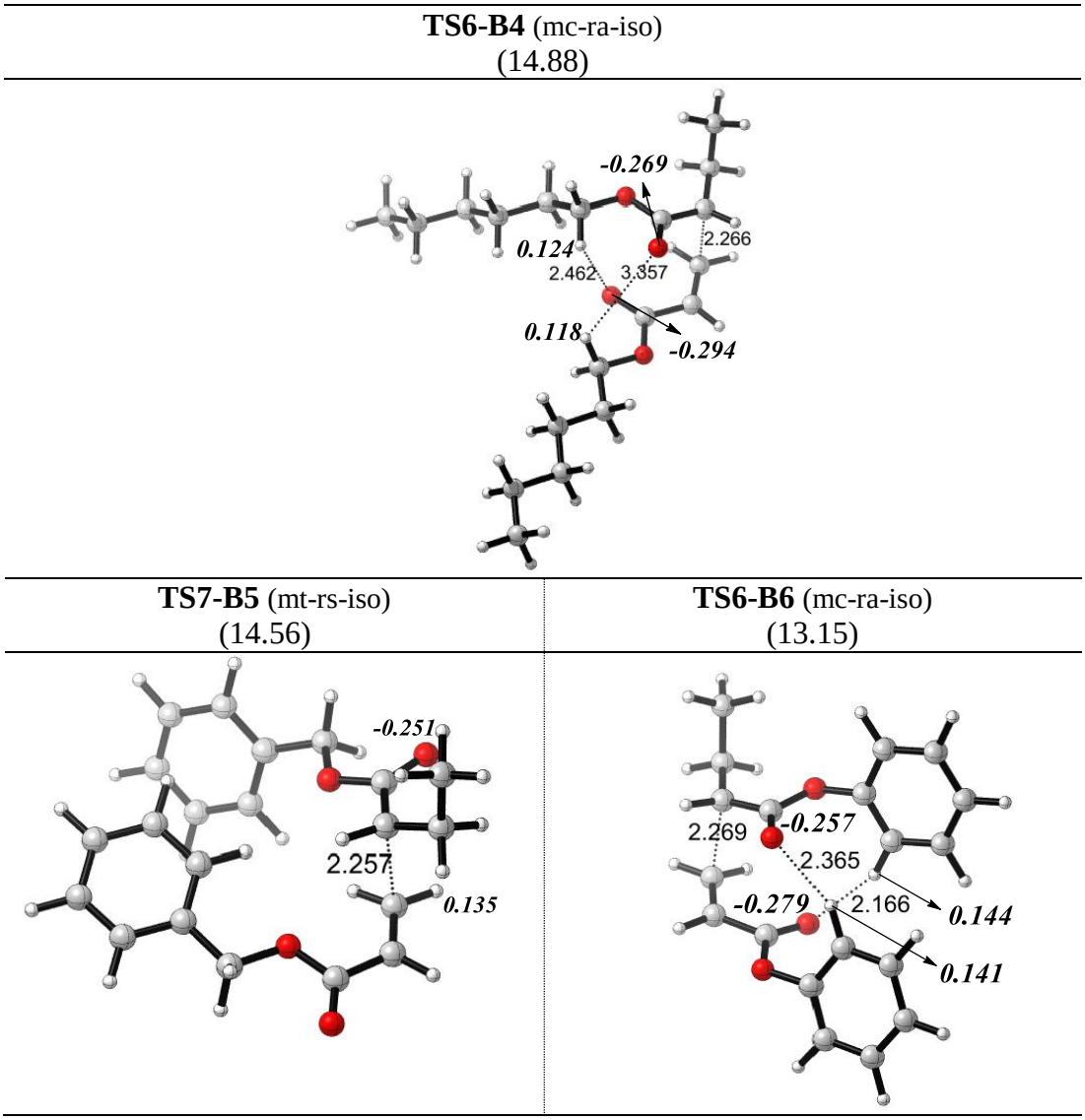

Gibbs free energies of activation are given in parentheses (kcal/mol).
NBO charges are displayed in italics and bold.

Figure 4.12. Most stable transition structures of acrylate monomers (**B4-B6**) (M06-2X/6-31+G*).

Table 4.5. Calculated propagation rate constant k_p (L/mol.s) for acrylate (**B4-B6**) monomers at T=298.15 K. (Relative k_p values are given in parenthesis)

Method	**B4**	**B5**	**B6**
M06-2X/6-31+G(d)	$1.92x10^{+3}$	$3.30x10^{+3}$	$35.5x10^{+3}$
MPWB1K/6-311+G(3df,2p)//M06-2X/6-31+G(d)	$5.22x10^{0}$	$3.71x10^{0}$	$3.29x10^{+1}$
Experimental rates of polymerization	$2.00x10^{-2*}$	$9.00x10^{-2*}$	$2.30x10^{-1*}$

*****Values are taken from Ref 81.

4.4. Conclusions

In this study, the free radical polymerization behavior of a series of RHMA and acrylate monomers has been modeled in order to to elucidate the role of the pendant groups on their polymerizabilities. The M06-2X/6-31+G(d) methodology reproduces the experimental trend qualitatively. Reaction barriers are lowered by the presence of stabilizing C=O…H-C nonbonded interactions in the case of **B1**, **B2** and **B3**. A similar picture emerges for acrylate monomers where the transition structures for **B4** are stabilized by C=O…H-C interactions and those of **B5**, **B6** are stabilized by C=O…H-Φ as well as by weak π-π interactions. Although benzyl acrylate (**B5**) and phenyl acrylate (**B6**) both have an aromatic group, they differ in their polymerization behavior because the transition structure of **B6** has greater negative charge on the carbonyl oxygen and has stronger C=O…H-Φ interactions. Overall the dimeric models used earlier to understand the effect of pendant groups (linear vs cyclic) on the polimerizability of acrylate derivatives [128], reproduce qualitatively the experimental trend in this study as well. The methodology used in this study can serve to understand the role of substituents in the free radical polymerization of RHMA derivatives and acrylates prior to synthesis.

5. A COMPUTATIONAL APPROACH TO THE FREE RADICAL POLYMERIZATION KINETICS OF RHMA MONOMERS: A STRUCTURE-REACTIVITY RELATIONSHIP

5.1. Introduction

Correlation between structure and reactivity is a fundamental problem in chemistry; successful correlations can aid our understanding and can allow us to predict the outcome of chemical reactions and rationally design optimal reagents. In the late forties Alfrey and Price [129] have developed an empirical model, the *Q-e* scheme for interpreting and predicting the reactivity of a vinylic monomer in copolymerizations. According to the *Q-e* model, each reactant is given a parameter, *Q* describes the reactivity of the monomer and *P* that of the radical. A second parameter e was used for the monomer or free radical related to its polar properties. The aim of the *Q-e* scheme, is to predict the relative reactivity in free radical copolymerizations without experimental determination of kinetic rate constants: it is based on a large database of kinetic rate constants. In the empirical equation developed by Alfrey and Price [129] for describing quantitative relationships for monomer activity in copolymerizations as showed in Equation 5.1. Q_2 describes the reactivity of monomer M2, P_1 denotes the general reactivity of radical M1, e_1 measures the permanent electric charge of M1, e_2 takes into account the permanent electric charge on M2 .

$$k_{12} = P_1 Q_2 \exp(-e_1 e_2) \tag{5.1}$$

Zhan and Dixon have found relationships for correlations of the *Q-e* parameters with DFT calculated electronegativities and reaction free energies reflecting the energetic and polar properties needed for the *Q-e* parameter development [130]. Later, density functional theory (DFT) based on quantitative structure-activity relationships (QSAR) of the reactivity parameters Q and e of the monomers has been used; stepwise multiple linear regression analysis (MLRA) and artificial neural networks (ANN) were adapted to generate models [131]. Furthermore parameters for the prediction of reactivity in free-radical copolymerizations have been developed and calculations were carried out for

radical structures; the multiple regression technique was used to select the descriptors as inputs for the artificial neural network (ANN). The latter study has shown that calculating quantum chemical descriptors from radicals to develop ANN models and predicting ln *Q* and *e* values was possible [132]. A structure-reactivity correlation was also presented a few years ago when the rate constants of dissociation of various alkoxyamines were correlated with three empirical factors [133]. Recently, high-level ab initio calculations have been used by Coote *et al.* to construct linear free-energy relationships describing the kinetics and thermodynamics of the combination and dissociation reactions between alkyl radicals and nitroxides [134]. A linear free energy relationship for modeling structure-reactivity trends in controlled radical polymerization was also proposed by the same group [135]. Morrill *et al*. have developed a quantitative structure-activity relationship for explanatory modeling of fast reacting methacrylate monomers bearing novel functionality [136]. Overall, the development of reliable quantitative structure-activity relationship models for the prediction of the reactivity of monomers is of real interest.

Alkyl α–(hydroxymethy1)acrylate monomers offer great versatility for functionalization and polymer formation [62, 63, 137, 138]. Recently, some of us have synthesized a series of novel alkyl α-hydroxymethacrylate (RHMA) derivatives with various secondary functionalities (ether, ester, carbonate and carbamate) and terminal groups (alkyl, cyano, oxetane, cyclic carbonate, morpholine) to investigate the effect of intermolecular interactions, H-bonding, π-π interactions and dipole moment on monomer reactivity. The polymerization rates of the synthesized monomers were determined by using photo-differential scanning calorimetry [106]. In this study, density functional theory (DFT) calculations are carried out to model the alkyl α-hydroxymethacrylate (RHMA) monomers synthesized earlier. The calculated quantum chemical descriptors have been used to construct a quantitative structure-activity relationships (QSAR) in order to predict the reactivity of these monomers. For this purpose, a correlation between the chosen descriptors and the experimentally measured maximum rates of photopolymerization (R_p) is proposed by making use of the multiple regression analysis (MRA).

The general structure of RHMA monomers used in this study is depicted in Figure 5.1. The RHMA monomers considered have ethyl or tertiary butyl as R_1; a secondary

functionality such as ether, ester, carbamate, cyclic carbonate as R_2 and a terminal functional group as R_3.

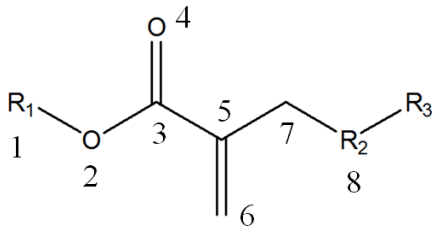

R_1: ethyl, t-butyl

R_2: secondary functionality (ether, ester, carbonate, carbamate)

R_3: terminal functional group (cyano, ether, morpholine, carbonate, cyclic carbonate, oxatane)

Figure 5.1. General structure of RHMA monomers.

The formation of a monomeric radical is modeled as depicted in Figure 5.2; the methyl radical adds to the ethylenic double bond of the monomer to yield a monomeric radical. The radical formed can attack the double bond of another monomer and the polymerization continues via propagation.

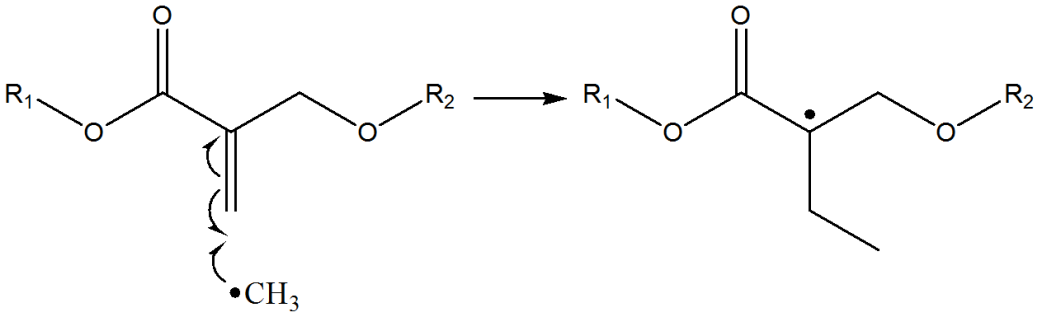

Figure 5.2. Model for the formation of the monomeric radical.

5.2. Methodology

5.2.1. Quantum Chemical Modeling

The conformational study of the monomers displayed in Table 5.1 and their monomeric radicals derived from them has been carried out. The geometries of all the monomers and their corresponding radicals are optimized with the B3LYP/6-31+G(d) methodology at 298.15 K in vacuum. All the conformations were screened systematically to find structures corresponding to the global minima on the potential energy surface (PES). Frequency calculations were run to characterize the minimum energy structures with positive vibrational frequencies.

Table 5.1. RHMA monomers modeled in this study.

Structure-Name
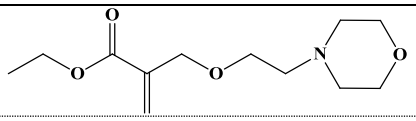 ethyl 2-((2-morpholinoethoxy)methyl)acrylate (**A1**)
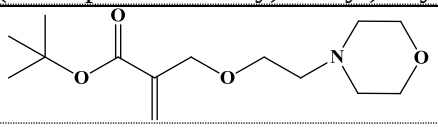 tert-butyl 2-((2-morpholinoethoxy)methyl)acrylate (**A2**)
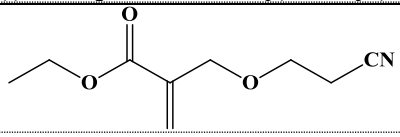 ethyl 2-((2-cyanoethoxy)methyl)acrylate (**A3**)
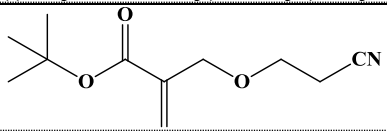 tert-butyl 2-((2-cyanoethoxy)methyl)acrylate (**A4**)
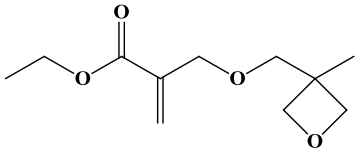 ethyl 2-(((3-methyloxetan-3-yl) methoxy)methyl)acrylate (**A5**)

Table 5.1. RHMA monomers modeled in this study (cont.).

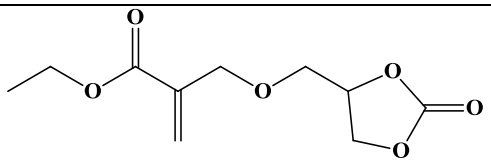 ethyl 2-(((2-oxo-1,3-dioxolan-4-yl)methoxy)methyl)acrylate (**A6**)
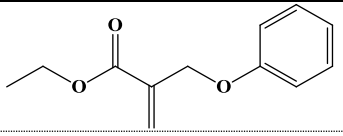 ethyl 2-(phenoxymethyl)acrylate (**A7**)
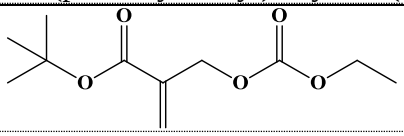 tert-butyl 2-(((ethoxycarbonyl)oxy)methyl)acrylate (**A9**)
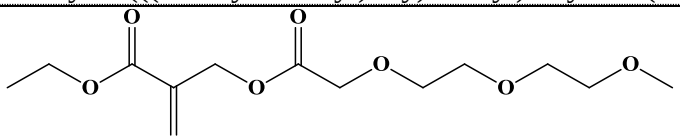 ethyl 2-(3-oxo-2,5,8,11-tetraoxadodecyl)acrylate (**A10**)
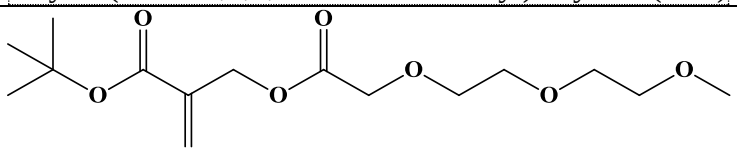 tert-butyl 2-(3-oxo-2,5,8,11-tetraoxadodecyl)acrylate (**A11**)
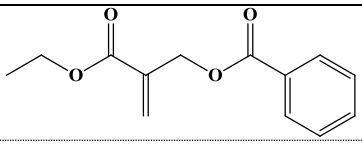 2-(ethoxycarbonyl)allylbenzoate (**A12**)
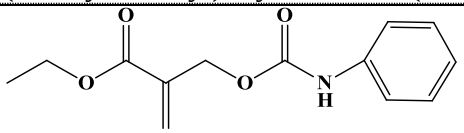 ethyl 2-(((phenylcarbamoyl)oxy)methyl)acrylate (**A13**)
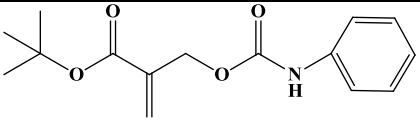 tert-butyl 2-(((phenylcarbamoyl)oxy)methyl)acrylate (**A14**)
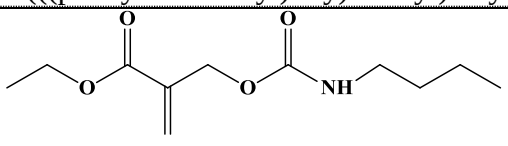 ethyl 3-((butylcarbamoyl)oxy)propanoate (**A15**)

Table 5.1. RHMA monomers modeled in this study (cont.).

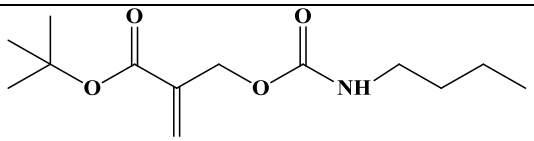 tert-butyl 3-((butylcarbamoyl)oxy)propanoate (**A16**)
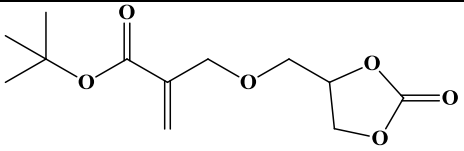 tert-butyl 2-(((2-oxo-1,3-dioxolan-4-yl)methoxy) methyl)acrylate (**C1**)
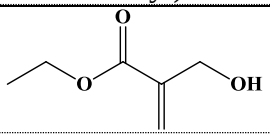 ethyl 2-(hydroxymethyl)acrylate (**C2**)
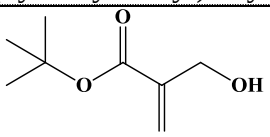 tert-butyl 2-(hydroxymethyl)acrylate (**C3**)
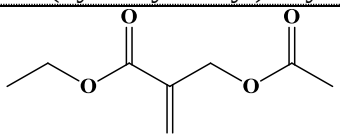 ethyl 2-(acetoxymethyl)acrylate (**C4**)

5.2.2. Quantitative Descriptors and Regression Analysis

In order to derive a relationship between the polymerization kinetics and the descriptors of the monomers of interest, a multiple regression analysis (MRA) was carried out [131, 133, 134]. The ultimate goal is to establish a correlation between the chosen descriptors and the experimentally known maximum rates of photopolymerization (R_p). The correlation between experimental and computational results is expected to be used for the prediction of the free radical polymerization kinetics of novel RHMA monomers prior to synthesis. The molecular descriptors utilized in this study are the Mulliken and APT charges of the backbone C atoms in proximity of the reactive center, the total dipole moment (μ), the energy of the highest occupied molecular orbital (E_{HOMO}), the energy of the lowest unoccupied molecular orbital (E_{LUMO}), the isotropic polarizability (α), the

Mulliken atomic spin density (ρ_s) of the atoms near the reactive center, the bond distances and the atom-atom overlap weighed NAO bond orders (C1-O2, O2-C3, C3-O4, C5-C6, C5-C7 and C7-O8 in Figure 5.1), the ionization energy (IE), the electron affinity (EA), the resonance parameter (Res) of the RHMA monomers and the corresponding radicals. These calculations were all carried out on the optimized geometries of the monomers and the radicals with the B3LYP/6-31+G(d) methodology. The ionization energy (IE) was calculated as the negative of the energy of highest occupied molecular orbital, $-E_{HOMO}$; the electron affinity (EA) is the energy of the lowest unoccupied molecular orbital, E_{LUMO}. The resonance stabilization parameter (Res) is the standart radical stabilization energy for the radical and was calculated as $1/(E_{LUMO}-E_{HOMO})$ for the monomeric radicals which were generated by the attack of the methyl radical to the monomer [135]. The calculation of bond orders was carried out with the NBO [96] method and the resulting atom-atom overlap weighed NAO bond order values were considered [136].

The multiple regression analysis (MRA) was performed using the Data Analysis Tools of Microsoft Excel 2010 (Microsoft, Redmond, USA). Determination of the best-fit parameters and the associated test statistics for the proposed equations was carried using the multiple linear regression techniques integrated in the Microsoft Excel software.

$$R_p = \boldsymbol{\beta_1} + \boldsymbol{\beta_2}\text{desc}_1 + \boldsymbol{\beta_3}\text{desc}_2 + \boldsymbol{\beta_4}\text{desc}_3 + \ldots \quad (5.2)$$

The 16 monomers displayed in Table 5.1 were used in the MRA to determine the descriptors that would show the best correlation. The best fit equation has been generated with the quantitative descriptors to construct the best correlation with a set of 16 observations (the training set). The data for 3 test monomers (i.e. **A4**, **A6, C4**, and **A4-R**, **A6-R**, **C4-R**) have been used to test the prediction potential of Equation 5.4. Finally the test monomers have also been included in data set and an improved equation for 19 compounds was generated.

The statistical quality of the descriptors in each equation is analyzed in terms of their standart error, t-test and p-values. Depending on these parameters and on the Principle of Parsimony, decisions for a descriptor to be dropped from the equation or to be added to the

model have been made [139]. The t-test shows how different the coefficients are from 0 and indicates the importance of a descriptor in the equation. The P-value of each descriptor tests the hypothesis that $\beta_i = 0$. If the P-value is not small enough to reject the hypothesis $\beta_i = 0$, the linear model is not useful for predicting the dependent variable. To reject the hypothesis that each coefficient is zero, the P-value should be lower than 0.05. The statistical quality of the proposed models was evaluated based on their R^2, the square of correlation coefficient adjusted R^2 (R^2_{adj}), F and significance F values. R^2_{adj} is calculated almost similarly as R^2, except that it has a factor of degrees of freedom ratio, to eliminate the bias of R^2 that comes from the number of observations and the number of descriptors. F is the mean square of regression divided by the mean square of error. The significance F is the probability that the predicted equation does not explain the corrolation, but the fit is purely by chance. The significance F is supposed to be lower than 0.1 to have a reliable correlation [139].

5.3. Results and Discussion

5.3.1. Conformational Analysis

The most stable conformers for monomers **A1**-**A3**, **A5**, **A7**, **A9**-**A16**, **C1**-**C3** and their corresponding radicals are displayed in Figure 5.3 and Figure 5.4. Three test RHMA monomers (**A4**, **A6**, **C4**) and the corresponding radicals are shown in Figure 5.5. The structures corresponding to global minima for the monomers have a planar zigzag backbone which is stabilized by resonance. The most stable conformers of monomers **A1**-**A3**, **A5**, **A7**, **A9**-**A16**, **C1**-**C3** were found to have the carbonyl group and the ethylenic double bond trans to each other; this relative position of the double bonds reduces the overall dipole moment increasing the stability of the molecule. In the case of radicals the anti orientation of the ethyl group with the carbonyl oxygen was preferred most of the time, except for **A9**-**R**, **A10**-**R** , **A11**-**R**, **A13**-**R**, , **A15**-**R**, **A16**-**R**, which have an ester group at R_2. In this way, these latter radicals which have the ethyl and carbonyl groups *syn* to each other, have the two carbonyl groups *anti* to each other minimizing the dipole moments of these structures. Note that while the monomers are quasi planar; the planarity of the radical is destroyed by the addition of the CH_3 radical to the ethylenic double bond, the methyl group of the monomeric radical is found to be always perpendicular to the backbone in the 3D structures of the radicals.

Monomer	Monomer
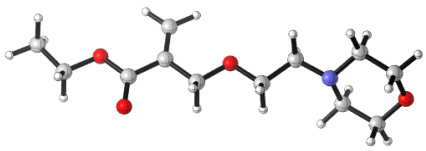 A1	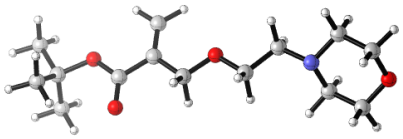 A2
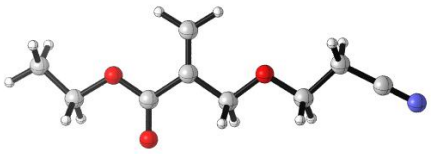 A3	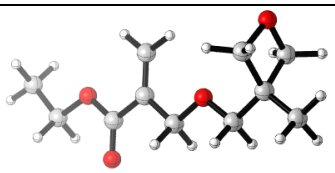 A5
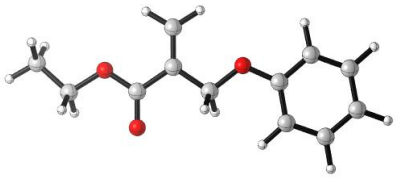 A7	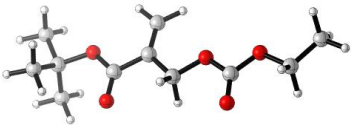 A9
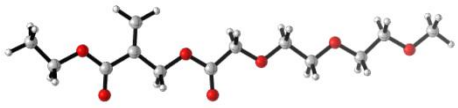 A10	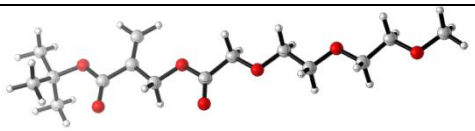 A11
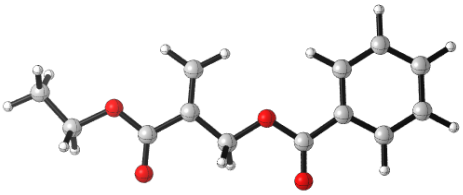 A12	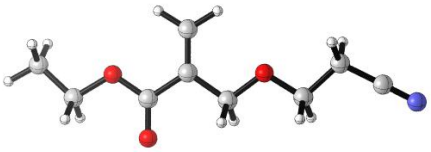 A3
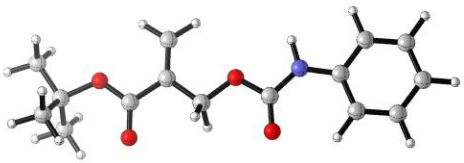 A14	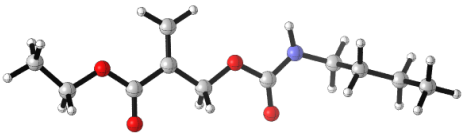 A15
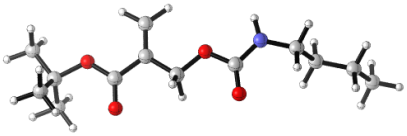 A16	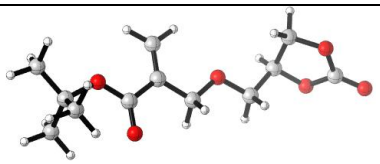 C1
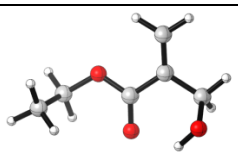 C2	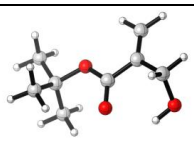 C3

Figure 5.3. 3D structures of the most stable conformers of RHMA monomers.

Radical	Radical
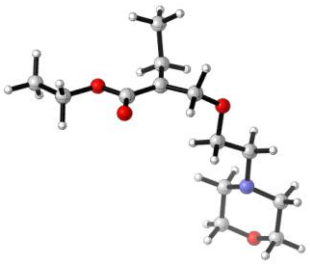 A1-R	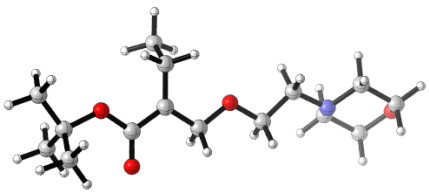 A2-R
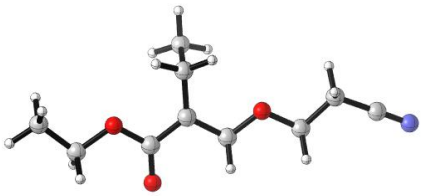 A3-R	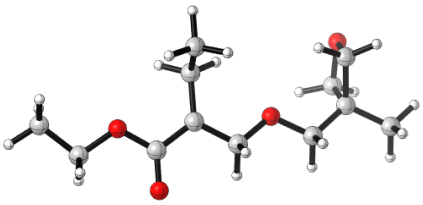 A5-R
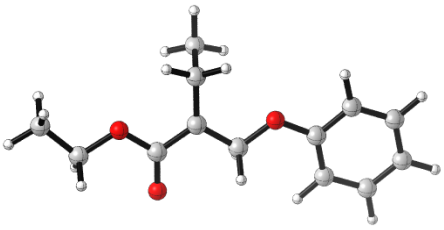 A7-R	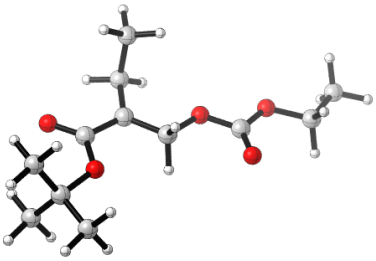 A9-R
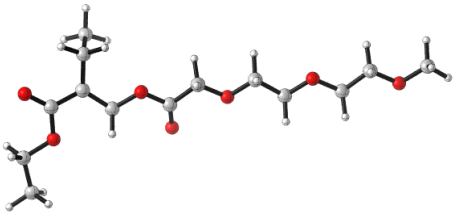 A10-R	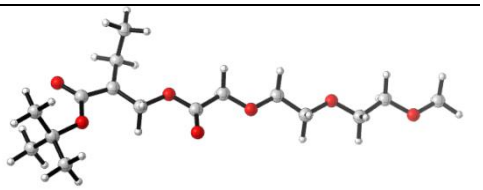 A11-R
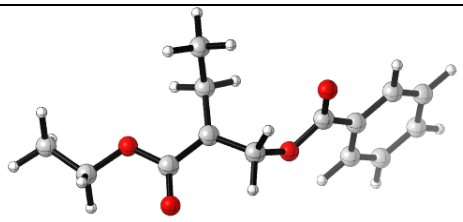 A12-R	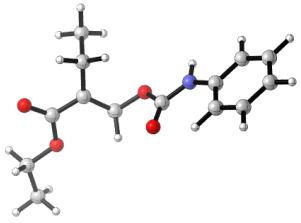 A13-R
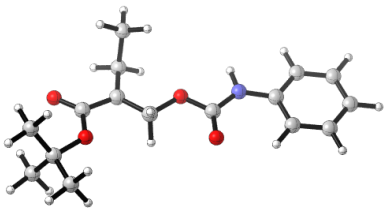 A14-R	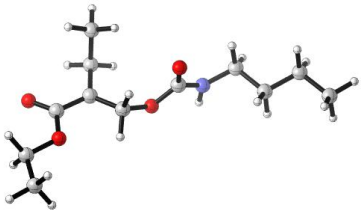 A15-R

Figure 5.4. 3D structures of the most stable conformers of RHMA radicals.

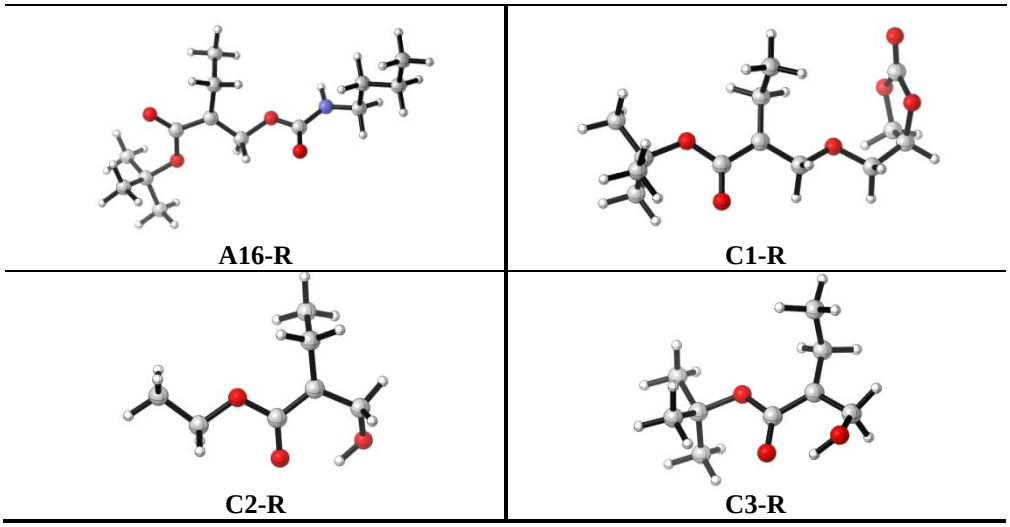

Figure 5.4. 3D structures of the most stable conformers of RHMA radicals (cont.).

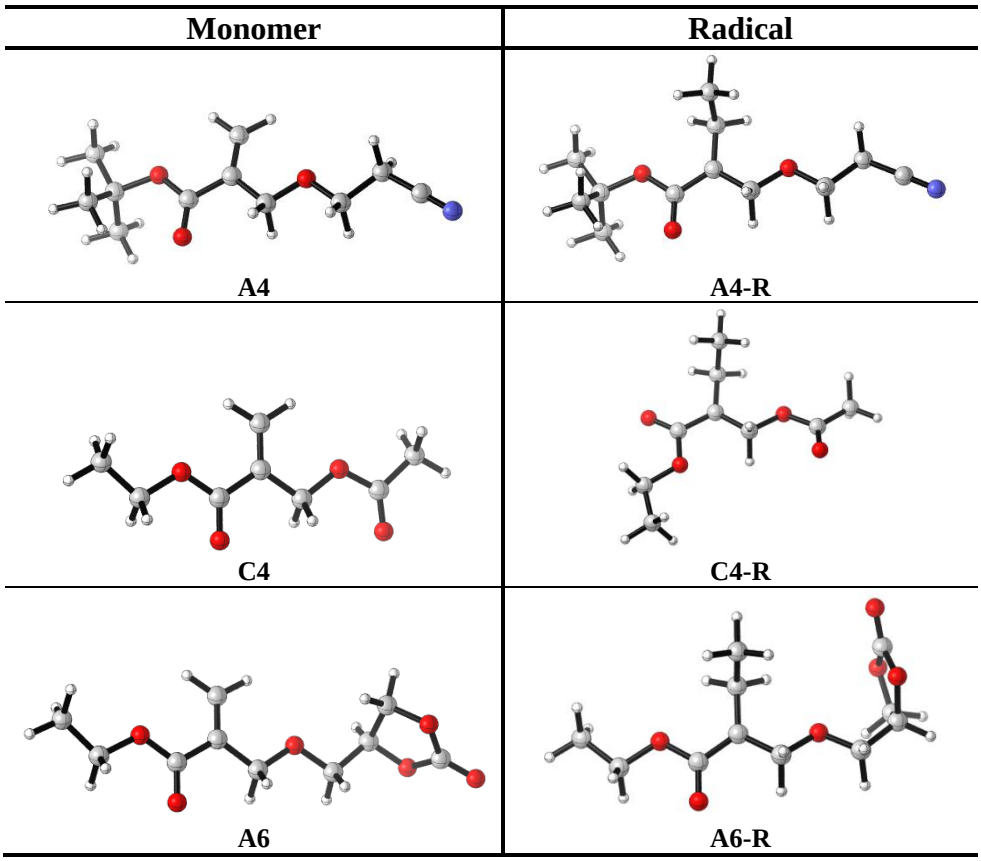

Figure 5.5. 3D structures of the most stable conformers of test RHMA monomers and radicals.

5.3.2. Regression Analysis

All of the proposed descriptors and their possible combinations have been considered to build a correlation with the rate of photopolymerization, R_p. The Mulliken and APT charges of the atoms close to the reactive center, the total dipole moment (μ), the energy gap between the HOMO (E_{HOMO}) and the LUMO (E_{LUMO}), the isotropic polarizability (α), the distance between heavy atoms failed to yield a plausible correlation with the experimental rate of polymerization, R_p.

$$R_p = \boldsymbol{\beta_1} + \boldsymbol{\beta_2} IE_m + \boldsymbol{\beta_3} EA_m + \boldsymbol{\beta_4} (BO_{C=O})_m + \boldsymbol{\beta_5} Res_r + \boldsymbol{\beta_6} \rho_s \quad (5.3)$$

The descriptors showing the best correlation with the experimental rates of polymerization, are the ionization energy (IE_m), the electron affinity (EA_m) and the bond order of the carbonyl double bond in the monomers (the atom-atom overlap weighed NAO bond order of carbonyl double bond of monomer -$BO_{C=O}$), the resonance stabilization parameter Res for the radical and the Mulliken atomic spin density (ρ_s) of C5 of the radical. The resulting linear equation proved to have high predictive power of R_p in case of the free radical polymerization of RHMA monomers. Equation 5.4 is obtained from the MRA of 16 monomers, using these promising descriptors.

$$R_p = -0.0663 - 0.3335\, IE_m - 2.1103\, EA_m + 0.0186\, BO_{C=O} + 0.0133\, Res_r - 0.0501\, \rho_s \quad (5.4)$$

A second equation with additional three test monomers (**A4**-**A6**-**C4**) has been derived. Different combinations of the proposed quantitative descriptors have been considered for the extended data set. Equation 5.5 was found to include the same descriptors as in Equation 5.4, but with slightly different coefficients, as expected. For the three test monomers **A4**, **A6** and **C4** the calculated R_p values based on Equation 5.4 were found to agree pretty well with the experimental ones (Figure 5.6). The R_p values calculated with Equation 5.5 shows also an acceptable correlation with the experiemental values. (Figure 5.7b)

$$R_p = -0.0779 - 0.3121\, IE_m - 2.2230\, EA_m + 0.0222\, BO_{C=O} + 0.0124\, Res_r - 0.0506\, \rho_s \quad (5.5)$$

Table 5.2. Coefficients for the descriptors chosen for RHMA monomers and the statistical characteristics of descriptors in Equation 5.4 and Equation 5.5.

	Descriptor	**Coefficient**	**Standart Error**	**t-test**	**P-value**
Eqn 5.4	Intercept	-0.0663 (β_1)	0.0279	-2.3763	0.0389
	IE_m	-0.3335 (β_2)	0.0473	-7.0437	3.53E-05
	EA_m	-2.1103 (β_3)	0.2611	-8.0808	1.08E-05
	$BO_{C=O}$	0.0186 (β_4)	0.0126	1.4707	0.1721
	Res_r	0.0133 (β_5)	0.0023	5.6634	0.0002
	ρ_s (rad C5)	-0.0501 (β_6)	0.0267	-1.8770	0.0900
Eqn 5.5	Intercept	-0.0779 (β_1)	0.0304	-2.5649	0.0235
	IE_m	-0.3121 (β_2)	0.0479	-6.5185	1.95E-05
	EA_m	-2.2230 (β_3)	0.2815	-7.8964	2.58E-06
	$BO_{C=O}$	0.0222 (β_4)	0.0129	1.7284	0.1076
	Res_r	0.0124 (β_5)	0.0026	4.7965	3.49E-04
	ρ_s (rad C5)	-0.0506 (β_6)	0.0289	-1.7476	0.1041

The standart error, t-test and p-value are used to analyze the statistical quality of each descriptor in the proposed models [Table 5.2]. Accordingly, the p-values of IE_m, EA_m and Res_r indicate very high statistical significance. Although, the p-values of $BO_{C=O}$ and ρ_s are higher than desired, this fact can be due to multicollinearity. The statistical quality of the proposed models was evaluated based on R^2, adjusted R^2 ($\mathbf{R^2_{adj}}$), F and Significance F values; both equations show high correlation (R^2 and $\mathbf{R^2_{adj}}$) and very high F values.

Table 5.3. Statistical quality of the proposed equations.

	N	**R**	**R^2**	**R^2_{adj}**	**Standart Error**	**F**	**Significance F**
Eqn 5.4	16	0.9703	0.9416	0.9123	0.0031	32.23	7.42E-06
Eqn 5.5	19	0.9585	0.9186	0.8873	0.0035	29.35	1.2E-06

In Equations 5.4 and 5.5 the negative coefficients of IE_m and EA_m indicate that as the ionization energy and the electron affinity of the monomers increase, the rate of polymerization decreases. This result can be justified by considering the free radical polymerization process: the easier an electron is taken from the monomer, the lower the ionization energy and the higher the polymerization rate. On the other hand, the larger the magnitude of the electron affinity, the greater the affinity of the monomer for an electron, the faster the polymerization proceeds.

(a) Equation 5.4

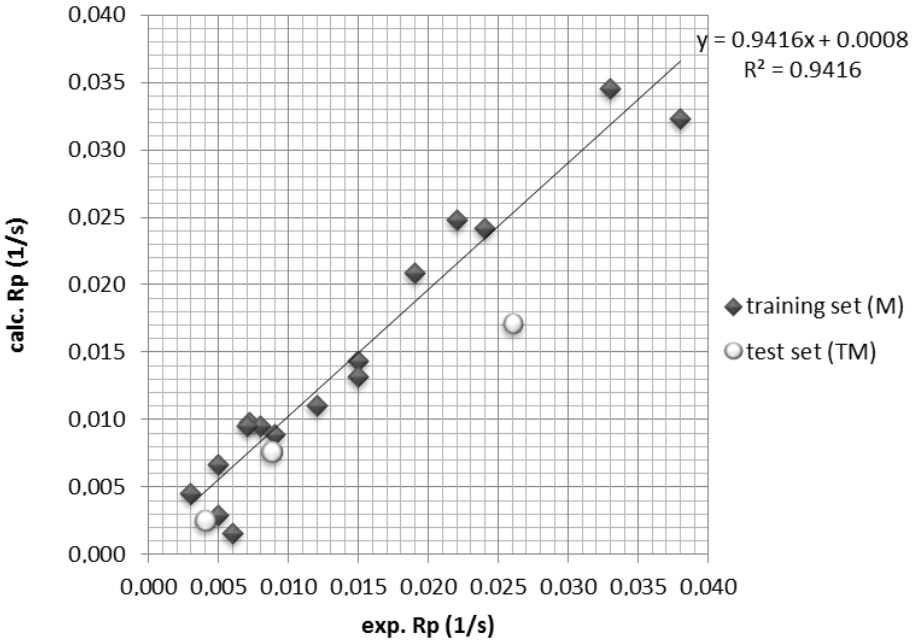

(b) Equation 5.5

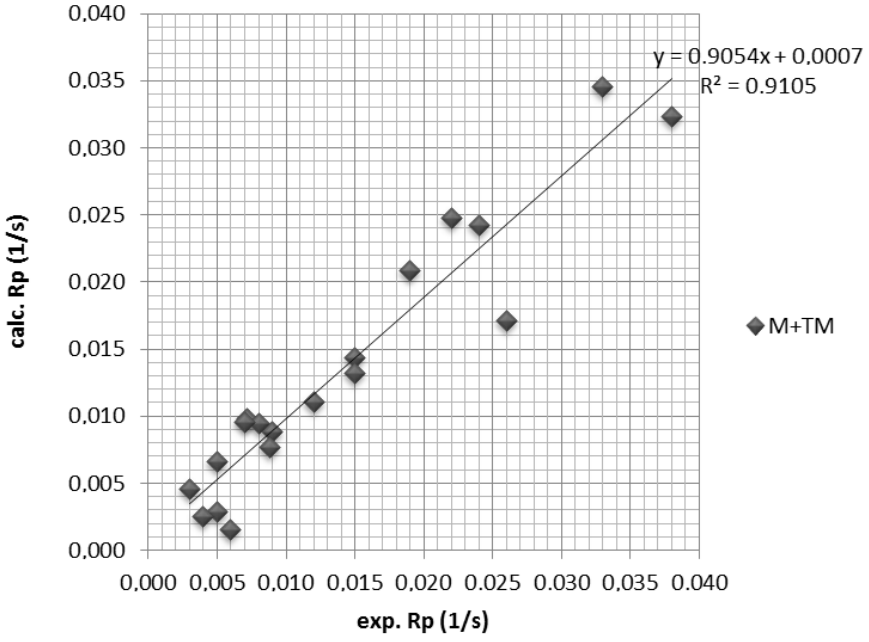

Figure 5.6. Calculated R_p values versus experimental $R_p$values of RHMA monomers. $R_p$values are calculated by using the MLR analysis in (a) Equation 5.4 and (b) Equation 5.5.

(a) Equation 5.4

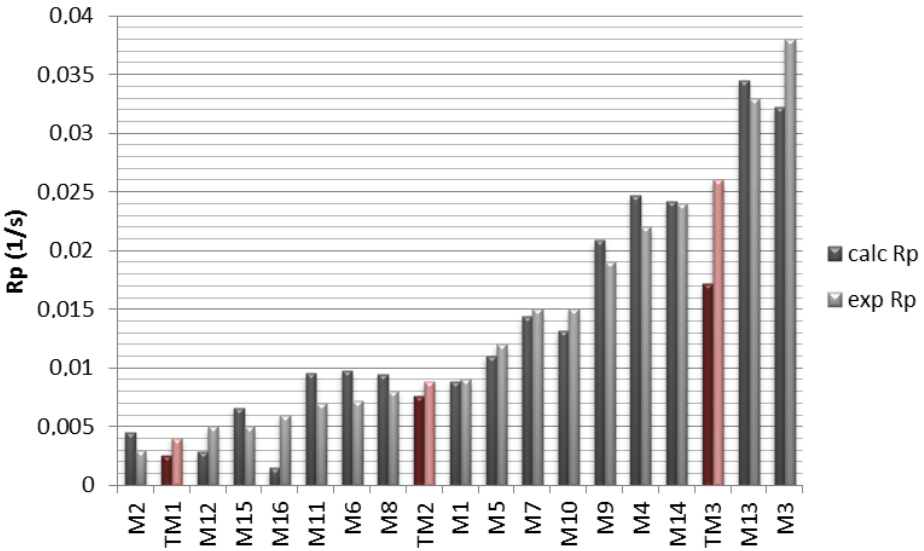

(b) Equation 5.5

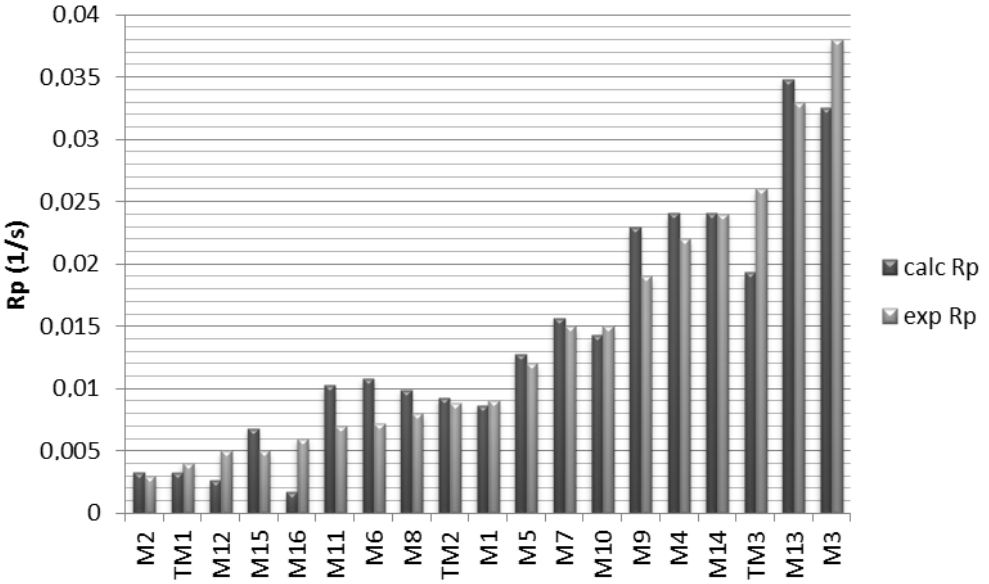

Figure 5.7. (a) Experimental and calculated R_p values according to Equation 5.4 for 16 RHMA (**A1**-**A3**, **A5**, **A7**, **A9**-**A16**, **C1**-**C3)**, in black. The predicted R_p values for the test monomers **A4**, **A6** and **C4** are given in red.

(b) Experimental and calculated R_p values according to Equation 5.5.

The coefficient of $BO_{C=O}$ indicates a direct proportionality between the bond order of the carbonyl double bond of the monomer and the rate of photopolymerization. This finding can be rationalized by taking into account the resonance in the RHMA monomers: as the bond order of the carbonyl double increases, the reactive center is more prone to be attacked by a radical. The carbonyl double bond being close to the reactive center is in resonance with the ethylenic double bond where the radical attacks. The MRA analysis indicates that the photopolymerization rate depends on the resonance parameter (Res) of the radical. In the Q–e scheme derived by Alfrey and Price [129] the rate constant was proportional to the parameter Q which indicates the resonance stabilization of a monomer (or a radical). Similarly, the MRA analysis indicates that the photopolymerization rate depends on the resonance parameter (Res) of the radical, the higher the contribution from Res, the faster the reaction. As the spin density of the radical on the radicalic center (C5) increases, Equation 5.5 predicts a decreasing value of R_p. As the spin density on C5 of the radicals decreases the resonace stability of the radical increases, and based on Alfrey and Price relationship the reaction rate increases.

5.4. Conclusions

The B3LYP/6-31+G* methodology has been used to model 19 RHMA monomers whose rates of photopolymerization have been experimentally measured. The most stable structures of the monomers and their radicals formed by attack of a radical (CH_3 in this study) to these monomers have been considered to derive their corresponding quantitative descriptors. Using the training set, we have established a linear relationship between the descriptors and the rate of polymerization. Among the various descriptors considered, the IE and AE of the monomers, the atom-atom overlap weighed NAO bond order of carbonyl double bond of monomer ($BO_{C=O}$), the resonance stabilization parameter of the monomeric radical (Res), and the Mulliken atomic spin density (ρ_s) of C5 of the radical were found to be correlated with the experimental rates of photopolymerization in Eqn 1. Three RHMA (**A4**, **A6** and **C4**) monomers whose rates of photopolymerizaion are known, have been tested against Equation 5.4 (R^2 = 0.9416). The agreement with experiment is remarkably well except for **A9** and **A6** bearing a carbonate and a cyclic carbonate group respectively.

The correlation with experiment is also reasonable when a new correlation including the test molecules is generated (R^2 = 0.9186). This study is expected to shed light on predicting the reactivities of RHMA monomers prior to their synthesis and thus to rank their photopolymerization abilities based on their structural properties.

6. DEVELOPMENT OF REACTIVE METHACRYLATES BASED ON GLYCIDYL METHACRYLATE

6.1. Introduction

2,2-Bis[4-(2-hydroxy-3-methacryloyloxy)phenyl]propane Bis-GMA is the most common methacrylate used in dental composites due to its high mechanical strength, low volatility and low polymerization shrinkage. However, it has very high viscosity and low polymerization conversion. Although reactive diluent monomers such as triethyleneglycol dimethacrylate (TEGDMA) are added to decrease viscosity and increase conversion, some drawbacks arise such as increased polymerization shrinkage, cytotoxicity, and water absorption. Therefore, development of highly reactive novel monomers as reactive diluents alternative to TEGDMA with lower water absorption, polymerization shrinkage, and cytotoxicity is one of the most important challenges in this area.

In recent years, several factors leading to the enhanced reactivity of (meth)acrylates were hypothesized. These are hydrogen abstraction from labile hydrogens in monomers, hydrogen bonding, and electronic effects (dipole moment and secondary functionalities).

Decker and Bowman formulated new monoacrylate monomers with carbonate, cyclic carbonate, carbamate, and oxazolidone groups that react extremely rapidly despite one vinyl group and form crosslinked polymers. They mentioned that crosslinking due to hydrogen abstraction reactions causes an increase in viscosity, earlier gelation, and autoacceleration, which lead to high rate of polymerization [50-55, 44].

Jansen *et al*. [56] investigated the rate of polymerization of different acrylates in terms of hydrogen bonding capability for systems containing amide, urethane, and urea groups and found that the monomers capable of forming hydrogen bonds show three to six times higher polymerization rates compared with their nonhydrogen bonding analogues

possessing ester and carbonate groups. The high reactivities were suggested to be due to preorganization via hydrogen bonding to bring the double bonds close to each other, enhancing the rate of polymerization, although reduction in termination rate may also be involved or be the cause. They also investigated the effect of monomer polarity on rate of polymerization and found a direct correlation between the maximum rate of polymerization and the dipole moment of the monomer above 3.5 Debye. However, Kilambi *et al.* [44] found no monotonic correlation between monomer reactivity and molecular dipole moments during bulk polymerization of various acrylate monomers. They suggested that a low dipole moment conformation of a monomer may be more reactive due to intermolecular hydrogen bonding than a conformation with a higher dipole moment.

It was observed that the presence of secondary functionalities (carbamates, carbonates, cyclic carbonates, cyclic acetals, morpholine, oxazolidones, hydroxyl, and aromatic rings) enhances reactivity by reducing activation energies in both Michael addition and photopolymerizations indicated by a monotonic correlation between them. The cyclic voltammetry experiments also proved a correlation between reduction potential of the monomers and Michael addition and photopolymerization reactivities [51].

In our previous works, we synthesized phosphonated methacrylates based on glycidyl methacrylate (GMA) for dental applications (Figure 6.1). These monomers showed high polymerization rates and crosslinking tendencies [140, 141]. Unexpectedly, monomers A and C that are monomethacrylates were found to be more reactive than dimethacrylate monomers such as glycerol dimethacrylate (GDMA) and Bis-GMA.

The factors for enhancement of monomer reactivity are not very clear yet, nor is their relative importance. To examine the relationship between monomer structure and reactivity, here, a series of monomers based on GMA and whose structures were changed in the third functionality were designed, synthesized, characterized, and evaluated for their rate of polymerization. (Figure 6.2)

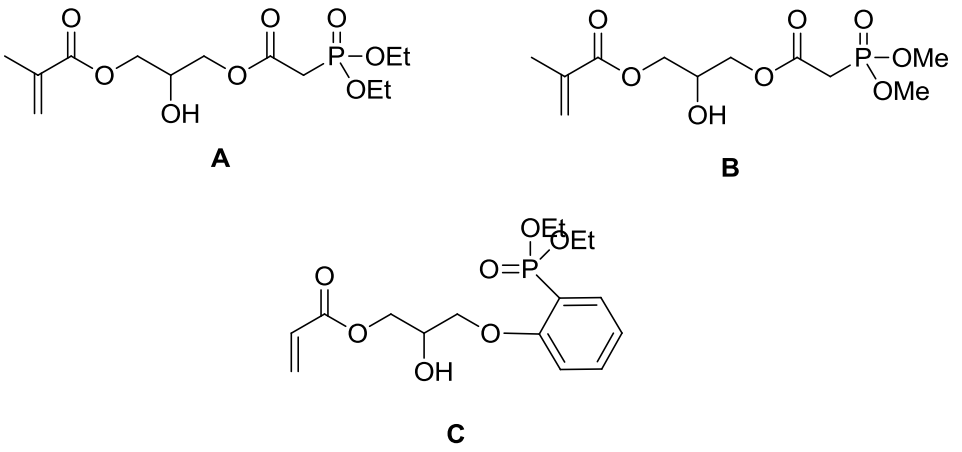

Figure 6.1. Structures of phosphonated methacrylates synthesized from GMA in our previous works.

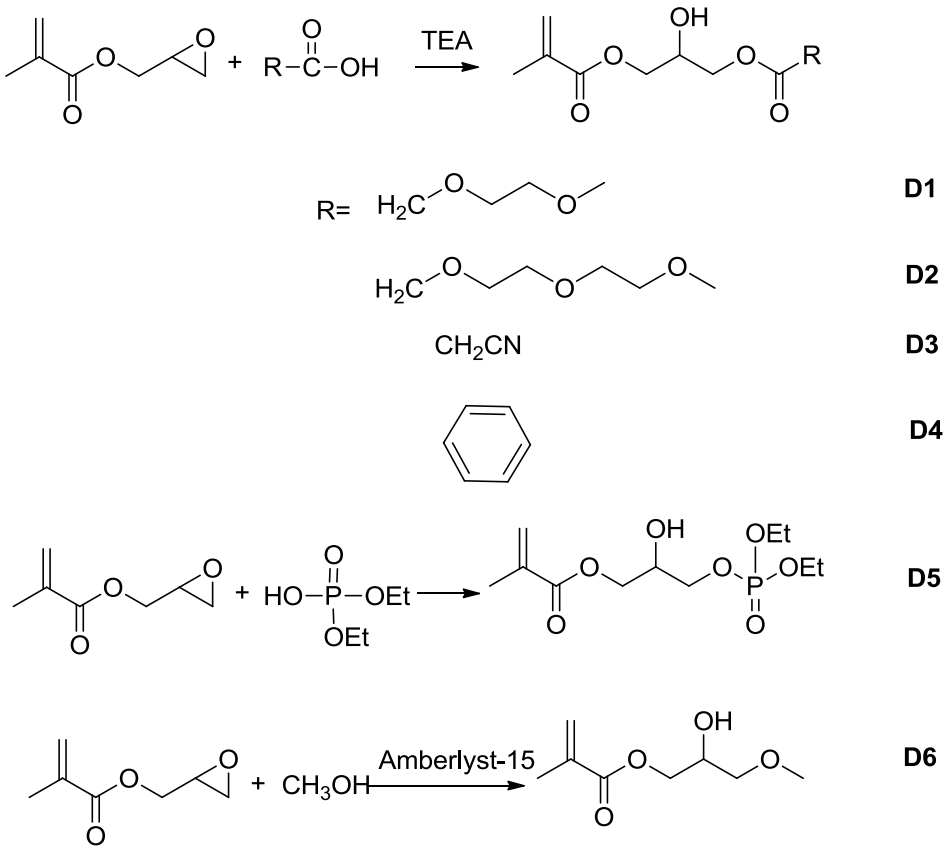

Figure 6.2. Synthesis of monomers.

6.2. Experimental Work

6.2.1. Materials and Apparatus

GMA, 2-(2-methoxyethoxy)acetic acid, 2-(2-(2-methoxyethoxy)ethoxy)acetic acid, diethylchlorophosphate, 2,6-di-tertbutyl-4-methylphenol (BHT), cyanoacetic acid, benzoic acid, hexyl acrylate (HA), 2-hydroxyethyl methacrylate (HEMA), Bis-GMA, TEGDMA, GDMA, and 2,2-dimethoxy-2-phenylacetophenone (DMPA) were used as received from Aldrich.

6.2.1.1. Materials. The monomer characterization involved ^{1}H and ^{13}C NMR spectroscopy (Varian Gemini 400 MHz) and Fourier-transform infrared (FTIR) spectroscopy (T 380). Photopolymerizations were carried out on a TA Instruments Q100 differential photocalorimeter (DPC). Thermogravimetric analysis was done with a TA Instrument (Q50). Viscosity measurements were carried out using Gemini 150 Rheometer system (Bohlin Instruments).

6.2.2. Synthesis of Monomers

6.2.2.1. Synthesis of 2-hydroxy-3-(2-(2-methoxyethoxy)acetoxy)propyl methacrylate (**D1**). GMA (1.01 g, 7.1 mmol), 2-(2-methoxyethoxy)acetic acid (0.99 g, 7.40 mmol), BHT (2.6 mg, 0.012 mmol) and TEA (102.2 mg, 1.0 mmol) were added to a round bottom flask with a water condenser and nitrogen inlet. The mixture was stirred at 60 °C for 18 h. The purification of the crude product by column chromatography (silica gel 0.063-0.200 mm) using dichloromethane initially and gradually changing to ethyl acetate as elutant resulted in a light yellow oil in 46.6 per cent yield.

^{1}H NMR (400 MHz, $CDCl_3$, δ, ppm): 1.87 (s, 3H, CH_3-C), 3.31 (s, 3H, CH_3-O), 3.51 (t, 2H, CH_2-O), 3.63 (t, 2H, CH_2-O), 4.04-4.30 (m, 7H, C*H*$_2$-C*H*, CH_2-C=O), 5.53, 6.06 (s, 2H, C=CH_2) ppm.

^{13}C NMR (400 MHz, $CDCl_3$, δ, ppm): 18.14 (*C*H_3-C), 58.89 (CH_3-O), 64.97, 65.56 (CH_2-O), 67.64 (CH-OH), 68.38, 70.72 (CH_2-O), 71.82 (*C*H_2-O-CH_3), 125.89 (*C*H_2=C), 135.65 (*C*=CH_2), 167.13 (CH_2=C-*C*=O), 170.33 (C=O) ppm.

FTIR: 3430 (O-H), 2888 (C-H), 1754 (C=O), 1716 (C=O), 1635 (C=C) cm^{-1}.

6.2.2.2. Synthesis of 13-hydroxy-10-oxo-2,5,8,11-tetraoxatetradecan-14-yl methacrylate (**D2**). Monomer **D2** was obtained with the same procedure using 2-(2-(2-methoxyethoxy)ethoxy)acetic acid. The purification of the crude product by column chromatography (silica gel 0.063-0.200 mm) using hexane initially and gradually changing to ethyl acetate as elutant resulted in a light yellow oil in 49.7 per cent yield. Characterization data are given next.

^{1}H NMR (400 MHz, $CDCl_3$, δ, ppm): 1.92 (s, 3H, CH_3-C), 3.35 (s, 3H, CH_3-O), 3.53-3.80 (m, 8H, CH_2-O), 4.14-4.60 (m, 7H, C*H*$_2$-C*H*, CH_2-C=O), 5.60, 6.13 (s, 2H, CH_2=C) ppm.

^{13}C NMR (400 MHz, $CDCl_3$, δ, ppm): 18.18 (*C*H_3-C), 58.93 (CH_3-O), 64.98, 65.6 (CH_2-O), 67.58 (CH-OH), 68.39, 69.4, 70.72 (CH_2-O), 71.83 (*C*H_2-O-CH_3), 126.25 (*C*H_2=C), 135.65 (*C*=CH_2), 167.15 (CH_2=C-*C*=O) , 170.34 (C=O) ppm.

FTIR: 3432 (O-H), 2883 (C-H), 1753 (C=O), 1716 (C=O), 1635 (C=C) cm^{-1}.

6.2.2.3. Synthesis of 3-(2-cyanoacetoxy)-2-hydroxypropyl methacrylate (**D3**). GMA (0.99 g, 6.99 mmol), cyano acetic acid (0.63 g, 7.41 mmol), BHT (2.9 mg, 0.013 mmol) and TEA (99.1 mg 0.98 mmol) were added to a round bottom flask with a water condenser and nitrogen inlet and stirred at 40 °C for 5 h. The residue was diluted with CH_2Cl_2 and extracted with $NaHCO_3$ (5%) solution. After the drying of the organic phase with anhydrous Na_2SO_4 and evaporation of the solvent, the crude product was purified by column chromatography (silica gel 0.063-0.200 mm) using hexane initially and changing to ethyl acetate as elutant. The pure product was obtained as colorless oil in 24.3 per cent yield.

^{1}H NMR (400 MHz, $CDCl_3$, δ, ppm): 1.93 (s, 3H, CH_3-C), 3.55 (s, 2H, CH_2-CN), 4.15-4.6 (m, 5H, CH_2-CH, CH), 5.61, 6.12 (s, 2H, CH_2=C) ppm.

^{13}C NMR (400 MHz, $CDCl_3$, δ, ppm): 18.14 (*C*H_3-C), 24.59 (*C*H_2-CN), 64.89, 67.09 (CH_2-O), 69.42 (CH-OH), 113.06 (*C*N-CH_2), 126.54 (*C*H_2=C), 135.54 (*C*=CH_2), 163.05 (CH_2=C-*C*=O), 167.22 (C=O) ppm.

FTIR: 3494 (O-H), 2963 (C-H), 1750 (C=O), 1712 (C=O), 1635 (C=C) cm^{-1}.

6.2.2.4. Synthesis of 2-hydroxy-3-(2-phenylacetoxy)propyl methacrylate (**D4**). Monomer **D4** was obtained with the same procedure using benzoic acid. The purification of the crude product by column chromatography (silica gel 0.063-0.200 mm) using hexane initially and gradually changing to ethyl acetate as elutant resulted in a colorless oil in 24.3 per cent yield. Characterization data are given next.

^{1}H NMR (400 MHz, $CDCl_3$, δ, ppm): 1.96 (s, 3H, CH_3), 4.20-4.50 (m, 5H, C*H*$_2$-C*H*), 5.62, 6.16 (s, 2H, CH_2=C), 7.40-7.50 (m, 2H, Ar-CH), 7.50-7.65 (m, 1H, Ar-CH), 8.00-8.15 (m, 2H, Ar-CH), ppm.

^{13}C NMR (400 MHz, $CDCl_3$, δ, ppm): 18.0 (*C*H_3-C), 65.50, 67.86 (CH_2-OH), 72.48 (CH-OH), 126.20 (*C*H_2=C), 128.20, 129.48, 133.05 (Ar-CH), 135.54 (*C*=CH_2), 166.44 (CH_2=C-*C*=O**)**, 167.24 (C=O) ppm.

FTIR: 3432 (O-H), 2958 (C-H), 1714 (C=O), 1636 (C=C) cm^{-1}.

6.2.2.5. Synthesis of 3-((diethoxyphosphoryl)oxy)-2-hydroxypropyl methacrylate (**D5**). Diethylchlorophosphate (5.00 g, 28.9 mmol) and water (3.10 g, 172.2 mmol) were added to a round bottom flask and the mixture was stirred at room temperature for 1 h. The solution was extracted with dichloromethane. After the drying of the organic phase and evaporation of the solvent, diethyl hydrogen phosphate was obtained.

The formed product, diethyl hydrogen phosphate (1.75 g, 11.36 mmol) and GMA (1.34 g, 9.43 mmol) were added to a round bottom flask with a nitrogen inlet. The mixture was stirred at 50 ^{o}C for 5 h. The crude product was washed with water, cyclohexane and petroleum ether and then further purified by column chromatography (silica gel 0.063-0.200 mm) using CH_2Cl_2 initially and gradually changing to 1 % methanol in CH_2Cl_2 as elutant. The pure product was obtained as a viscous yellow oil in a 31.5 % yield.

^{1}H NMR (400 MHz, $CDCl_3$, δ, ppm): 1.34 (s, 3H, C*H*$_3$-CH$_2$), 1.94 (t, 3H, CH$_3$-C), 2.6 (bs, 1H, OH), 4.07-4.24 (m, 9H, C*H*$_2$-C*H*), 5.59, 6.13 (s, 2H, *C*H$_2$=C) ppm.

^{13}C NMR (400 MHz, $CDCl_3$, δ, ppm): 16.35 (*C*H$_3$-CH$_2$), 18.59 (*C*H$_3$-C), 64.64, 68.92 (CH$_2$-O), 64.97 (*C*H$_2$-CH$_3$), 69.09 (CH-OH), 126.60 (*C*H$_2$=C), 136.06 (*C*=CH$_2$), 167.55 (C=O) ppm.

FTIR: 3379 (O-H), 2983 (C-H), 1717 (C=O), 1637 (C=C), 1249 (P=O), 1017 cm^{-1} (P-O-Et).

6.2.2.6. Synthesis of 2-hydroxy-3-methoxypropyl methacrylate (**D6**). GMA (0.84 g, 5.92 mmol), 30 mL methanol and Amberlyst-15 (600.4 mg) were added to a round bottom flask and placed in an ultrasonic bath. After 2 h at 22-30 ^{o}C, the catalyst was filtered, methanol was evaporated and the residue was washed with hexane to remove unreacted GMA. The pure product was obtained as a colorless liquid after column chromatography (silica gel 0.063–0.200 mm), starting CH_2Cl_2 elutant and changing to EAc : CH_2Cl_2 (20:80) gradually.

^{1}H NMR (400 MHz, $CDCl_3$, δ, ppm): 1.95 (s, 3H, CH$_3$-C), 3.4-3.6 (m, 5H, CH$_3$-O, C*H*$_2$-O-CH$_3$), 4.00-4.40 (m, 3H, CH-OH, CH$_2$-O), 5.59, 6,13 (s, 2H, CH$_2$=C) ppm.

^{13}C NMR (400 MHz, $CDCl_3$, δ, ppm): 18.25 (*C*H$_3$-C), 59.20 (CH$_3$-O), 65.69, 68.73 (CH$_2$-O), 73.43 (CH-OH), 126.01 (*C*H$_2$=C), 135.92 (*C*=CH$_2$), 167.40 (C=O), 170.34 (C=O) ppm.

FTIR: 3434 (O-H), 2929 (C-H), 1715 (C=O), 1635 (C=C) cm^{-1}.

6.2.3. Photopolymerizations

6.2.3.1. Photopolymerization Procedure. Approximately 3.0 or 4.0 mg of sample was placed in an aluminium DSC pan. The photoinitiator which was dissolved in CH_2CI_2 was added with a micro-syringe to give a final concentration in the monomer of 2.0 mol per cent after evaporation of the solvent. The sample and the reference pans were placed in the DSC chamber, the system was purged with nitrogen flow to remove air and CH_2Cl_2 for 10 min before polymerization and purging was continued during polymerization. Heats of photoreactions were measured using a DPC equipped with a mercury arc lamp. The samples were irradiated for 10 min at 40 ^oC with an incident light intensity of 20 mW/cm^2. The heat flux as a function of reaction time was monitored using DSC under isothermal conditions and both the rate of polymerization (R_p) and conversion were calculated as a function of time. The theoretical values used for the heats of reaction (ΔH_p) were 13.1 and 20.6 kcal/mol and for methacrylate and acrylate double bonds [73, 74]. Rates of polymerization were calculated according to the following formula:

$$\text{Rate} = \frac{(Q/s)\, M}{n\, \Delta H_p\, m} \qquad (6.1)$$

where Q /s is heat flow per second, M the molar mass of the monomer, n the number of double bonds per monomer molecule, ΔH_p is the heat released per mole of double bonds reacted and m the mass of monomer in the sample.

6.2.4. Computational Simulation

All monomers were fully optimized by density fuctional theory (DFT) using Gaussian 03 program at the B3LYP/6-31+G(d) in order to obtain some quantum chemical descriptor to find experimental and computational correlation [90]. Four descriptors were

calculated, which are dipole moment, the energy of the lowest unoccupied molecular orbital (E_{LUMO}), Natural Bond Orbital (NBO) charges of the carbon alpha to the carbonyl group and terminal vinylic carbon.

6.2.4.1. Calculation of dipole moments. Boltzman-averaged dipole moments *(μ_{calc})* were calculated using the following method. First, all free rotations around single bonds were considered for a given monomer. Spartan '04 program was used to calculate the Boltzmann-averaged dipole moments [75]. The number of conformations generated is dependent on both the number of bonds and their types. All these conformations were minimized at the PM3 level of theory. The convergence criterion for the maximum gradient was 0.0001 a.u. and the maximum number of geometry optimization cycles was taken to be 20 + the number of independent geometrical parameters for geometry optimization. The unique structures were sorted in the order of increasing energy. The dipole moments of the first 100 conformers are Boltzmann averaged at 298.15 K according to the following formula:

$$\langle \mu_{calc} \rangle = \sum D_j \frac{e^{\Delta H_j / RT}}{\sum_i e^{\Delta H_i / RT}} = \sum_j D_j p_j \qquad (6.2)$$

where D_j is the dipole moment of the conformation j, ΔH_j is the difference between the heat of formation of conformation j and the heat of formation of the global minimum conformation, T is the absolute temperature, R is the ideal gas constant and p_j is the probability of finding the monomer in conformation j at the temperature T [53].

6.2.4.2. Calculation of E_{LUMO} and NBO charges. E_{LUMO} and NBO charges of vinylic carbon atoms have been performed with the Gaussian03 package at the B3LYP/6-31+G(d) level.

6.3. Results and Discussion

6.3.1. Monomer Synthesis

The ring opening reaction of GMA with four carboxylic acids, a phosphoric acid derivative and an alcohol was used for the preparation of new functional monomers with the following structure:

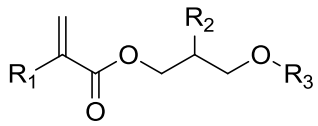

Figure 6.3. General structure of synthesized monomers.

where R_1 is methyl due to methacrylates, R_2 is a secondary functionality which is an OH group and R_3 is a third functionality (Figure 6.3). The hydrogen bonding ability of the monomers will be similar due to OH group. The structure of the third functionality is varied to obtain highly polar monomers.

The general procedure for the synthesis of monomers **D1**–**D4** involved a simple one-step ring-opening reaction of GMA with different acids in the presence of TEA as catalyst (Figure 6.2). The following acids were used to provide monomers with high polarities: 2-(2-methoxyethoxy)acetic acid, 2-(2-(2-methoxyethoxy)ethoxy)acetic acid, cyanoacetic acid, and benzoic acid. Monomers **D1** and **D2** are novel, **D3** seems to be novel (we could not find its synthesis procedure18). In the literature, monomer **D4** was synthesized using tetrabutylammonium bromide as catalyst in acetonitrile [143]. The reactions were conducted at 60 ^{o}C, and BHT was used to prevent homopolymerization of GMA during reactions. Monomers were obtained as viscous oils after purification with column chromatography. The solubilities and viscosities of the monomers are reported in Table 6.1. All of the synthesized monomers were found to be more viscous than TEGDMA due to hydrogen bonding.

GMA was reacted with diethyl hydrogen phosphate, which was prepared from the reaction of diethylchlorophosphate and water (Figure 6.2). The pure product was obtained after column chromatography as a colorless oil. It was soluble almost in all organic solvents except hexane, and it was also soluble in water (Table 6.1).

The ring-opening reaction of the epoxides is not regiospecific. There are two possible sites for attack of alcohols, acids, and anhydrides [145, 146]. If the attack occurs from the less- hindered side, the linear isomer is obtained otherwise the branched isomer or both isomers are produced. The crude product yields of acid reactions were very high, containing mostly the linear isomer with different amounts of the branched isomer.

The ^{1}H NMR of monomer **D1** showed methyl protons at 1.87 ppm, methoxy protons at 3.31 ppm, two methylene protons at 3.51 and 3.63 ppm, other methylene and methine protons between 4.04 and 4.30 ppm, and double bond protons at 5.53 and 6.06 ppm (Figure 6.4). The small peaks ~4.4, 5.2, and 6.0 ppm are due to the branched isomer. The ratios of linear to branched isomers for monomers **D1**, **D2**, and **D5** were found to be greater than 7.5:1.

The ^{13}C NMR spectrum of monomers **D3** and **D4** also showed two isomers (Figures 6.5 and 6.6). For example, the spectrum of monomer **D4** showed characteristic peaks for methyl carbon at 17.97 ppm, a tertiary carbon at 67.81 ppm, methylene carbons at 65.25 and 65.47 ppm, double bond carbons at 126.20 and 135.52 ppm, aromatic carbons at 128.17, 129.45, and 133.01 ppm, and carbonyl carbons at 166.41 and 167.21 ppm (Figure 6.6). The small peaks at 61.02 (CH_2) and 62.75 (CH_2) ppm are due to the branched isomer, small CH peak is difficult to see. The ratio of CH_2 peaks for linear isomer to that of branched isomer indicates relative ratios of the isomers, which is about 4:1. This ratio was also confirmed by ^{1}H NMR. Another fraction of column chromatography indicated a ratio of 14:1. Similarly, the ratio of linear to branched isomers for monomer **D3** was also found to be high (4:1). These results indicated the amount of branched isomers formed is greater for the acids with more rigid structures.

The FTIR spectra of the monomers **D1**–**D4** showed the presence of alcoholic OH bond at ~3400 cm^{-1}, the double bonds at 1634 cm^{-1}, two different ester C=O bonds at ~1750 and 1716 cm^{-1} (Figure 6.7) except monomer **D4** where two C=O peaks overlap at 1713 cm^{-1}. Monomer **D5** showed one C=O peak at 1717 cm^{-1} and also showed P=O and P-OEt group peaks at 1249 and 1017 cm^{-1}.

The alcoholysis of epoxides is conducted under acidic and basic conditions and requires long reaction times and high temperature. Liu *et al*. [147] have demonstrated that Amberlyst-15 is an efficient heterogeneous catalyst for the regioselective ring-opening reactions of epoxides (such as phenyl glycidyl ether, styrene oxide, and cyclohexene oxide) by alcohols in the formation of β-alkoxy alcohols under ultrasonication at room temperature. We used the same method for the synthesis of our last monomer (monomer **D6**; Figure 6.2). GMA was reacted with methanol in the presence of Amberlyst-15 in an ultrasonic bath at 25–30 ^{o}C. However, the major product was found to be a α-alkoxy alcohol (linear isomer: 78%) with a small amount of β-alkoxy alcohol (branched isomer: 22%) determined from ^{1}H NMR of the crude product. In the literature, the reaction of GMA with methanol at room temperature using BF_3 as catalyst gave a mixture of products with similar regioselectivity (branched:linear 20/80%) [148, 149].

When the crude product was subjected to a chromatographic separation on silica gel, fractions containing mixture of isomers were obtained. The ^{13}H NMR spectra of three isomer mixtures were shown at Figure 6.8. The ratio of double bond peaks or double bond to CH peak of branched isomer (~5.0 ppm) indicates relative ratios of the isomers. Mixture **D1** contains mainly the linear isomer with a very small amount of branched isomer. Mixtures **D2** and mixture **D3** contain linear to branched isomers with the ratio of 3.4:1 and 1:1. The FTIR spectrum of this monomer showed the characteristic peaks of hydroxyl, carbonyl, and C=C groups at 3434, 1715, and 1635 cm^{-1}.

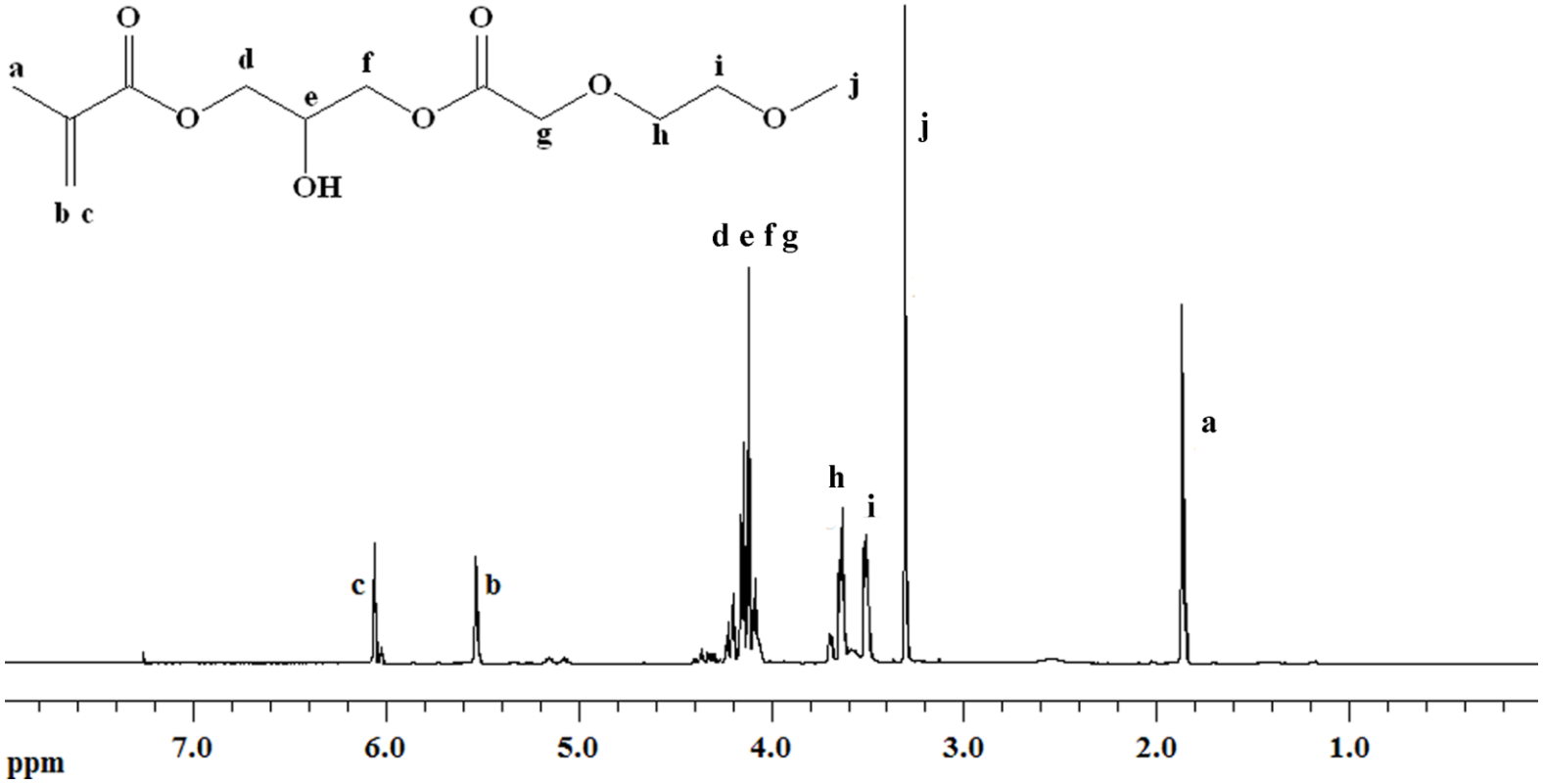

Figure 6.4. ^{1}H NMR spectra of monomer **D1**.

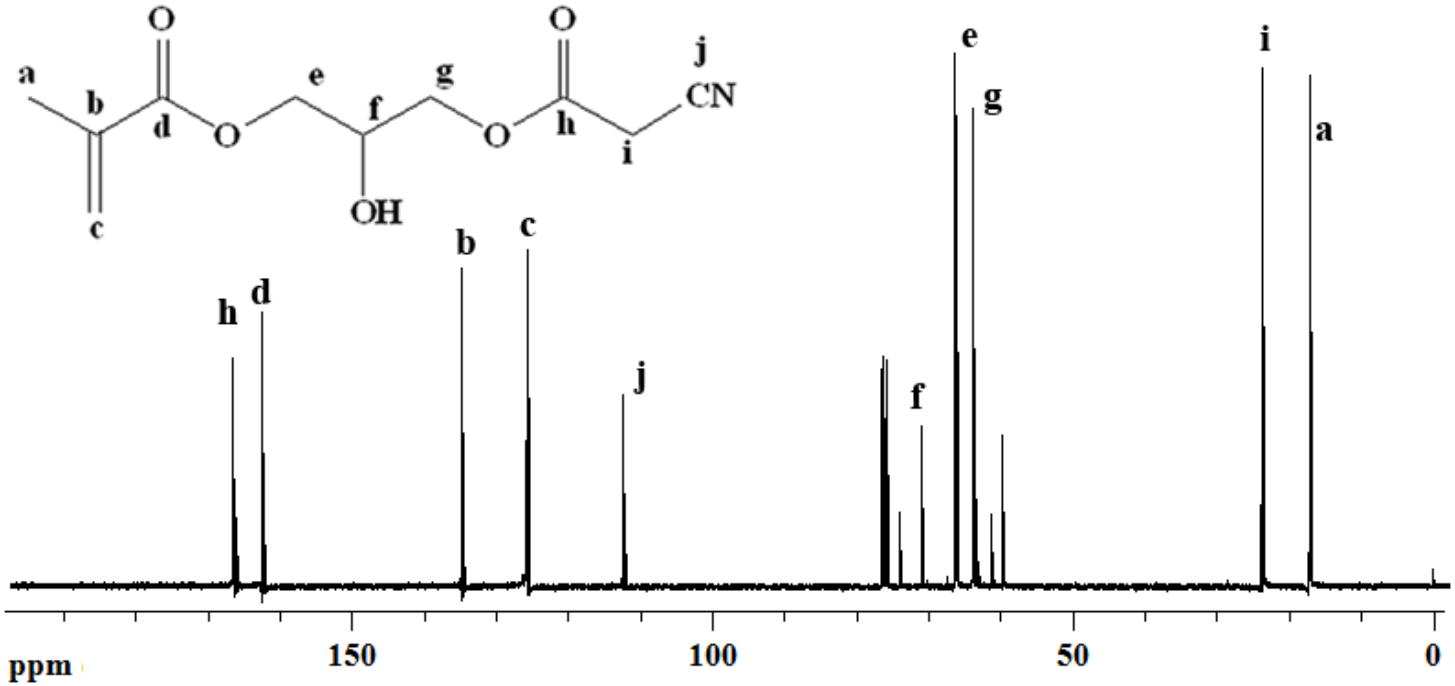

Figure 6.5. ^{13}C NMR spectra of monomer **D3**.

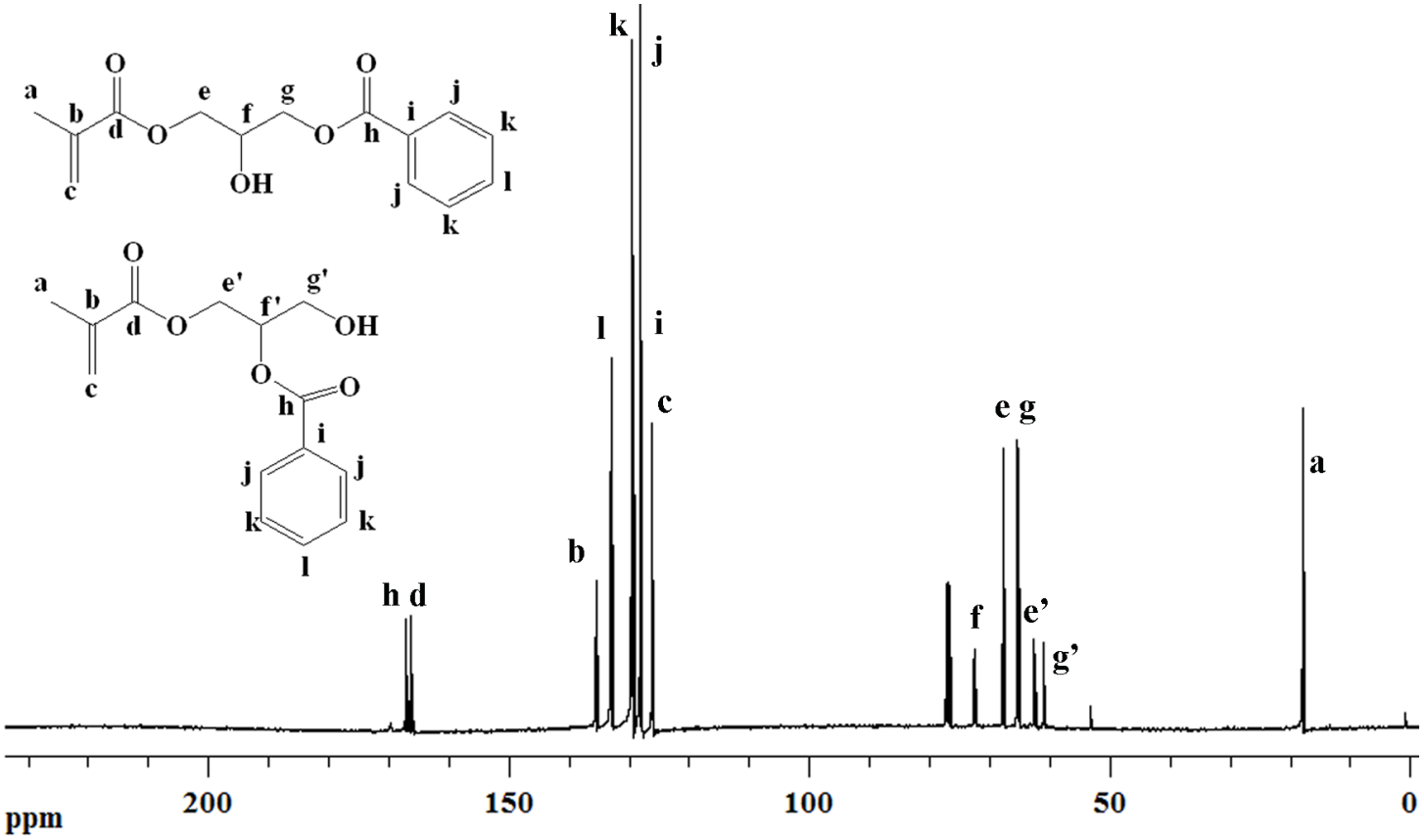

Figure 6.6. ^{13}C NMR spectra of monomer **D4**.

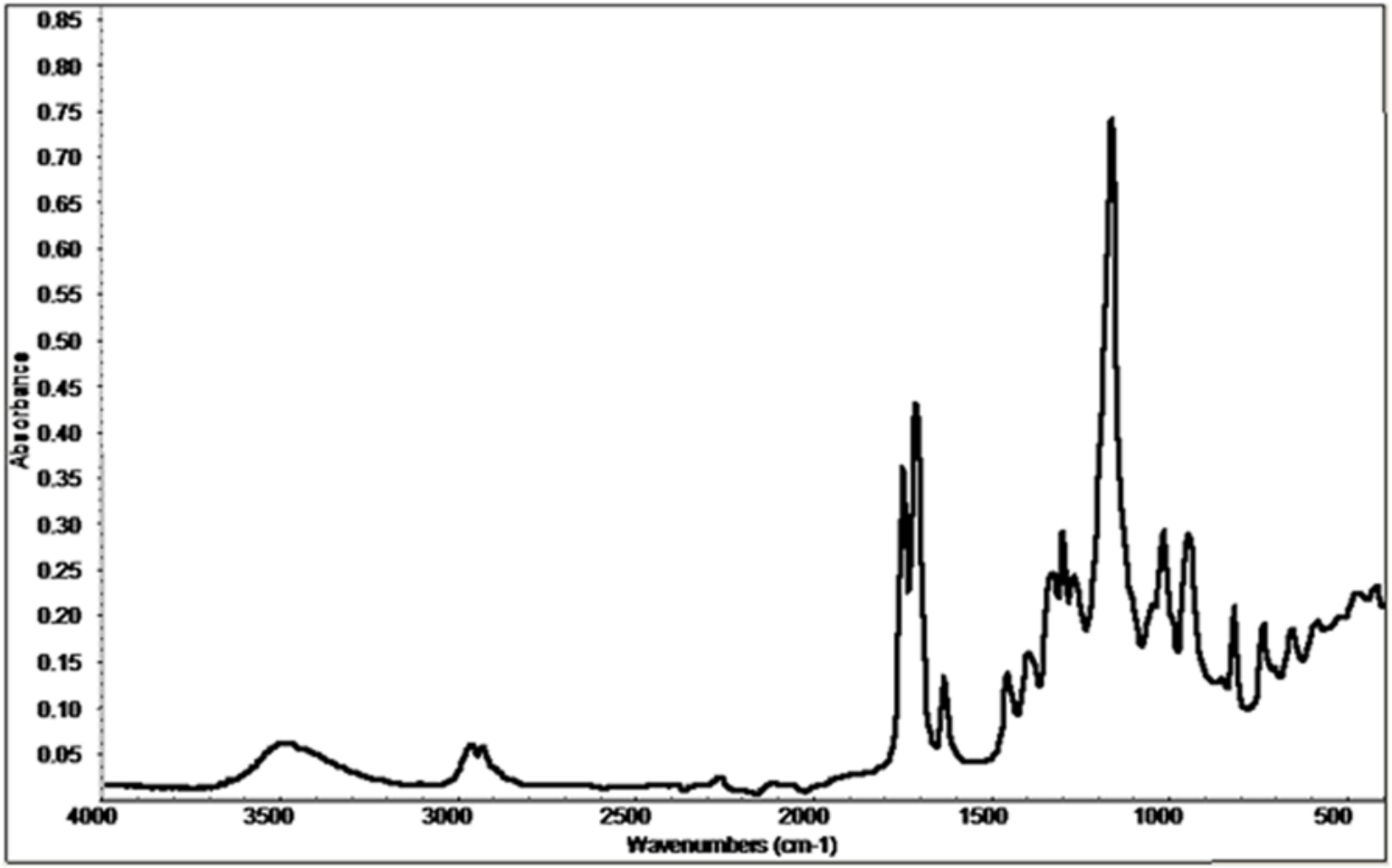

Figure 6.7. FTIR spectra of monomer **D3**.

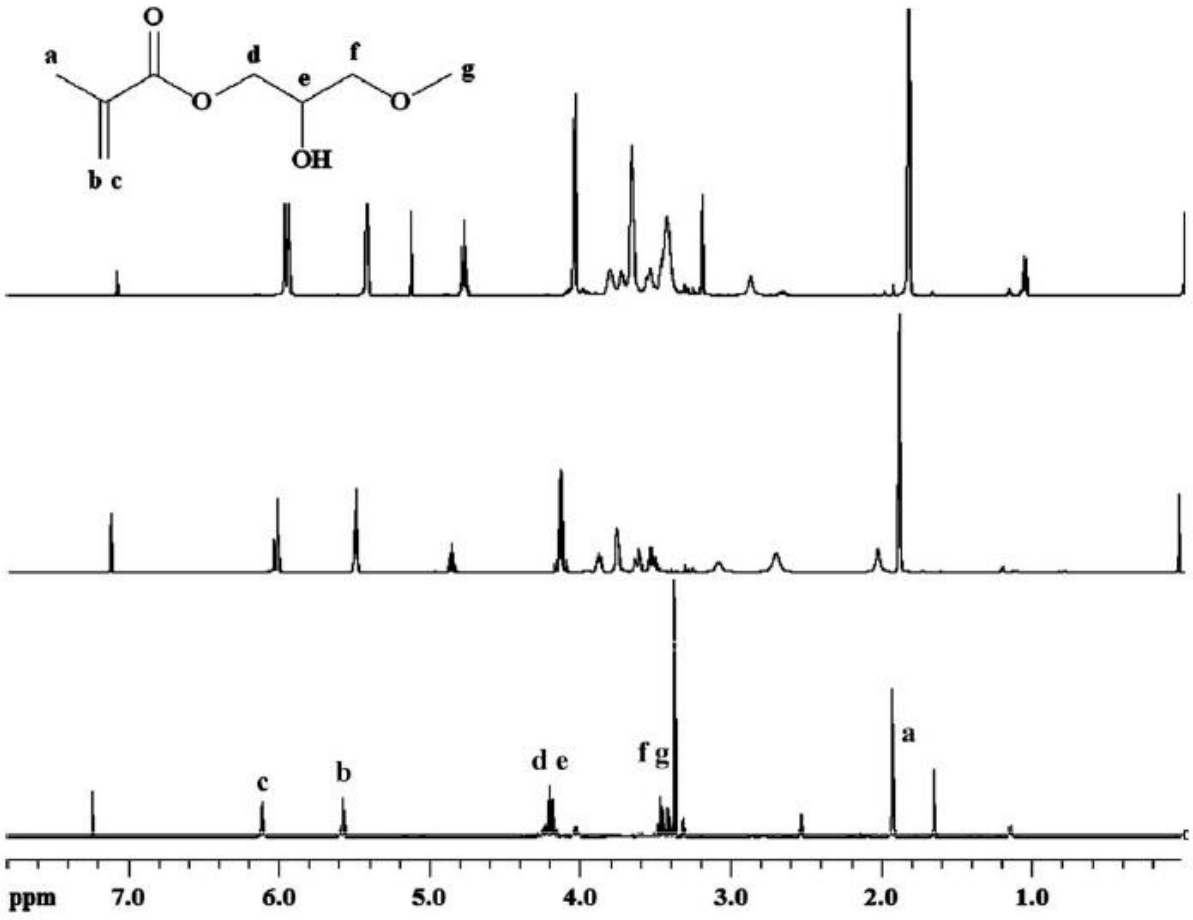

Figure 6.8. ^{1}H NMR spectra of isomer mixtures of monomer **D6** (mixture 1-bottom, mixture 2-middle, and mixture 3-top).

Table 6.1. Viscosities and solubilities of the synthesized monomers and TEGDMA.

Monomer	**Viscosity Pa s**	**H_2O**	**ether**	**methanol**	**CH_2Cl_2**	**THF**	**hexane**	**acetone**
TEGDMA	0.009	-	+	+	+	+	+	+
D1	0.047	+	+	+	+	+	-	+
D2	0.072	+	+	+	+	+	-	+
D3	0.960	-	+	+	+	+	-	+
D4	0.258	-	+	+	+	+	-	+
D5	0.059	+	+	+	+	+	-	+
D6	0.136	+/-	-	+	+	+	-	+

6.3.2. Thermal Polymerizations

Bulk polymerizations of monomers **D1**–**D6** were carried out with azobisisobutyronitrile (AIBN) (0.5 wt %) at 60 ^{o}C. These monomers polymerized very fast to give crosslinked polymers, as indicated by swelling in various solvents. This behavior can be explained by a hydrogen abstraction chain transfer mechanism from the labile hydrogens on the carbons attached to oxygen, which can be followed by reinitiation. The crosslinking will result high mechanical properties, which is an important property for dental materials.

The crosslinked polymer obtained from monomer **D5** may also have potential as flame retardant due to its phosphate group. The thermal gravimetric analysis of this polymer (residual monomer was removed by several washings with methylene chloride) showed a major weight loss around 270 ^{o}C and a char yield of 33.3%. This char yield was higher than those of GMA-based crosslinked phosphonated polymers (poly-A, poly-B and poly-C) with the char yields of 25-30%. The enhanced char production of phosphates compared with phosphonates is due to formed phosphoric acid which is more effective at promoting further crosslinking of polymers instead of the weaker phosphonic acid [150].

6.3.3. Photopolymerization

Photopolymerization of the monomers were followed by DPC. First, the homopolymerization behavior of the synthesized monomers was investigated and compared with those of commercial monomers such as HEMA, Bis-GMA, GDMA and TEGDMA. Table 2 shows the results in terms of rate of polymerizations and conversions.

Table 6.2. Rate of polymerizations and conversions of monomers **D1-D6**, Bis-GMA,TEGDMA, HEMA and GDMA.

Monomer (linear:branched)	**R_p (s^{-1})**	**Conversion (%)**
D1 (>7.5:1)	0.034±0.003	91±3
D2 (>7.5:1)	0.060±0.001	95±2
D3 (5:1)	0.074±0.002	88±2
D4(14:1)	0.070±0.002	72±2
D4 (4:1)	0.061±0.002	74±2
D5 (>7.5:1)	0.066±0.003	64±3
D6 (>7.5:1)	0.065±0.001	81±3
D6 (1:1)	0.058±0.001	68±1
TEGDMA	0.056±0.002	79±2
Bis-GMA	0.037±0.003	47±2
HEMA	0.037±0.002	92±1
GDMA	0.040±0.00	58±1

It is known that, as the monomer functionality increases, the rate of polymerization increases while the conversion decreases. However, the synthesized monofunctional monomers except one (monomer **D1**) showed higher rates of polymerization (0.057-0.074 s^{-1}) than Bis-GMA (0.037 s^{-1}) and GDMA (0.040 s^{-1}) and similar or higher rates of polymerization than TEGDMA (0.056 s^{-1}). In addition to hydrogen abstraction mechanism, the high reactivity of the synthesized monomers can be explained by their hydrogen bonding capabilities leading to high viscosity and earlier Trommsdorf effect. Monomer **D1** was found to be the least reactive monomer, which also correlates with its low viscosity, as

expected. These properties may be understood to be due to a combination of low dipole moment (in dipole moment section) and low hydrogen bonding capability. The conversions of all the synthesized monomers (64–95%) were higher than Bis-GMA (47%) and GDMA (58%). Monomers **D1** and **D2** with very flexible structure gave very high conversions (91 and 95%).

It was observed that the rate and conversion data of a given monomer is different for different fractions of column chromatography, which indicated different reactivities of the two isomers. To see the effect of isomer structure on the rate of polymerization, two fractions obtained from column chromatography of monomer **D4** and **D6** were polymerized. It was observed that as the branched isomer content in the isomer mixture is increased, the maximum rate of polymerization is decreased. For example, the maximum rate of polymerization of monomer **D4** decreased from 0.070 (14:1, linear:branched) to 0.061 s^{-1} (4:1, linear:branched). Similarly, rates were found to be 0.065 (mixture 1) and 0.058 s^{-1} (mixture 3) for two different isomer mixtures of monomer **D6**. We observed similar behavior during polymerizations of ethyl a-chloromethacrylate-GDMA isomer mixtures [151]. The reason for the higher reactivity of the linear isomers is not obvious. We suggest an explanation by the polarity differences of isomers in the next section.

The synthesized monomers were also evaluated as reactive diluents to Bis-GMA. The maximum rate and conversion values of Bis-GMA:monomer (50:50 mol %) mixtures were measured and compared with a control Bis-GMA:TEGDMA (50:50 mol %) system. It was observed that on addition of monomers (except monomer **D1**), both maximum rate of polymerizations and conversions were improved, and the values are comparable with the control (Table 6.3). We could not explain why addition of a very flexible monomer (monomer **D1**) to Bis-GMA did not increase the conversion. The maximum rate of polymerization and conversion of the mixtures (except Bis-GMA:**D1**) were between the rates of polymerizations and conversions of the two monomers. For example, the maximum rate of polymerization of Bis-GMA and monomer **D2** were 0.037 and 0.060 s^{-1}, whereas the mixtures of Bis-GMA with monomer **D2** gave maximum rate of polymerization of 0.056 s^{-1}.

Table 6.3. Rate of copolymerizations and conversions of monomers **D1**-**D6** and TEGDMA with Bis-GMA.

Monomers (50:50 mol%)	**R_p (s^{-1})**	**Conversion (%)**
Bis-GMA:**D1**	0.035±0.002	43±2
Bis-GMA:**D2**	0.056±0.003	70±2
Bis-GMA:**D3**	0.040±0.03	50±2
Bis-GMA:**D4**	0.050±0.003	57±2
Bis-GMA:**D5**	0.043±0.001	57±2
Bis-GMA:**D6**	0.049±0.002	52±3
Bis-GMA:TEGDMA	0.052±0.003	56±3

6.3.4. Effect of Monomer Structure on Oxygen Inhibition

Although free radical polymerizations are inhibited by oxygen, most of the curing processes are conducted in air. The presence of oxygen results in long induction times, low conversions, slow polymerization rates, short chains, and poor polymer properties [47]. In general, oxygen inhibition depends on viscosity of the medium that is effected by monomer functionality, molecular weight, and functional groups present in the monomer structure (such as OH). When the viscosity is high or increases during polymerization, diffusion rate of oxygen to the monomer will be low. Other than viscosity, monomers with abstractable hydrogens such as ether groups were showed to reduce oxygen inhibition by forming peroxy radical. For example, Hoyle and coworkers found that TEGDMA shows oxygen inhibition in air with less than 15% decrease in polymerization rate, while 1,12-dodecane dimethacrylate shows ~35% reduction in rate. They also concluded that methacrylates were less sensitive to oxygen than acrylates. The reduction of rate of polymerization of HA was found to be ~80% [47].

Since we propose a hydrogen abstraction mechanism for the formation of crosslinked structures from our monomers, we investigated their photopolymerization behavior in the presence and absence of oxygen. Figures 6.9 and 6.10 show the polymerization exotherms and conversions of monomer **D2** together with HA in the presence and absence of oxygen. The photopolymerization results of monomers **D2**, **D3**, and **D4** were listed in Table 6.4. The synthesized monomers showed little oxygen inhibition in air (10–13% decrease in rate), whereas HA (76% decrease in air) was found to be very sensitive to air. These findings support our proposed hydrogen abstraction chain transfer mechanism.

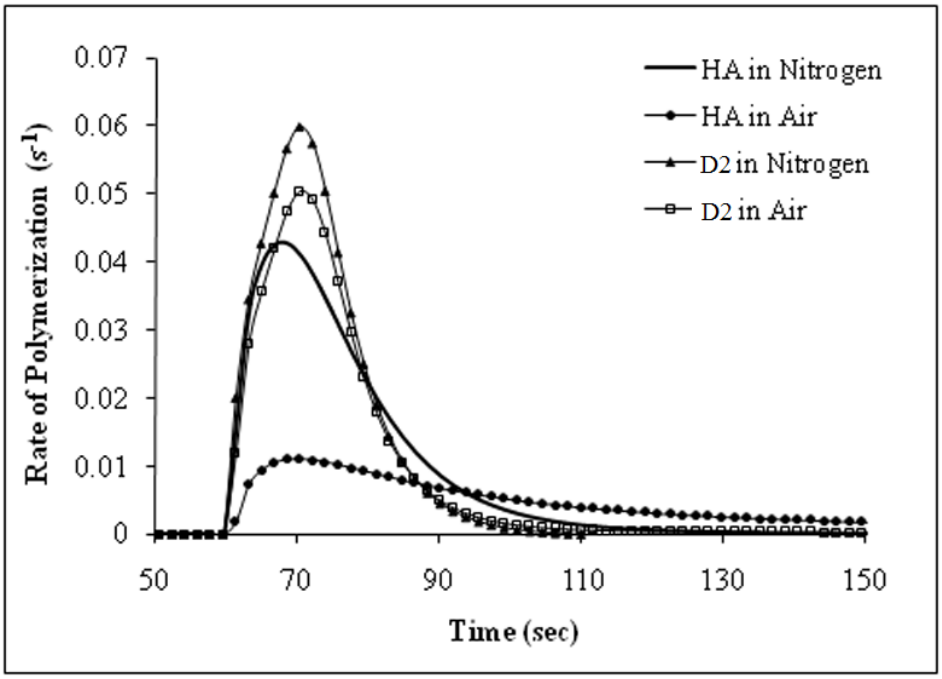

Figure 6.9. Photopolymerization rate versus time for monomer **D2** and HA in nitrogen and air.

6.3.5. Dipole Moment

The synthesized monomers were evaluated in terms of dipole moment to find a relation between monomer structure and reactivity. The Boltzmann-averaged dipole moments of monomers were calculated for minimum energy conformers (Table 6.5).

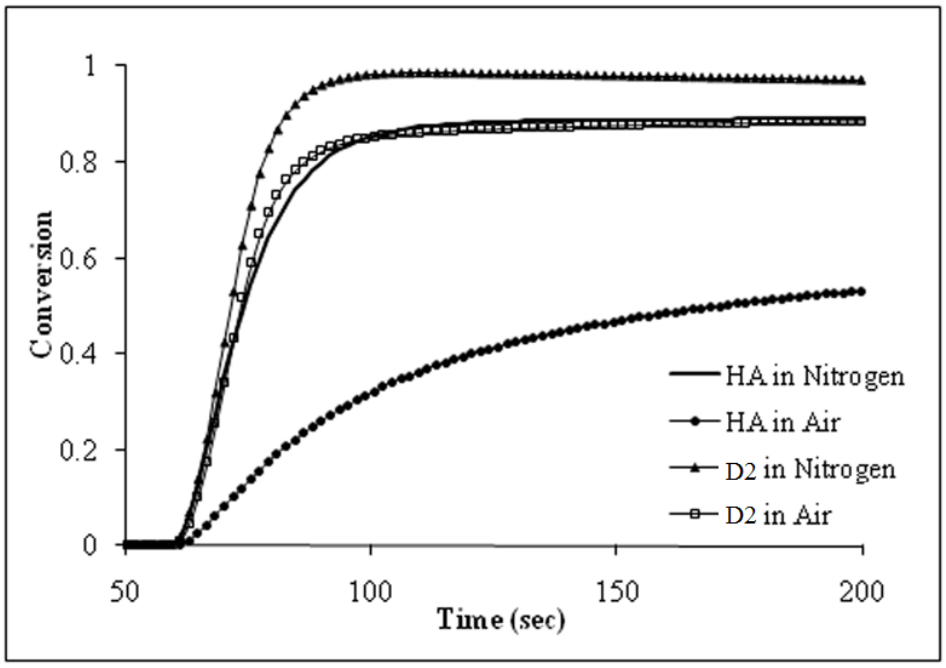

Figure 6.10. Conversion versus time for monomer **D2** and HA in nitrogen and air.

Table 6.4. Photopolymerization rates and conversions of monomers **D2**, **D3**, **D4** and HA in the presence and absence of oxygen.

Monomer	**R_p (s^{-1})**	**Conversion (%)**
D2	0.060±0.001	95±2
D2[a]	0.050±0.002	89±2
D3	0.074±0.002	88±2
D3[a]	0.069±0.002	80±2
D4	0.070±0.002	72±2
D4[a]	0.061±0.001	75±2
HA	0.043±0.003	82±4
HA[a]	0.010±0.002	60±2

[a] in air

When we consider ester linked monomers (**D1**–**D5**), there seems to be a correlation: the most reactive monomer has the highest dipole moment, the least reactive one, lowest; with the other three in between (the intermediate ones are too close together for their differences to have meaning).

We also calculated dipole moments of some of the branched isomers. They were found to be lower than those of the linear isomers as expected. For example, linear isomers of monomers **D3**, **D4**, and **D6** were found to have dipole moments of 5.30, 3.97, and 3.04, whereas branched isomers gave values of 3.49, 3.22, and 2.82 (Table 6.5). The difference for monomer **D3** was very significant, which may explain the lower reactivity of monomer **D3** (isomer mixture) than expected.

6.3.6. Calculation of NBO Charges and E_{LUMO}

Computer simulations were used to observe the electron density surfaces and partial charges on double bond carbons of the synthesized monomers. These values were compared with the chemical shift differences of these carbons determined by ^{13}C NMR spectra.

The calculated charges on the terminal vinyl carbons and the carbon alpha to the carbonyl group of the monomers were similar to indicate a correlation with reactivities (Table 6.5).

Bowman and coworkers [51] said that a molecule with smaller ELUMO value shows higher susceptibility toward attack by nucleophiles or radicals. Thus, during a polymerization of a monomer with a lower LUMO energy, the activation energy for the propagation is reduced, which results in an increase in rate of polymerization. We also calculated the LUMO energies of the synthesized monomers using B3LYP DFT to explain reactivity differences between them (Table 6.5). We observed a correlation between the polymerization rate and LUMO energies for the ester linked monomers (**D1**–**D5**); the most reactive monomer (monomer **D3**) has the lowest LUMO energy, whereas the least reactive

one (monomer **D1**) has the highest LUMO energy. The ether linked monomer with the highest LUMO energy did not follow this trend.

Table 6.5. Dipole moments, chemical shift differences, LUMO energies and NBO charges of the monomers.

Monomer	**Dipole moment**	**Δδ**	**LUMO energies (eV)**	**Charges on the terminal vinylic carbon**	**Charges on the carbon alpha to the carbonyl group**
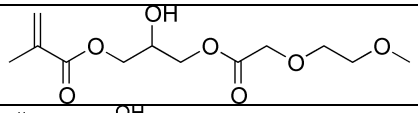	2.81	9.76	-0.06817	-0.3749	-0.1238
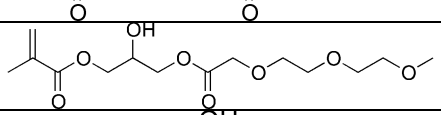	3.94	9.40	-0.07487	-0.3659	-0.1302
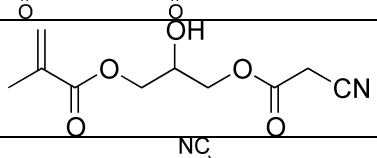	5.30	9.00	-0.08463	-0.3733	-0.1301
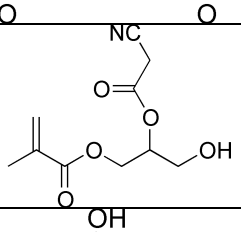	3.49	-	-0.07391	-0.3894	-0.1247
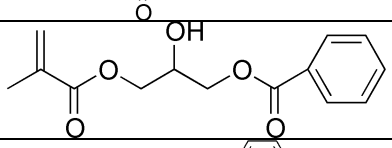	3.97	9.35	-0.07198	-0.3877	-0.1235
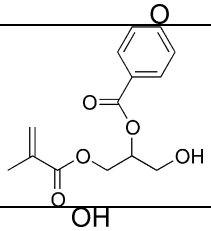	3.22	-	-0.06757	-0.3713	-0.1206
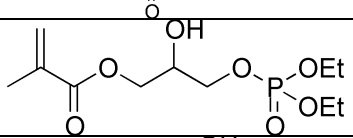	3.34	9.50	-0.07361	-0.3872	-0.1243
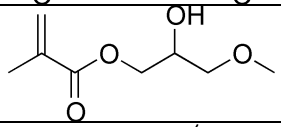	3.04	9.91	-0.06295	-0.3879	-0.1268
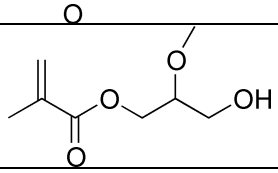	2.82	-	-0.06295	-0.3719	-0.1243

^{13}C NMR can be used to predict free radical polymerizability of monomers. The chemical shift differences of the C=C double bonds ($C_\beta H_2$=Cα-) of the synthesized monomers are given in Table 6.5. Vaidya *et al.* have reported that δC_β and δC_α shift to lower and higher fields, respectively, with an increase in electron withdrawing power of the substituents. Therefore, (δC_β-δC_α) shows the effects of substituents on polymerizability. The stronger the electron-withdrawing power of the substituents, the smaller the difference and the higher the radical polymerizability [152, 153]. Also, bulky substituents may cause differences in chemical shifts and/or lead to lower propagation enthalpy through steric hindrance. Comparison of the $\Delta\delta$ values of the ester-linked monomers shows that the most reactive monomer (monomer **D3**) has the lowest (9.0 ppm) value and the least reactive one (monomer **D1**) has the highest value (9.76 ppm). The monomers with similar polymerization tendencies gave values in between (9.35–9.50). The aforementioned correlation was not applicable to the ether-linked monomer **D6**.

6.4. Conclusions

Six hydroxyl-containing methacrylate monomers with various third functionalities were synthesized as mixtures of isomers. Photopolymerization studies of these monomers indicated that the monomers they can be used as alternative reactive diluent to TEGDMA in Bis-GMA. Monomer **D2** was found to be the best monomer between all the monomers studied. Low sensitivity of the monomers to oxygen is consistent with the crosslinked polymer formation during thermal polymerization due to a proposed hydrogen abstraction chain transfer reaction. Although we could not see a monotonic correlation between computationally calculated dipole moment and LUMO energies these values can be used to roughly estimate relative reactivities of the monomers with similar structures.

7. SYNTHESIS AND EVALUATIONS OF NOVEL POLYMERIC PHOTOINITIATORS WITH SIDE-CHAIN BENZOPHENONE DERIVED FROM ALKYL α-HYDROXYMETHACRYLATES

7.1. Introduction

In recent years, photopolymerizable initiators receive continuous interest due to their advantages in comparison with their corresponding low molecular weight analogues [124, 154, 155]. Some of these advantages are compatibility improvement in the formulation, low odor, non-toxicity, and reduced migration to the film surface which is important for the synthesis of environmentally friendly materials. In addition, the efficiency of photoinitiation can be enhanced due to the energy migration along the polymer chain, or intramolecular reactions responsible for generating more reactive species. Also, polymer chain can prevent coupling of the reactive species, thus favoring their reaction with the monomers. Further improvements in the efficiency of photoinitiation, which result in reduction of exposure time and increase productivity, can be achieved by designing new polymeric structures containing photoinitiator groups.

Polymeric photoinitiators contain side chain or main chain photoinitiator moiety which generates free radicals upon absorption of UV light and are able to initiate polymerization and crossinking of monomers and oligomers. A variety of polymeric photoinitiators containing Type I and *Type II* free radical photoinitiators are described in the literature [157-161]. Most of the *Type II* polymeric photoinitiators are based on benzophenone, thioxanthone, anthraquinone, camphorquinone or benzyl moieties, and among them benzophenone-containing ones are more common [162-174]. Also, *Type II* photoinitiators require the presence of a coinitiator (usually an amine) in the solution to work, hence polymeric photoinitiators were tried that contain both benzophenone and amine groups in the same macromolecule; and some of them were found to show higher

photoinitiation activity compared with the polymeric photoinitiators without amine groups where the amines are supplied externally. This result can be explained by the favorable excitation energy transfer when both groups are in close proximity. For example, Wei and coworkers studied copolymerization of a polymerizable photoinitiator 4-[(4-maleimido)thiophenyl]benzophenone (MTPBP) and an unsaturated coinitiator amine N,N-dimethylaminoethyl methacrylate (DMAEM) [27]. The results indicated that P(MTPBP-co-DMAEM) is most efficient for the polymerization of both HDDA and TMPTA compared to their low molecular weight analogs, BP/DMAEM and MTPBP/poly-DMAEM and poly-MTPBP/DMAEM.

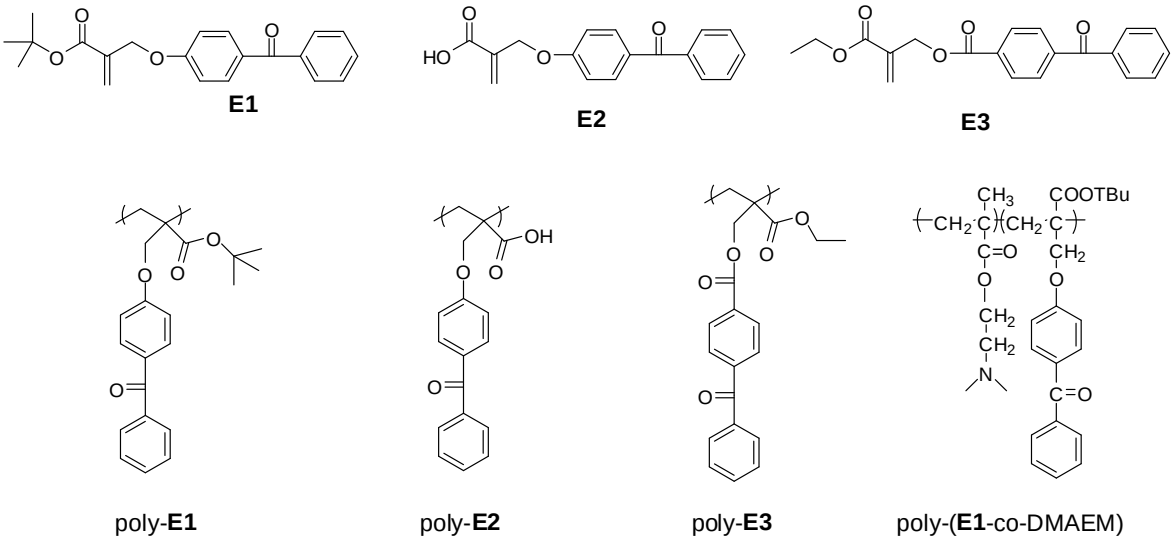

Figure 7.1. Structures of polymerizable and polymeric photoinitiators.

It is suggested that the choice of polymeric backbone might also effect the photoinitiation activity. While polymeric photoinitiators were prepared with different polymeric backbones, no RHMA-based ones are reported in the literature. The purpose of this work is to develop such new polymeric photoinitiators and investigate their structure-activity for UV curable coatings. We report synthesis and characterization of three polymerizable and three polymeric photoinitiators bearing side-chain benzophenone groups (Figure 7.1). Their photopolymerization efficiencies were compared with non-bound benzophenone in the polymerizations of TEGDMA, HDDA and HEMA using

photodifferential scanning calorimeter (photo-DSC). Also one copolymeric photoinitiator from one of the polymerizable initiators and a coinitiator (DMAEM) was prepared in order to observe the effect on the photoinitiation activity of having the coinitiator also on the polymer, hence always in close vicinity to BP group.

7.2. Experimental Work

7.2.1. Materials and Apparatus

7.2.1.1. Materials. Ethyl α-bromomethacrylate (EBBr) and *tert*-butyl α-bromomethacrylate (TBBr) were synthesized according to literature procedures [71, 72]. 4-hyroxybenzophenone, 3-benzoylbenzoic acid, trifluoroacetic acid (TFA), triethylene glycol dimethacrylate (TEGDMA), 1,6-hexanedioldiacrylate (HDDA), N,N-dimethyl para toluidine, N-methyldiethanolamine (MDEA), N,N-dimethylaminoethyl methacrylate (DMAEM), benzophenone (BP), 2-hydroxyethylmethacrylate (HEMA), 2,2'-azobis(isobutyronitrile) (AIBN), 2,2'-dimethoxy-2-phenyl acetophenone (DMPA) and all other reagents and solvents were obtained from Aldrich Chemical Co. and used as received.

7.2.1.2. Apparatus. ^{1}H and ^{13}C-NMR spectra were taken on Varian Gemini (400 MHz) spectrometer. IR spectra were obtained on a T 380 FTIR spectrometer. Elemental analysis were obtained from Thermo Electron SpA FlashEA 1112 elemental analyser (CHNS separation column, PTFE; 2m; 6x5 mm). The photopolymerizations were carried out on a TA Instruments Q100 differential photocalorimeter (DPC). Gel permeation chromatography (Viscotek) was carried out with THF solvent using polystyrene standards. UV spectra were recorded on a Shimadzu UV-1601 spectrometer.

7.2.2. Synthesis of Polymerizable Photoinitiators

7.2.2.1. Synthesis of *Tert*-butyl 2-((4-benzoylphenoxy)methyl)acrylate (**E1**). To a mixture of 4-hyroxybenzophenone (0.476 g, 2.4 mmol) and K_2CO_3 (3.44 g, 24.9 mmol) in acetone

(5 mL) under a stream of nitrogen, TBBr (0.575 g, 2.6 mmol) was added dropwise at room temperature. The mixture was stirred at 60 °C for 48 h under nitrogen. After removal of the solvent, the mixture was diluted with CH_2Cl_2 and extracted with water (3x5mL). The organic phase was dried over anhydrous sodium sulfate, filtered and evaporated under reduced pressure. The residue was recrystallized from methanol and dried under vacuum to give pure product as a white solid in 68% yield (mp 53-54 °C).

^{1}H-NMR ($CDCl_3$, 400 MHz, δ): 1.5 (s, 9H, CH_3), 4.8 (s, 2H, CH_2-O), 5.9 (s, 1H, CH_2=C), 6.3 (s, 1H, CH_2=C), 6.9 (d, 2H, CH-C), 7.5 (m, 3H, CH-CH), 7.8 (m, 4H, CH-C).

^{13}C-NMR ($CDCl_3$, 400 MHz, δ): 28.0 (CH_3), 66.5 (CH_2-O), 81.5 (C-CH_3), 114.5 (Ar-CH), 125.7 (C=*C*H_2), 128.1 (Ar-CH), 130.4 (Ar-CH), 131.9 (Ar-C), 132.5 (Ar-CH), 132.7, (CH-CH), 136.7 (Ar-C), 138.7 (*C*=CH_2), 161.9 (C-O), 164.5 (C=O ester), 195.6 (C=O ketone).

FTIR (ATR, cm^{-1}): 2976 (C-H), 1696 (C=O), 1643 (C=C), 1142 (C-O). Anal. Calcd for :

ELEM. ANAL., Calcd. For $C_{21}H_{22}O_4$: C, 74.54%; H, 6.55%; O, 18.91%. Found: C, 74.27%; H, 6.72%; O, 18.78%.

7.2.2.2. Synthesis of 2-((4-Benzoylphenoxy)methyl)acrylic acid (**E2**). Trifluoroacetic acid (0.5 mL) was added dropwise to **E1** (0.2 g, mol) in an ice bath under a stream of nitrogen. The mixture was stirred at room temperature for 1 day. After removal of excess trifluoroacetic acid, the crude product was recrystallized from methanol. The pure product was obtained as a white solid in 47% yield (mp 70-71 °C).

^{1}H-NMR ($CDCl_3$, 400 MHz, δ): 4.9 (s, 2H, CH_2-O), 6.2 (s, 1H, CH_2=C), 6.6 (s, 1H, CH_2=C), 7.0 (d, 2H, CH-C), 7.5 (t, 2H, CH-CH), 7.6 (t, 1H, CH-CH), 7.7 (d, 2H, CH-C), 7.8 (d, 2H, CH-C).

^{13}C-NMR ($CDCl_3$, 400 MHz, δ): 65.8 (CH_2-O), 114.3 (CH-C), 128.2 (CH-CH), 129.5, 129.8 (CH-C), 130.7 (*C*-CH_2), 132.6 (C-CO, CH-CH), 134.6 (C-CO), 138.7 (*C*H_2-C), 161.7 (C-O), 170.2 (CO ester), 195.7 (CO ketone).

FTIR (ATR, cm^{-1}): 1713 (C=O), 1683 (C=O), 1646 (C=C), 1115 (C-O).

7.2.2.3. Synthesis of 2-(Ethoxycarbonyl)allyl 4-benzoylbenzoate (**E3**). A mixture of 3-benzoylbenzoic acid (2.26 g, 10 mmol), EBBr (1.93 g, 10 mmol), K_2CO_3 (1.38 g, 10 mmol) and methyl ethyl ketone (MEK) (25 mL) was stirred at 60 ºC for 24 h under a stream of nitrogen. After removal of the solvent, the mixture was diluted with CH_2Cl_2 and extracted with water (3x5 mL). The organic phase was dried over anhydrous sodium sulfate, filtered and evaporated under reduced pressure. The crude product was recrystallized from methanol to give pure product as a white solid in 78% yield (mp 61-62 °C).

^{1}H-NMR ($CDCl_3$, 400 MHz, δ): 1.2 (t, 3H, CH_3), 4.2 (q, 2H, CH_2-CH_3), 5.0 (s, 2H, CH_2-O), 5.9 (s, 1H, CH_2=C), 6.4 (s, 1H, CH_2=C), 7.4 (t, 2H, CH-CH), 7.5 (t, 1H, CH-CH), 7.7 (d, 2H, CH-C), 7.9 (d, 2H, CH-C), 8.2 (d, 2H, CH-C).

^{13}C-NMR ($CDCl_3$, 400 MHz, δ): 14.2 (CH_3), 61.1 (CH_2-CH_3), 63.2 (CH_2-O), 127.5, 128.5, 130.0, 131.0 (CH-C), 133.2, 134.3, 138.0 (C-CH), 132.9 (*C*-CH_2), 136.9 (*C*-CH_2), 165.0, 165.2 (C=O ester), 195.67 (C=O ketone).

FTIR (ATR, cm^{-1}): 1735 (C=O), 1723 (C=O), 1705 (C=O), 1652 (C=C), 1104 (C-O). Anal. Calcd for : C, 71.01; H, 5.33; . Found: C, 70.69; H, 5.47.

ELEM. ANAL., Calcd. For $C_{20}H_{18}O_5$: C, 70.99%; H, 5.36%; O, 23.64%. Found: C, 70.69%; H, 5.47%; O, 23.79%.

7.2.3. Synthesis of Polymeric Photoinitiators

The thermal homo- and copolymerizations were carried out with standard freeze-evacuate-thaw procedures:

(i) The homopolymerizations of monomers **E1** and **E3** were carried out in bulk at 60 °C with AIBN (0.5 wt%) as initiator. After six hours, the viscous polymer solutions were dissolved in methylene chloride and precipitated into a large excess of methanol. The precipitated polymers were repeatedly dissolved in methylene chloride and precipitated again in methanol, filtered, dried under vacuum and stored in the dark. Poly-**E1** and poly-**E3** was obtained in 23 and 35% yields. The homopolymerization of monomer **E2** was carried out in THF ([M]= 0.36 M, [AIBN]= $3x10^{-3}$ M). After eight hours, the viscous polymer solution was dissolved in DMF and precipitated into a large excess of methanol twice, filtered, dried under vacuum and stored in the dark. Poly-**E2** was obtained in 46% yield.

(ii) The copolymerization of monomer **E1** with DMAEM was carried out in bulk (**E1**: DMAEM, 1 : 1 mol%) at 60 °C with AIBN as initiator. After six hours, the viscous polymer solution was dissolved in methylene chloride and precipitated into a large excess of hexane. Poly(**E1**-co-DMAEM) was obtained in % 19 yield. The properties of the copolymer are reported in Tables 7.1 and 7.2.

7.2.4. Photopolymerizations

7.2.4.1. Photopolymerization Procedure. The samples (3-4 mg) were irradiated in an isothermal mode at 40 ^{0}C for 10 min with an incident light density of 20 mW/cm^2 under a nitrogen flow of 20 mL min^{-1}. Rates of polymerization were calculated according to the following formula:

$$\text{Rate} = \frac{(Q/s)\, M}{n\, \Delta H_p\, m} \qquad (7.1)$$

where Q/s is the heat flow per second, M the molar mass of the monomer, n the number of double bonds per monomer molecule, ΔH_p the heat released per mole of double bonds

reacted and m the mass of monomer in the sample. The theoretical value used for ΔH_p is 13 kcal/mol for methacrylate double bonds [73, 74].

7.3. Results and Discussion

7.3.1. Synthesis and Characterization of Polymerizable Photoinitiators

Three new polymerizable photoinitiators (**E1-E3**) comprising benzophenone groups were synthesized by one step reaction according to Figure 7.2, and their structures were confirmed by spectroscopic and elemental analysis. Photoinitiator **E1** was synthesized through nucleophilic substitution reaction of 4-hydroxybenzophenone with TBBr under basic conditions using acetone as the solvent. Hydrolysis of the *tert*-butyl groups of **E1** with CF_3COOH gave a new photoinitiator **E2** with both benzophenone and carboxylic acid functionality. This initiator may not require an additional coinitiator due to the presence of a hydrogen donating carboxylic acid group in its structure. Photoinitiator **E3** was synthesized from reaction of EBBr with 3-benzoylbenzoic acid using potassium carbonate as catalyst and acetone as the solvent. All the initiators were obtained as white solids (melting points of 53-54, 70-71 and 61-62 ºC for **E1**, **E2** and **E3**) in 47-78 % yield after recrystallization from methanol. They are soluble in polar organic solvents such as methylene chloride, acetone, ether, methanol and THF but insoluble in water (Table 7.1).

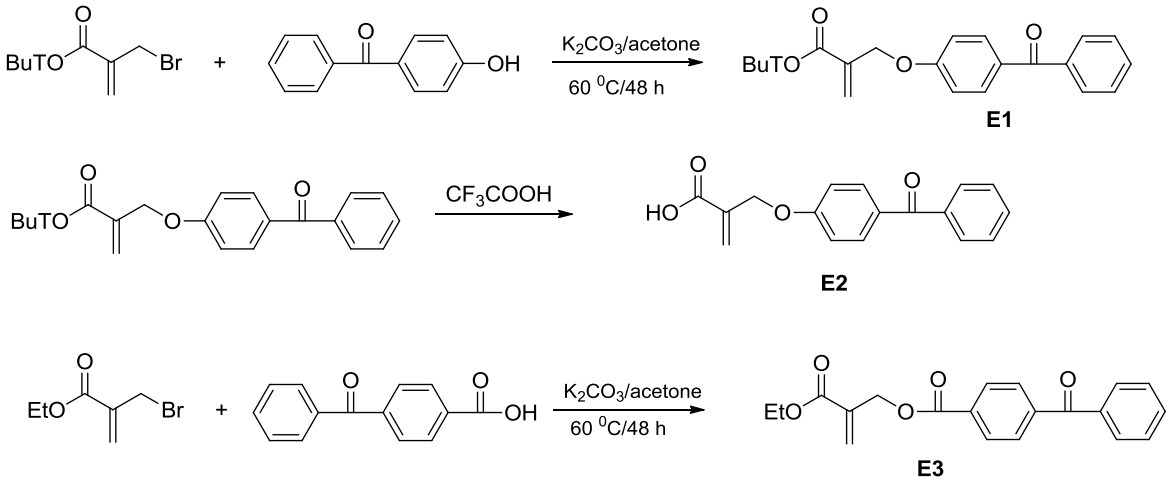

Figure 7.2. Synthesis of novel polymerizable benzophenone-containing photoinitiators.

Table 7.1. Solubilities of polymerizable and polymeric photoinitiators.

Photoinitiators	**Acetone**	**THF**	**CH_2CI_2**	**MeOH**	**ether**	**H_2O**	**DMSO**
E1	+	+	+	+	+	-	+
E2	+	+	+	+	+	-	+
E3	+	+	+	+	+	-	+
Poly-**E1**	+	+	+	-	-	-	-
Poly-**E2**	-	-	-	-	-	-	+
Poly-**E3**	+	+	+	-	-	-	+
P(**E1**-co-DMAEM)	+	+	+	-	-	-	-

The spectral data are in agreement with the expected structure of the initiators. For example, ^{13}C NMR spectrum of **E1** is characterized by *tert*-butyl carbons at 28.0 and 81.5 ppm, aromatic carbons in the range of 114.5-136.7 ppm, double bond carbons at 125.7 and 138.7 ppm and two different carbonyls at 164.5 (ester) and 195.6 (ketone) ppm (Figure 7.3). The structure of **E2** is supported by the complete disappearance of the *tert*-butyl carbons of **E1**. ^{1}H-NMR spectrum of initiator **E3** is characterized by aromatic protons at 7.4-8.3 ppm, double bond protons at 5.9 and 6.4 ppm, methylene protons adjacent to oxygen at 5.0 ppm and methyl protons at 1.2 ppm (Figure 7.4). In the FTIR spectrum of the **E1**, characteristic of the stretching vibration of the two different C=O bonds at 1696(ester), 1643(ketone) cm^{-1} was observed. In the FTIR spectra of the poly-**E1**, characteristic of the stretching vibration of the two different C=O bonds at 1723(ester), 1654(ketone) cm^{-1} was observed (Figure 7.5). On the other hand, in the FTIR spectra of the **E3**, characteristic of the stretching vibration of the three different C=O bonds at 1735 (ester), 1723 (ester) and 1705 (ketone) cm^{-1} was observed.

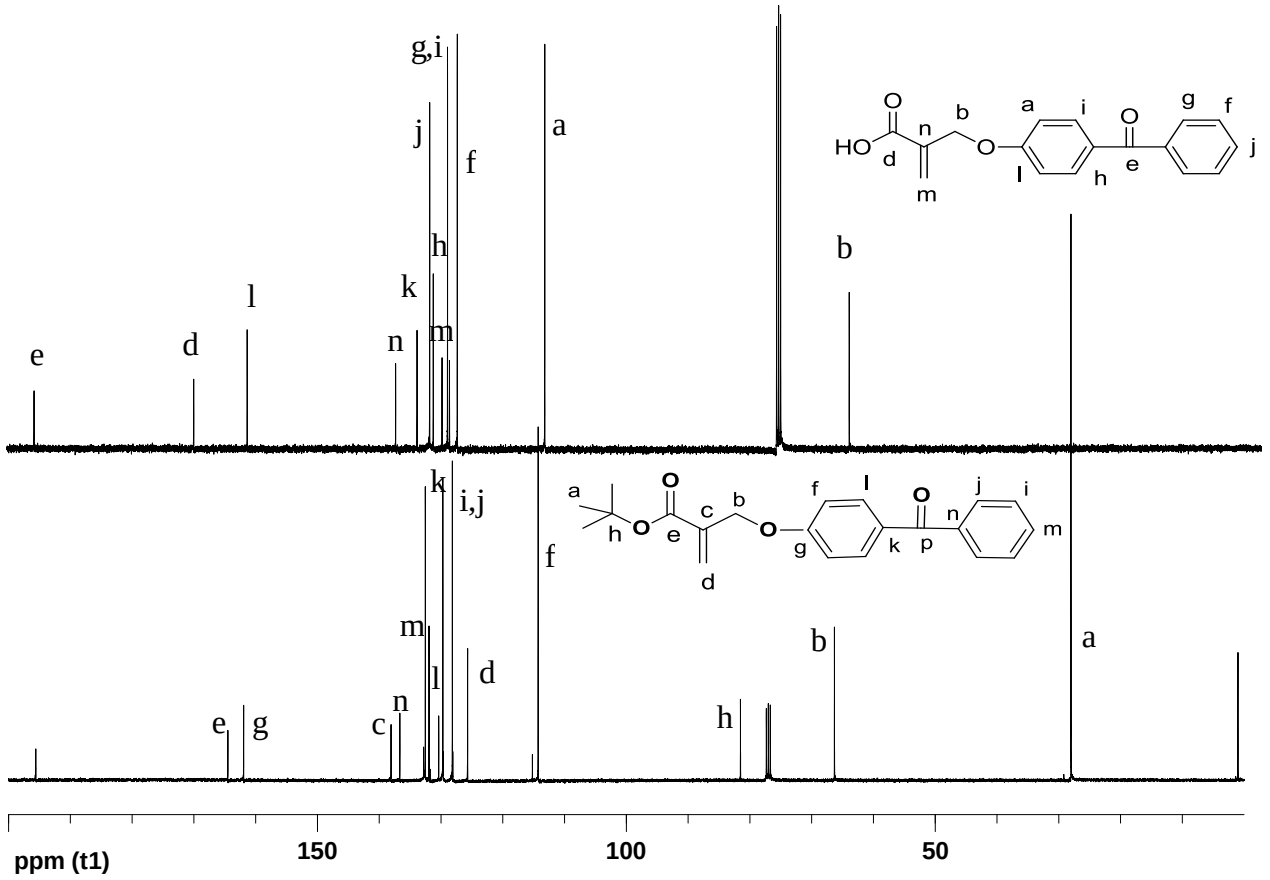

Figure 7.3. ^{13}C NMR spectra of **E1** and **E2**.

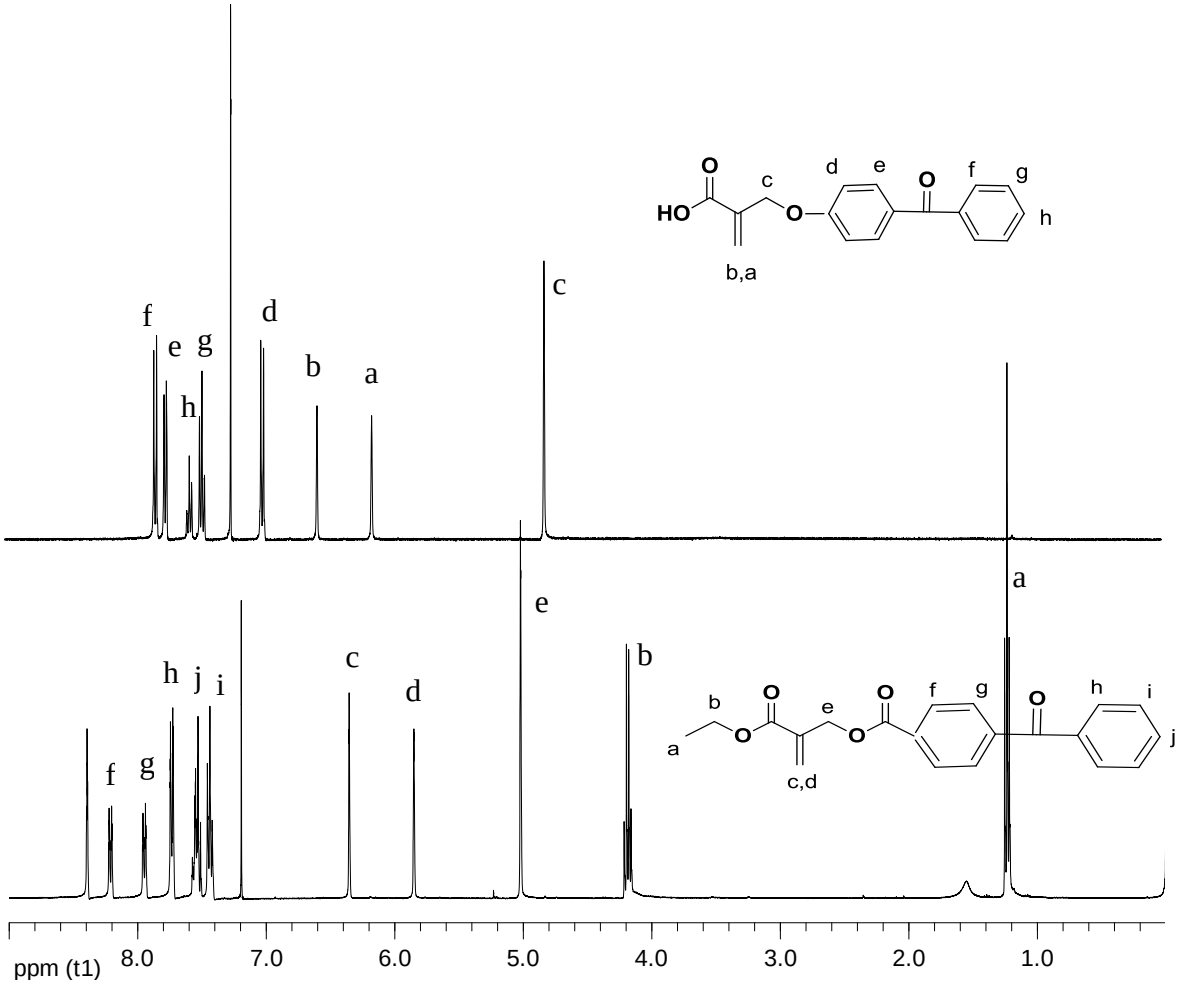

Figure 7.4. ^{1}H NMR spectra of **E2** and **E3**.

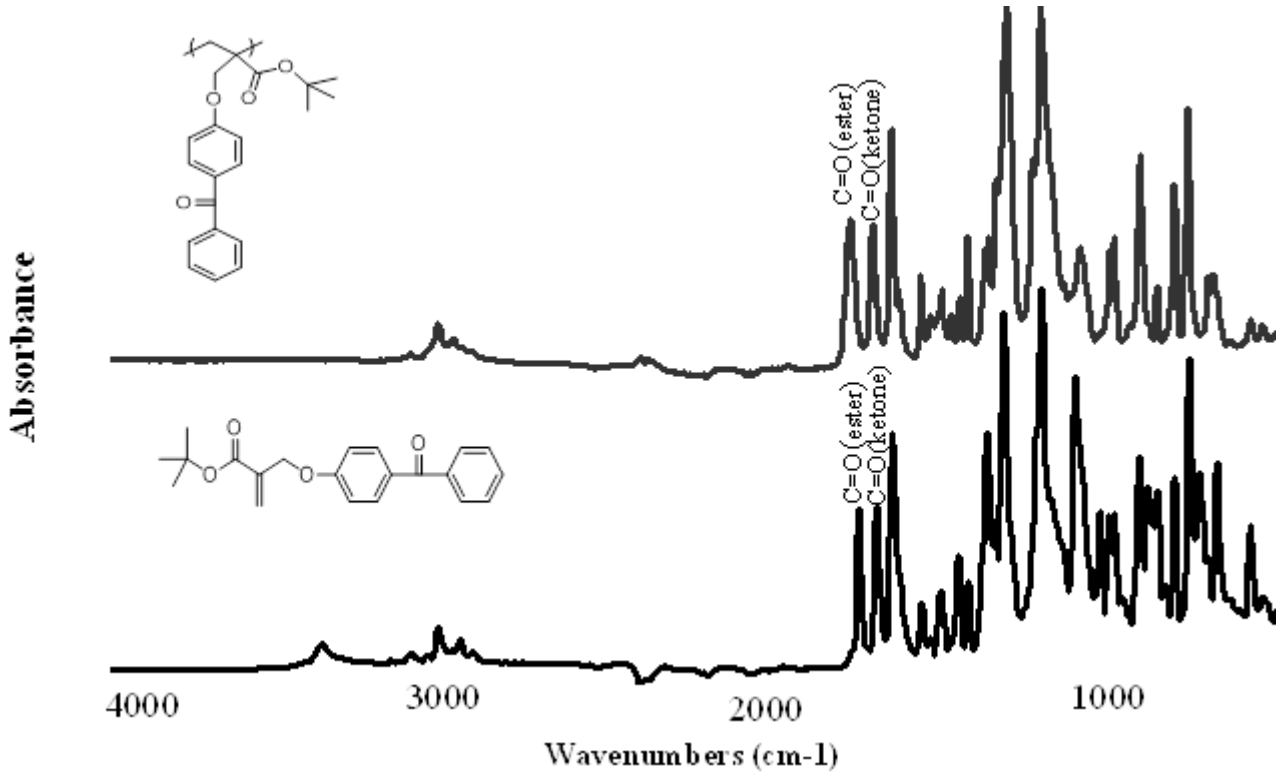

Figure 7.5. FTIR spectra of **E1** and poly-**E1.**

7.3.2. Synthesis and Characterization of Polymeric Photoinitiators

In order to synthesize novel polymeric photoinitiators bearing side-chain BP, polymerizable photoinitiators **E1-E3** were bulk and solution polymerized with AIBN at 60 ºC using standard freeze-evacuate-thaw procedures (Table 7.2). The polymers were obtained as white solids with 23-46 % yield after repeated precipitations into methanol and characterized by ^{1}H NMR, FTIR spectrometry, GPC and DSC. ^{1}H NMR spectra of the polymers showed no peaks at around 5.9 and 6.3 ppm related to the unsaturated methacrylate protons. The peaks in the 1.0-2.5 ppm region are due to ethyl or *tert*-butyl and backbone protons, in the 3.5-4.5 ppm region due to methylene protons attached to oxygen atom as well as the peaks in 6.5-8.5 ppm the region due to aromatic protons (Figure 7.6). Also, the occurrence of polymerizations were confirmed by the occurrence of the C=O peak due to saturated *ethyl* or *tert*-butyl ester in the FTIR spectra. The number average molecular weight of the polymer obtained from **E3** (M_n= 63350) was found to be much higher than those obtained from **E1** (M_n= 17360). Experience has shown higher k_p to k_t ratios for ester derivatives than for ether derivatives, leading to inherently longer kinetic chain length. In particular, evaluation of k_p and k_t for ethyl α-benzoyloxymethacrylate in benzene gave values of 990 and 2.9x10^6 L/mol s^{-1} compared to methyl 2-(phenoxymethyl)acrylate with k_p and k_t values of 182 and 1.6x10^6 L/mol s^{-1}, respectively at 60 ^{0}C.

Poly-**E1** and poly-**E3** are well soluble in common organic solvents such as acetone, THF, methylene chloride and DMSO but insoluble in methanol, ether and water. However, poly-**E2** was only soluble in dimethyl sulfoxide. DSC analysis of poly-**E1** and poly-**E3** showed a decrease in T_g as the bulkiness of the ester group decreased, from 138 ^{o}C for poly-**E1** to 96 ^{o}C for poly-**E3**. No T_g was observed for poly-**E2** upon heating to 190 ^{o}C. Monomer **E1** was copolymerized with DMAEM (1:1 ratio of **E1**:DMAEM) using AIBN as thermal initiator to obtain the corresponding polymer, poly(**E1**-co-DMAEM), having the coinitiator also on the polymer. The copolymer composition was determined by ^{1}H NMR analysis by integration of aromatic protons of **E1** with respect to other protons in the copolymer and found to be 2.3:1 (**E1**:DMAEM) (Figure 7.7). T_g value of the copolymer was around 71 ^{o}C.

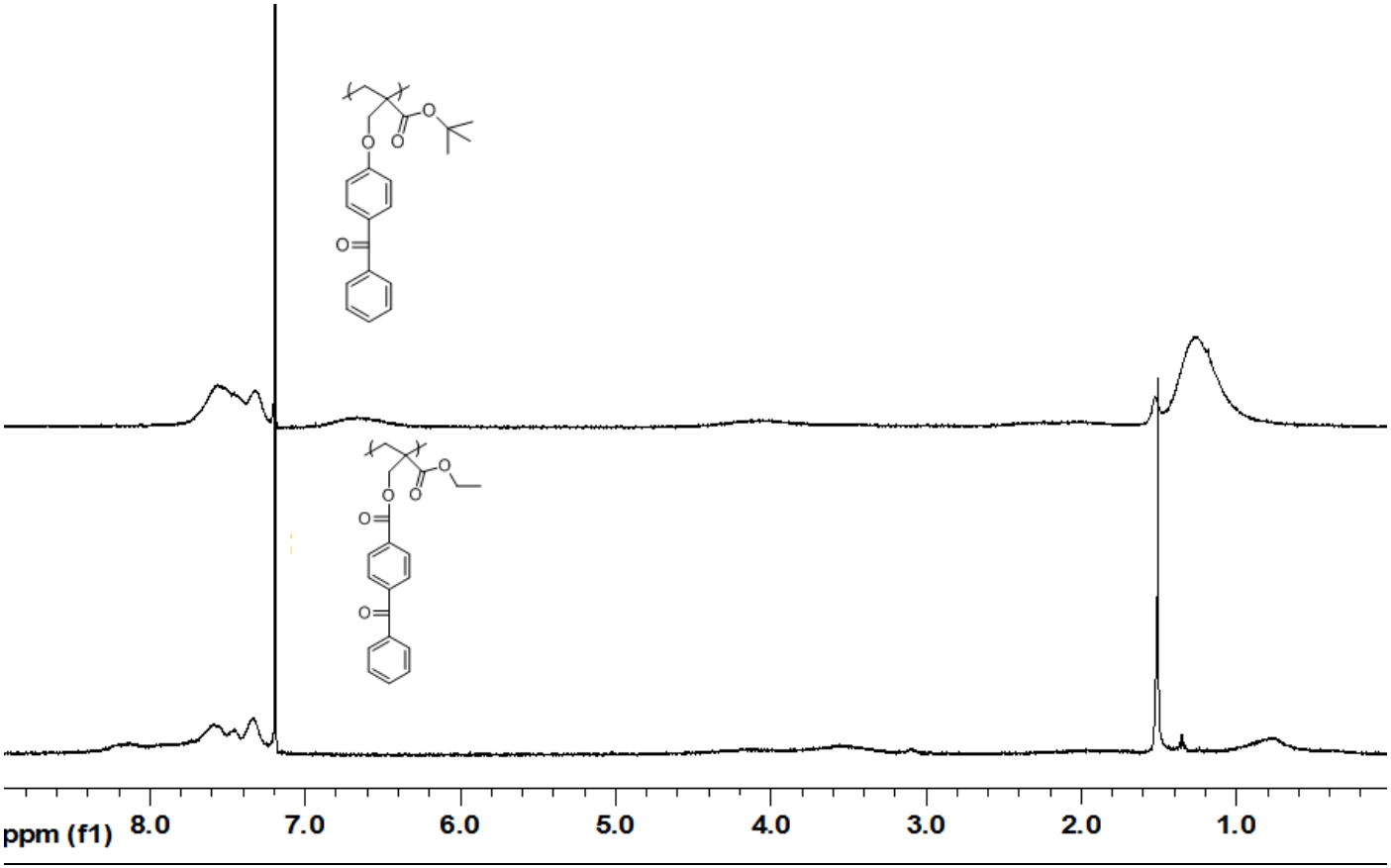

Figure 7.6. ^{1}H NMR spectra of poly-**E1** and poly-**E3**.

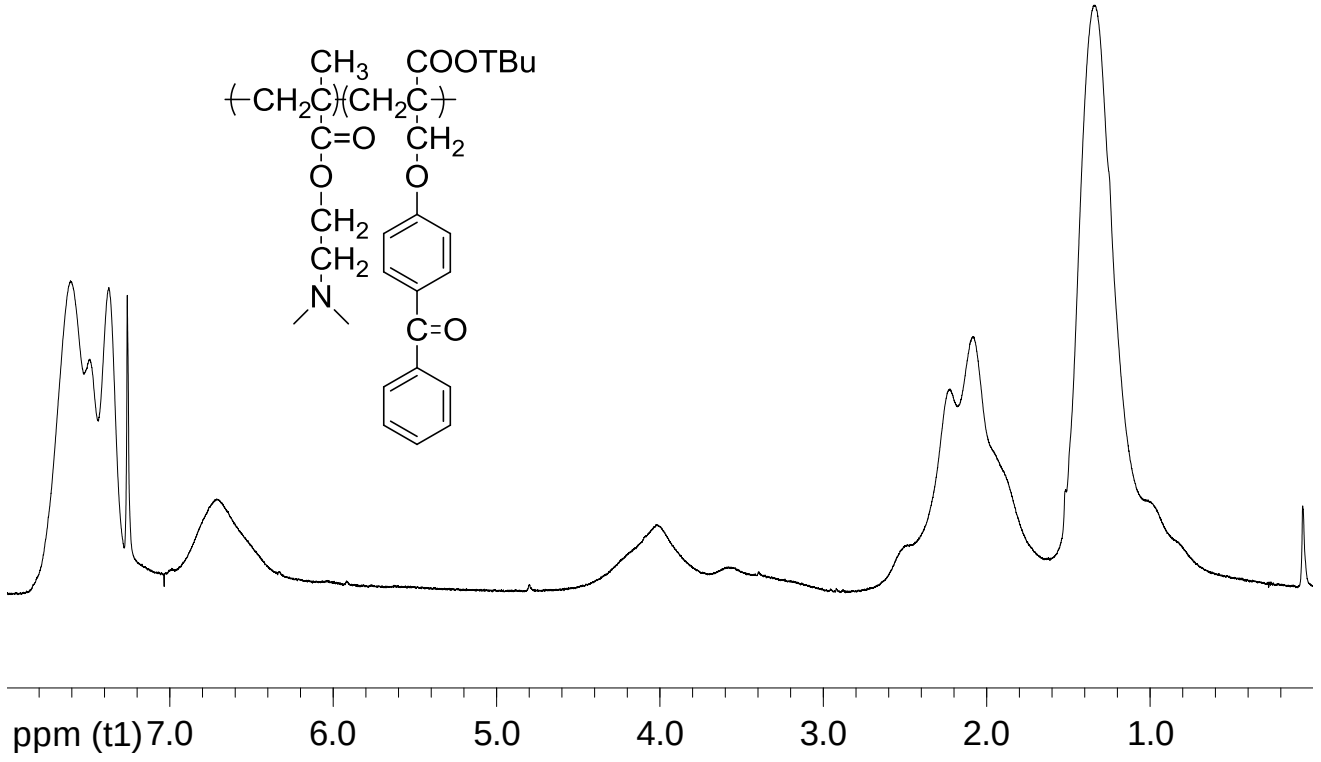

Figure 7.7. ^{1}H-NMR spectrum of poly(**E1**-co-DMAEM).

Table 7.2. Physical properties of polymeric photoinitiators.

PI	**Yield (%)**	**M_n**	**M_w/M_n**	**T_g (^oC)**
Poly-**E1**	23	17360	1.4	138
Poly-**E2**	35	-	-	-
Poly-**E3**	46	63350	1.7	96
P(**E1**-co-DMAEM)	19	54995	1.6	71
P(DMAEM)	-	325741	0.5	-

Poly- **E2** is not soluble in THF

7.3.3. UV/Vis Spectral

UV-vis spectroscopy in DMF was carried out to investigate the absorption characteristics of the monomeric and polymeric photoinitiators (**E1**-**E3**, poly-**E1**, poly-**E2**, poly-**E3** and poly(**E1**-co-DMAEM)) together with BP as the reference (Figure 7.8 and 7.9). The wavelength of maximum absorption (λ_{max}) and molar extinction coefficient (ε) are summarized in Table 7.3. BP has π-π^* transitions as a distinct maximum in 250 nm region and n-π^* transitions as a shoulder of π-π^* transitions in the range of 300-350 nm. The n-π^* transitions have low extinction coefficient due to the spin forbidden transition. In polymerizable initiators **E1** and **E2**, a significant red-shift of the π-π^* transition (289 nm) was observed, probably due to the electron donating effect of oxygen directly attached to the benzophenone unit (Figure 7.8, Table 7.3). This red-shifted transition can provide UV-curing near to the wavelength of visible light. The n-π^* transitions of these initiators was also observed as a shoulder around 350 nm. Monomeric initiator **E3** showed completely different maximum of absorption (255 nm) compared to **E1** and **E2** and similar to BP. The difference can be explained by the electron withdrawing effect of ester group attached to the benzophenone unit. The different maximum absorptions indicate that the structures of the initiators have significant influence on the UV-vis absorption of BP groups. Both the maximum of absorption and the molar extinction coefficient are important parameters to determine the photoefficiency of the photoinitiators.

Polymeric photoinitiators exhibit the similar characteristic absorption with their monomers, indicating that the chain structure has an important effect on the maximum absorption of BP groups.

Figures 7.10-7.16 show the UV spectral changes of monomeric, polymeric and copolymeric initiators in the presence of an amine, MDEA upon photolysis. As the photolysis proceeds, the photoinitiators are consumed and their absorption spectra change. At the end of the irradiation, the absorption bands of both polymerizable and polymeric photoinitiators at 280 nm were almost completely disappeared and new bands at around 330 nm due to formation of ketyl radicals were appeared.

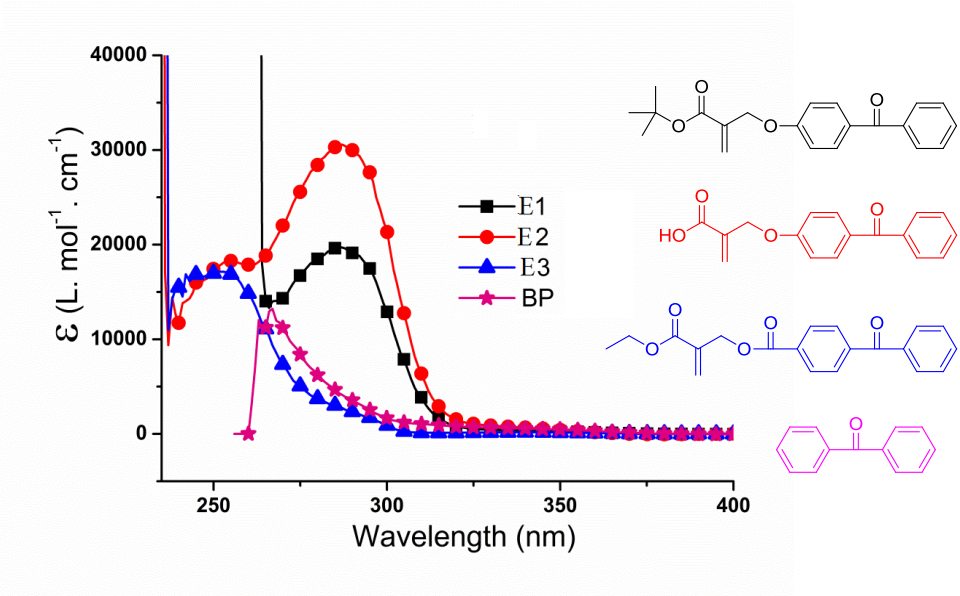

Figure 7.8. UV/Vis absorption spectra of **E1-E3** and BP in DMF solution.

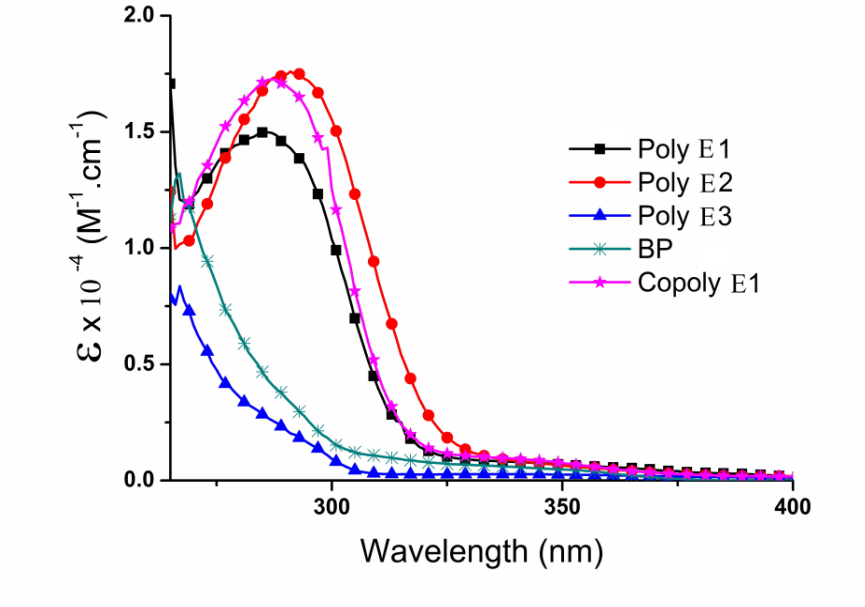

Figure 7.9. UV/Vis absorption spectra of polymeric photoinitiators and BP in DMF solution.

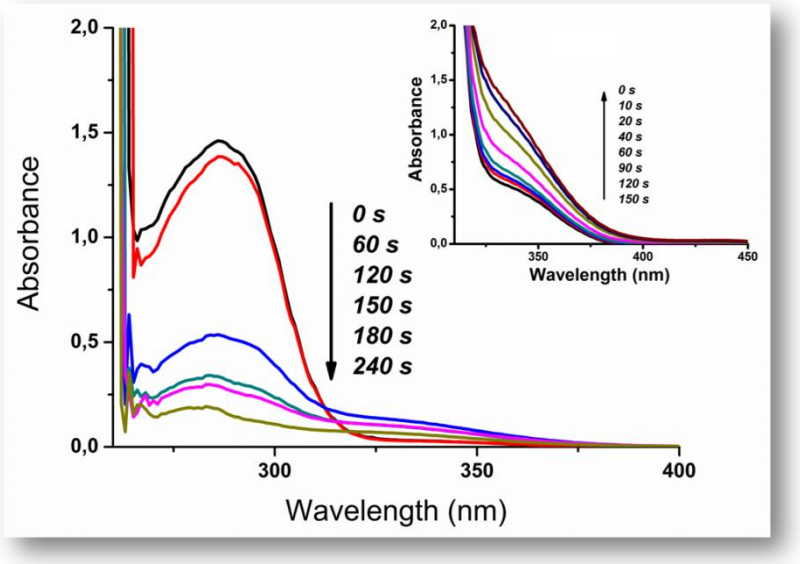

Figure 7.10. Absorption spectra of **E1** (7.4×10^{-5} mol L^{-1})/MDEA(1.0×10^{-2} mol L^{-1}) at 280 nm and **E1** (1.0×10^{-3} M), MDEA (1×10^{-2} M) at 330 nm in DMF solution.

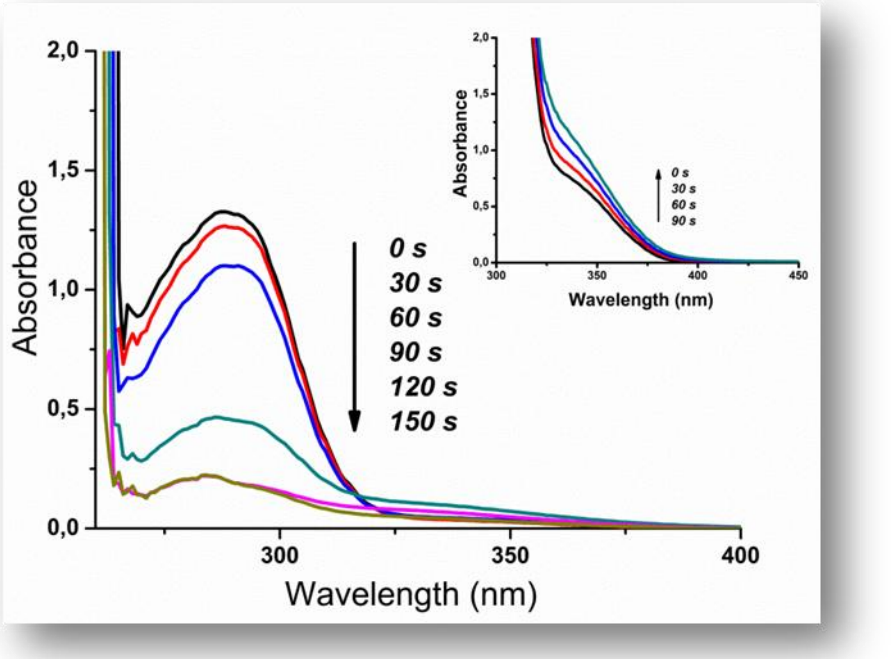

Figure 7.11. Absorption spectra of **E2** (4.8×10^{-5} mol L^{-1})/MDEA(1.0×10^{-2} mol L^{-1}) at 280 nm and **E2** (2.0×10^{-3} M), MDEA (1×10^{-2} M) at 330 nm in DMF solution.

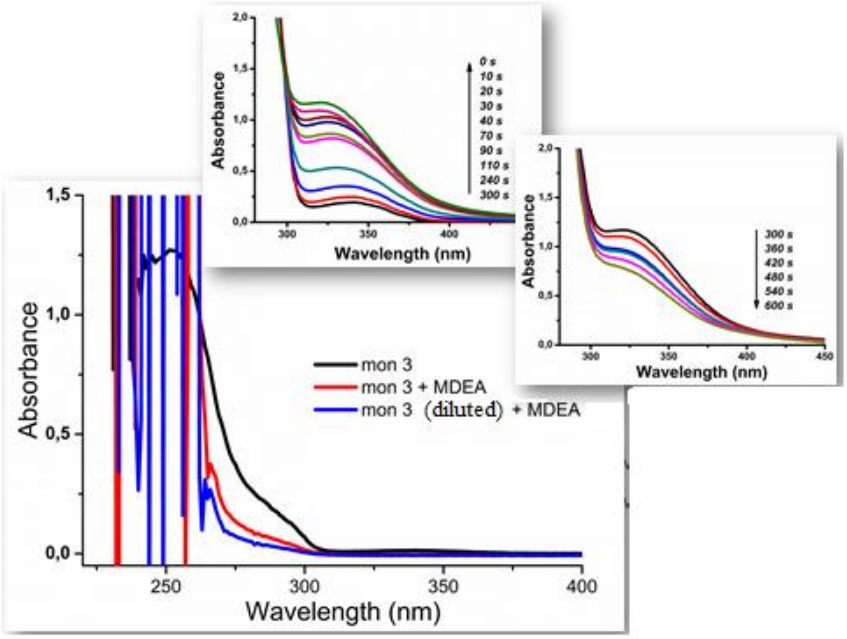

Figure 7.12. Absorption spectra of **E3** (7,4 x 10^{-5} mol L^{-1})/MDEA(1.0x10^{-2} mol L^{-1}) at 280 nm and **E3** (1.0 x 10^{-3} M), MDEA (1x10^{-2} M) at 330 nm in DMF solution.

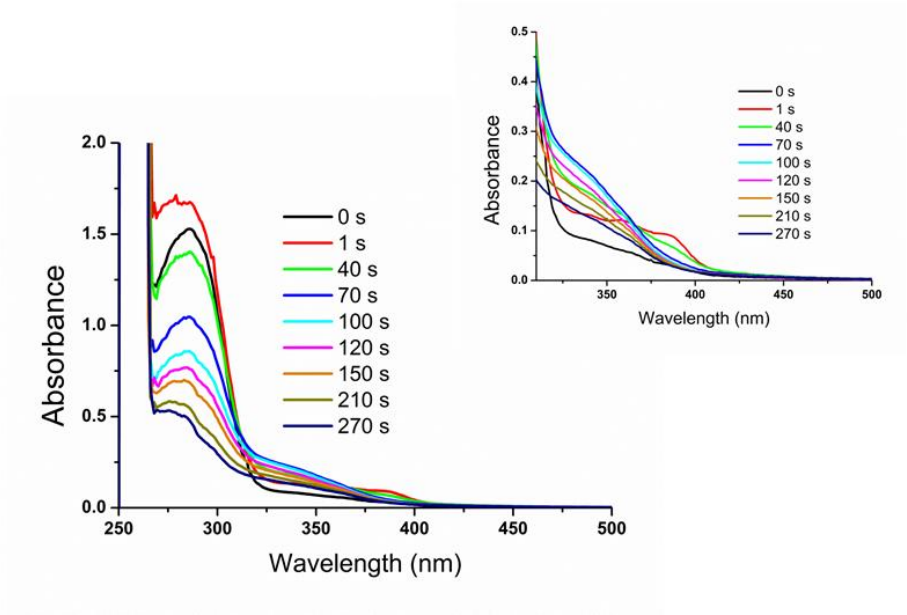

Figure 7.13. Absorption spectra of poly-**E1** (2 x 10^{-6} mol L^{-1})/MDEA(1.0x10^{-2} mol L^{-1}) at 280 and 330 nm in DMF solution.

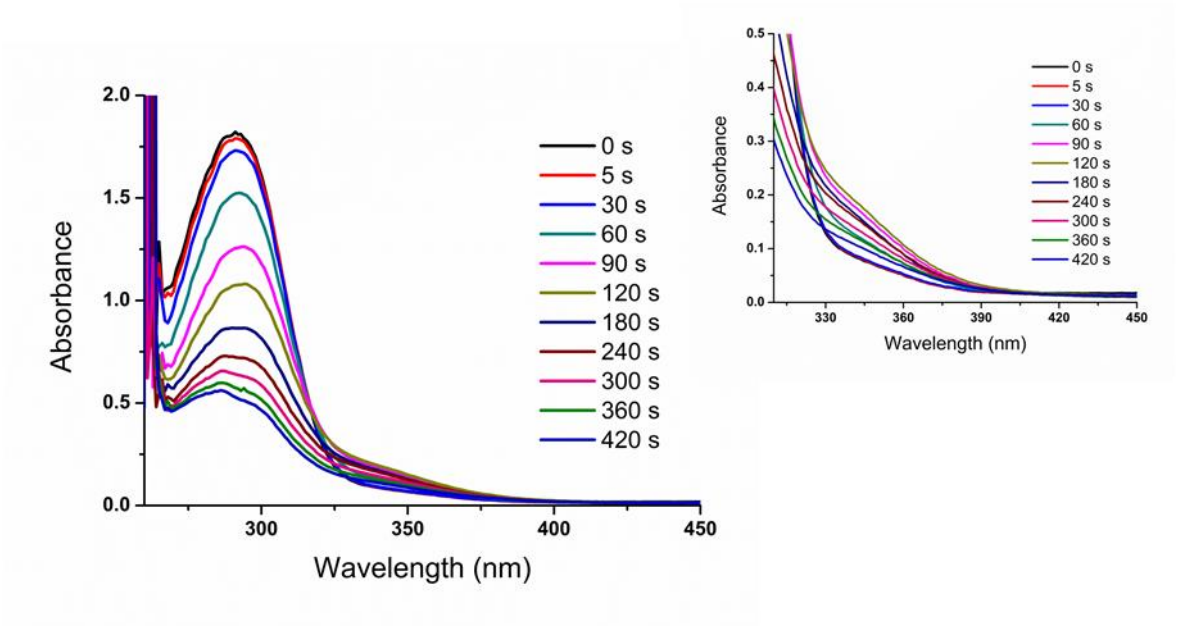

Figure 7.14. Absorption spectra of poly-**E2** (2 x 10^{-6} mol L^{-1})/MDEA(1.0x10^{-2} mol L^{-1}) at 280 and 330 nm in DMF solution.

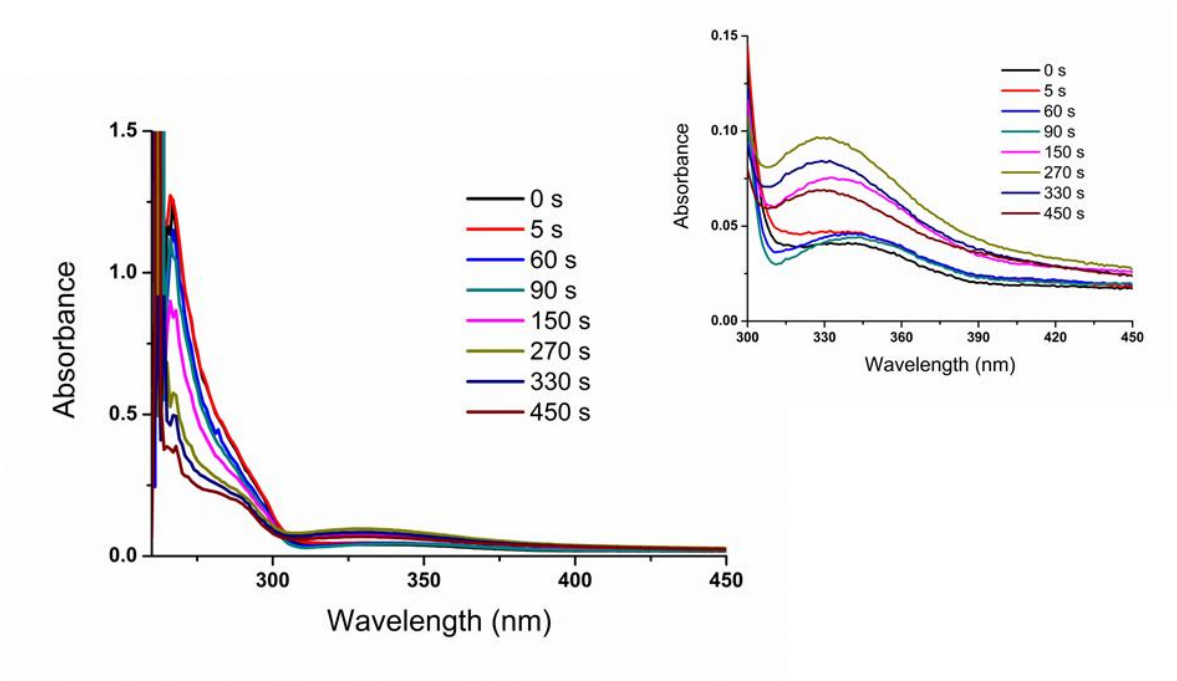

Figure 7.15. Absorption spectra of poly-**E3** (8 x 10^{-7} mol L^{-1})/MDEA(1.0x10^{-2} mol L^{-1}) at 280 and 330 nm in DMF solution.

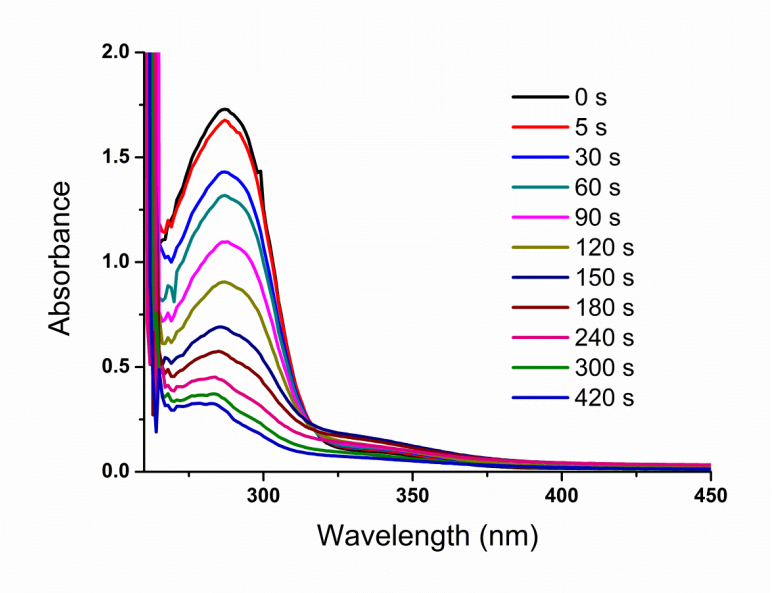

Figure 7.16. Absorption spectra of **E1**-co-DMAEM (9 x 10^{-7} mol L^{-1})/MDEA(1.0x10^{-2} mol L^{-1}) at 280 and 330 nm in DMF solution.

Table 7.3. λ_{max} and ε values of the synthesized polymerizable and polymeric photoinitiators and BP in DMF.

Photoinitiator	λ_{max} (nm)	**ε (L mol^{-1} cm^{-1})**
E1	289	19323
E2	289	30107
E3	255	16873
BP	267	13220
poly-**E1**	288	17288
poly-**E2**	294	14846
poly-**E3**	268	7730
poly(**E1**-*co*-DMAEM)	289	17086

Table 7.4. t_{max}, R_{pmax} and conversion values during photopolymerizations of TEGDMA.

Photoinitiator	**t_{max} (s)**	**R_{pmax} (s^{-1})x10^{-3}**	**Conversion (%)**
E1	198.0	4.04	59
E2	169.2	5.12	62
E3	167.4	4.57	59
BP	221.4	2.95	45
Poly-**E1**	120.6	12.89	72
Poly-**E2**	-	-	-
Poly-**E3**	109.8	11.81	64

7.3.4. Photoinitiating Activity

The photopolymerization efficiencies of polymerizable (**E1-E3**) and polymeric initiators (poly-**E1**, poly-**E3** and poly(DMAEM-*co*-**E1**) bearing benzophenone groups together with benzophenone were investigated in the photopolymerizations of TEGDMA using N,N-dimethyl-p-toluidine as coinitiator. Figure 7.17 and Table 7.4 show photopolymerization results such as time to reach the maximum polymerization rate (t_{max}), maximum rate of polymerization (R_{pmax}) and conversion obtained, using photo-DSC. It was clearly seen that the synthesized polymerizable photoinitiators exhibit improved t_{max}, R_{pmax} and conversion compared to BP. Among these initiators, **E2** and **E3** showed similar photoinitiation activity, with the lower t_{max} values of 169 and 167 s compared to **E1** and BP with t_{max} values of 198 and 221 s. The slightly lower photoinitiaton reactivity of monomeric initiator **E1** compared to the other two may be due to its bulky *tert*-butyl group. The better performance of polymerizable initiators compared to BP may be attributed to their higher light absorption properties.

The polymeric initiators were found to perform much better than their monomeric counterparts. The maximum rate of polymerization for TEGDMA initiated with the polymeric photoinitiators (poly-**E1** and poly-**E3**) were similar and 2.4-4 times greater than

that of TEGDMA initiated with the polymerizable photoinitiators. The conversions reached were 45, 59 and 72 % for benzophenone, **E1** and poly-**E1**, respectively. The t_{max} values of polymeric photoinitiators were even lower than monomeric ones, 121 and 110 s for poly-**E1** and poly-**E3**. Since poly-**E2** was not soluble in TEGDMA, we could not test its polymerization reactivity with this monomer. Therefore the properties of the three polymeric initiators were also investigated in HEMA using the same amine as coinitiator and BP was also used as reference initiator.

All of the polymeric initiators showed similar but improved t_{max}, reactivity and conversion in HEMA with respect to BP (Figure 7.18).

Figure 7.19 shows the photo-DSC profiles of HDDA initiated by benzophenone, poly-**E1** and poly-**E3** in the presence of coinitiater amine. Their polymerization behaviors appear to be similar to multifunctional TEGDMA monomer.

We also investigated photopolymerization of HDDA initiated by BP/DMAEM, **E1**/DMAEM, poly-**E1**/DMAEM, poly-**E1**/poly-DMAEM, poly(**E1**-*co*-DMAEM) at 40 ^{0}C (Figure 7.20). It was observed that there is a remarkable differences among photoinitiating systems. The systems constituted by combinations polymeric BP with both low and high molecular weight amine such as poly-**E1**/DMAEM and poly-**E1**/poly-DMAEM showed higher activity compared to the copolymer poly(**E1**-*co*-DMAEM). The copolymeric photoinitiator showed similar efficiency with the monomer combinations.

It is known that macromolecular radicals can be prevented from coupling reactions due to steric hindrance and results in higher initiation reactivity compared to low molecular weights counterparts. Therefore, poly-**E1**/DMAEM and poly-**E3**/poly-DMAEM systems were found have the highest efficiency. The lower initiating ability of the copolymer can be explained by the lower amount of DMAEM (**E1**:DMAEM ratio of 2.3:1) in the copolymer.

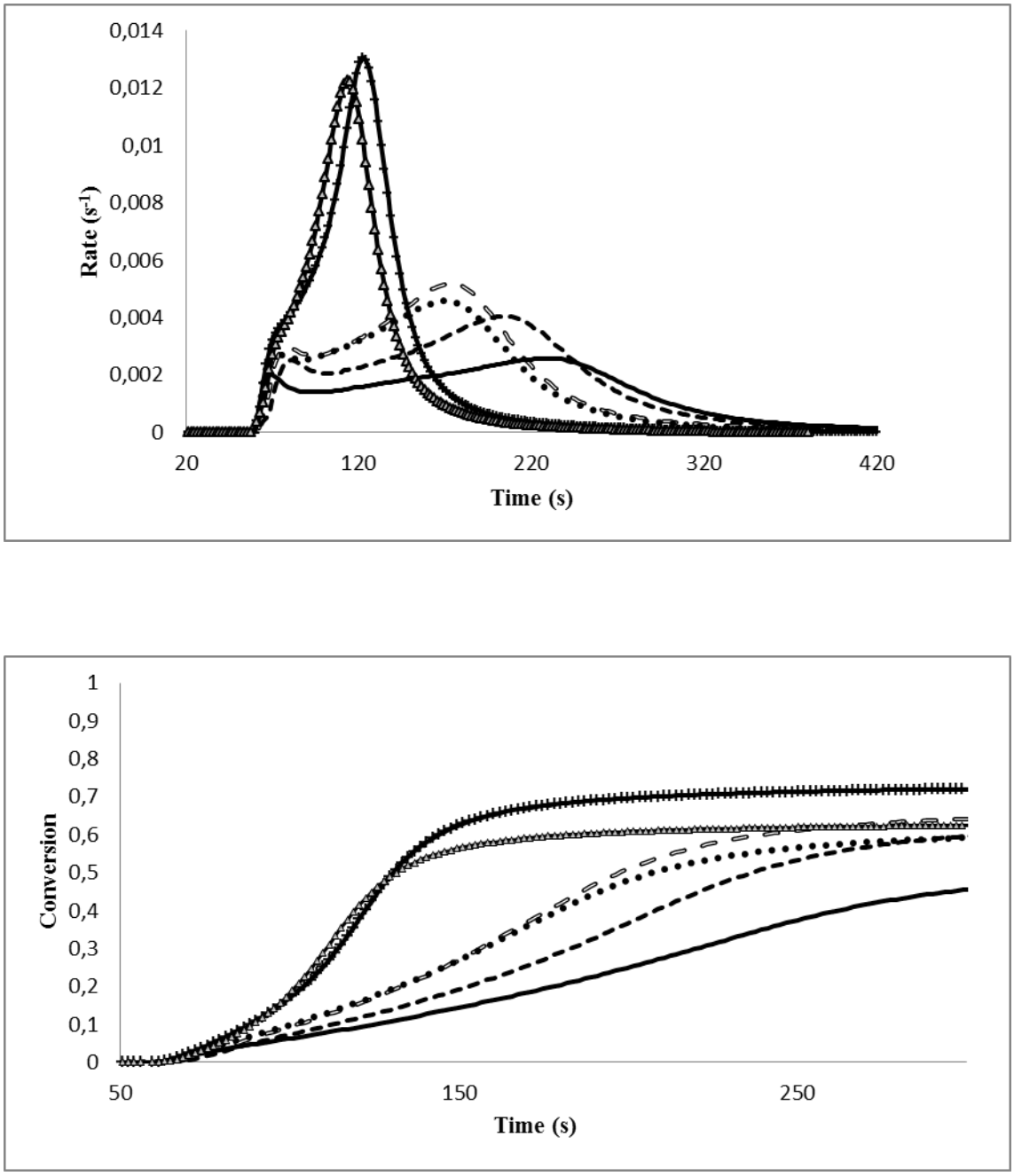

Figure 7.17. Rate-time and conversion-time plots for the photopolymerization of TEGDMA initiated by (-) BP, (--) **E1**; (═) **E2**; (•) **E3**; (+) poly-**E1**; (▲) poly-**E3**. Photoinitiator and amine (N,N-dimethyl-p-toluidine) concentration in monomer are 1 and 3 mol%.

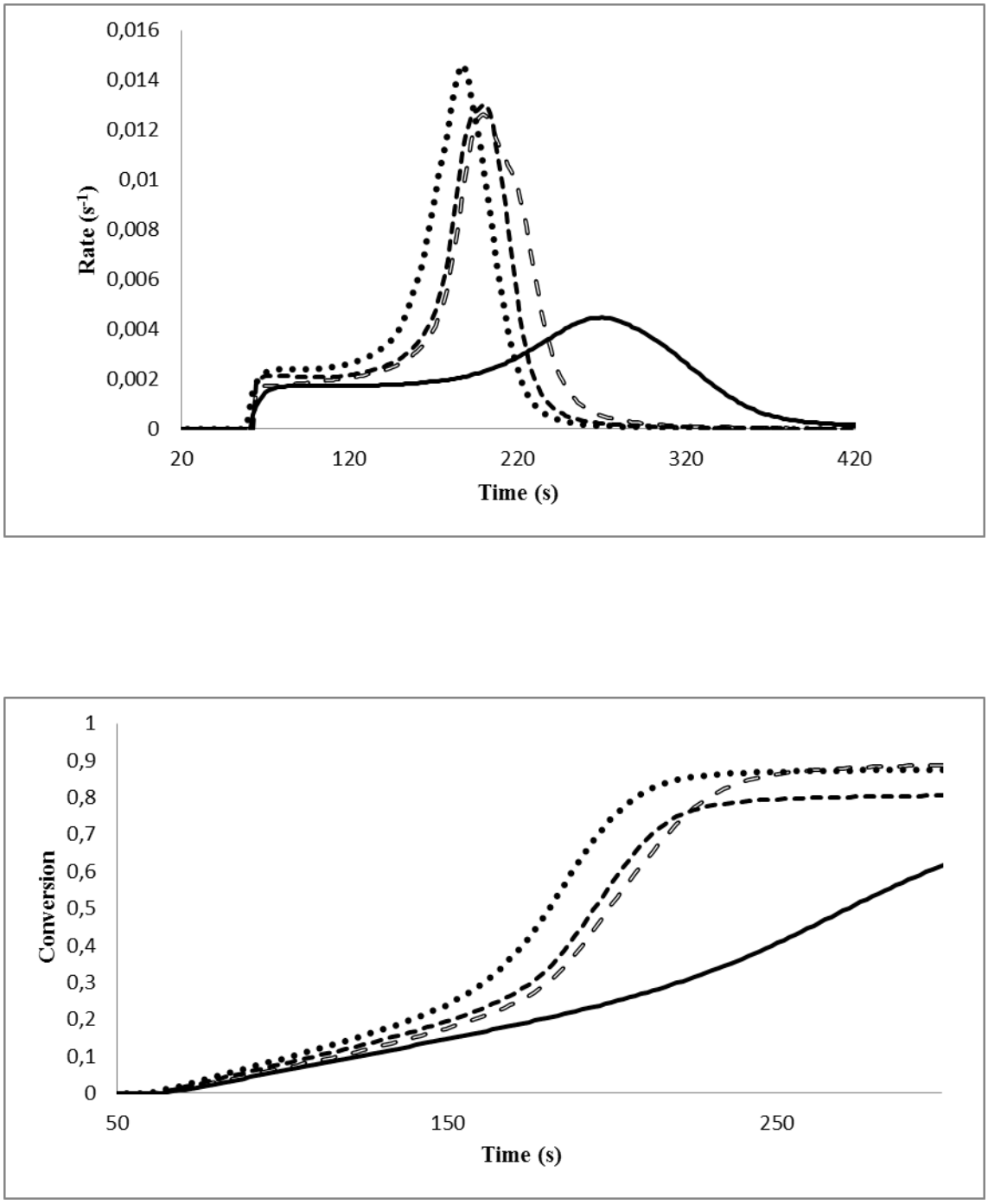

Figure 7.18. Rate-time and conversion-time plots for the photopolymerization of HEMA initiated by (-) BP; (--) poly-**E1**; (═) poly-**E2**; (•) poly-**E3**. Photoinitiator and amine (N,N-dimethyl-p-toluidine) concentration in monomer are 1 and 3 mol%.

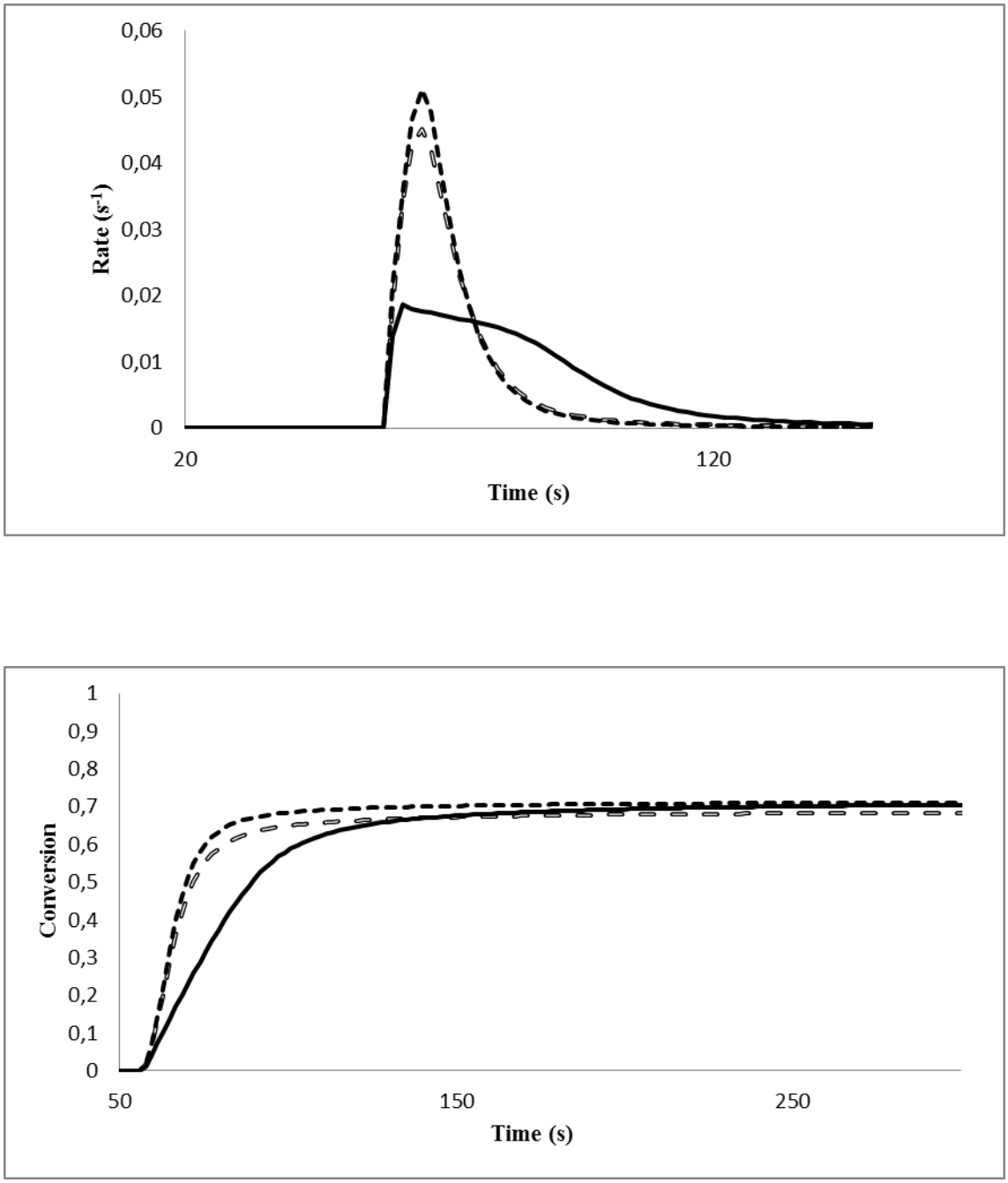

Figure 7.19 Rate-time and conversion-time plots for the photopolymerization of HDDA initiated by (-) BP; (--) poly-**E1**; (═) poly-**E3**. Photoinitiator and amine (N,N-dimethyl-p-toluidine) concentrations in monomer are 1 and 3 mol%.

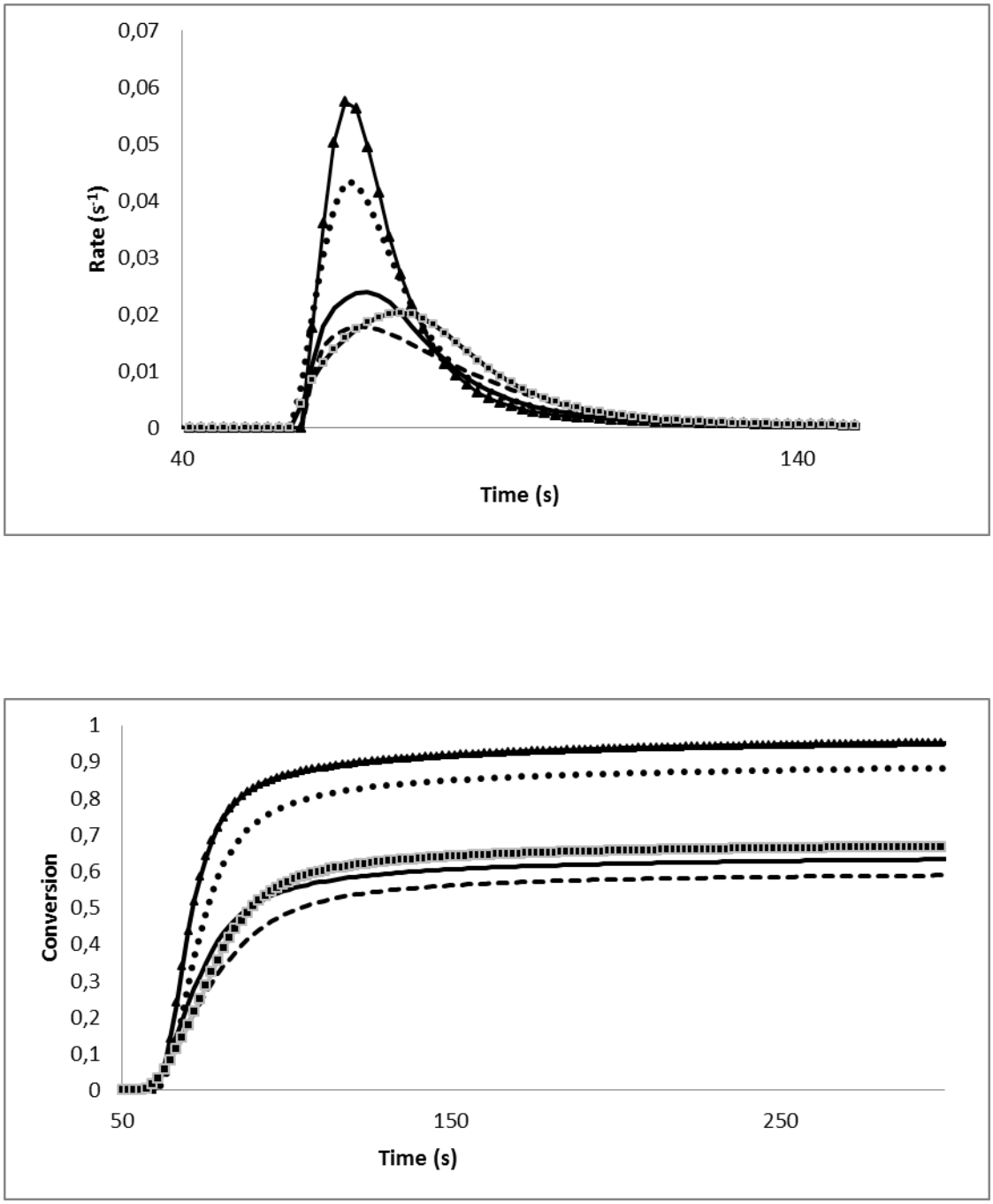

Figure 7.20. Rate-time and conversion-time plots for the photopolymerization of HDDA initiated by (-) BP/DMAEM; (--) P(**E1**-*co*-DMAEM) 1/1; (■) **E1**/DMAEM, (•) poly-**E1**/poly-DMAEM; (▲) poly-**E1**/DMAEM. Photoinitiator and amine (N,N-dimethyl-p-toluidine) concentrations in monomer are 1 and 3 mol%.

7.4. Conclusions

Three novel polymerizable photoinitiators containing side-chain benzophenone group were synthesized from RHMA's. Their homo- and copolymerization with an amine monomer, DMAEM, gave four novel polymeric initiators.

The polymerizable photoinitiators were found to initiate polymerization of TEGDMA more efficiently than benzophenone.

The polymeric initiators (homopolymers) in combination with low molecular weight tertiary amine resulted in photopolymerization of TEGDMA, HEMA and HDDA with a higher rate of polymerization compared to all low molecular weight combination (polymerizable photoinitiators and BP with low molecular weight amine).

8. CYCLIZATION TENDENCIES IN FREE RADICAL POLYMERIZATION OF ALLYL ACRYLATE DERIVATIVES: A COMPUTATIONAL STUDY

8.1. Introduction

Free-radical homopolymerization of allylic monomers, which have the general structure CH_2=CH-CH_2-X, are well known to polymerize at low rates and to yield polymers of low molar mass [175]. This is commonly believed to be due to "auto inhibition" arising from hydrogen abstraction from the allylic methylene group, followed by loss of the resulting allylic radicals via radical coupling reactions [176]. ESR experiments have shown that although allylic radicals are formed in polymerization of allylic monomers, they are only present at low concentration [177]. Monomers containing two double bonds of different reactivities may result in regioselective reactions. Allyl methacrylate (AMA), though frequently used as a cross-linker, belongs to this class of monomers since it contains both a methacrylic and an allylic double bond. NMR studies of the structure of poly(allyl methacrylate) formed by both bulk and dilute solution polymerization have provided no evidence for the in-chain lactone rings which may result from intramolecular cyclopolymerization of allyl methacrylate, the signals in the NMR spectra of poly(allyl methacrylate) are entirely consistent with "normal" polymerization at the methacrylic bonds with pendant allyl groups. Usanmaz et al. have polymerized AMA in CCl_4 by α,α - azoisobutyronitrile where about 98-99% of the allyl side groups remained pendant even after completion of the polymerization [178]. The spectroscopic and thermal results showed that polymerization is not a cyclopolymerization type, but may have end group cyclization. The authors have also concluded from ^{1}H NMR measurements, that cyclopolymerization reactions are produced in a very low proportion. Matsumoto *et al*. have carried out the radical cyclopolymerization of allyl methacrylate, the structure of the polymer showed no existence of unreacted pendant methacrylic groups which

suggested that the polymerization mechanism occurs exclusively with methacrylic groups.[5] The authors also claim that the formation of five-membered ring by intramolecular head-to-head addition of uncyclized methacrylic radical to allyl group is sterically favored as the result of the introduction of two successive methylene units, which separate adjacent bulky structural units [179]. The free radical polymerization of allyl 2-cyanoacrylate (ACA) has been carried out by some of us and the cross-linking behavior of these polymers has been detected [180]. Mathias *et al.* have synthesized and polymerized ethyl α-[(allyloxy)methyl)]acrylate. Their two-dimensional INADEQUATE NMR analysis has conclusively confirmed monomer cyclization exclusively to five-membered rings with a ratio of *trans* to *cis* ring configurations in the polymer backbone of approximately 2.2 [181]. This study aims in understanding the main features that govern cyclopolymerization as opposed to homopolymerization in the free radical polymerization of difunctional acrylate derivatives such as allyl methacrylate, allyl 2-cyanoacrylate and methyl -[α (allyloxy)methyl] acrylate. For this purpose the free radical polymerization behavior of the monomers displayed in Figure 8.1 has been modeled.

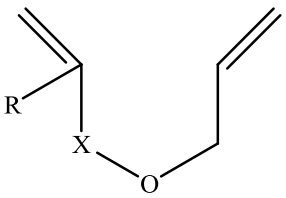

X : C=O R : CH_3 (allyl methacrylate, **F1**)

X : C=O R : CN (allyl 2-cyanoacrylate, **F2**)

X : CH_2 R : $COOCH_3$ (methyl -[α(allyloxy)methyl] acrylate, **F3**)

Figure 8.1. Monomers modeled in this study

As shown in Figure 8.2, initially, the initiator attacks the end-carbon of the double bond of the monomer and a radical is formed (a). The radical attacks either the double bond of the other monomer (b) or the other double bond in the same unit and

intramolecular cyclization occurs (c). The cyclized radical can propagate by attacking the double bond of another monomer (d). Chain transfer occurs via abstraction of a hydrogen atom from the monomer (e), yielding a different kind of radical which can attack the double bond of another monomer (f).

8.2. Theory and Computational Details

The elementary steps shown in Figure 8.2 have been modeled for allyl methacrylate (**F1**), allyl 2-cyanoacrylate (**F2**) and methyl α-[(allyloxy)methyl]acrylate (**F3**). The rate constant for a bimolecular reaction is calculated as shown in chapter for given as[9]

For unimolecular reactions such as

A ⟶ B

the rate constant is given as [94],

$$k = \frac{k_B T}{h} e^{-\Delta G^{\neq}/RT}$$

Mulliken charges [182] have been calculated for all the reactants and the transition structures. The energetics in terms of Gibbs free energies of activation, $\Delta G^{\neq}$ for all the elementary steps shown in Figure 8.2 have also been reported. These findings are discussed to elucidate the free radical polymerization efficiencies, the regioselectivity and the stereoselectivity of the monomers.

In some cases, the reactivity will be investigated by using concepts introduced in DFT based reactivity theory ("conceptual DFT") [183-190]. The Fukui function $f(r)$, introduced by Parr and Yang, is often used to investigate the regioselectivity. The Fukui function is defined as the initial response of the electron density due to an infinitesimal perturbation in the total number of electrons N, at constant external potential $V(r)$ [191, 192].

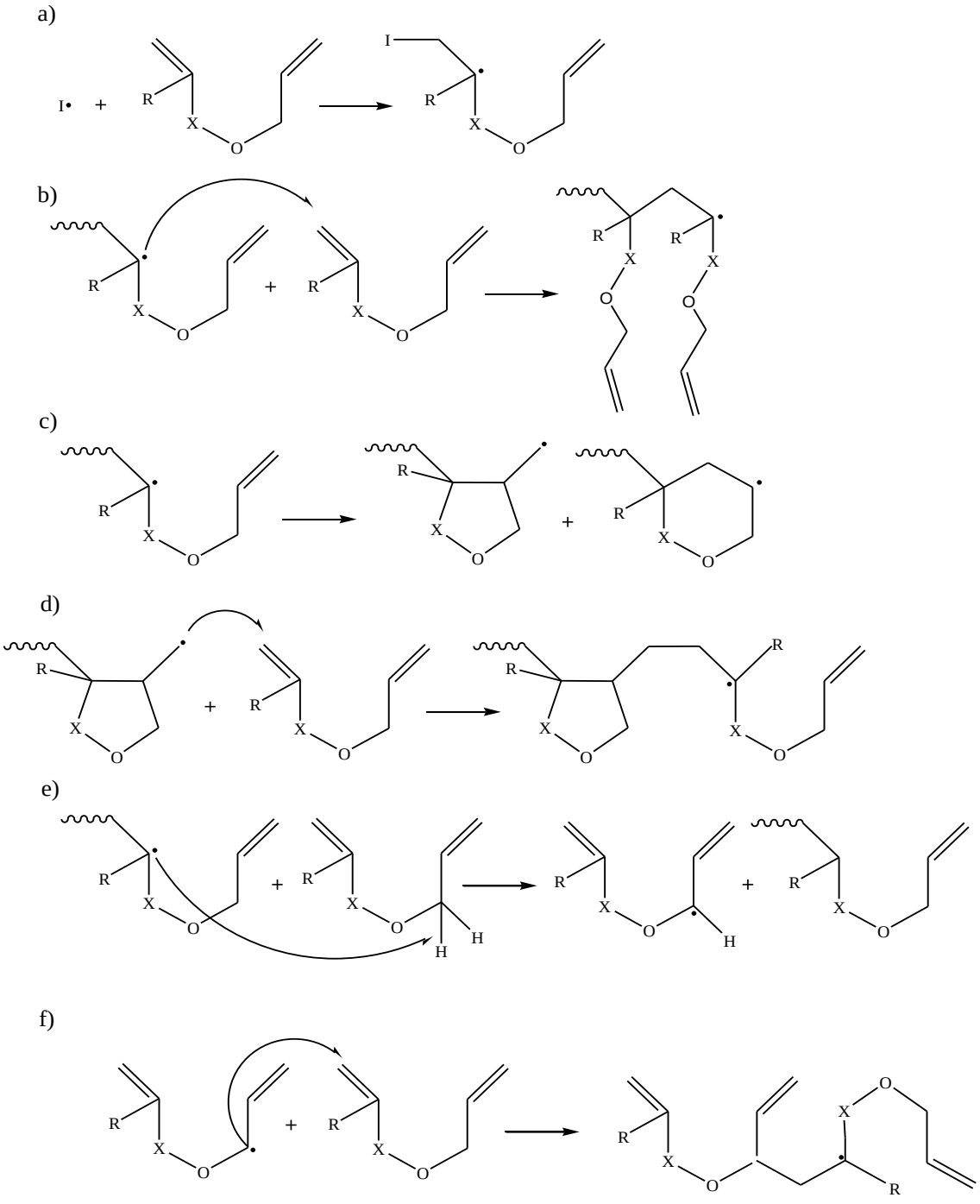

Figure 8.2. Elementary steps of free radical polymerization: initiation (a), homopolymerization (b), cyclization (c), propagation (d), chain transfer (e), reinitiation (f).

$$f(r) = \left(\frac{\delta\rho(r)}{\delta N}\right)_{\vartheta}$$

Three different Fukui functions can be introduced, representing the case of a nucleophilic attack, f^{+}(r); an electrophilic attack, f^{-}(r); or a neutral (radical) attack, f^{0}(r) [193]. For a system of *N* electrons, the nucleophilic and electrophilic Fukui functions can be computed

$$f^{+}(r) = \rho_{N+1}(r) - \rho_{N}(r)$$

$$f^{+}(r) = \rho_{N}(r) - \rho_{N-1}(r)$$

and f^{0}(r) can be the averaged

$$f^{0}(r) = \frac{f^{+}(r) + f^{-}(r)}{2}$$

ρ_{N+1} (r), ρ_{N}(r), ρ_{N-1} (r) represent the electron densities for systems of *N* + 1, *N*, and *N* - 1 electrons computed by using the geometry of the *N* electron system. High values of Fukui functions f^{0}(r) will indicate high reactivities towards free radical attacks. The effect of a polar environment was taken into account as mentioned in chapter 4.

8.3. Results and Discussion

8.3.1. Initiation

In **F1** and **F3**, the most stable structures of the monomers (Figure 8.3) exhibit extended structures with the alkene and carbonyl groups *anti* to each other. The anti-position of these groups in **F1** and **F3** allows a favorable interaction between the hydrogens of the methyl group and the carbonyl oxygen. In **F2**, the CN and carbonyl groups are anti to each other stabilizing this molecule by diminishing its dipole moment (Table 8.1).

F1	F2	F3
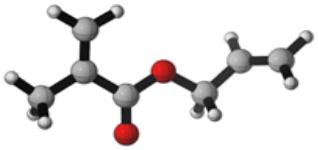	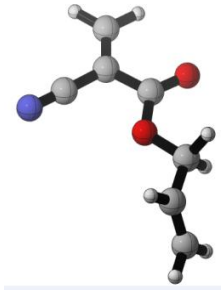	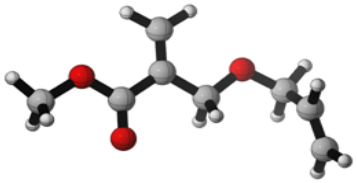

Figure 8.3**.** 3D structures of the most stable conformers of **F1**, **F2** and **F3**.

Table 8.1. Relative Gibbs free energies (G_{rel}) and dipole moment (μ) of **syn** and **anti** conformations of **F1**, **F2** and **F3**.

	M1		**M2**		**M3**	
	syn	**anti**	**syn**	**anti**	**syn**	**anti**
G_{rel}	0.4	0.0	0.0	0.7	0.4	0.0
μ	2.05	1.93	2.29	6.17	3.02	0.64

M1-TS-i	**M2-TS-i**	**M3-TS-i**
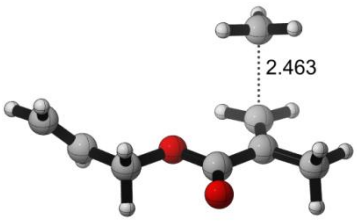	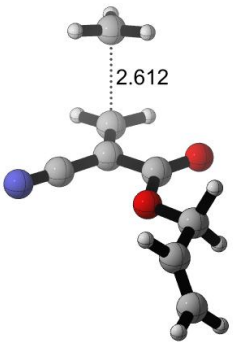	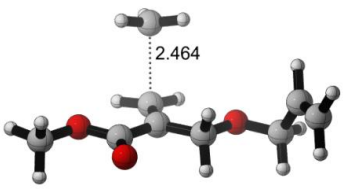
14.18	11.09	13.91

Figure 8.4**.** 3D structures and Gibbs free energies of activation ($\Delta G^{\neq}$) at 298 K for initiation (B3LYP/6-31+G*).

The initiation reaction where the incoming radical is CH_3 has been depicted in Figure 8.4. The initiation reaction is earliest for **F2** as illustrated by the longest critical bond (2.612 Å) and the lowest Gibbs free energy of activation (11.09 kcal/mol) in **F2-TS-i**. This low barrier is probably due to the electron-withdrawing character of the CN group which renders the C terminal more prone to the attack by the free radical exemplified by CH_3. The regioselectivity for the CH_3 radical is also investigated by using the Fukui function f^0(r) (Table 8.2). The terminal allylic carbon, C1, has the highest f^0(r) values in all the species showing that this carbon has the highest affinity for a radical attack in agreement with Matsumoto's results claiming that the polymerization of allyl methacrylate occurs exclusively with methacrylic groups [179].

Table 8.2. Fukui function (f^0(r)) for **F1**, **F2** and **F3**(B3LYP/6 -311++G(d,p))

f^0(r)	**F1**	**F1**	**F3**
C1	0.200310	0.233430	0.189835
C2	0.096350	0.094965	0.071820
C6	0.049840	0.136495	0.017965
C7	0.117905	0.059175	0.082475

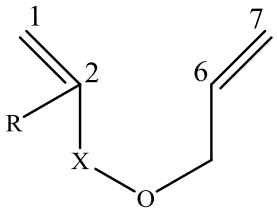

The free radicals formed after attack of the CH_3 radical- **F1-R**, **F2-R** and **F3-R** have extended conformations. We have also located the quasi-cyclic reactive rotamers in order to monitor the ease of cyclization in these species. Our computational findings indicate that the cyclic rotamers **F1-RR** and **F2-RR** are considerably higher in energy than their corresponding extended conformations **F1-R** and **F2-R.** Thus the radicalic forms of **F1** and **F2** exist exclusively as extended chains, whereas in the case of **3f** the energy difference between the extended **(F3-R)** and cyclic conformations (**F3-RR)** is only 1.79 kcal/mol indicating that about 5% of the molecules at 298K will already exist in the cyclized conformation; this percentage is expected to be higher at higher temperatures. Also note that the distance between the radical center and the double bond is already 3.158 Å, quite close to the one in the transition structure (Figure 8.5).

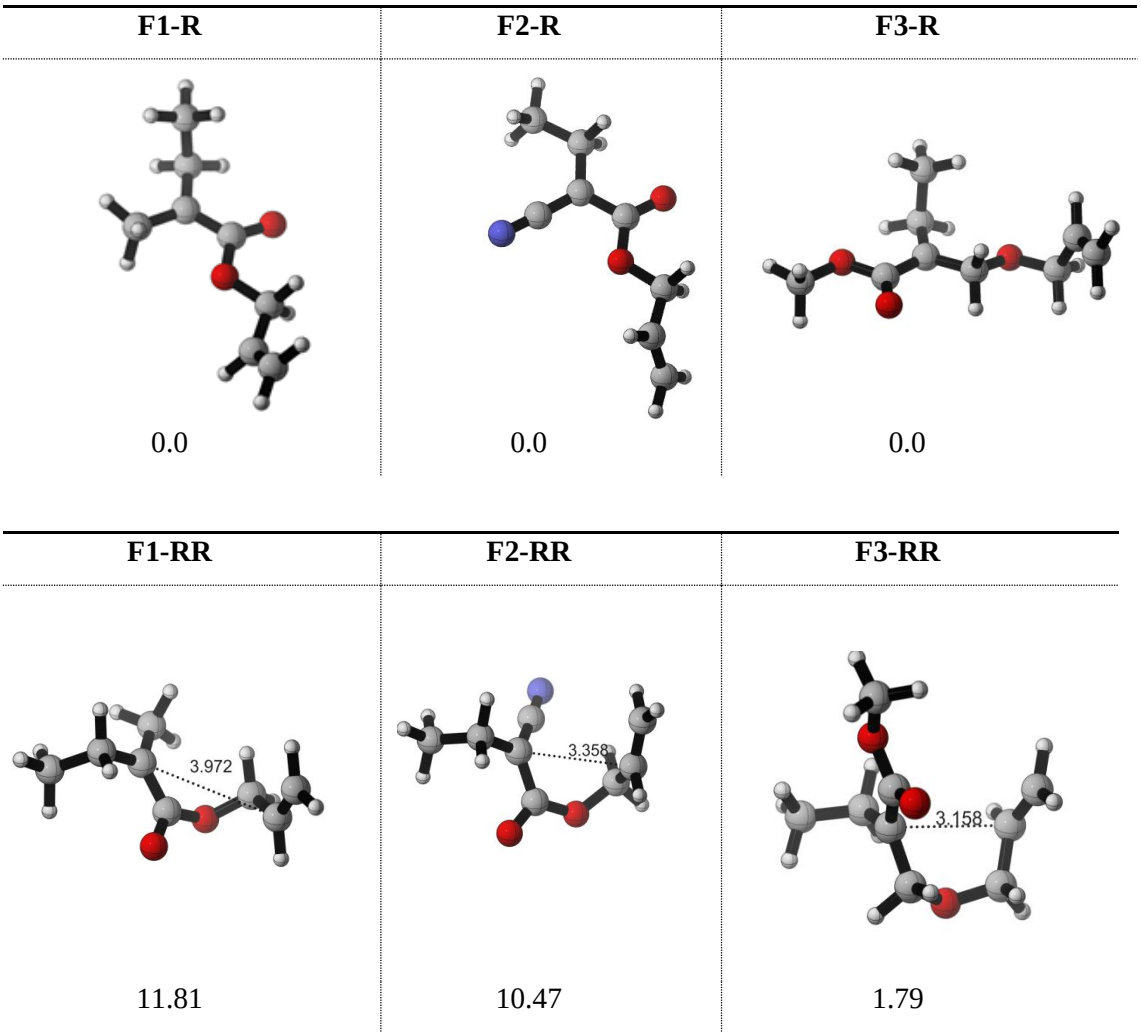

Figure 8.5. 3D structures, relative Gibbs free energies (ΔG_{rel}) for the global minima of the radicals and their reactive rotamers (B3LYP/6-31+G*) at 298 K .

8.3.2. Cyclization Tendency of Monomers

The free radicals either attack the double bond of a new monomer or the double bond of the monomer itself to form 5-membered (exo-cyclization) or 6-membered rings (endo-cyclization). The transition structures for homopolymerization are quite similar to each other in terms of geometrical features and energy barriers. Cyclization preferentially occurs via 5 membered rings: exo-cyclization is preferred to endo-cyclization by far in all cases (Figure 8.6 and Figure 8.7). The exo preference of the

diallyl monomers in cyclization was interpreted to be kinetically controlled [194]. In one of our studies, the 5 membered ring formation of **F3** has been rationalized by using DFT based reactivity indices such as non-spin polarized (f^0), spin polarized Fukui functions (f_{NN}^0), spin densities ρ_s, and dual descriptors ($f^{(2)}$(r)) [195]. For similar systems, it is also known that 5-membered ring formation is facilitated due to the favorable overlap efficiency, the regioselectivity being governed mostly by steric factors rather than by electronic factors [196-199]. It has been noted that, for approach of the radical to the double bond with the p orbitals in a common plane, formation of five-membered rings would be less sterically hindered [200]. One of the terminal hydrogens lies in the nodal plane directly between the radical carbon and the carbon on the terminal end of the double bond, thus hindering six-membered ring formation [201]. Nevertheless, a suggestion that there may be an electronic interaction between the initially formed radical and the neighboring double bond of the diene has also received considerable attention [202]. Capon and Rees have interpreted the unexpected exo preference of hexenyl systems in terms of the activation entropy, $\Delta S^{\neq}$. They propose that higher strain energy in the smaller ring is overcome by the more favorable activation entropy of the exo cyclization [203]. Exocyclization of **F1** and **F2** is considerably slower when compared to **F3**; this is illustrated in their respective free energy activation barriers: 23.03, 22.52 and 13.23 kcal/mol. The relative energies of the reactive rotamers of **F1-RR, F2-RR** and **F3-RR** display the same trend and are 11.81, 10.47, 1.79 kcal/mol higher in energy than their ground state counterparts. This finding confirms the ease of cyclization of **F3** (1.79 kcal/mol) as compared to **F1** (11.81 kcal/mol) and **F2** (10.47 kcal/mol). Also note that cyclization of **F3** is less endothermic than the others in agreement with Hammond's postulate [204].

The geometrical parameters of the reactive rotamers (**F1-RR**, **F2-RR**, **F3-RR**) and those of their exo-cyclization transition states have been compared with the ones of the 5-membered ring THF (Table 8.3). Besides the resemblance of **F3-RR** and **F3-TS-exo** with THF in terms of the angle α, their dihedral angles are also in line with each-other.

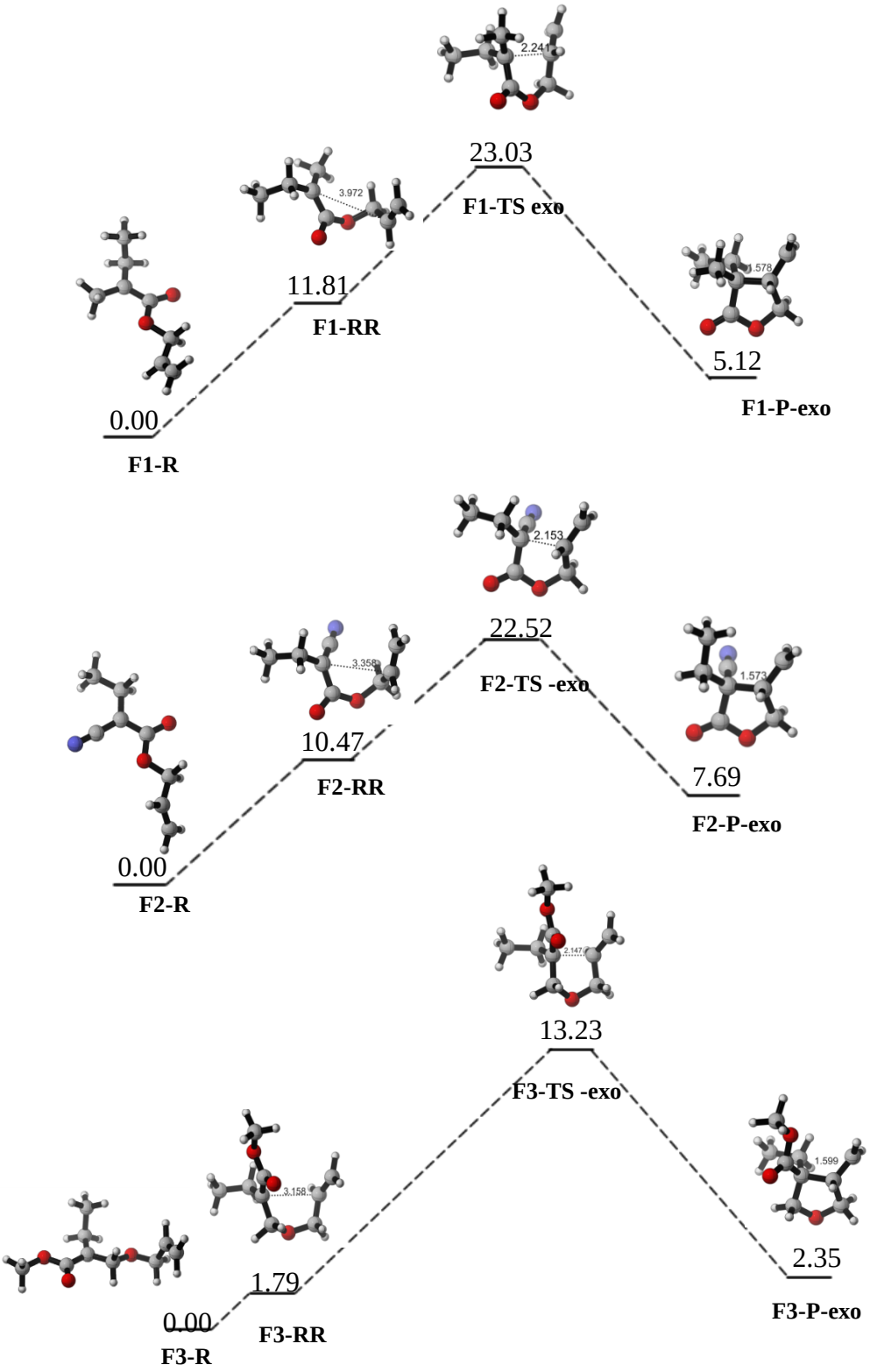

Figure 8.6. Gibbs free energy profiles for exo-cyclization of **F1-R**, **F2-R** and **F3-R** (B3LYP/6-31+G*).

Table 8.3. Angles which are significant for the ring formation.

	Angle	Dihedral		
	α (2-3-4)	**2-3-4-5**	**3-4-5-6**	**4-5-6-2**
F1-RR	117.1	76.8	68.4	52.1
F2-RR	121.7	29.0	59.5	-52.1
F3-RR	113.7	81.6	-76.3	30.4
F1-TS-exo	115.7	12.6	25.6	-35.3
F2-TS-exo	114.5	10.6	28.7	-30.6
F3-TS-exo	109.8	53.4	-52.2	26.8
THF	105.6	39.7	-39.6	23.3

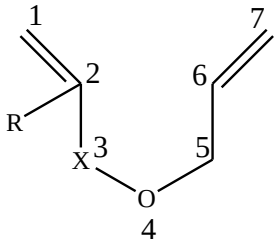

In order to confirm the role of the hybridization of C3 in exo-cyclization, hypothetical molecules have been modeled. **F1**, a model for **F1**, has the carbonyl group at C3 replaced with an sp^3 hybridized carbon ($-CH_2-$). A substantial decrease of the cyclization energy barrier has been observed in the case of **F1'** (11.70) as compared to **F1** (23.03). The finding confirms the fact that the presence of the carbonyl group at C3 inhibits the cyclization because of the widening of the angle α. Nevetheless, Butler et al. have reported the cyclopolymerization of methacrylic anhydride via 6-membered rings [205]. Notice that in the latter both C3 and C5 are sp^2 hybridized, in the case of **F1** and **F2** it is rather the incompatibility in the hybridization of C3 (sp^2) and C5 (sp^3) that disfavors cyclization. The 5-membered cyclic structure (**F3-P-exo**) attacks C1 of another monomer via **F3-TS-prop** and the polymerization continues.

Depending on the relative orientation of the methyl formate group ($COOCH_3$) and the double bond, *cis* and *trans* isomers of **F3-TS-exo** have been located (Figure 8.8). The energy difference between the *cis* and *trans* transition structures in favor of the **F3-TS-exo-cis** is 1.11 kcal/mol in line with our previous calculations with B3LYP/6-31G*.[17] The two-dimensional INADEQUATE analysis has confirmed monomer cyclization exclusively to five-membered rings with a ratio of *trans* to *cis* ring configurations in the polymer backbone of approximately 2.2 [181].

F1-TS-homopol	F2-TS-homopol	F3-TS-homopol
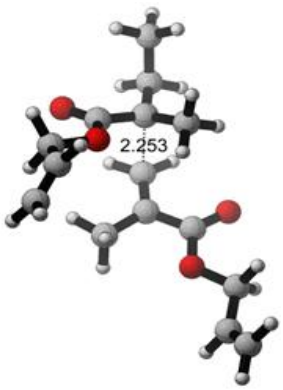	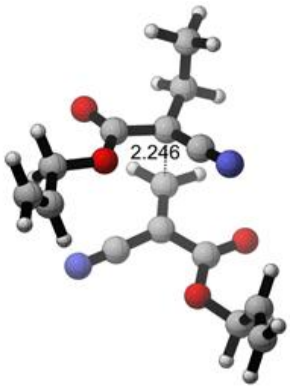	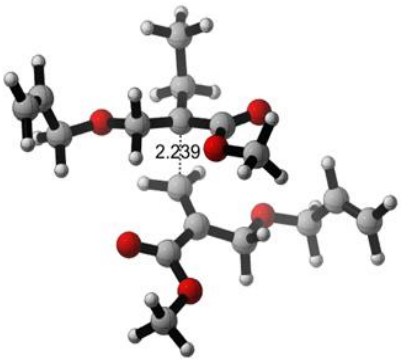
22.94	22.44	22.39
F1-TS-exo	**F2-TS-exo**	**F3-TS-exo**
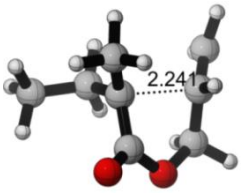	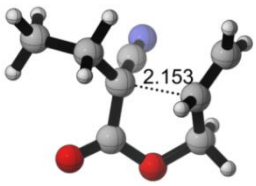	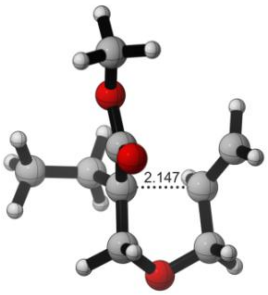
23.03	22.52	13.23
F1-TS-endo	**F2-TS-endo**	**F3-TS-endo**
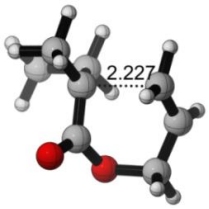	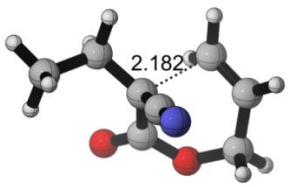	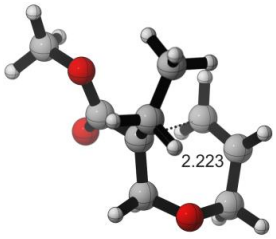
30.21	29.82	18.94

Figure 8.7. 3D structures and Gibbs free energies of activation ($\Delta G^{\neq}$) for linear homopolymerization, cyclopolymerization and further propagation at 298K (B3LYP/6-31+G*).

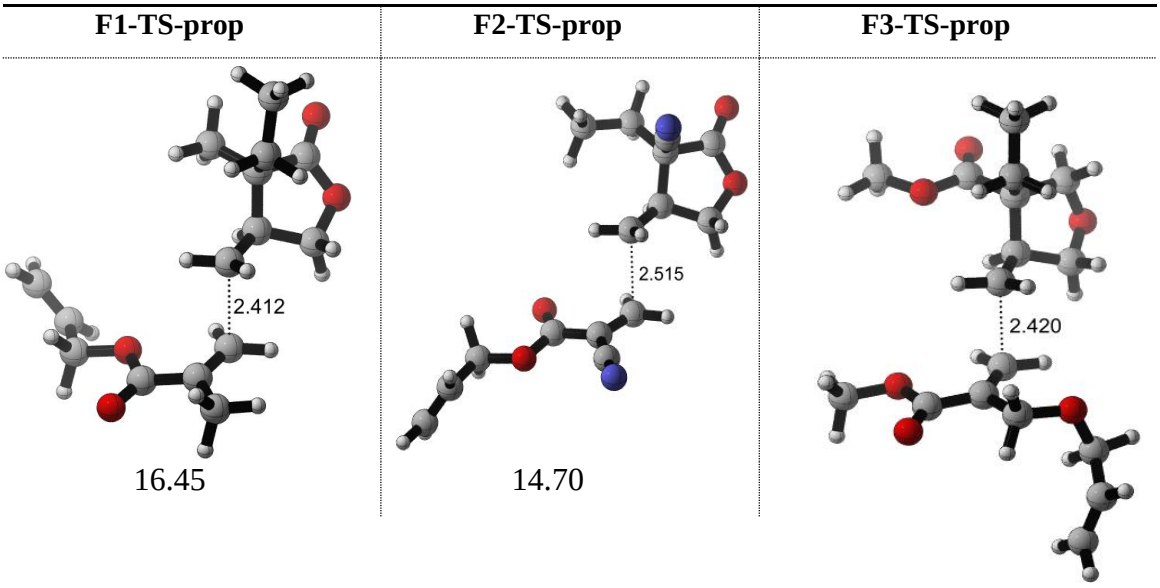

Figure 8.7. 3D structures and Gibbs free energies of activation ($\Delta G^{\neq}$) for linear homopolymerization, cyclopolymerization and further propagation at 298K (B3LYP/6-31+G*) (cont.).

The model used in this study reproduces the attractive interactions between the carbonyl oxygen and the methylene group and its repulsion with the alkyl chain, however it does not reflect the steric effects of the backbone and a one to one comparison with experiment would be irrelevant.

8.3.3. Chain Transfer and Reinitiation

The radicals present in the reaction vessel can also abstract H from the monomer, this reaction, termed as chain transfer, may compete with the initiation reaction where the free radical would add to the double-bond. For each one of these species the barriers for chain transfer are higher than those for initiation. Overall the chain transfer process doesn't compete with the initiation reaction. The radical formed after chain transfer would propagate as expected, this side reaction termed as reinitiation is even slower than the chain transfer process. The reinitiation for **F2** is favored over the others as it is in the case of the initiation: the electron-withdrawing CN group renders the terminal carbon more positive than the other substituents (Figure 8.9).

F3-TS-exo-cis	F3-TS-exo-trans
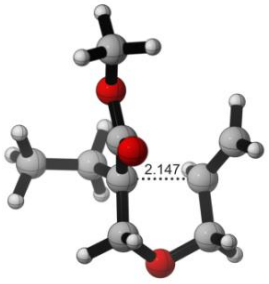	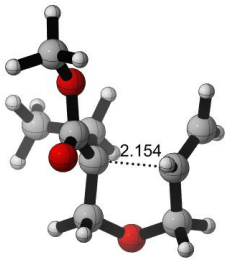
0	1.11

Figure 8.8. 3D structures and Gibbs free energies of the *cis* and *trans* transition states for exo cyclization of **F3** at 298K (B3LYP/6-31+G*).

Fukui functions have also been used to identify the location of the most plausible hydrogen to be abstracted in the chain transfer process (Table 8.4). In **F1** and **F2** the hydrogens of the CH_2 group between the ester functionality and the ethylenic double bond are more prone to abstracted H than the others. One of these hydrogen atoms is stabilized by the carbonyl oxygen while the other is being abstracted. In **F3** there are 2 sets of hydrogens to be abstracted by the methyl group, the ones close to the ester functionality will be abstracted because of the electron withdrawing ability of the later.

Table 8.4. Fukui functions ($f^0(r)$) for abstractable H's (B3LYP/6-311++G(d,p)//B3LYP/6-31+G*).

$f^0(r)$	F1	F2	F3
H_a	0.030465	0.021625	0.050975
H_b	0.022535	0.030275	0.052750
H_c			0.029040
H_d			0.027485

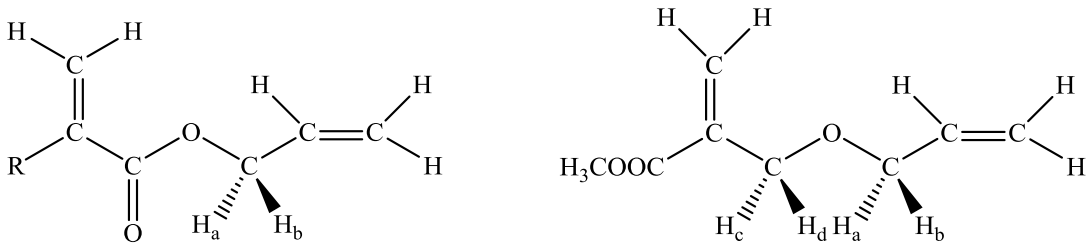

(R = CH_3 for **F1** and CN for **F2**)

F1-TS-ct	**F2-TS-ct**	**F3-TS-ct**
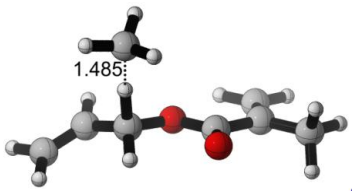	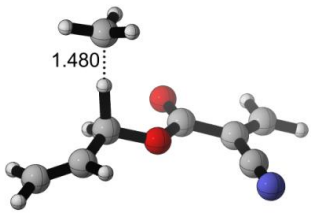	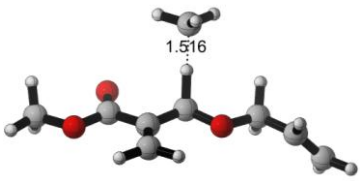
16.83	16.61	15.91

F1-TS-re	**F2-TS-re**	**F3-TS-re**
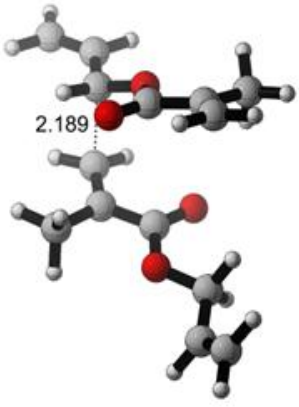	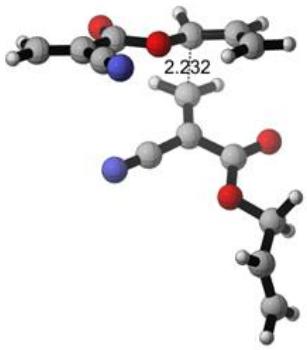	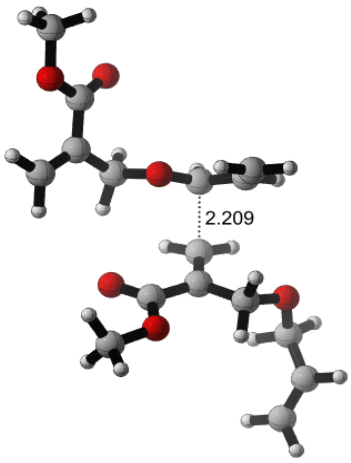
24.50	19.63	25.46

Figure 8.9. 3D structures and Gibbs free energies of activation ($\Delta G^{\neq}$) (kcal/mol) for chain transfer and reinitiation transition statesat 298 K [B3LYP/6-31+G(d)].

Table 8.5. Gibbs free energies of activation ($\Delta G^{\neq}$, kcal/mol), electronic energies of activation ($\Delta E^{\neq}$, kcal/mol) and rate constants (B3LYP/6-31+G*) at 298.15 K. Values in solution (benzene) are displayed in parenthesis.

	F1				**F2**		**F3**		
	$\Delta G^{\neq}$	**$\Delta E^{\neq}$**	**Rate constant***	**$\Delta G^{\neq}$**	**$\Delta E^{\neq}$**	**Rate constant***	**$\Delta G^{\neq}$**	**$\Delta E^{\neq}$**	**Rate constant***
Initiation	14.18 (12.27)	4.81 (2.90)	6.21E+03 (1.54E+05)	11.09 (9.13)	1.97 (0.01)	1.14E+06 (3.09E+07)	13.91 (12.05)	4.61 (2.75)	9.81E+03 (2.22E+05)
Homopolymerization	22.94 (21.58)	8.93 (7.57)	2.34E-03 (2.28E-02)	22.44 (21.93)	9.05 (8.55)	5.49E-03 (1.26E-02)	22.39 (21.63)	8.0 (7.24)	6.66E-03 (2.09E-02)
Chain transfer	16.83 (15.28)	7.59 (6.04)	7.11E+01 (9.54E+02)	16.61 (15.15)	7.39 (5.92)	1.02E+02 (1.20E+03)	15.91 (14.13)	7.04 (5.25)	3.32E+02 (6.67E+03)
Reinitiation	24.50 (23.16)	11.73 (10.39)	1.70E-04 (1.59E-03)	19.63 (18.88)	7.28 (6.07)	6.34E-01 (2.17E+00)	25.46 (24.14)	12.59 (11.26)	3.33E-05 (3.03E-04)
Cyclopolymerization									
Exo-cyclization	23.03 (20.72)	19.69 (18.77)	8.16E-05 (3.95E-03)	22.52 (21.79)	19.89 (19.16)	1.92E-04 (6.44E-04)	13.23 (12.96)	10.54 (10.31)	1.24E+03 (1.92E+03)
Endo-cyclization	30.21 (28.05)	26.65 (25.88)	4.43E-10 (1.65E-08)	29.82 (28.97)	27.03 (26.19)	8.62E-10 (3.50E-09)	18.94 (18.80)	15.79 (15.65)	8.08E-02 (1.01E-01)
Intermolecular Propagation	16.45 (17.83)	5.39 (6.77)	1.34E+02 (1.28E+01)	14.70 (13.00)	4.11 (2.41)	2.60E+03 (4.52E+04)	17.57 (15.62)	5.88 (3.93)	2.03E+1 (5.39E+02)

*The unit of the rate constant is (1/s) for exocyclization and endocyclization and (L/s.mol) for the other steps.

8.4. Kinetics

The kinetics of the free radical polymerization steps of monomers **F1, F2** and **F3** are displayed in Table 8.5. Initiation of the monomers by a free radical is the fastest step for all the monomers. The CN group at position 2 of **F3** faciliates the initiation step due to its electron withdrawing ability. The kinetics for linear homopolymerization display the same trend for all the monomers, however **F3** cyclopolymerizes via 5-membered rings, while **F1** and **F2** do not. As demonstrated earlier, the latter do not cyclize because of the fact that carbon atoms attached to the heteroatom - C3 (sp^2) and C5 (sp^3) - have different hybridization characters. As claimed by Butler, in monomers which tend to cyclopolymerize, the intramolecular cyclization step requires greater energy than the intermolecular step [205]. **F3** satisfies this expectation and has activation barriers of 10.54 kcal/mol and 5.88 kcal/mol for cylization and propagation respectively. However the rate of cyclization ($1.92x10^3$) is considerably larger than that for intermolecular propagation ($5.39x10^2$) demonstrating that cyclization is favored entropically. It is also worth noting that chain transfer reactions ($7.11.x10^1 < k_{ct} < 3.32x10^2$) do not compete with initiation ($1.14.x10^3 < k_i < 6.21x10^3$). The trends in the vacumm are also reproduced in a polar environment.

8.5. Conclusions

This study has used the DFT methodology to shed light on how the free radical polymerization mechanism of allyl acrylate derivatives depends on the structure of the monomer. While allyl methacrylate (AMA) and allyl 2-cyanoacrylate (ACA) tend to polymerize to give polymers with pendant unsaturation as demonstrated experimentally [179, 180], methyl α-[(allyloxy)methyl]acrylate cyclopolymerizes. It has also been claimed that the presence of the carbonyl group at C3 in AMA and ACA inhibits cyclization because of its incompatibility in hybridization with the other unsaturated carbon next to the oxygen. Furthermore it has been shown that while the quasi cyclic reactive rotamer of methyl α-[(allyloxy)methyl]acrylate is present at room temperature by 5%, the quasi cyclic reactive rotamers of AMA and ACA do not form at all at room temperature. It has been

pointed out that the rate determining step in the cyclopolymerization mechanism is the cyclization via 5-memberd rings rather than the intermolecular propagation even though the latter is favored energetically. The solvent as a polar medium did not alter the polymerization trends in vacuum.

9. ORIGINS OF THE SOLVENT EFFECT ON THE PROPAGATION KINETICS OF ACRYLIC ACID AND METHACRYLIC ACID

9.1. Introduction

Water-soluble polymers are of high importance, finding widespread applications in hydrogels, flocculants, thickeners, coatings, and have adhesion characteristics [206, 207]. Pulsed-laser polymerization in conjunction with size-exclusion chromatography (PLP-SEC) has been carried out to monitor the influence of solvents on the propagation kinetics of free radicals [207]. The effect of solvent on the kinetics of the free radical polymerization (FRP) of acrylates, methacrylates and other vinylic monomers has been investigated [208]. It is known that rate enhancement or retardation depends not only on the monomer structure and the nature of the solvent separately but also on the specific type of interactions between the reacting species and the solvent.

It is known that the propagation rate coefficients for styrene and methyl methacrylate (MMA) in a wide variety of solvents (acetonitrile, dimethyl formamide, anisole, methyl isobutyrate, bromobenzene, benzene and 1,2-dichloroethane) only change mostly by 10 % [208]. On the other hand, certain solvents, such as benzyl alcohol [209, 210], dimethylsulfoxide [209, 210], N-methylpyrrolidinone [209, 210], 2,6-dithiaheptane [211] and 1,5-dithiacyclooctane [211] induce a significant increase in k_p. In many cases hydrogen bonding is responsible for this observed rate acceleration. The usage of alcohols as solvents in the FRP of acrylates has caused a rate enhancement which was attributed to a decrease in electron density around the C=C bond of the monomer due to the hydrogen bonding between the solvent and the oxygen atom of carbonyl group. The rate of propagation, k_p, of MMA in benzyl alcohol has been reported to increase by almost one order of magnitude as compared to bulk polymerization [209,210].

When there are no specific interactions between the monomer and the solvent, a correlation between the propagation rate constant $k_{p,}$ the size of the solvent molecules and

the monomer has been established.[5] Thus, one expects an increase in the propagation rate constant when the solvent is larger in size than the monomer. When the solvent size is smaller than the monomer, the propagation rate constant decreases. These results were explained by a change in local concentration of the monomer around the growing chain end: a larger solvent size leads to an increase in local monomer concentration around the growing chain end increasing the propagation rate constant and vice-versa [208].

For the free radical polymerization of styrene (in ethanol, methanol, toluene, ethylbenzene), methacrylic acid (in methanol, tetrahydrofuran, 2-propanol, toluene, acetic acid), methyl methacrylate (in methanol, ethyl acetate, ethanol, toluene, 2-butanone), and butyl acrylate (in toluene, tetrahydrofuran) it was shown that the propagation rate constant k_p is invariant with monomer concentration [212-218]. Increase in k_p with dilution of monomer concentration was observed for acrylamide and methacrylamide derivatives [219-222], acrylic acid and methacrylic acid [213, 216, 223-229]. This strong solvent effect was attributed to dimerization [219-222] or to local monomer concentrations at the radical site being different from the overall monomer concentration [228]. These studies have revealed the fact that polar monomers, that are capable of forming hydrogen bonds, are affected substantially by the solvent [230-233]. When the bulky system is diluted, the propagation rate constant k_p of MAA and AA has been reported to increase by at least one order of magnitude. This change was reflected in an increase in the Arrhenius pre-exponential factor, due to the disorder created by strong hydrogen bonding between the growing species and water molecules [224, 234-236].

In the last two decades quantum chemical studies on the free radical polymerization of vinyl monomers [237-253], acrylate and methacrylate derivatives [104, 105, 122, 124, 125, 248, 254-258] and their copolymerization [254, 255, 261], have been carried out. In these studies at least two units were considered to mimic the growing polymer chain and to obtain reliable kinetic results. Implementation of the solvent by a polarizable continuum model (PCM) has lead to serious underestimation of the experimentally obtained propagation rate constant in the case of ethyl α-hydroxymethacrylate [122, 262]. Usage of the PCM methodology, in bulk for methyl acrylate (MA) and methyl methacrylate (MMA)

has lead to a very good qualitative agreement with the experimentally observed trends [263]. Thicket *et al*. [259] have monitored the effect of the solvent on the propagation reaction of the monomers: a decrease in the activation barrier was attributed to a greater resonance stabilization of the transition state in a polar medium.

Recently, the COSMO-RS methodology has yielded promising results to simulate the solvent effect [249, 263]. Coote *et al.* have obtained highly accurate propagation rate constants for methyl acrylate and vinyl acetate by using the thermodynamic cycle in which G3(MP2)-RAD calculations in the gas phase are corrected by the solvation energies obtained from COSMO-RS [245, 246, 264, 265]. The latter have used the G3(MP2)-RAD methodology that approximates CCSD(T) calculations with a large triple-ζ basis from calculations with a double-ζ basis set, via basis set corrections carried out at the R(O)MP2 level of theory [264, 265]. They calculated the rate coefficients and Arrhenius parameters with this composite method for dimer models and have corrected their gas phase results by computing solution phase calculations with the COSMO-RS method [266-268]. Warshel *et al.* have carried out a comparative study between continuum, explicit and mixed implicit/explicit solvation models in the context of phosphate hydrolysis [269]. Some of us have used successfully the mixed implicit/explicit solvation model to study the propagation reaction of methyl methacrylate (MMA), n-isopropylacrylamide (NIPAM), acrylamide (AM) and methacrylamide (MAM) [104, 127, 260]. In these studies, the experimentally observed head to tail propagation [270] which is assumed to be the most favorable mode of attack was proven by theoretical methods [251].

Thus, the elucidation of the solvent effects on the reaction kinetics of free radical polymerization is of utmost importance and quantum chemical calculations can give insight at the molecular level. In this study we focus on acrylic and methacrylic acid and we compare the geometrical features of the propagating species in bulk and in solution to unravel the role of water on the propagation rate constants of AA and MAA. The propagation ratio of AA/MAA which is around 35 in bulk, lowers slightly to 31 in water [226, 228] and it is the goal of this study to understand the mode of acceleration of the

propagation of the free radical polymerization of AA and MAA by a protic and polar medium.

9.2. Computational Procedure

Addition of R· -the methyl (CH_3·) radical for unimeric species- to a monomer yields a backbone with three carbon atoms. The unimeric radical then adds to the monomer to generate the propagating polymer chain (propagation reaction) (Figure 9.1). In this study we systematically located the transition states for both unimeric and dimeric radical models, to evaluate the influence of the length of the radical chain on the propagation kinetics.

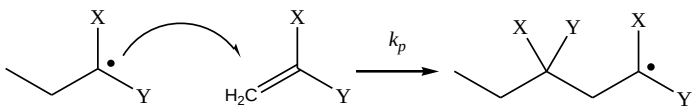

X=-H for AA and -CH_3 for MAA
Y=-COOH

Figure 9.1. Propagation of AA and MAA.

The B3LYP methodology combined with 6-31+G(d) basis. COSMO-RS calculations were performed with ADF [272]. The energetics and kinetics in vacuum and in solution have been evaluated with the MPWB1K/6-311+G(3df,2p)//B3LYP/6-31+G(d), M05-2X/6-311+G(3df,2p)//B3LYP/6-31+G(d) and M06-2X/6-311+G(3df,2p)//B3LYP/6-31+G(d) methodologies to further refine the energy at another level of theory. The MPWB1K method was chosen because it has been proven to be successful for describing thermochemistry, reaction kinetics, hydrogen bonding, and weak interactions [256, 273]. This method has also been found to be successful in studies concerning the free radical polymerization reactions of acrylates [105, 124, 125, 127, 258, 260]. The M05-2X [92] and M06-2X [91] functionals have been chosen because they are recommended for thermochemistry, kinetics, and noncovalent interactions [91, 92]. The M05-2X functional is further known to be successful for radical species [124, 274-284]. According to Zhao and Truhlar, the M05-2X functional implicitly accounts for “medium-range” electron correlation because of the way it is parametrized, and this is sufficient to describe the

dispersion interactions within many complexes [91]. These authors define “medium-range”correlation to be that found in complexes separated by about 5Å or less [285]. The main intermolecular interactions in the species analyzed in this study are hydrogen bondings thus M05-2X and M06-2X functionals are expected to reproduce these interactions quite well. The conventional transition state theory (TST) is used to calculate the rate constants. The rate constant of a bimolecular reaction as shown in chapter 4.

For implicit solvation, the effect of a polar environment was taken into account by use of SCRF theory, and IEF-PCM model as explained in chapter 4 and 8 [97]. For the case where the solvent has been modeled explicitly and implicitly, the contribution resulting both from the explicit coordination with solvent molecules in the reactants and transition states and the one originating from the bulk solvent effect as in earlier publications have been considered [269, 287-290]. In the latter case all gas phase geometries were re-optimized in polarizable continuum medium (PCM) with explicit water molecules (implicit/explicit solvation model) in order to access the effect of the solvent. These structures were further used to calculate the solvation energies with the new generation method COSMO-RS [266-268]. All the energies reported in this study are in kcal/mol.

Classical MD simulations were performed on the dimers of poly(AA) and poly(MAA). The simulation box was composed of 3 dimeric chains and 250 water molecules, a solution with a density of 1 g/cm^3 having 9 weight % poly(AA/MAA). Each side of the cubic box was 20.2 Å. The box was constructed with the Amorphous Cell module of Accelrys Materials Studio suite of programs [291]. The COMPASS forcefield [292] was used with a cutoff distance of 10 Å, and a switching function with spline and buffer widths of 1.0 and 0.5 Å, respectively. The system was initially minimized with 5000 steps of conjugate gradients up to a convergence of 1 kcal/mol/Å. Then, periodic boundary conditions were imposed and MD simulations were performed in the NVT ensemble at 298 K using the Andersen thermostat as the temperature control method with a collision ratio of 1.0 [293]. 200 ps equilibration run was followed by a production run of 1 ns. The time step was set to 1 fs and coordinates from the production stage were recorded every 1 ps for further analysis. The radial distribution functions analyzed in this study are based on 1000 snapshots.

9.3. Results and Discussion

A conformational search was carried out for the monomers and the radicals at the B3LYP/6-31+G(d) level of theory. The s-*cis* geometry has the lowest energy for AA, while the s-*trans* conformer is preferred in case of MAA. Although the energy difference between s-*cis* and s-*trans* conformers is only 0.31 kcal/mol and 0.45 kcal/mol for AA and MAA respectively (Figure 9.2). These results are consistent with previous theoretical studies on MA and MMA [105]. Notice that in both cases long range electrostatic interactions between the carbonyl oxygen and hydrogens stabilize these structures. In the case of MAA s-*trans* is preferred because of the bifurcation of the carbonyl oxygen between the hydrogens of the methyl group. A similar conformational study was performed for the radicals formed by addition of CH_3 radical to the monomers, as they may adopt either a *syn* or *anti* configuration (Figure 9.2).

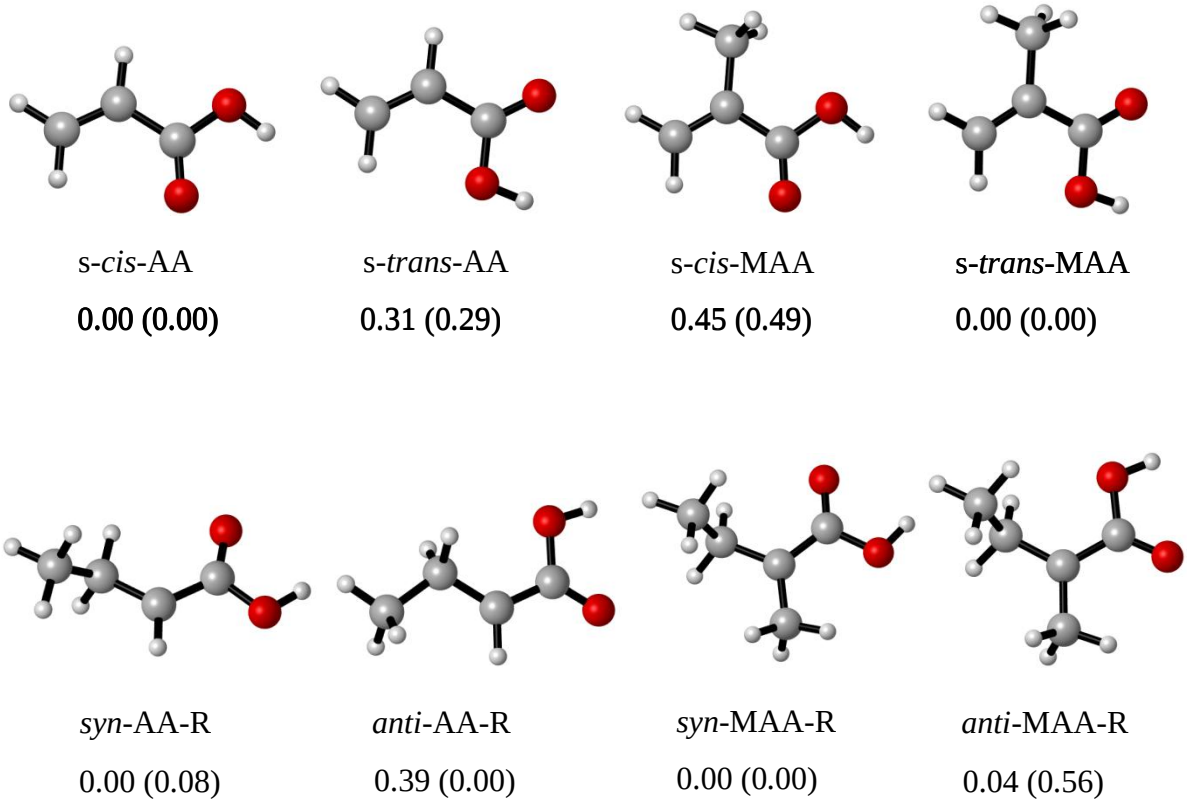

Figure 9.2. Relative electronic energies (Gibbs free energies in parenthesis) for the most stable conformers of the monomers and the radicals of AA and MAA (B3LYP/6-31+G(d)).

Racemo and meso dimeric radicals may be formed by attack of the most stable conformation of the radical (*syn/anti*) to the most stable conformation of the monomer (s-*cis*/s-*trans*) as schematically depicted in Figure 9.3.

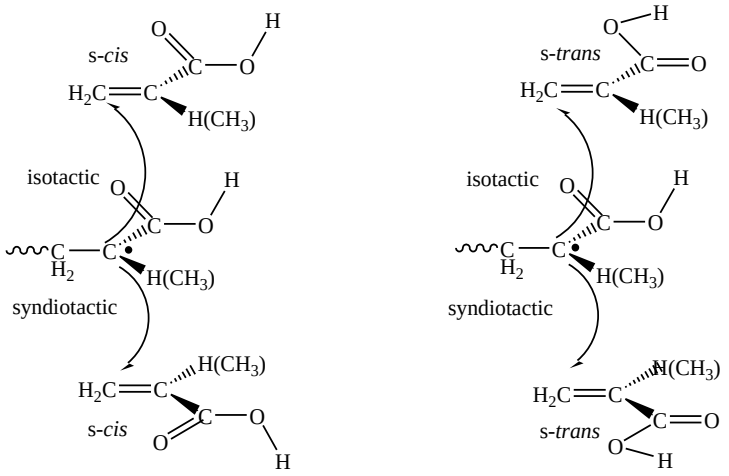

Figure 9.3. Stereoselective radical (*syn*) addition to **AA** and **MAA** (s-*cis* and s-*trans*).

All the plausible combinations for the radical addition to the monomer were used giving rise to eight different transition states. For each of these transition structures a relaxed potential energy scan was carried out around the forming bond; in this way the most stable transition state structures were located. The most stable structures for the unimeric and dimeric transition structures of **AA** and **MAA** are displayed in Figure 9.4.

In vacuum, the pro-racemo (syndiotactic) transition state of AA is preferred whereas the pro-meso (isotactic) attack is prefered for MAA as seen from Table 9.1, where the relative electronic energies are tabulated for the eight different transition structures of AA and MAA. In the case of MAA (TS-MAA and TS-MAA-dimer) for the meso chain the *gauche* addition is preferred. In the case of AA (TS-AA and TS-AA-dimer), due to the absence of a methyl group at the alpha position which leads to steric repulsions, the *anti* addition is preferred. These trends are dictated by steric effects as well as by long range stabilizing interactions between the carbonyl oxygen and the hydrogens of the methyl group.

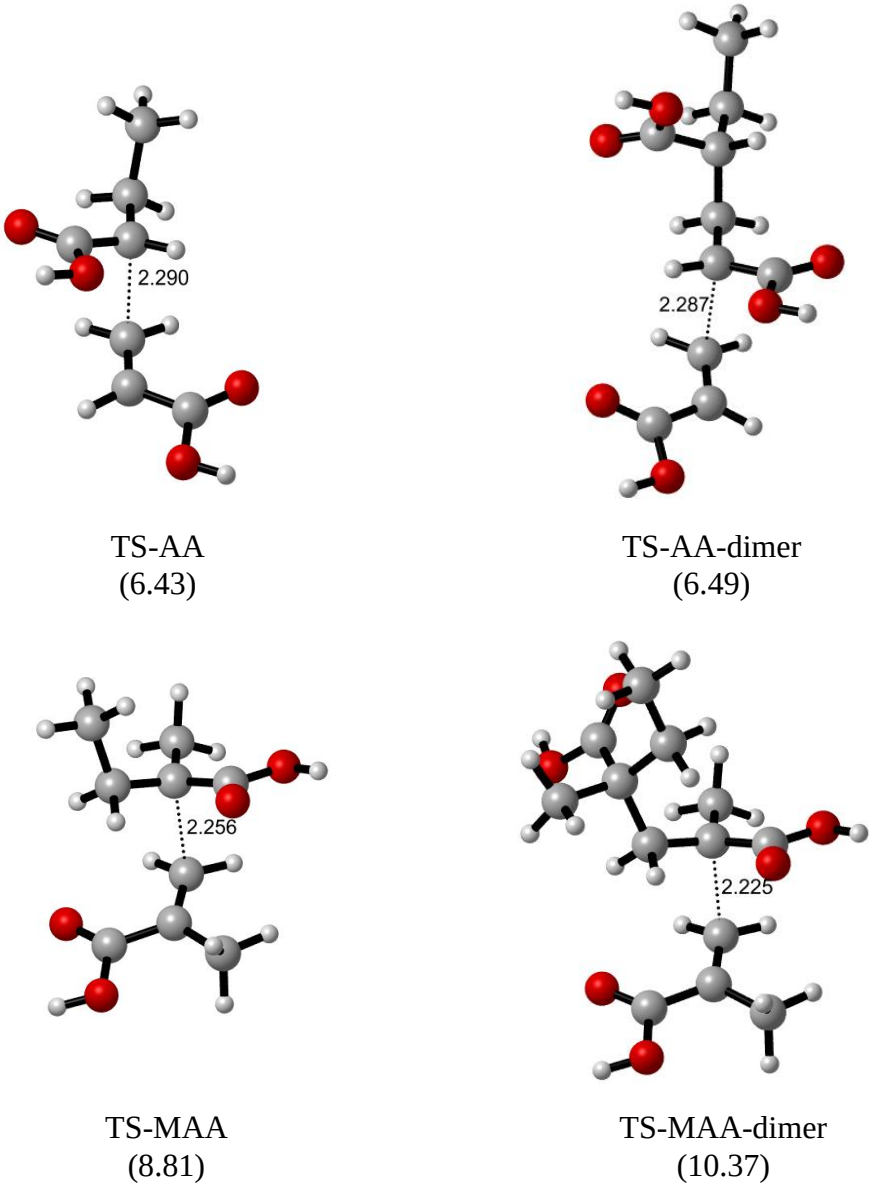

TS-AA
(6.43)

TS-AA-dimer
(6.49)

TS-MAA
(8.81)

TS-MAA-dimer
(10.37)

Figure 9.4. Most stable transition state structures of AA and MAA in vacuum (B3LYP/6-31+G(d)) (Electronic activation barriers are given in parenthesis (kcal/mol)).

AA has an earlier transition state (2.290 Å) and lower activation barrier of 6.43 kcal/mol (B3LYP/6-31+G(d)) than MAA which has a late transition state (2.256 Å) with an activation barrier of 8.81 kcal/mol (Figure 9.4). Most probably these geometrical features can be ascribed to additional steric effects present in MAA due to the methyl group at the α position of the monomer. The early transition state and the absence of the

steric group in the proximity of the reactive center lead to a higher rate for the propagation reaction in the case of AA.

The most stable transition states have been chosen (pro-racemo in case of AA and pro-meso in case of MAA) and the chains were extended to dimeric chains to mimic better the propagating radical. The dimeric transition states show similar features as compared to the unimeric model for AA with an early transition, a critical bond distance of 2.287 Å, and an activation barrier of 6.49 kcal/mol and a relatively late transition state for MAA with higher activation energy (10.37 kcal/mol) and critical bond distance of 2.225 Å (Figure 9.4). As the chain extends, the activation barrier for AA does not change significantly, whereas that of MAA increases by 1.5 kcal/mol, because the radical center is even more hindered in the alpha position.

Table 9.1. Relative electronic energies (ZPE included, kcal/mol) leading to pro-racemo and pro-meso unimeric transition states (B3LYP/6-31+G(d)).

Stereoregularity	**Radical**	**AA**		**MAA**	
		s-*cis*	s-*trans*	s-*cis*	s-*trans*
pro-racemo	*Syn*	**0.00***	0.87	0.09	0.34
pro-meso	*Syn*	0.31	1.38	**0.00****	0.39
pro-racemo	*Anti*	0.98	1.74	0.11	0.44
pro-meso	*Anti*	0.86	1.62	0.23	1.62

* TS-AA (pro-racemo) in Figure 2 has an electronic activation barrier of 6.43 kcal/mol (B3LYP/6-31+G(d)).

** TS-MAA (pro-meso) in Figure 2 has an electronic activation barrier of 8.81 kcal/mol (B3LYP/6-31+G(d)).

We have also considered transition structures where the propagation occurs via the attack of cyclic dimers of AA and MAA. The activation barriers for the latter are slightly lower than the others in vacuum (Figure 9.5, Table 9.2).

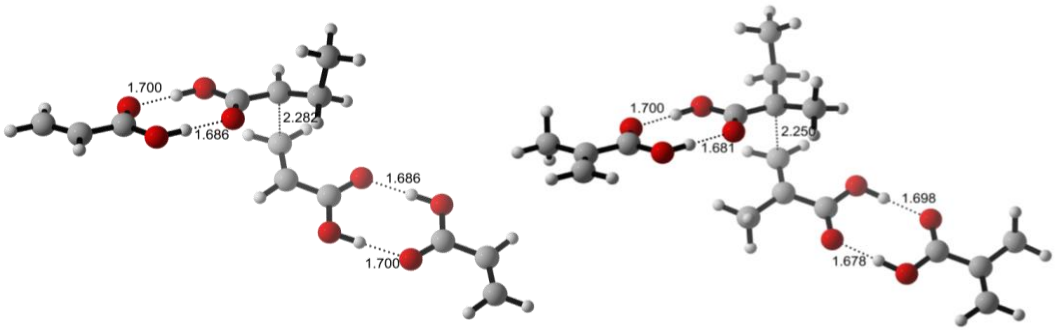

TS-AA-cyclic TS-MAA-cyclic

Figure 9.5. Propagation transition state structures for cyclic dimers of AA and MAA (B3LYP/6-31+G(d)).

9.3.1. Propagation of AA and MAA in Solution

Molecular dynamic simulations were carried out to understand the location of water molecules around the propagating species. Thus dimeric chains of AA (HOOC-CH_2-CH_2-C(H)(CH_3)(CO-OH) and MAA (HOOC-CH(CH_3)-CH_2-C(CH_3)(CH_3)(COOH) are chosen as models for PAA and PMAA respectively and were placed separately in a box of water as described earlier. Analysis of the radial distribution functions for PAA shows that the water molecules are trapped in the vicinity of the acidic ends of the dimeric chains (Figure 9.6) with the closest distance being the one between the -OH moiety of the carboxyl group of the polymeric chain and water. Almost all of the snapshots have recorded a water molecule to be within a hydrogen bond distance (1.7 Å) from the acidic proton on each end of the chain. A snapshot from the MD simulation of PAA displays the water molecules in the proximity of the acidic end (Figure 9.7). In view of these results we decided to use an explicit water molecule on the polymeric chain in the proximity of the acidic functionality to mimic explicit interactions with the solvent environment of PAA and PMAA in water. The bulk solvent effects on the geometry were further included by systematically optimizing the structures using a bulk electrostatic model (PCM), as explained in the methodology section.

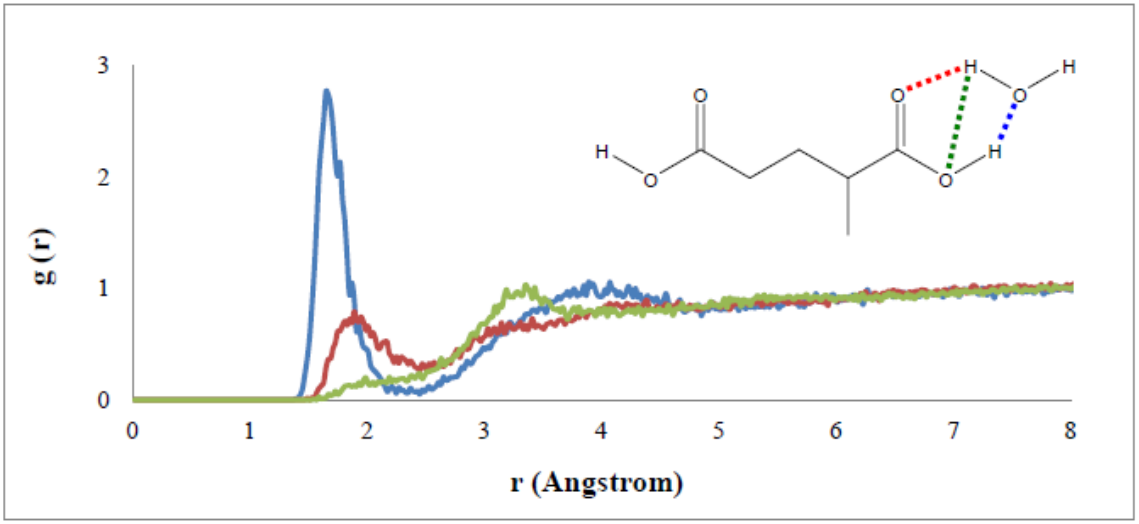

Figure 9.6. Radial distribution functions for a dimeric AA chain. The interactions between acidic protons of AA and oxygen of water are shown in blue (—); the interactions between the carbonyl oxygens of AA and the protons of water are in red (—); the interactions between the –OH oxygens of AA and the protons of the water are in green (—).

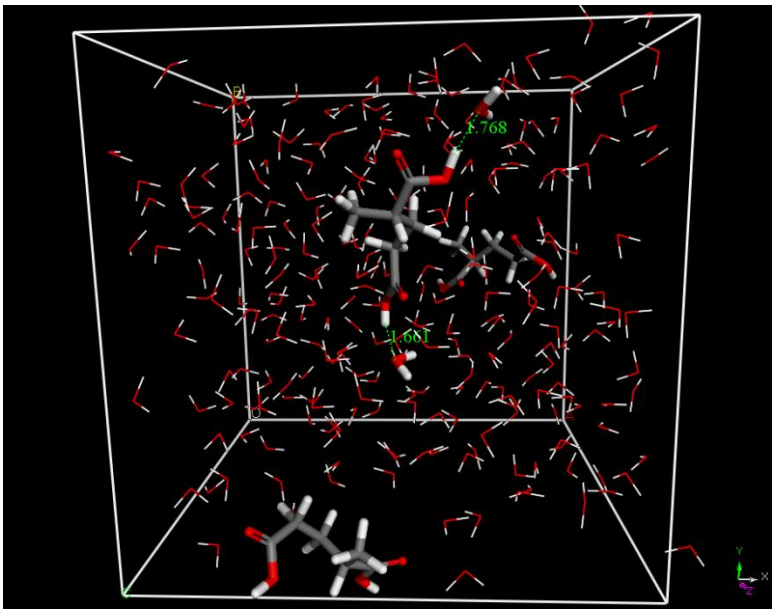

Figure 9.7. A snapshot from the MD simulation of PAA (model).

We constructed unimeric and dimeric transition states by adding one explicit water molecule to each acidic end of the monomer and the radical. The optimized transition structures in implicit solvent states are depicted in Figure 9.8. All the transition structures with explicit water molecules have longer critical bond distances than their counterparts in vacuum, indicating slightly earlier transition structures. Note that long critical bonds lead to an increase in the disorder of the polymeric chain and thus are an indication of rate acceleration. Both for AA and MAA critical distances slightly shorten while passing from the unimeric to the dimeric case, due to an increase of steric factors.

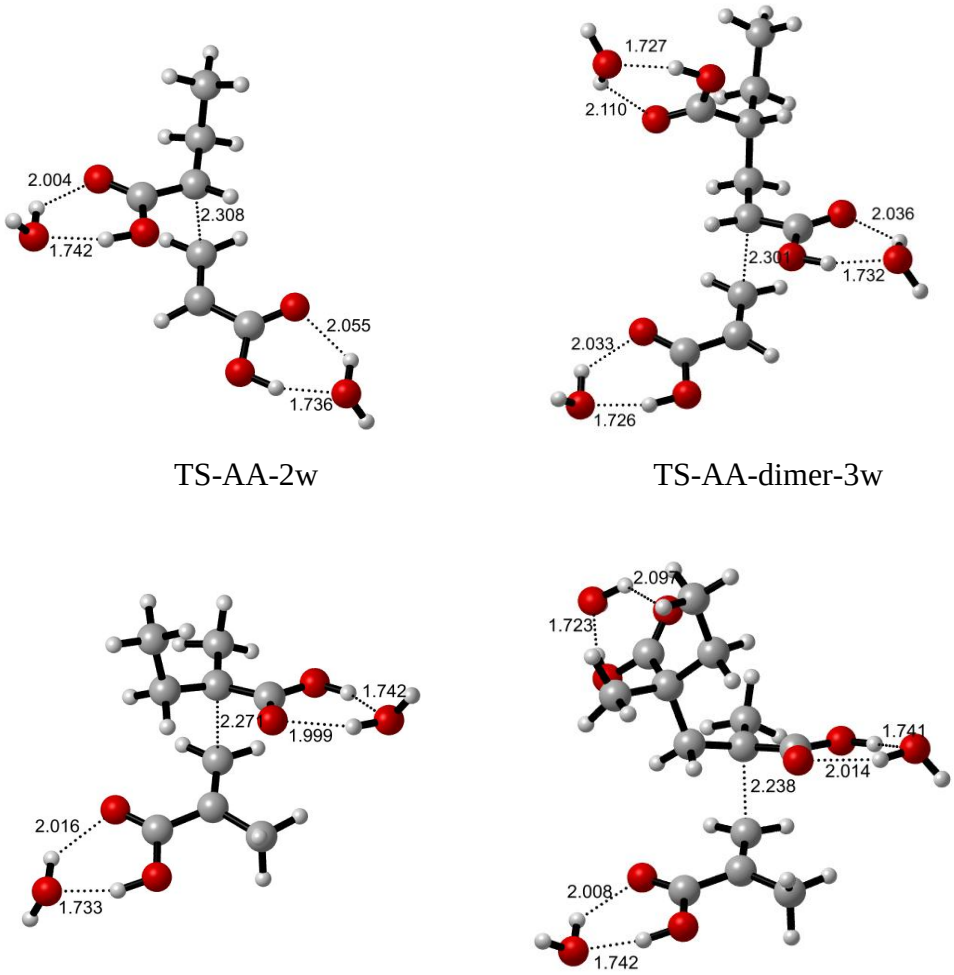

TS-AA-2w TS-AA-dimer-3w

TS-MAA-2w TS-MAA-dimer-

Figure 9.8. Most stable transition state structures of AA and MAA in water (B3LYP/6-31+G(d) -PCM).

A general overview of the electronic activation energies for AA and MAA in the various models, using different levels of theory together with the experimental values is given in Table 2. Polymeric chains with cyclic dimers have not been observed in MD simulations with water, thus the corresponding transition structures have not been considered.

For AA, the activation barrier increases slightly (0.79 kcal/mol) as passing from the gas phase to aqueous medium, whereas for MAA this change is even smaller (0.26 kcal/mol) [216, 226, 228]. Except for the B3LYP methodology all the other functionals - MPWB1K, M05-2X and M06-2X - predict the change in the activation barriers in the correct direction and magnitude. The experimental values are better described using a dimeric model. Note that the M06-2X functional reproduces the experimental values in solvent quite satisfactorily.

The Gibbs Free energies of activation as well as the propagation rate constants for both monomers in bulk and water are given in Table 9.3 together with the experimental data. Notice that in bulk polymerization the monomer acts just as one particular solvent and that it is the difference in intermolecular interactions between the transition structure and different solvent environments which determines whether there is a solvent dependence of k_p. Since the activation barriers in water and in vacuum are very close to each other (Table 9.2), the rate enhancement must be attributed to the increase of entropy in aqueous medium.

It is worthwhile noticing that the kinetic parameters obtained with the M06-2X/6-311+G(3df,2p)//B3LYP/6-31+G(d) methodology and the dimeric model are closer to the experimental ones than those obtained with the other methodologies.

Table 9.2. Activation energy barriers (kcal/mol) for the unimeric propagating chains of AA and MAA .The corresponding values for the dimers are given in parenthesis, those for the cyclic structures are displayed in brackets and italics. ΔE_a is defined as the difference between the activation barrier in gas phase ($E_{a\text{-}gas}$) and in water environment ($E_{a\text{-}water}$).

		E_{a_gas}	E_{a_water}	ΔE_a
	B3LYP[a]	6.43 (6.49) [*6.38*]	8.78 (9.41)	-2.35 (-2.92)
AA	MPWB1K[b]	5.09 (5.20) [*4.76*]	5.16 (5.53)	-0.07 (-0.33)
	M05-2X[b]	1.98 (2.23) [*1.62*]	2.08 (2.48)	-0.10 (-0.25)
	M06-2X[b]	3.02 (3.24) [*2.59*]	3.03 (3.40)	-0.01 (-0.16)
	Exp.	2.89[c]	3.68[d]	-0.79
	B3LYP[a]	8.81 (10.37) [*8.61*]	11.73 (14.07)	-2.92 (-3.70)
MAA	MPWB1K[b]	6.13 (6.86) [*5.88*]	5.20 (6.45)	0.93 (0.41)
	M05-2X[b]	2.26 (3.20) [*2.02*]	1.38 (2.77)	0.88 (0.43)
	M06-2X[b]	3.06 (3.76) [*2.61*]	1.96 (3.25)	1.10 (0.51)
	Exp.	3.85±0.4[e]	3.47±0.1[f]	0.26

[a] Gas phase optimizations are carried out at the B3LYP/6-31+G(d) level and aqueous phase optimizations are carried out for the explicitly solvated structures by PCM methodology with B3LYP/6-31+G(d).

[b] The 'Functional'/6-311+G(3df,2p)//B3LYP/6-31+G(d)-PCM methodology has been used for aqueous phase calculations.

[c] extrapolated from 40 wt% at 25°C. Ref 228

[d] 10 wt% AA at 2.1-20.1°C. Ref 228

[e] extrapolated from 40 wt% at 25°C. Ref 226

[f] 15 wt% MAA at 25°C. Ref 226

Table 9.3. Gibbs Free energies of activation (25°C, kcal/mol) and propagation rate constants k_p ($L.mol^{-1}.s^{-1}$) in bulk and aqueous media. The corresponding values for the dimers are given in parenthesis, those for the cyclic structures are displayed in brackets and italics.

		Bulk		**Water**	
		$\Delta G^{\ddagger}$	k_p	$\Delta G^{\ddagger}$	k_p
AA	MPWB1K[a]	14.53 (14.93) [*14.45*]	3.36E+03 (1.71E+03) [*3.85E+03*]	14.88 (14.70)	1.85E+03 (2.51E+03)
	M05-2X[a]	11.42 (11.95) [*11.31*]	6.37E+05 (2.60E+05) [*7.74E+05*]	11.80 (11.66)	3.35E+05 (4.27E+05)
	M06-2X[a]	12.46 (12.96) [*12.28*]	1.10E+05 (4.75E+04) [*1.51E+05*]	12.76 (12.58)	6.71E+04 (0.91E+05)
	Exp.	-	2.01E+04[b]	-	1.32E+05[c]
MAA	MPWB1K[a]	17.51 (19.23) [*15.57*]	2.21E+01 (1.20E+00) [*5.78E+02*]	16.61 (17.89)	1.01E+02 (1.16E+01)
	M05-2X[a]	13.63 (15.57) [*11.71*]	1.54E+04 (5.81E+02) [*3.91E+05*]	12.79 (16.11)	6.37E+04 (2.34E+02)
	M06-2X[a]	14.43 (16.13) [*13.67*]	3.95E+03 (2.24E+02) [*1.44E+04*]	13.37 (14.69)	2.36E+04 (2.58E+03)
	Exp.	-	5.74E+02[d]	-	3.83E+03[e]

[a] COSMO-RS is used for calculations in bulk, optimized structures in vacuum are used. The 'Functional'/6-311+G(3df,2p)//B3LYP/6-31+G(d) methodology is used for the energetics. For the aqueous phase calculations, explicitly solvated structures are optimized with B3LYP/6-31+G(d) in a continuum (PCM), the 'Functional'/6-311+G(3df,2p)//B3LYP/6-31+G(d)-PCM methodology is used for the energetics and is followed by COSMO-RS calculations in water at 25 ºC.
[b] extrapolated from 40 wt% at 25°C. Ref 228
[c] 10 wt% AA in water at 2.1-20.1°C. Ref 228
[d] extrapolated from 40 wt% at 25°C. Ref 226
[e] 15 wt% MAA in water at 25°C. Ref 226

The rate acceleration of AA_{bulk} as compared to MAA_{bulk} can be attributed to the presence of the methyl group in the alpha position of MAA that hinders the radical center for further attack. A direct relationship between the reactivity and the electron density on the atoms where the reaction occurs was suggested in the work of Beuermann [208]. The solvent is expected to change the electron density of the carbon atoms of the double bond and alter the reactivity as discussed in the literature [226]. In order to validate this suggestion, we performed a charge analysis on the various monomers, with and without explicit solvent interactions. Based on the calculated NBO charges for the monomers and the radicals in the gas phase and in water some qualitative trends can be drawn (Figure 9.9). C1 of *s-cis*-AA has a charge of -0.334, whereas C1 of ***s****-trans*-MAA is -0.355; C1 of s-*cis*-AA is more electron deficient and more susceptible to be attacked by a radical. The radical center C2 (secondary radical) of *syn*-AA-R is richer in electrons as compared with the radical center of *anti*-MAA-R (tertiary radical). Overall based on the electronic charges one can predict AA to polymerize faster than MAA. In solution, the electron densities do not change much and this in agreement with our previous findings on the origin of rate acceleration in solution: rate acceleration in solution is due to a change in entropy rather than a change in electronic charges.

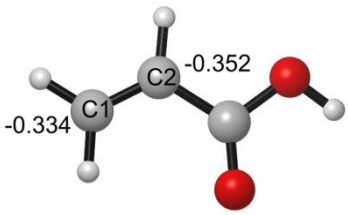

s-*cis*-AA

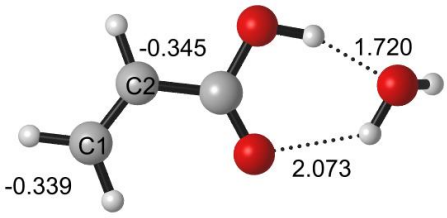

s-*cis*-AA-1w

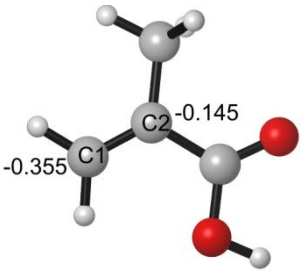

s-*trans*-MAA

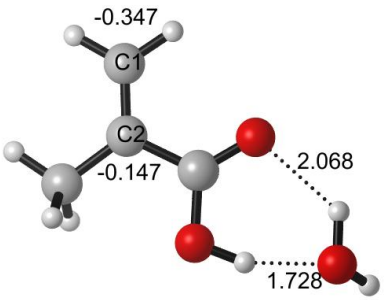

s-*trans*-MAA-1w

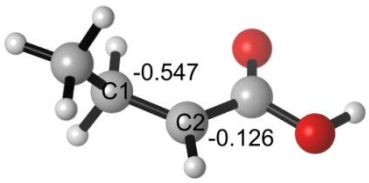

syn-AA-R

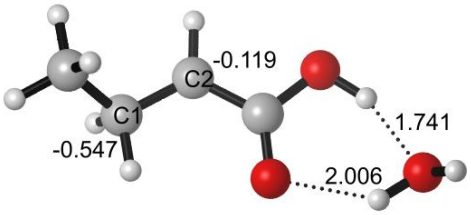

syn-AA-R-1w

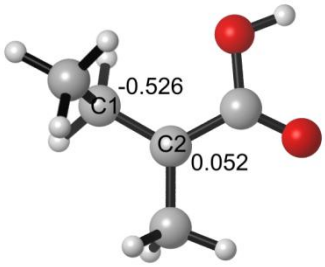

anti-MAA-R

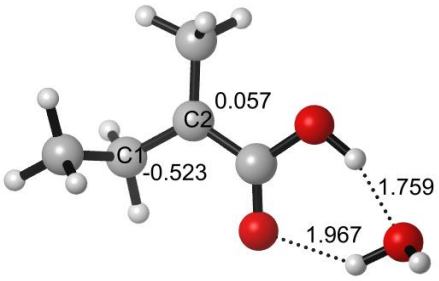

anti-MAA-R-1w

Figure 9.9. NBO charges and geometrical parameters for the monomers and radicals in vacuum and in aqueous medium (optimized in water with the PCM methodology) (B3LYP/6-31+G(d)).

9.4. Conclusions

In this study, we have used static and molecular dynamics computational tools to rationalize the rate acceleration in the free radical polymerization of AA and MAA in water and assess their relative rates of polymerization. Experimentally, it was found that AA polymerizes faster than MAA both in bulk and in water. Furthermore the rate of polymerization is faster in water than in bulk both for AA and MAA. Molecular dynamics calculations were performed to understand the explicit interactions between the polymer chain and the water molecules. It was found that water prefers a coordination with the carboxyl group of the propagating chains. Extensive transition state searches were performed for MAA and AA in gas phase and water environment. The slower propagation for AA compared to MAA, was ascribed to additional steric effects present in MAA due to the methyl group at the α position of the monomer in both media. In both cases, in water, the acidic end of the reacting species is captured by water. In water, the electronic distribution at the reactive centers in the transition states diminishes, the critical bonds are longer, the entropy of activation increases, the rate of propagation increases. This study emphasizes the fact that M06-2X/6-311+G(3df,2p)//B3LYP/6-31+G(d) methodology reproduces quantitatively the experimental rate accelerations of AA and MAA in water and is more suitable for modeling their free radical polymerization kinetics. Overall, quantum chemical tools have been used to enlighten the rate acceleration of the free radical polymerization of both species in water. The dimeric models and the methodology proposed in this study can be used for further understanding of the solvent effect on the propagation kinetics of acrylate derivatives. The propagation of cyclic dimers plays also a role in the free radical polymerization kinetics of AA and MAA in bulk, conclusive results about the propagation mechanism can further be drawn by taking into consideration longer propagating chains.

10. CONCLUSION

The experimental part of this study consists of the synthesis of a series of alkyl α-hydroxymethacrylate (RHMA) derivatives with various secondary functionalities (ether, ester, carbonate, and carbamate) and terminal groups (alkyl, cyano, oxetane, cyclic carbonate, phenyl and morpholine) to understand the effect of intermolecular interactions, H-bonding, π-π interactions, and dipole moment on monomer reactivity. All of the monomers except one ester and one ether derivative are novel. The polymerization rate, are determined by using photo-DSC. The π-π interactions were found to be an important rate enhancing factor. Among the monomers studied here, aromatic carbamates capable of both π-π interactions and hydrogen bonding were found to show the highest rate of polymerization. There is a correlation between the chemical shift differences of the double bond carbons, the calculated dipole moments, and the reactivities only for nonhydrogen bonded monomers.

Another point of interest concerns the reactive diluents. Six hydroxyl-containing methacrylate monomers with various third functionalities have been synthesized to investigate the relationship between molecular structure and monomer reactivity. The photo-, homo-, and copolymerization behavior of the monomers with 2-2-bis[p-(2'-hydroxy-3'-methacryloxypropoxy)phenylene]propane (Bis-GMA) were investigated. The maximum rates of polyerization of monomer 13-hydroxy-10-oxo-2,5,8,11-tetraoxatetradecan-14-yl methacrylate (D2), 3-(2-cyanoacetoxy)-2-hydroxypropyl methacrylate (D3), 2-hydroxy-3-(2-phenylacetoxy)propyl methacrylate (D4), 3-((diethoxyphosphoryl)oxy)-2-hydroxypropyl methacrylate (D5), and 2-hydroxy-3-methoxypropyl methacrylate (D6) were found to be greater than that of triethylene glycol dimethacrylate (TEGDMA) and Bis-GMA. For the more reactive monomers (D2, D3 and D4), the oxygen sensitivity of polymerization was found to be low due to a hydrogen abstraction/chain transfer reaction.

Another study includes the synthesis and evaluations of polymerizable (*tert*-butyl 2-((4-benzoylphenoxy)methyl)acrylate (E1), 2-((4-benzoylphenoxy)methyl)acrylic acid (E2) and 2-(ethoxycarbonyl)allyl 4-benzoylbenzoate (E3)) and their polymeric photoinitiators (poly-E1, poly-E2, poly-E3) bearing side-chain benzophenone (BP) for the UV-curing coatings. TEGDMA, 1,6-hexanedioldiacrylate (HDDA) and 2-hydroxyethylmethacrylate (HEMA) initiated by E1-E3, poly-E1, poly-e2, poly-E3 and BP were studied by photo-DSC using N,N-dimethyl para toluidine as coinitiator. Both monomeric and polymeric initiators were found to have high efficiencies than BP and polymeric ones were even more reactive than polymerizable ones.

In the computational part, the polymerization trends of RHMA and acrylates were modeled by using density functional methods in order to understand the structure-reactivity relationship between the monomer and its overall rate of polymerization. The kinetics of the various reactions was modeled by means of the Transition State Theory Various levels of theory were tested to investigate the influence of the methodology on the kinetics. Reaction barriers are lowered by the presence of stabilizing C=O…H-C interactions. A similar picture emerges for acrylate monomers where the transition structures for hexyl acrylate are stabilized by C=O…H-C interactions and those of benzyl and phenyl are stabilized by C=O…H-Φ as well as by weak π-π interactions. Overall the dimeric models used earlier to understand the effect of pendant groups (linear vs cyclic) on the polimerizability of acrylate derivatives reproduce qualitatively the experimental trend in this study as well. The M06-2X/6-31+G(d) methodology reproduces the experimental trend qualitatively.

The structure-reactivity of RHMA monomers was also evaluated by using the Multiple Regression Analysis (MRA) methodogy in order to predict the polymerization kinetics. 19 RHMA monomers, whose rate of photopolymerization have been measured, and their corresponding radicals have been modeled by using the B3LYP/6-31+G(d) methodology. Quantitative descriptors were evaluated and among the various descriptors, the ionization energy (IE) and electron affinity (EA), the atom-atom overlap weighed NAO bond order of carbonyl double bond ($BO_{C=O}$) of the monomers, the resonance stabilization parameter of the monomeric radical (Res), and the Mulliken atomic spin density (ρ_s) of the

radical were found to be correlated with the experimental rates of photopolymerization. A linear relationship between the descriptors and the rate of polymerization was established. This study is expected to shed light on predicting the reactivities of RHMA monomers prior to their synthesis and thus to rank their photopolymerization abilities based on their structural properties.

Another highly relevant but difficult issue concerns the influence of solvent on the free radical polymerization behavior. In most cases a combination of an explicit and implicit solvation model has been used. The effect of the solvent on the reactivity of acrylic acid (AA) and methacrylic acid (MAA) has been explained by using static and molecular dynamics computational tools. Experimentally, it was found that AA polymerizes faster than MAA both in bulk and in water. Furthermore the rate of polymerization is faster in water than in bulk both for AA and MAA. Classical Molecular Dynamics calculations have been carried out to determine the location of the solvent molecules in the proximity of the dimeric poly(AA) and poly(MAA) units. A combined implicit/explicit solvent model was used for the evaluation of the kinetics of the dimeric polymer chains. We show that the rate acceleration of both polymers in water is mainly due to entropic rather than electrostatic effects and is in agreement with experimental findings. Moreover the slower propagation rate of MAA versus AA is ascribed to additional steric effects present in MAA due to the methyl group at the α position of the monomer. Among the functionals used, the M06-2X/6-311+G(3df,2p)//B3LYP/6-31+G(d) methodology reproduces the experimental rate constants quantitatively the best.

APPENDIX A: SPECTROSCOPY DATA

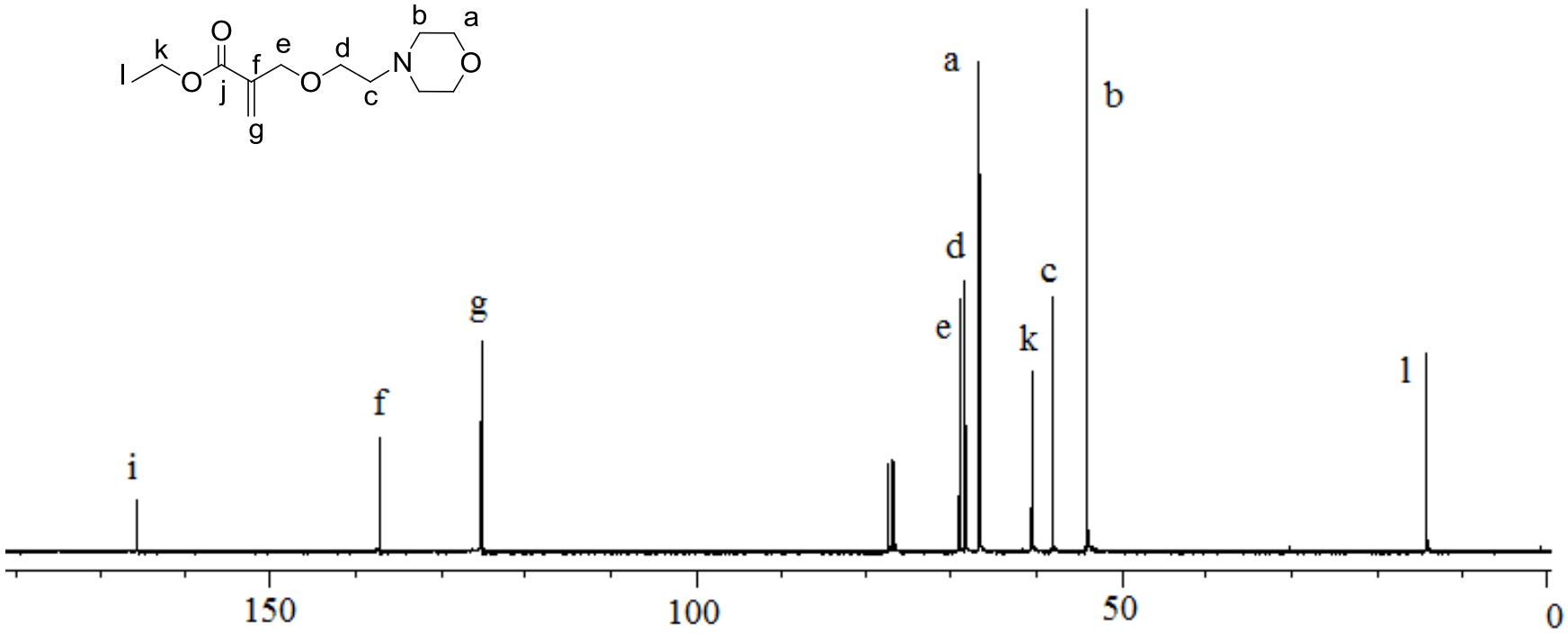

Figure A.1. ^{13}C-NMR spectra of monomer **A1**.

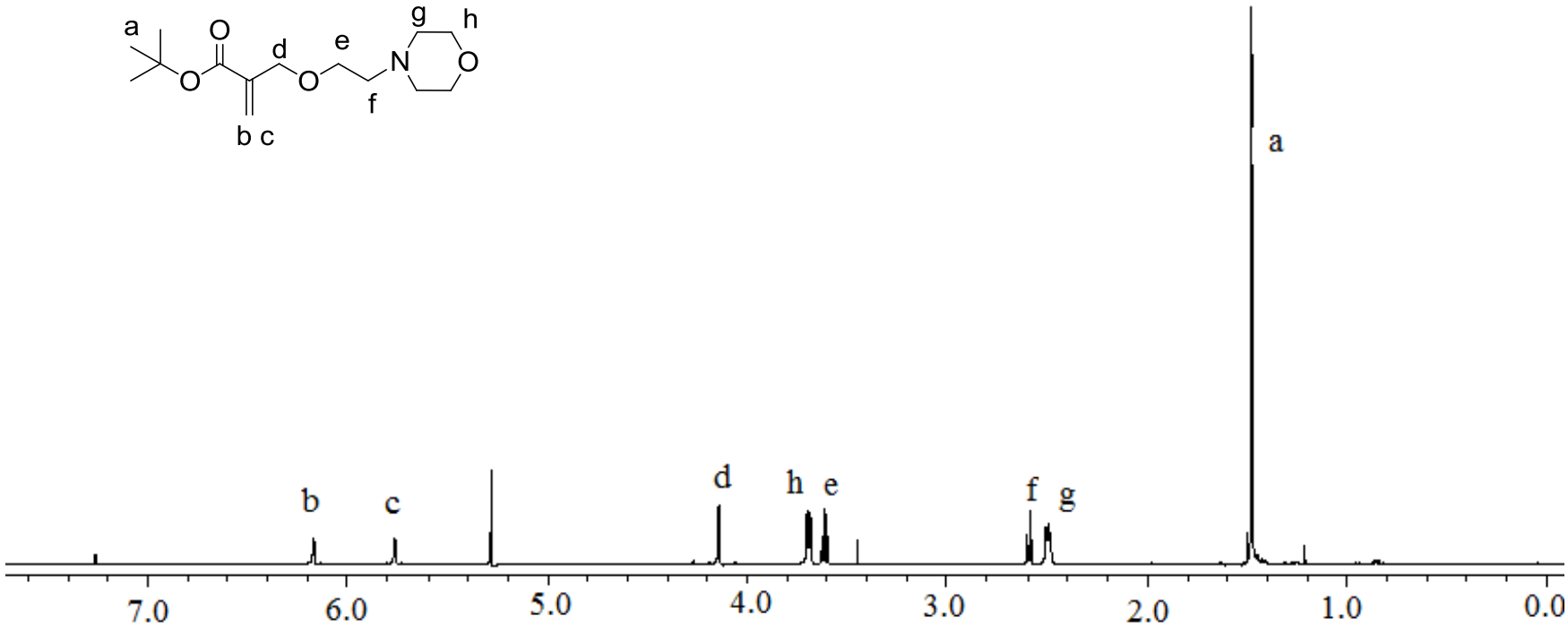

Figure A.2. ^{1}H-NMR spectra of monomer **A2**.

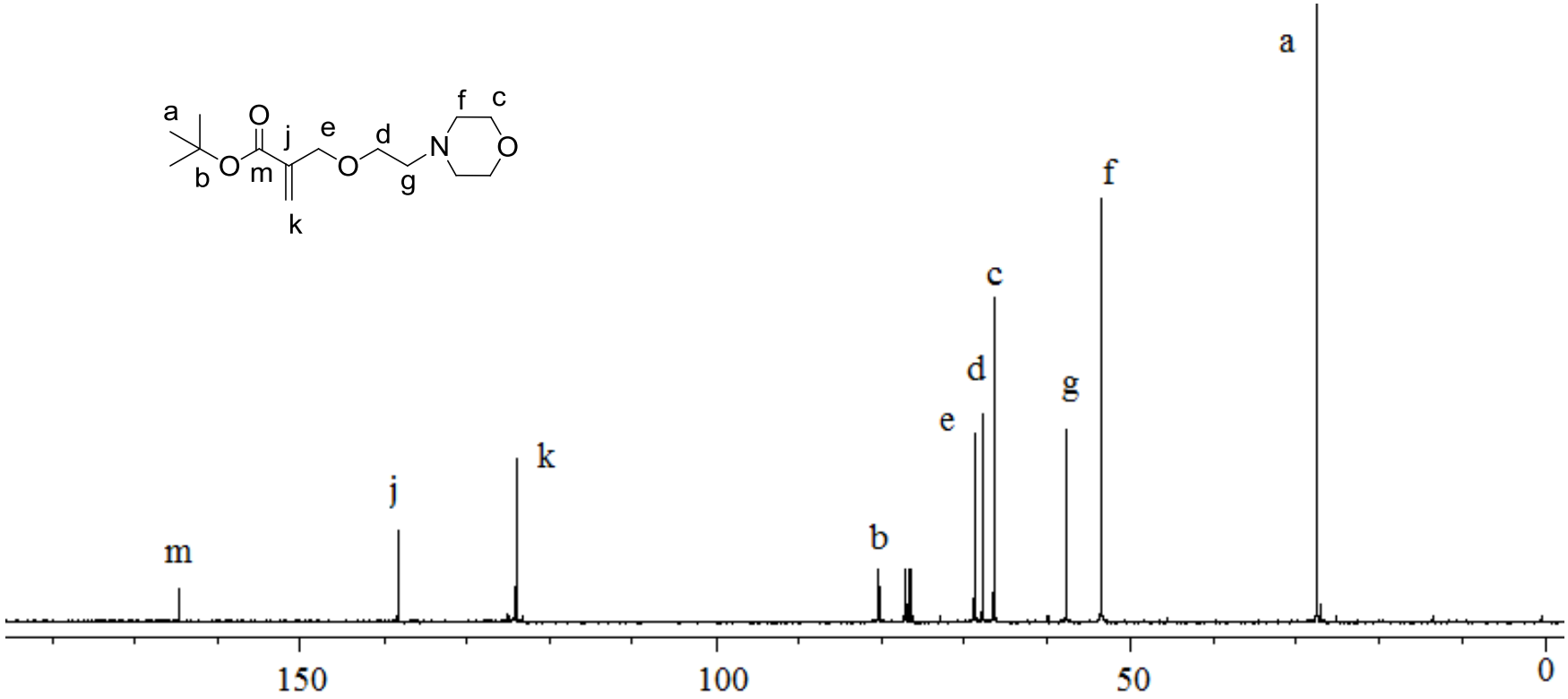

Figure A.3. ^{13}C-NMR spectra of monomer **A2**.

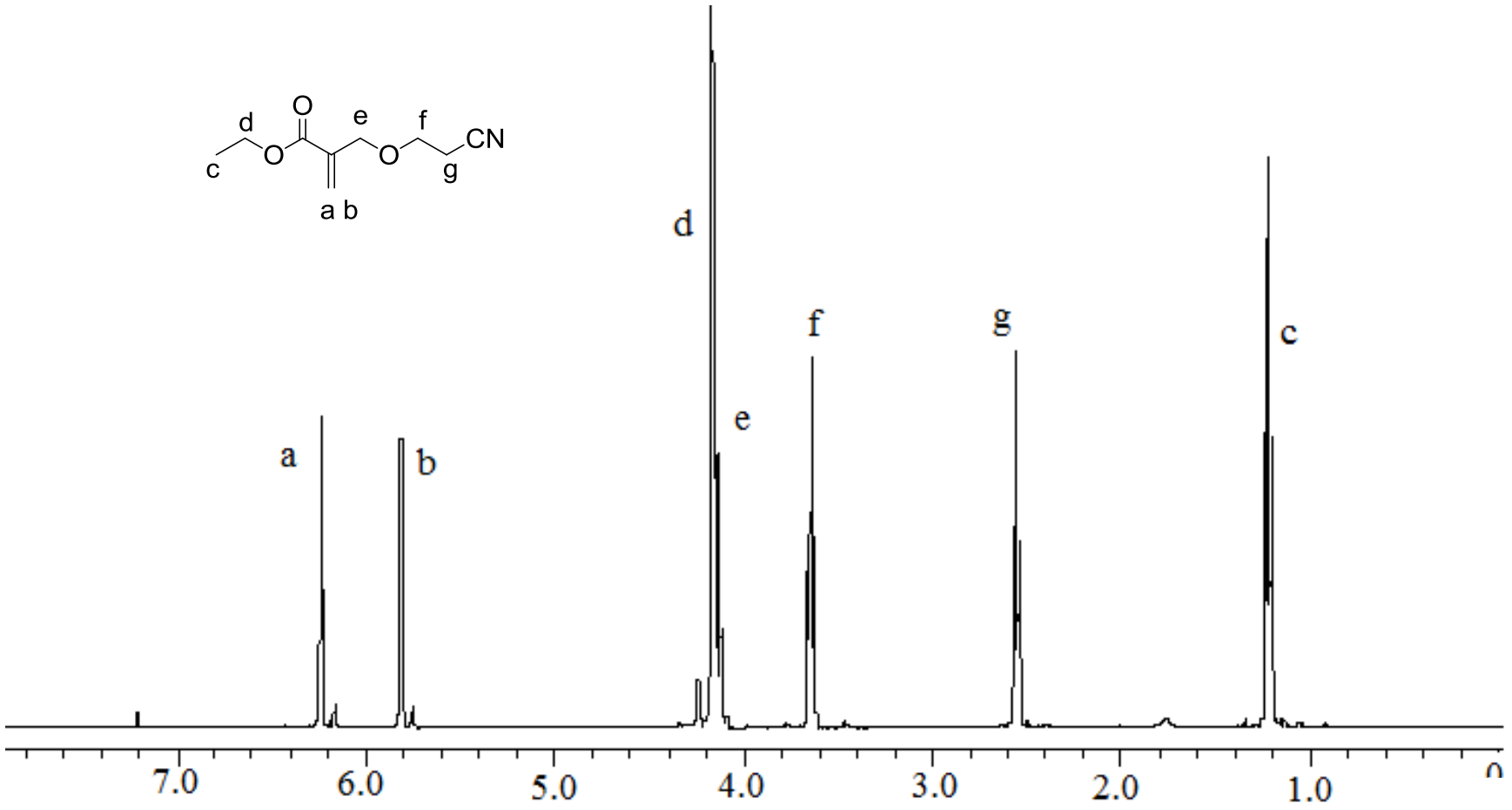

Figure A.4. ^{1}H-NMR spectra of monomer **A3**.

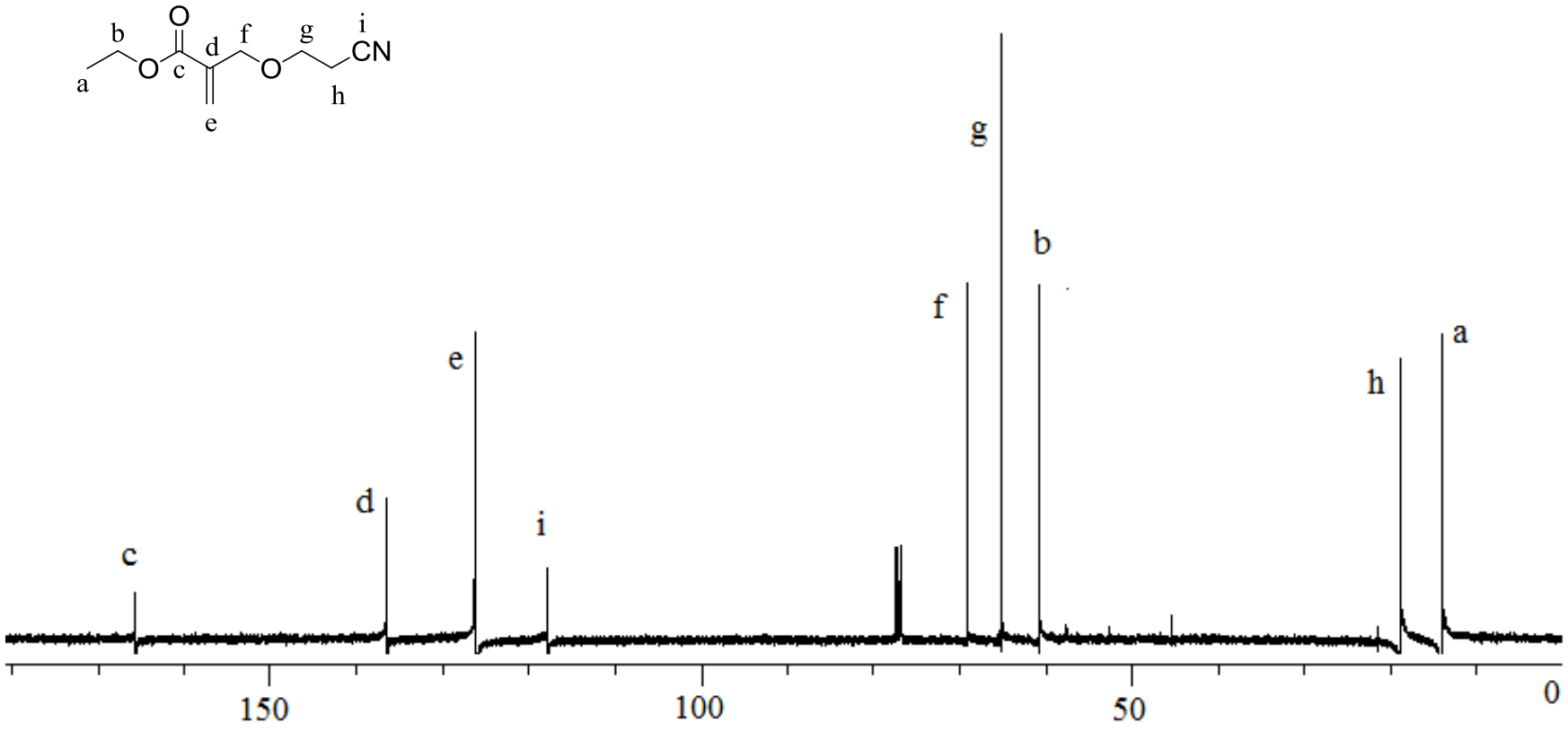

Figure A.5. ^{13}C-NMR spectra of monomer **A3**.

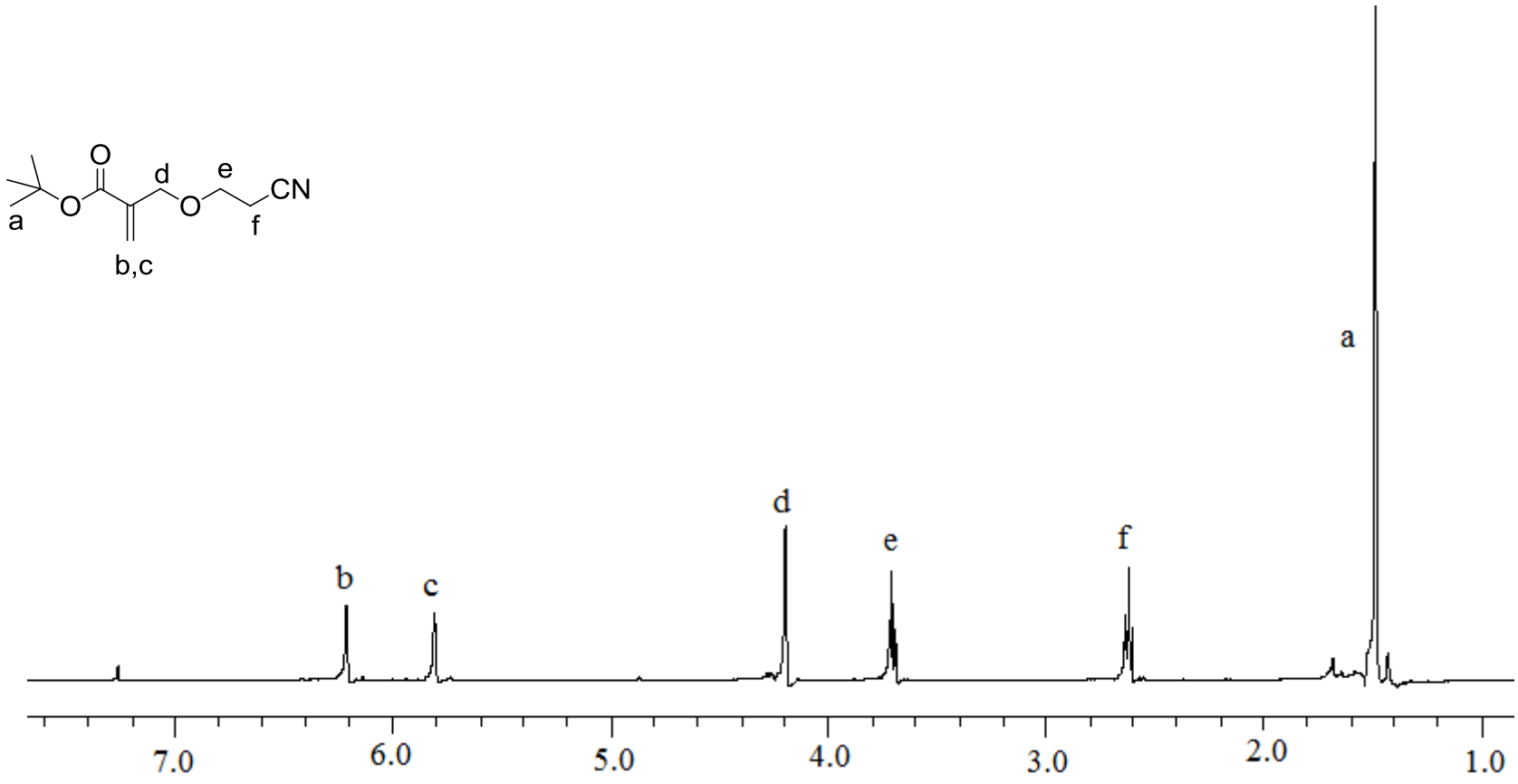

Figure A.6. ^{1}H-NMR spectra of monomer **A4**.

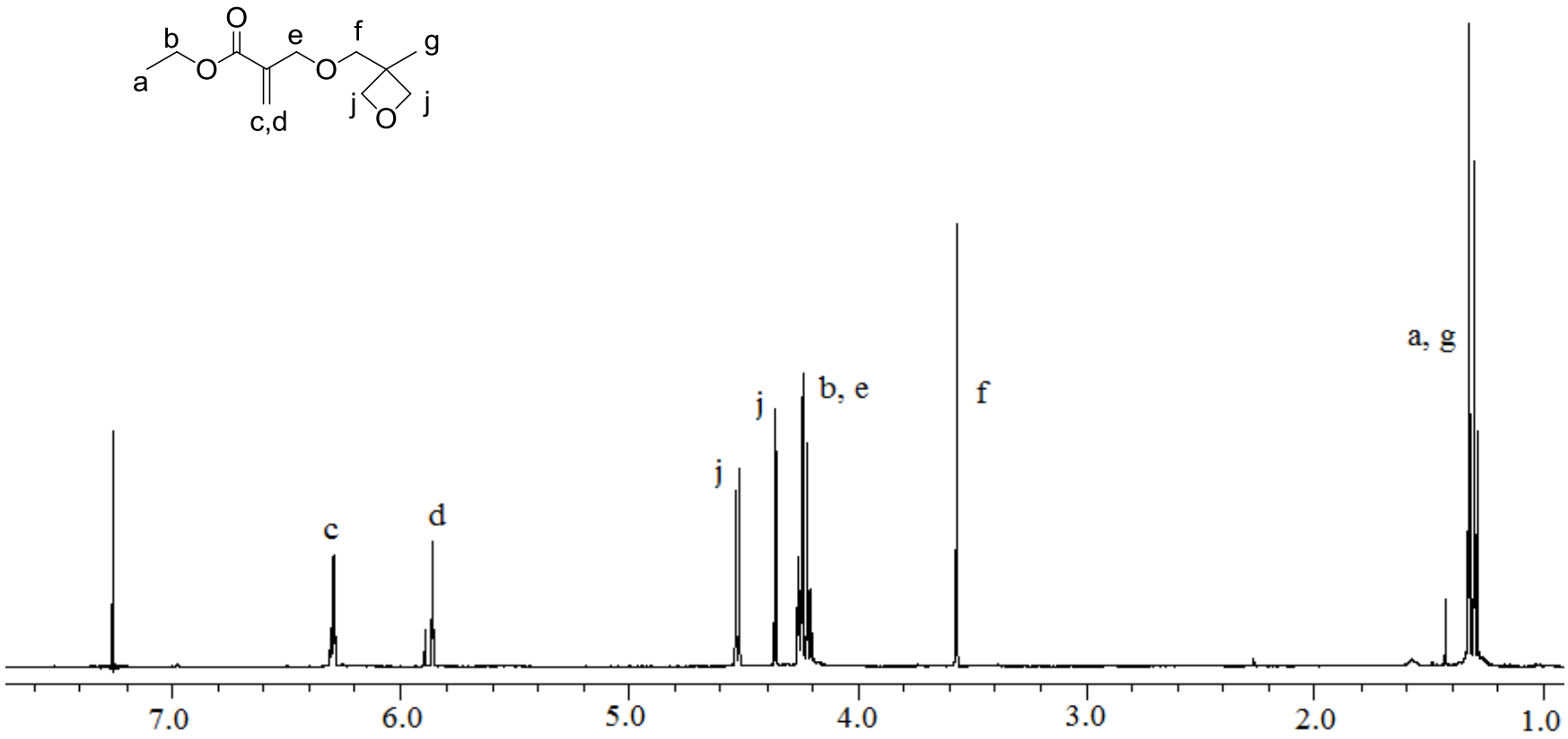

Figure A.7. ^{1}H-NMR spectra of monomer **A5**.

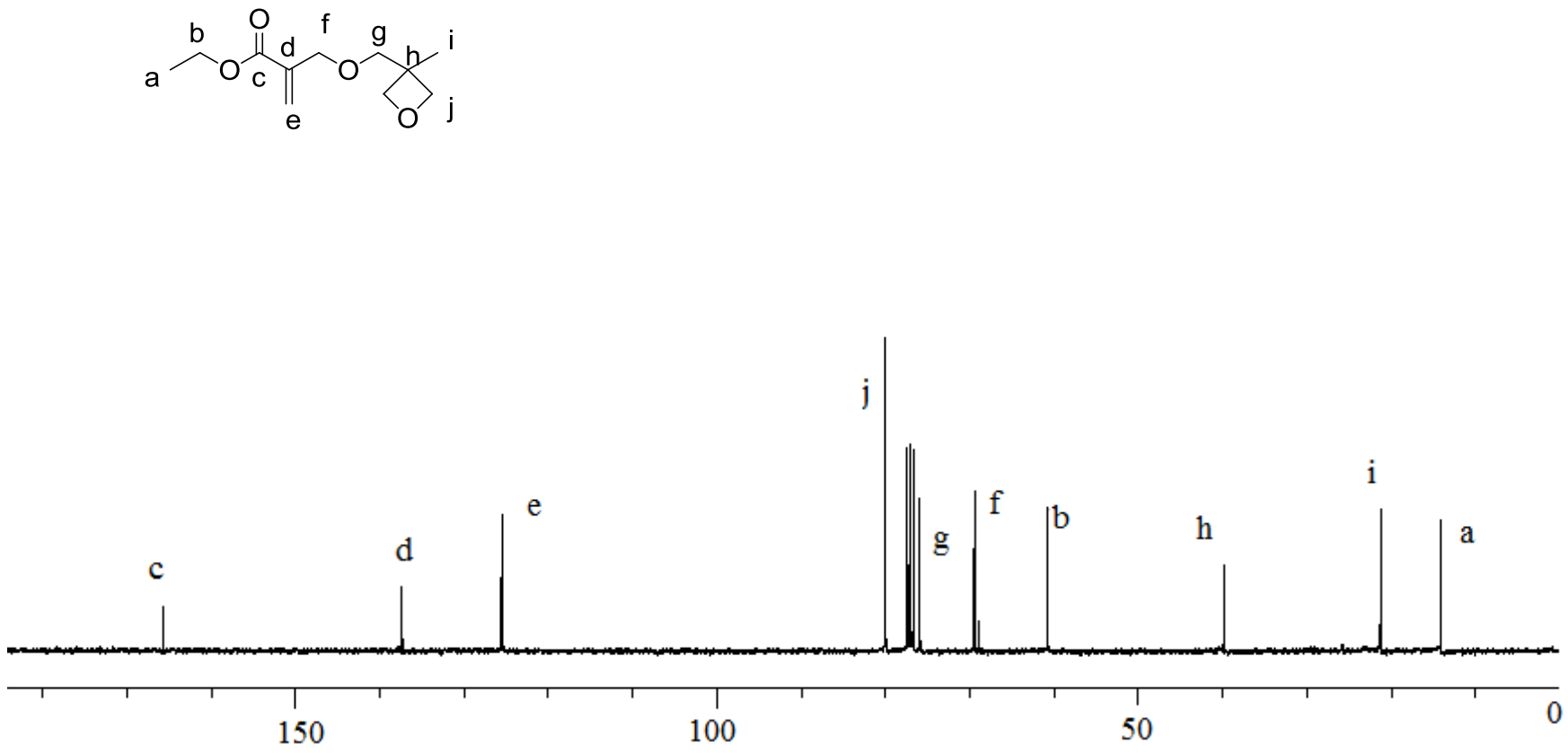

Figure A.8. ^{13}C-NMR spectra of monomer **A5**.

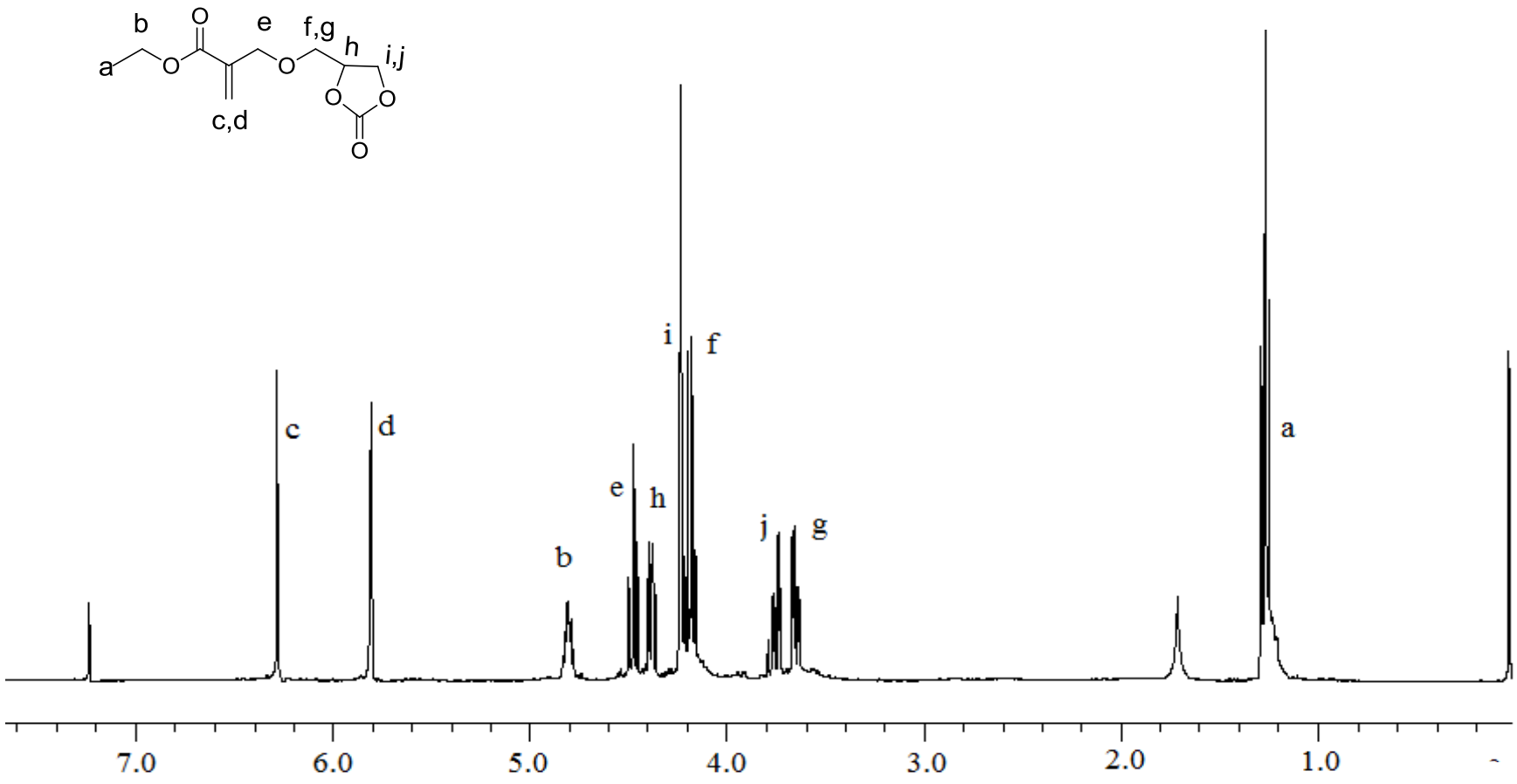

Figure A.9. ^{1}H-NMR spectra of monomer **A6**.

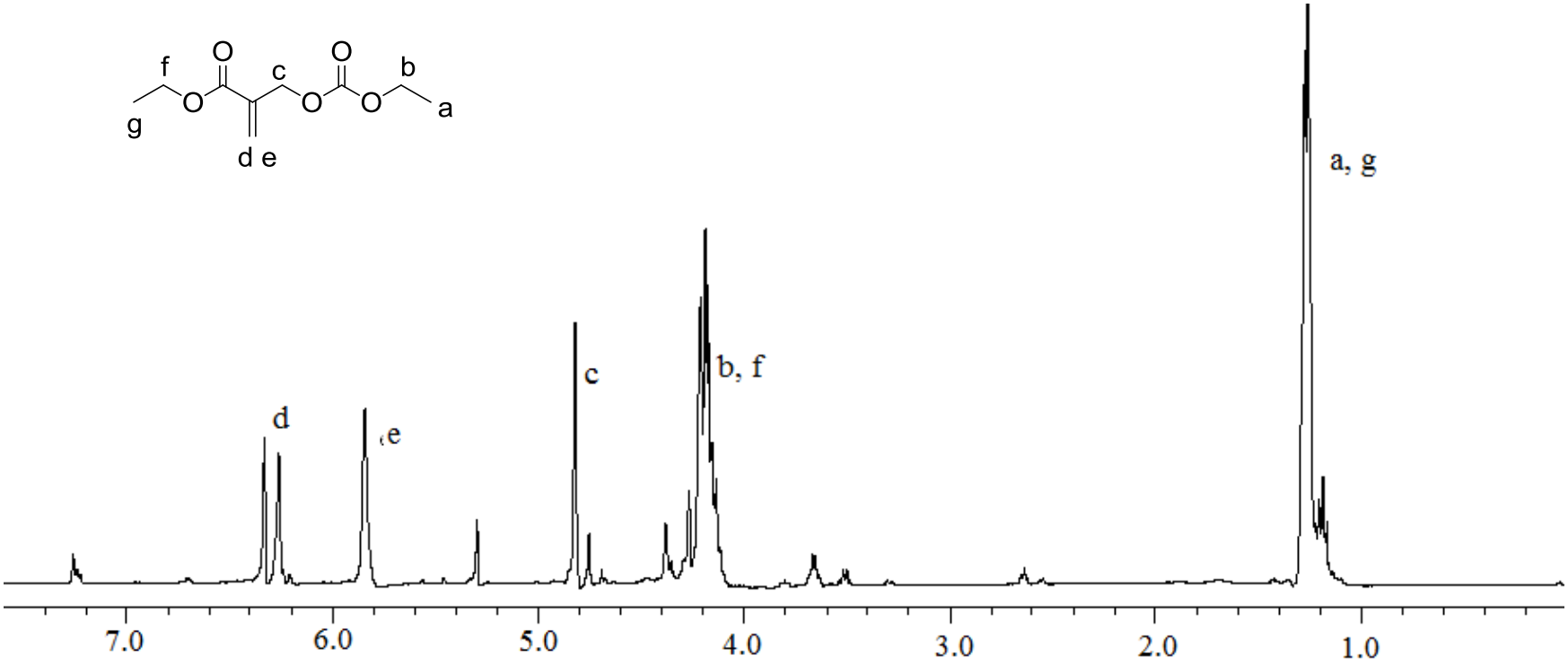

Figure A.10. ^{1}H-NMR spectra of monomer **A8**.

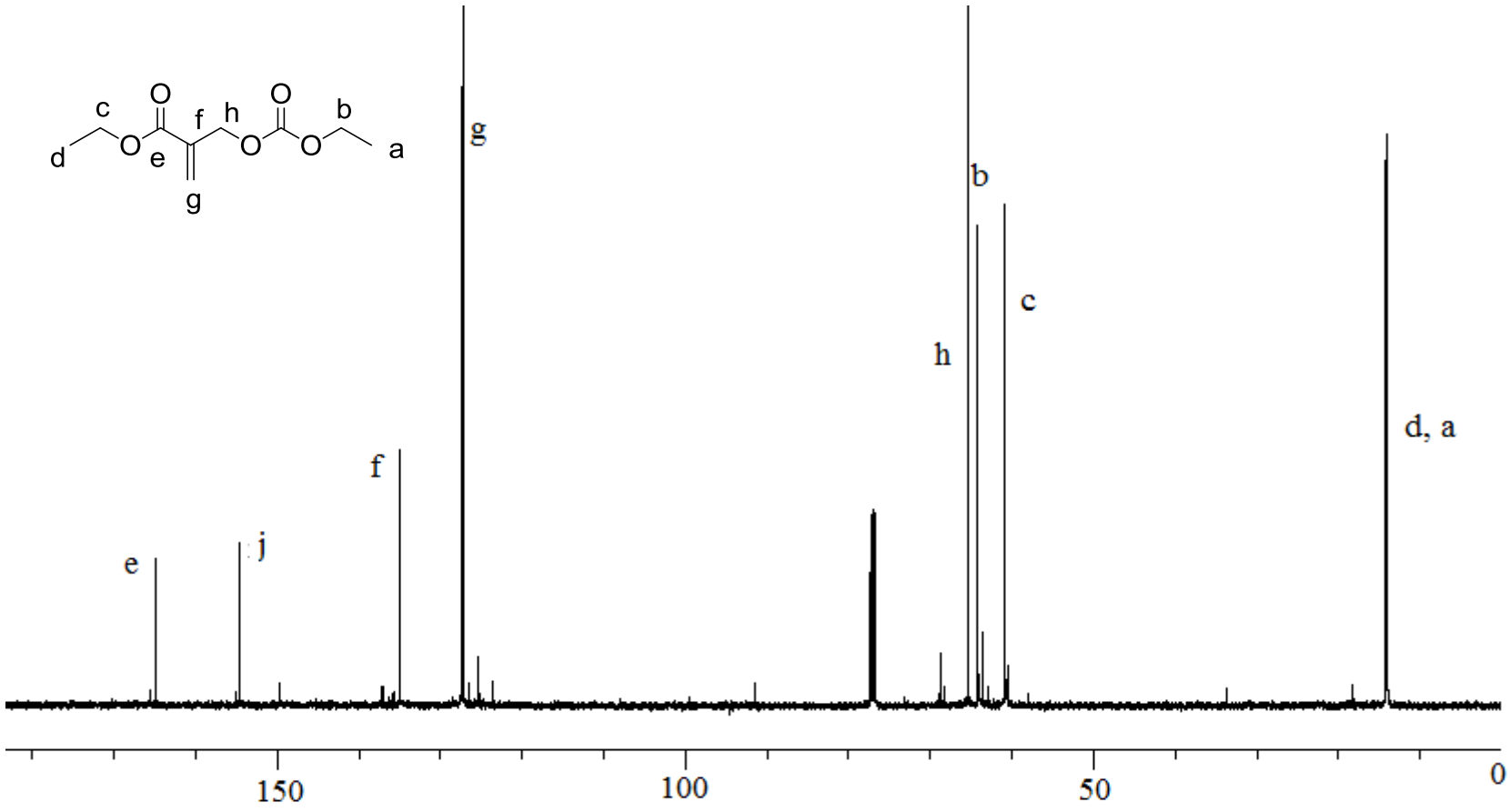

Figure A.11. ^{13}C-NMR spectra of monomer **A8**.

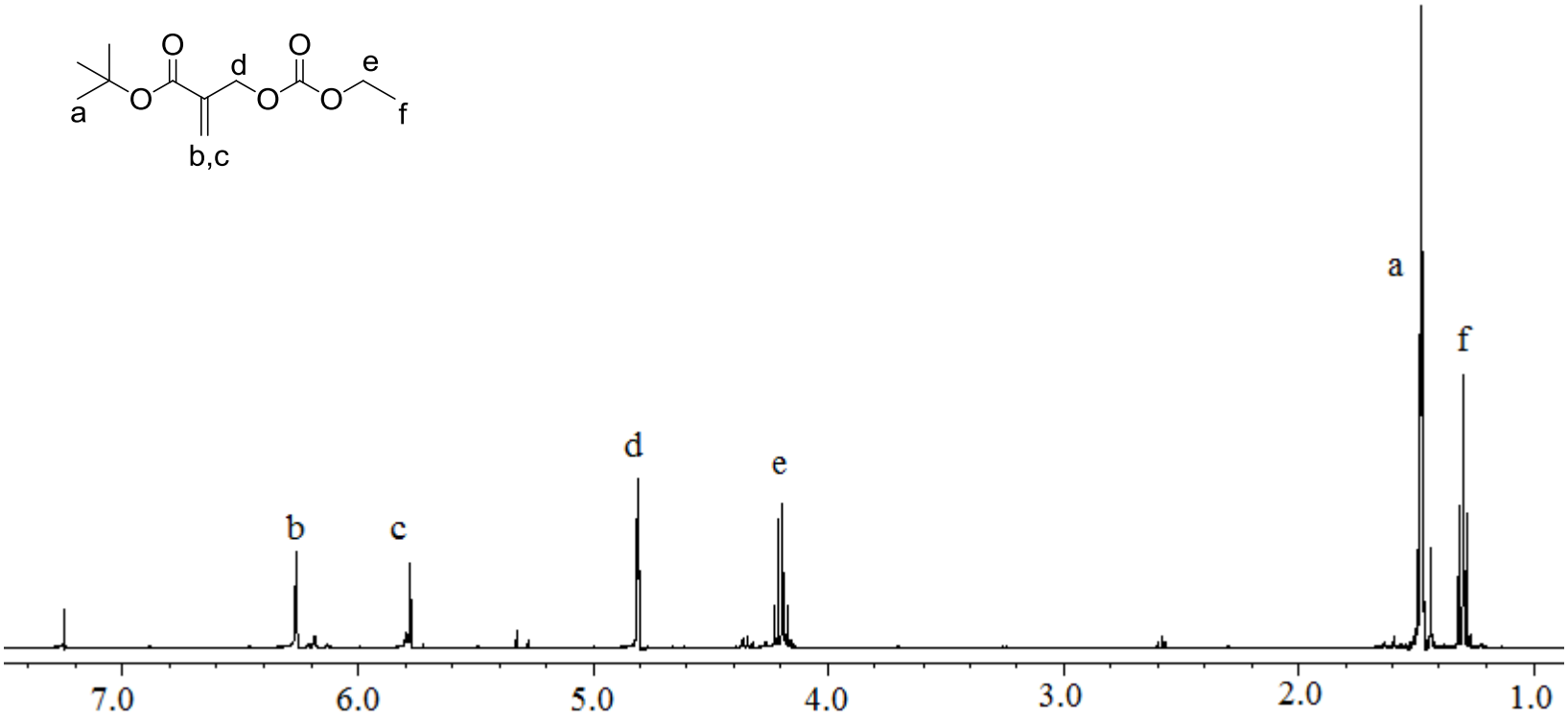

Figure A.12. ^{1}H-NMR spectra of monomer **A9**.

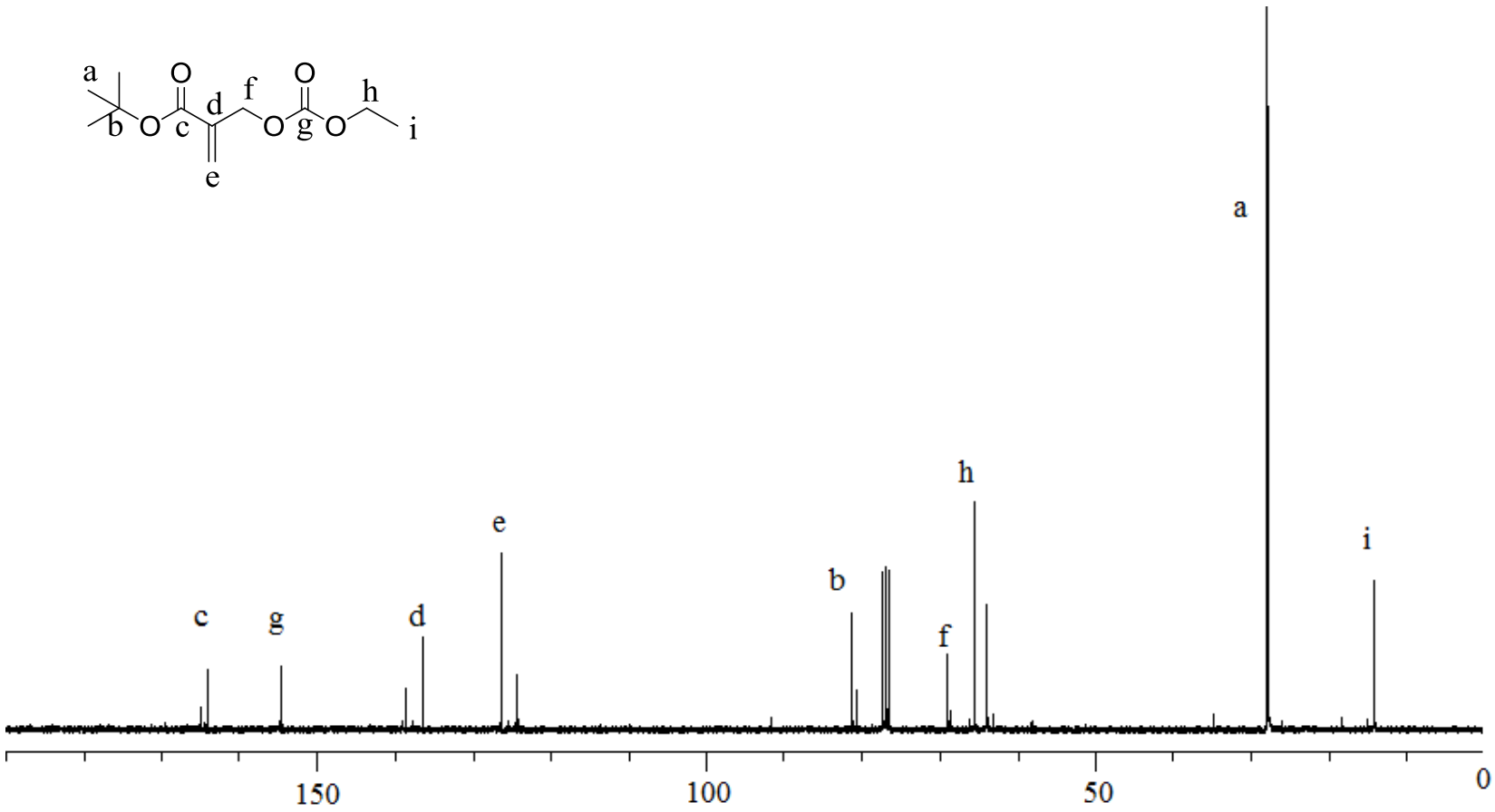

Figure A.13. ^{13}C-NMR spectra of monomer **A9**.

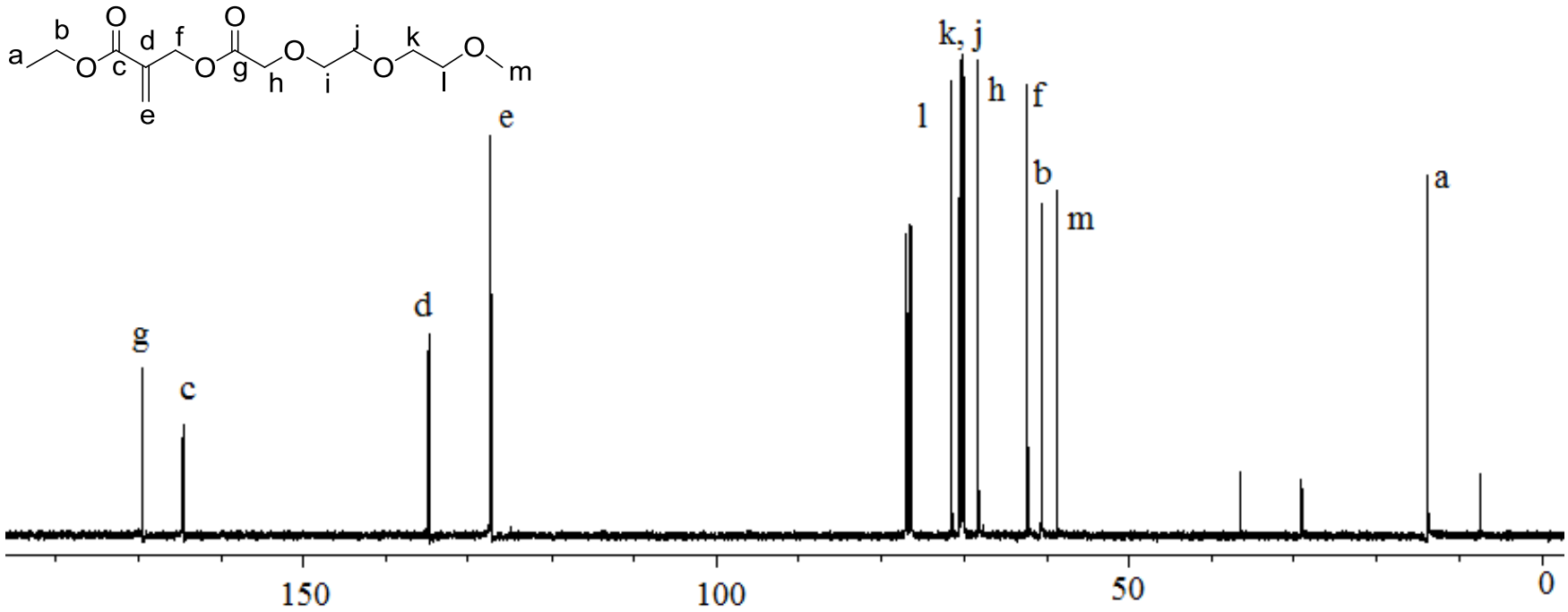

Figure A.14. ^{13}C-NMR spectra of monomer **A10**.

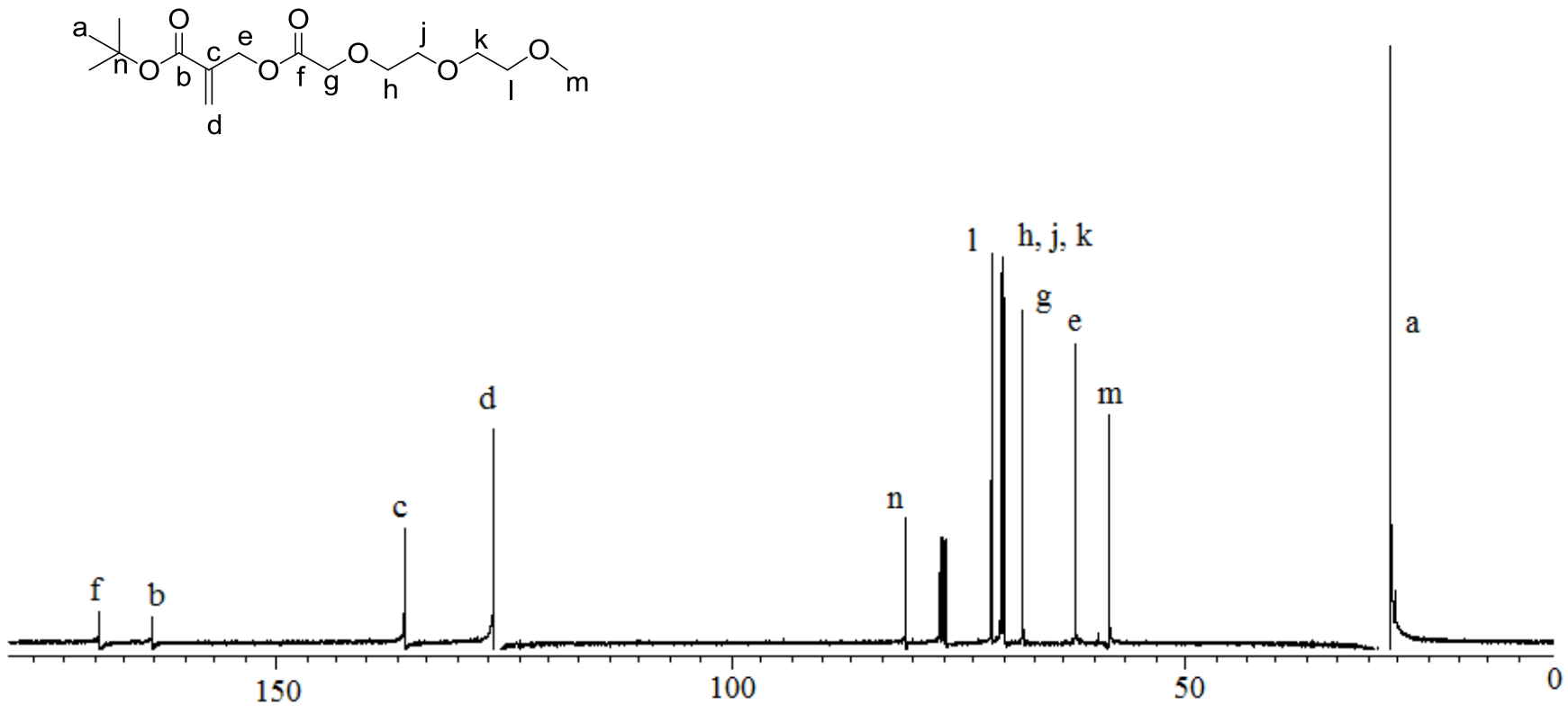

Figure A.15. ^{13}C-NMR spectra of monomer **A11**.

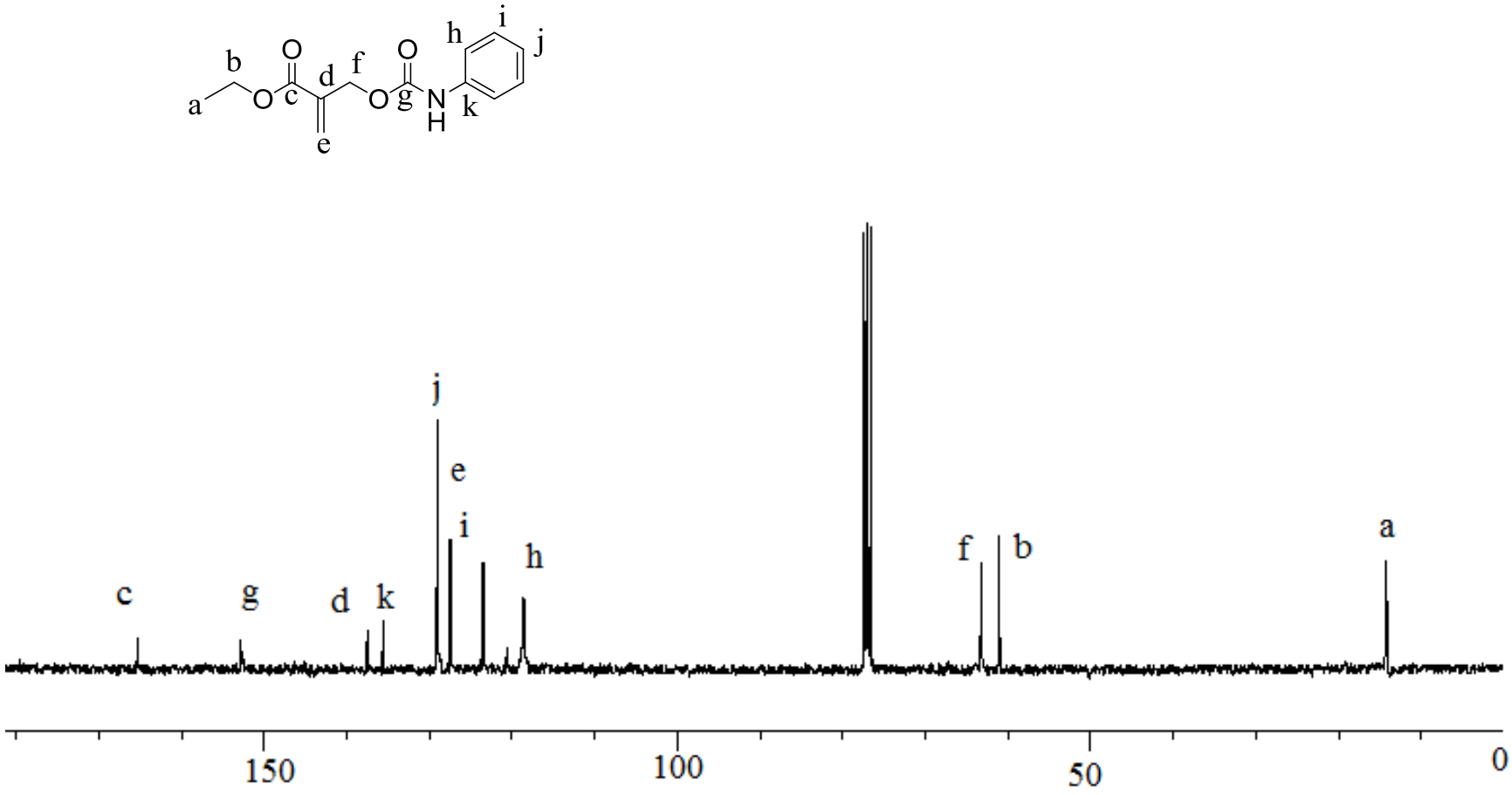

Figure A.16. ^{13}C-NMR spectra of monomer **A12**.

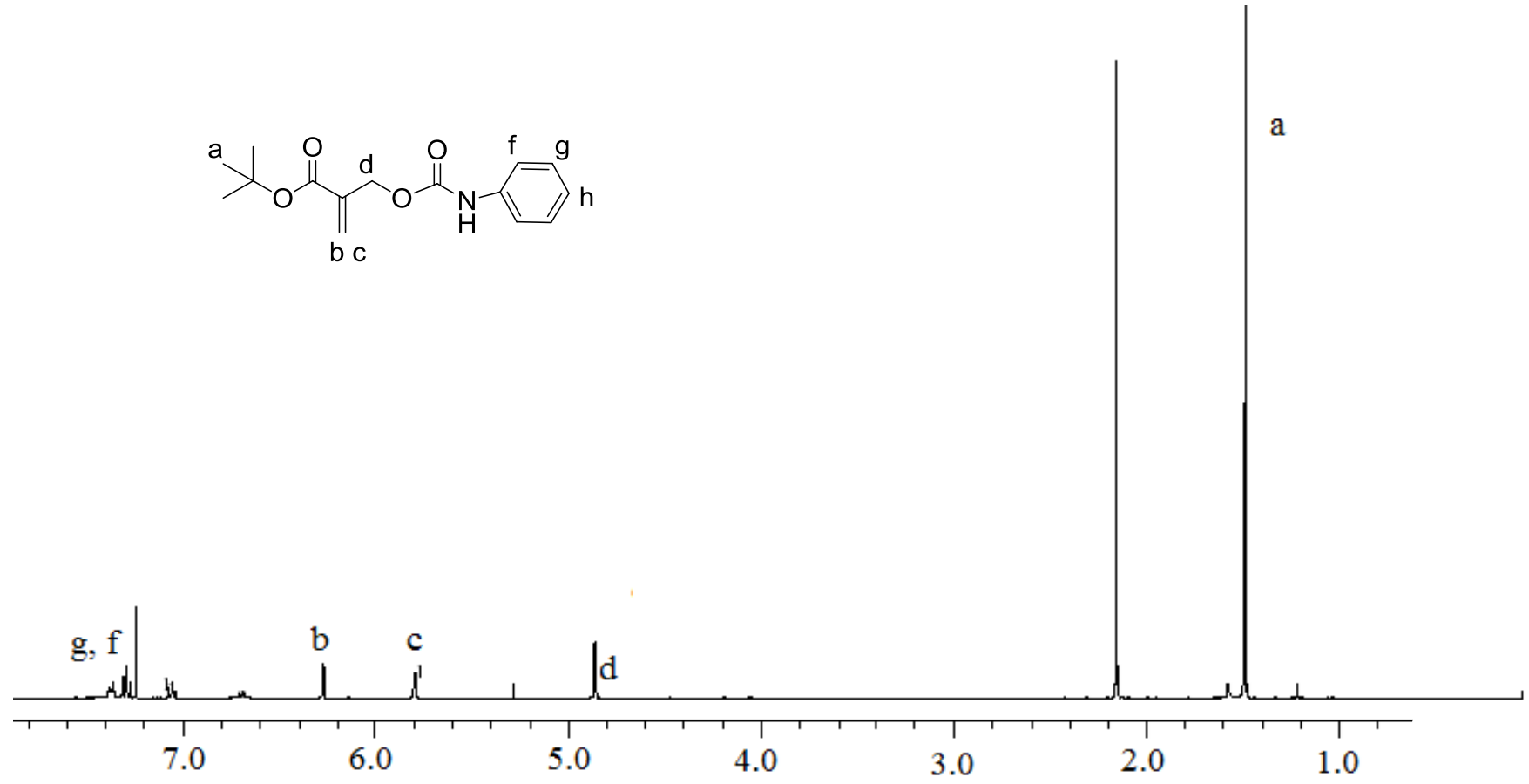

Figure A.17. ^{1}H-NMR spectra of monomer **A14**.

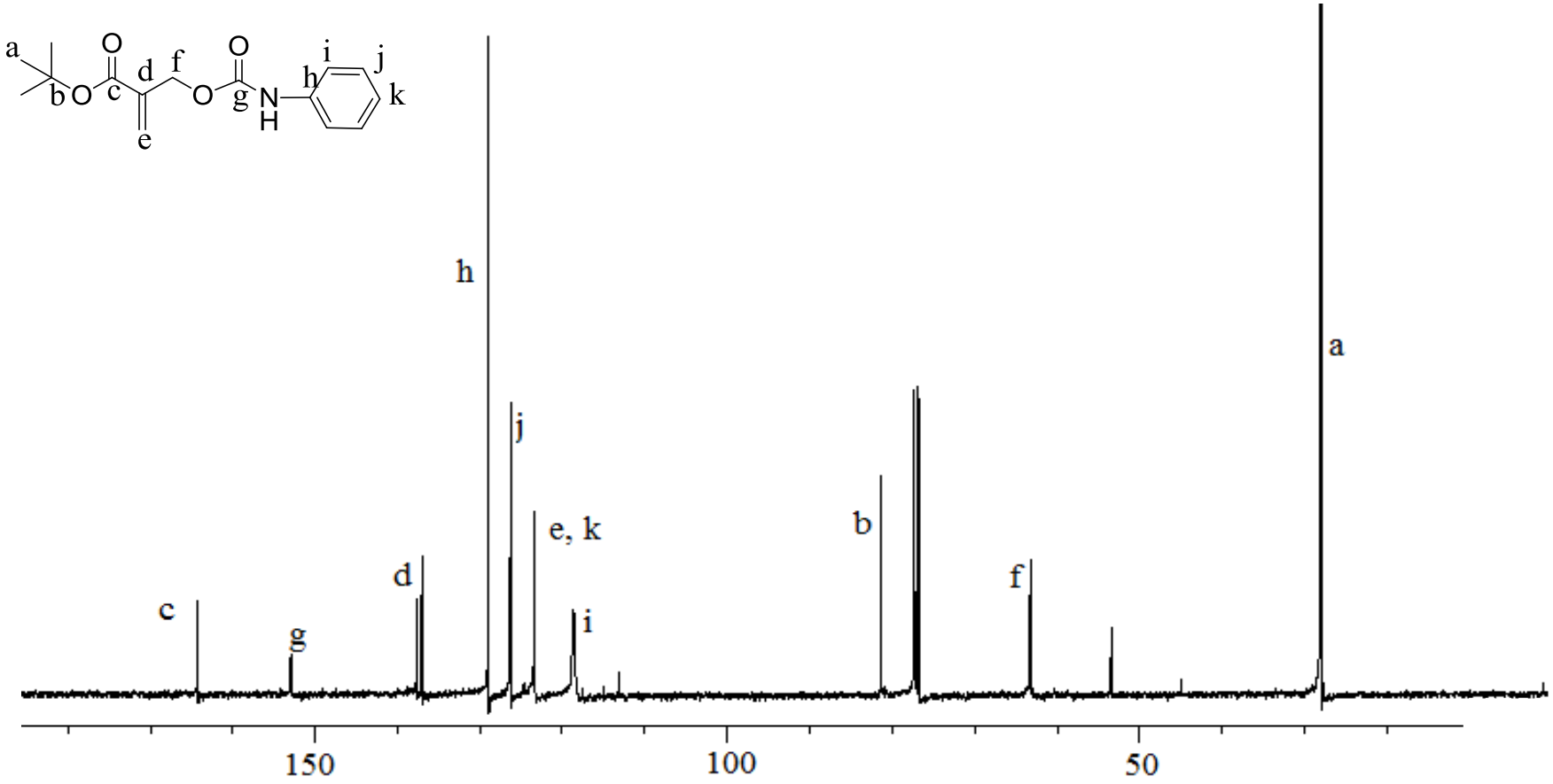

Figure A.18. ^{13}C-NMR spectra of monomer **A14**.

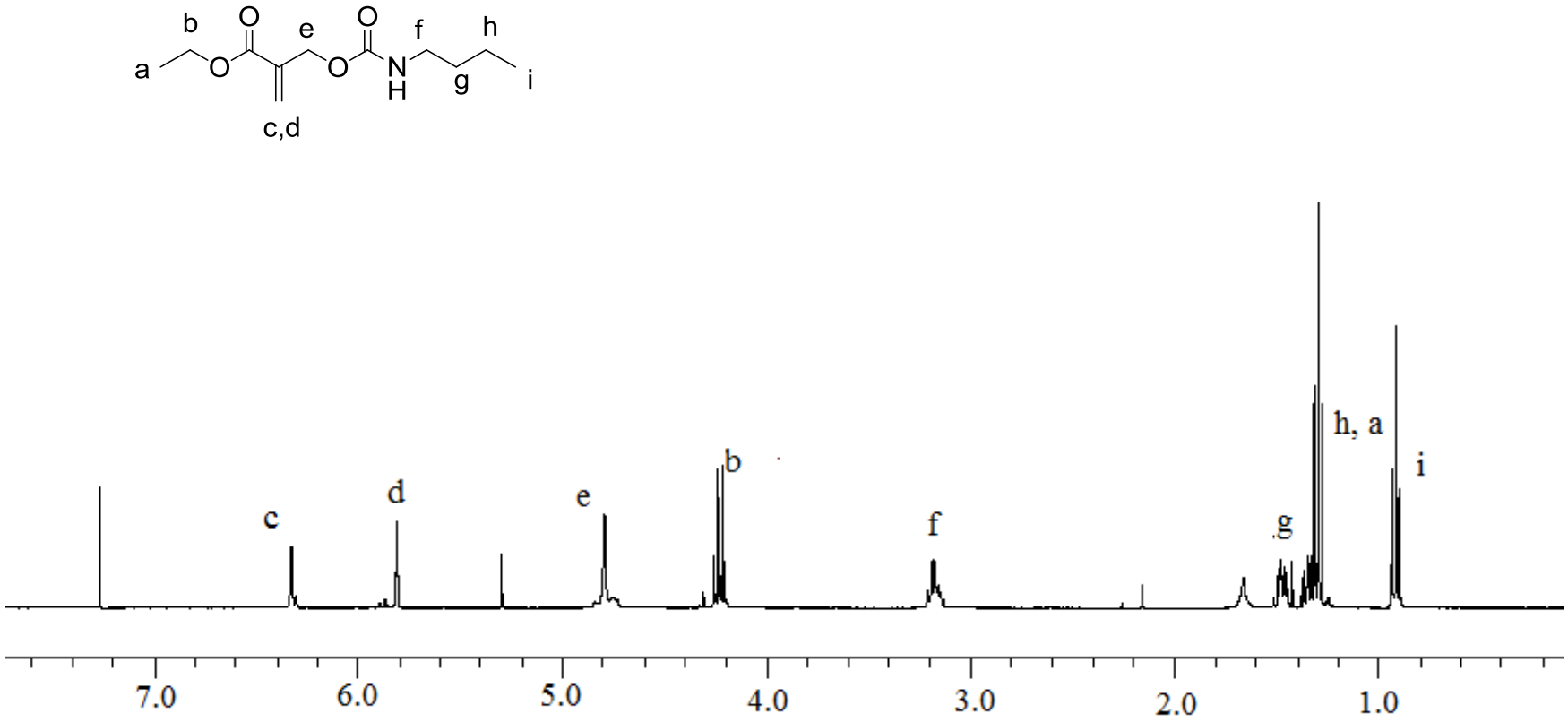

Figure A.19. ^{1}H-NMR spectra of monomer **A15**.

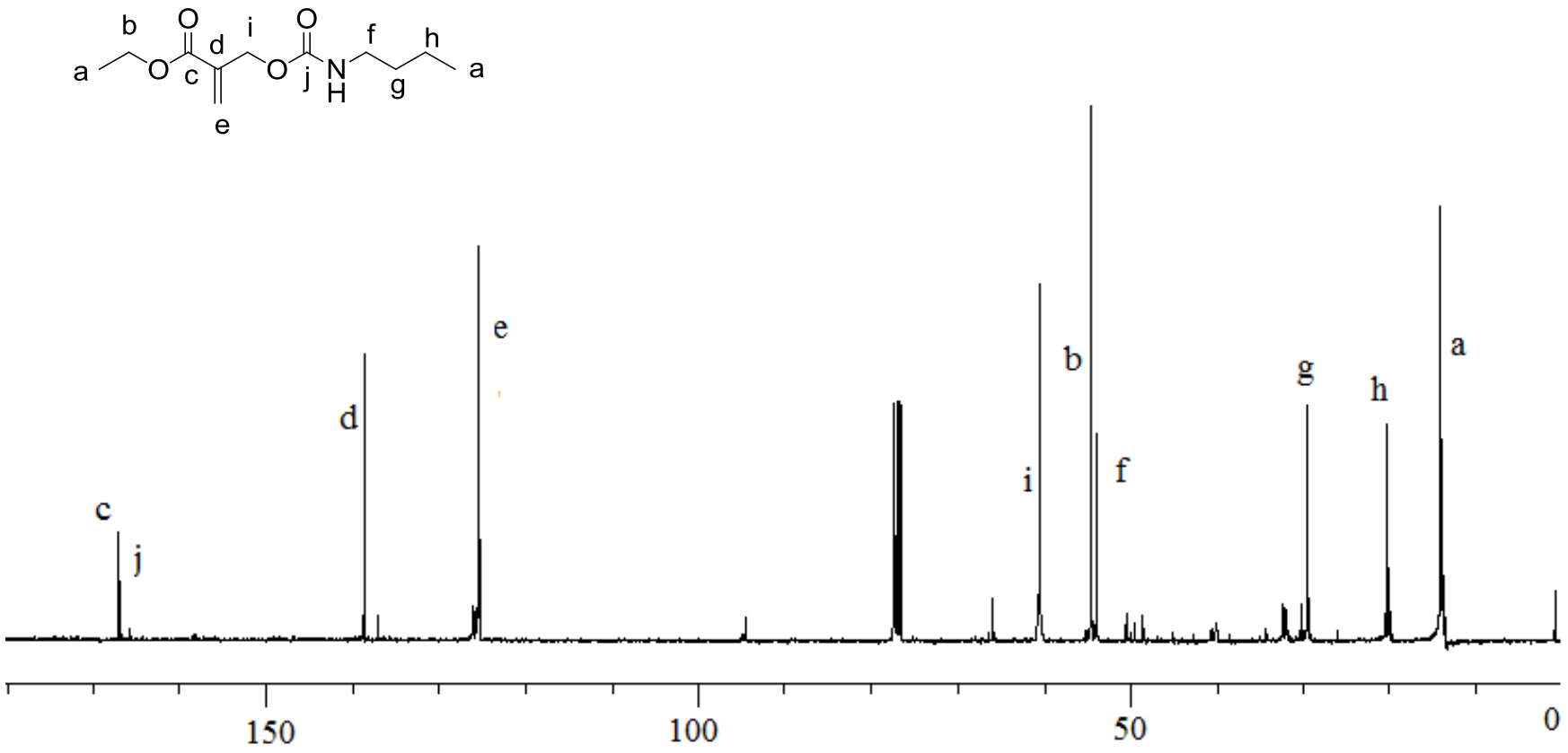

Figure A.20. ^{13}C-NMR spectra of monomer **A15**.

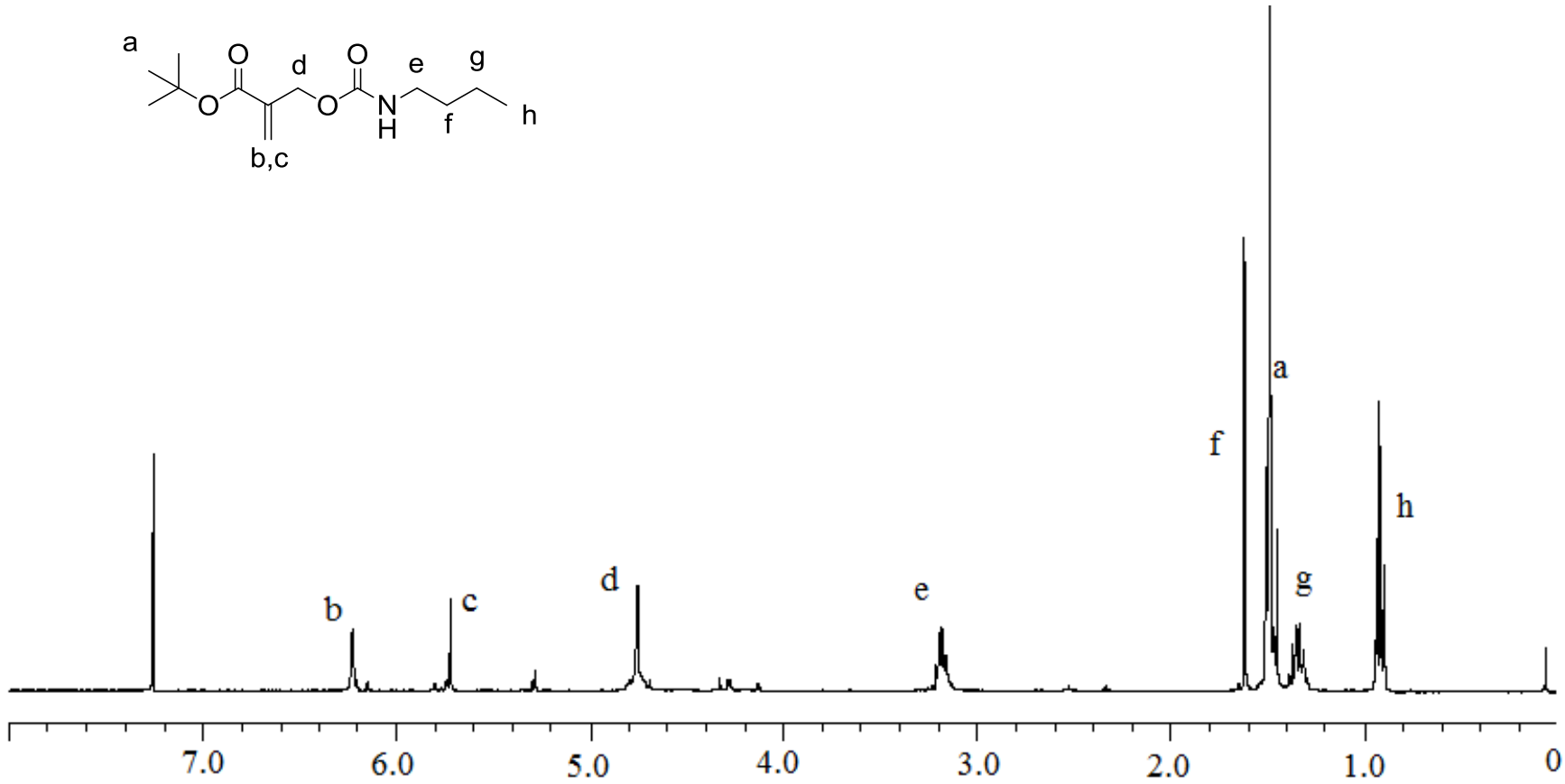

Figure A.21. ^{1}H-NMR spectra of monomer **A16**.

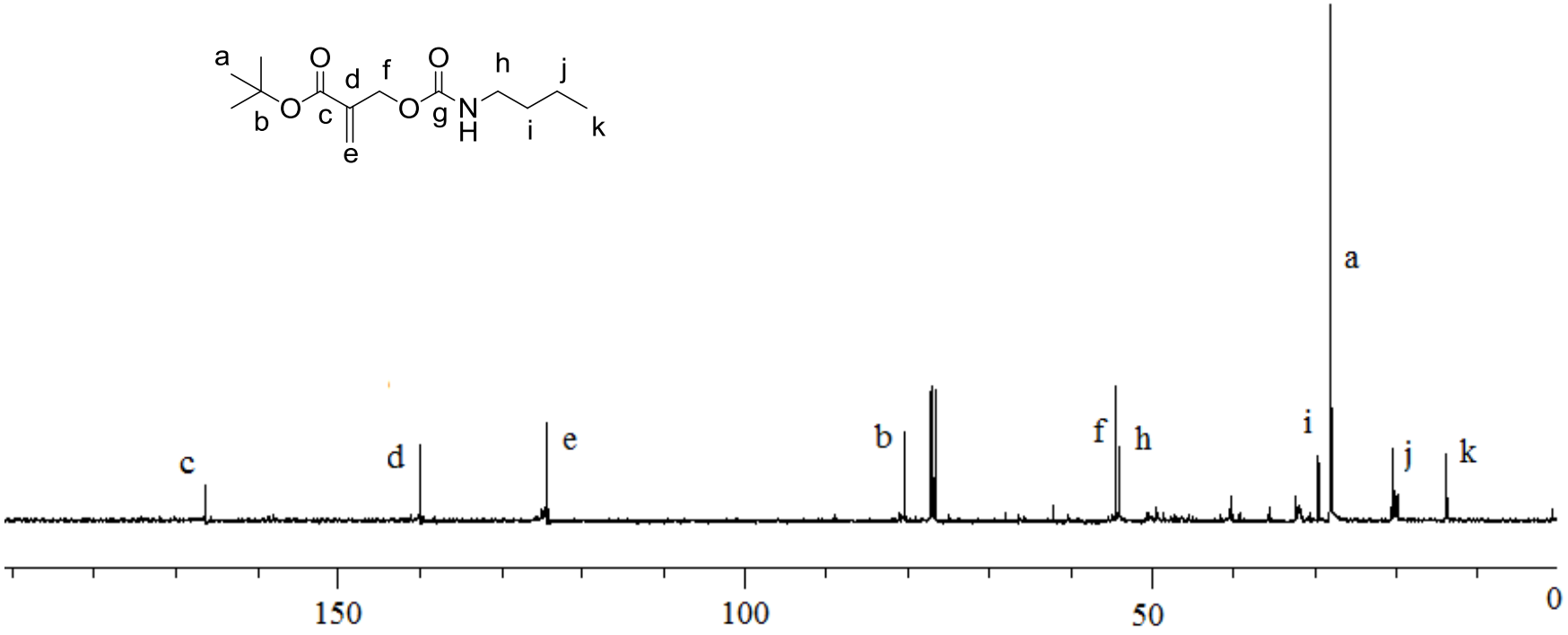

Figure A.22. ^{13}C-NMR spectra of monomer **A16**.

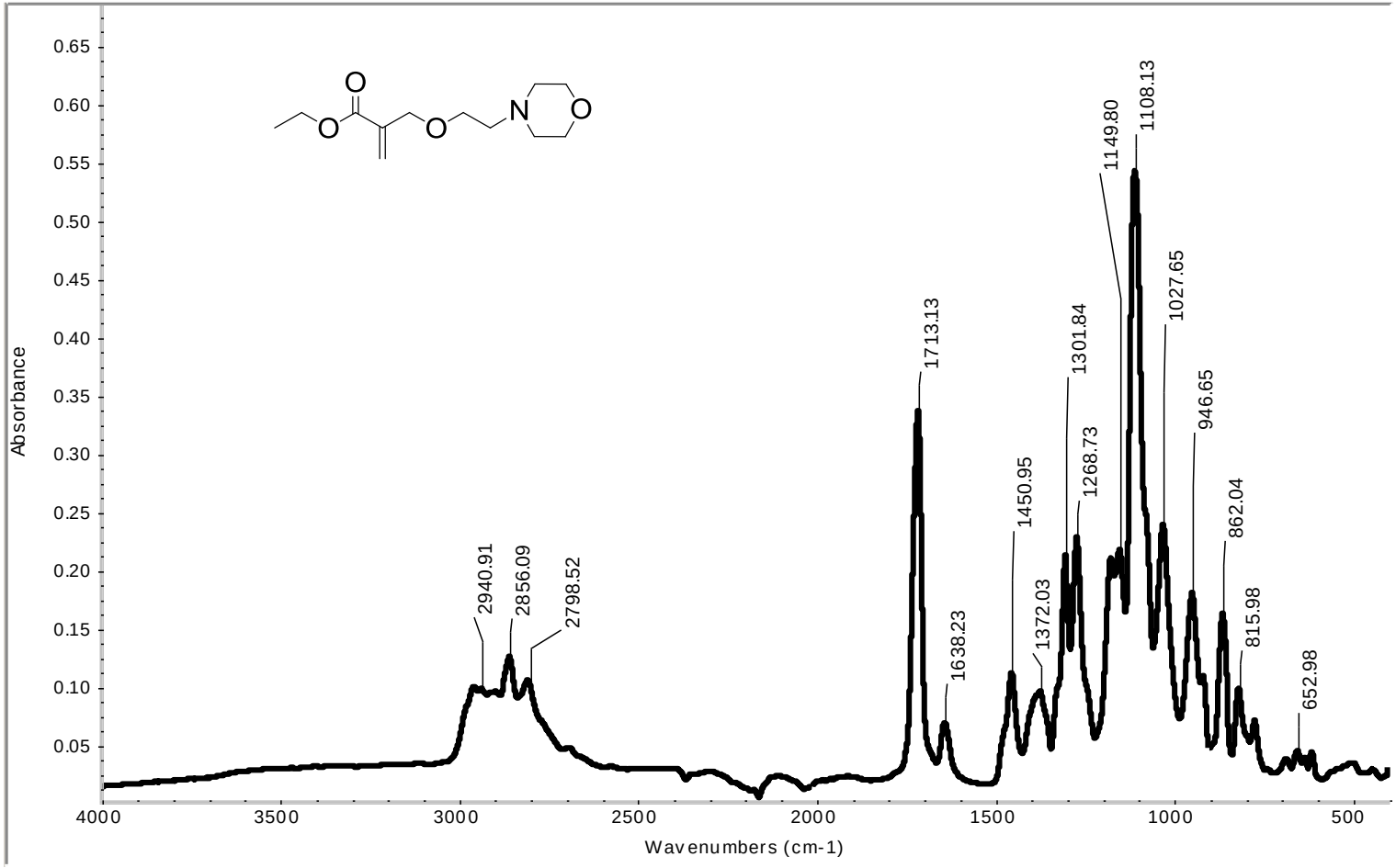

Figure A.23. FTIR spectra of monomer **A1**.

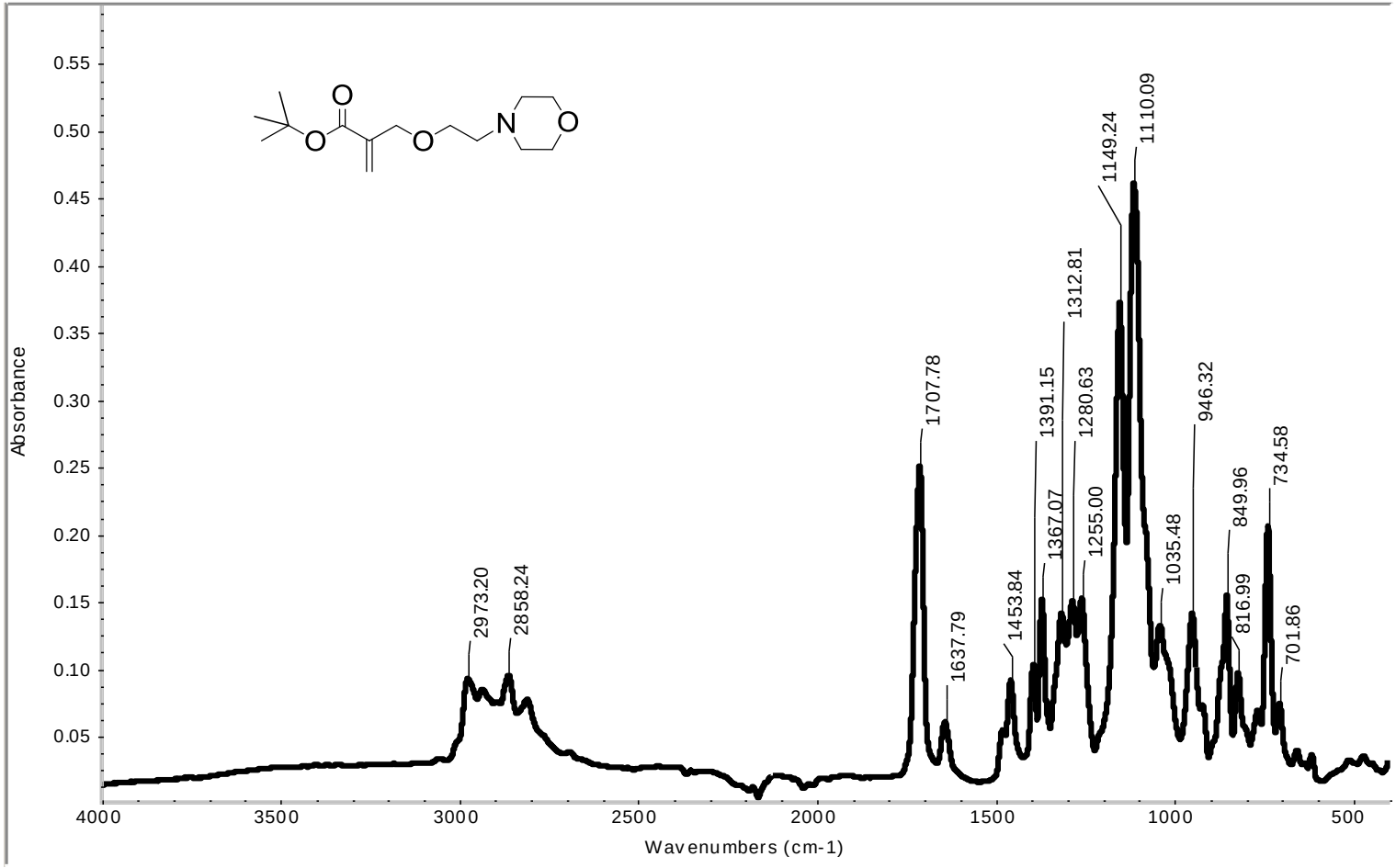

Figure A.24. FTIR spectra of monomer **A2**.

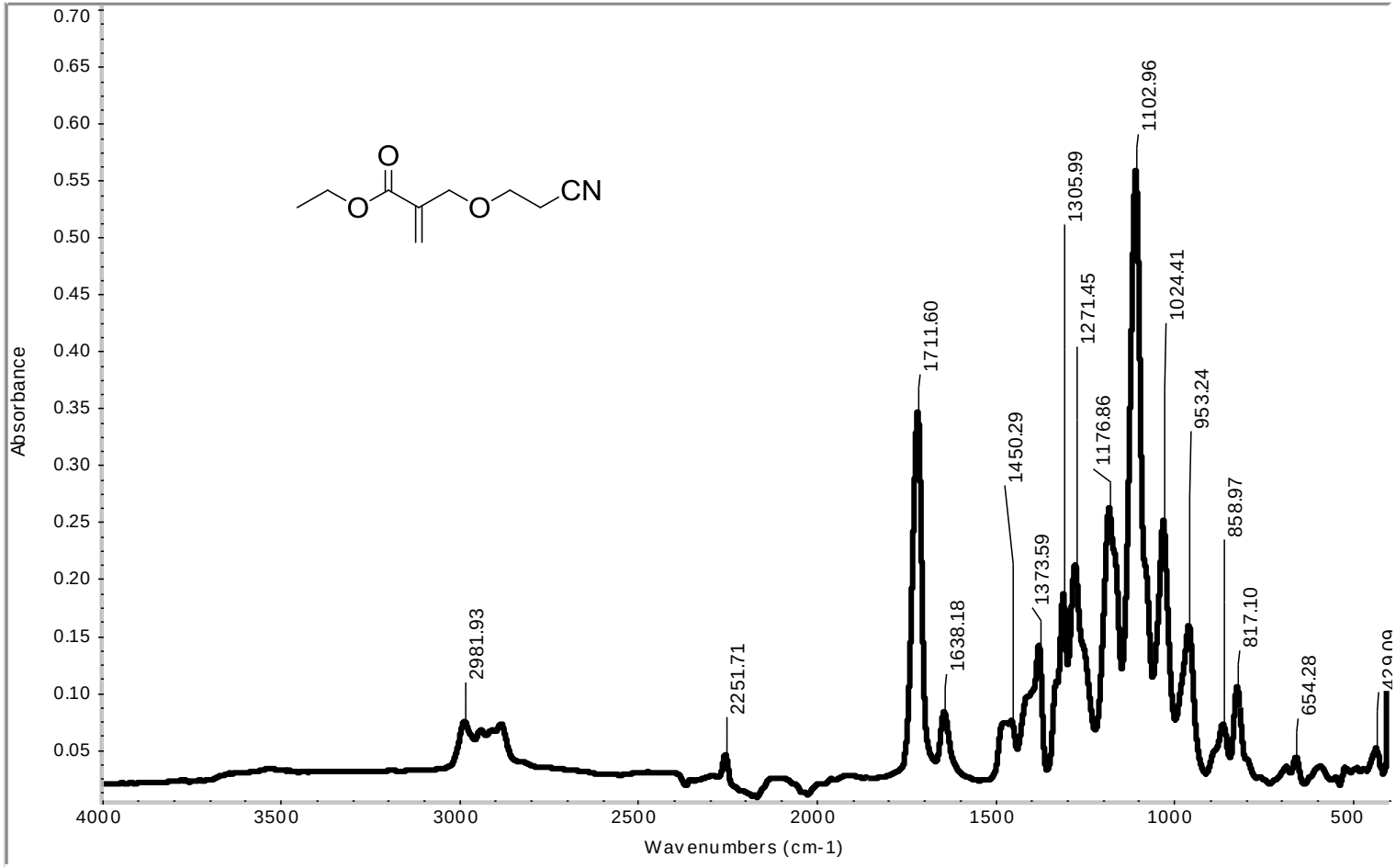

Figure A.25. FTIR spectra of monomer **A3**.

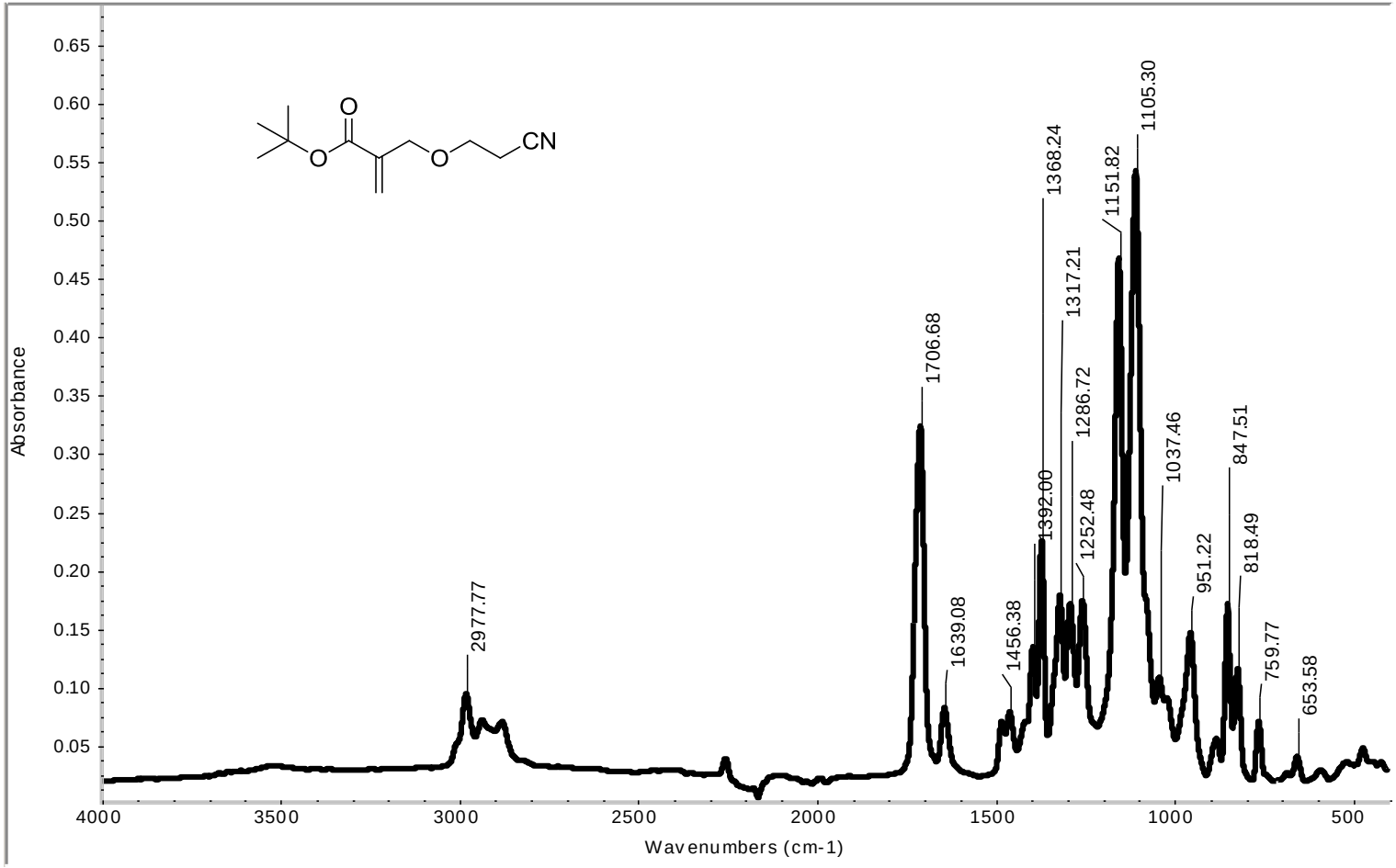

Figure A.26. FTIR spectra of monomer **A4**.

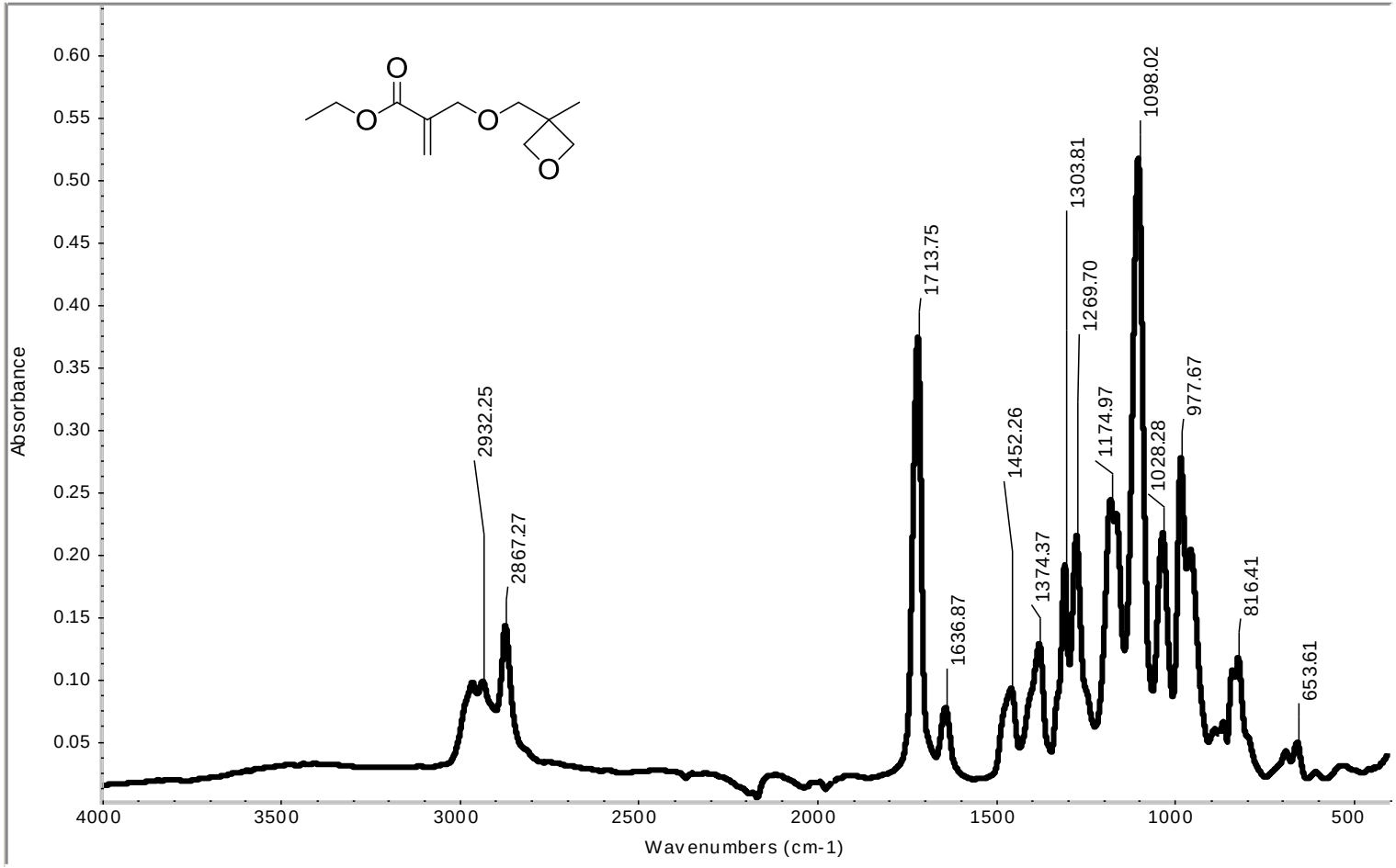

Figure A.27. FTIR spectra of monomer **A5**.

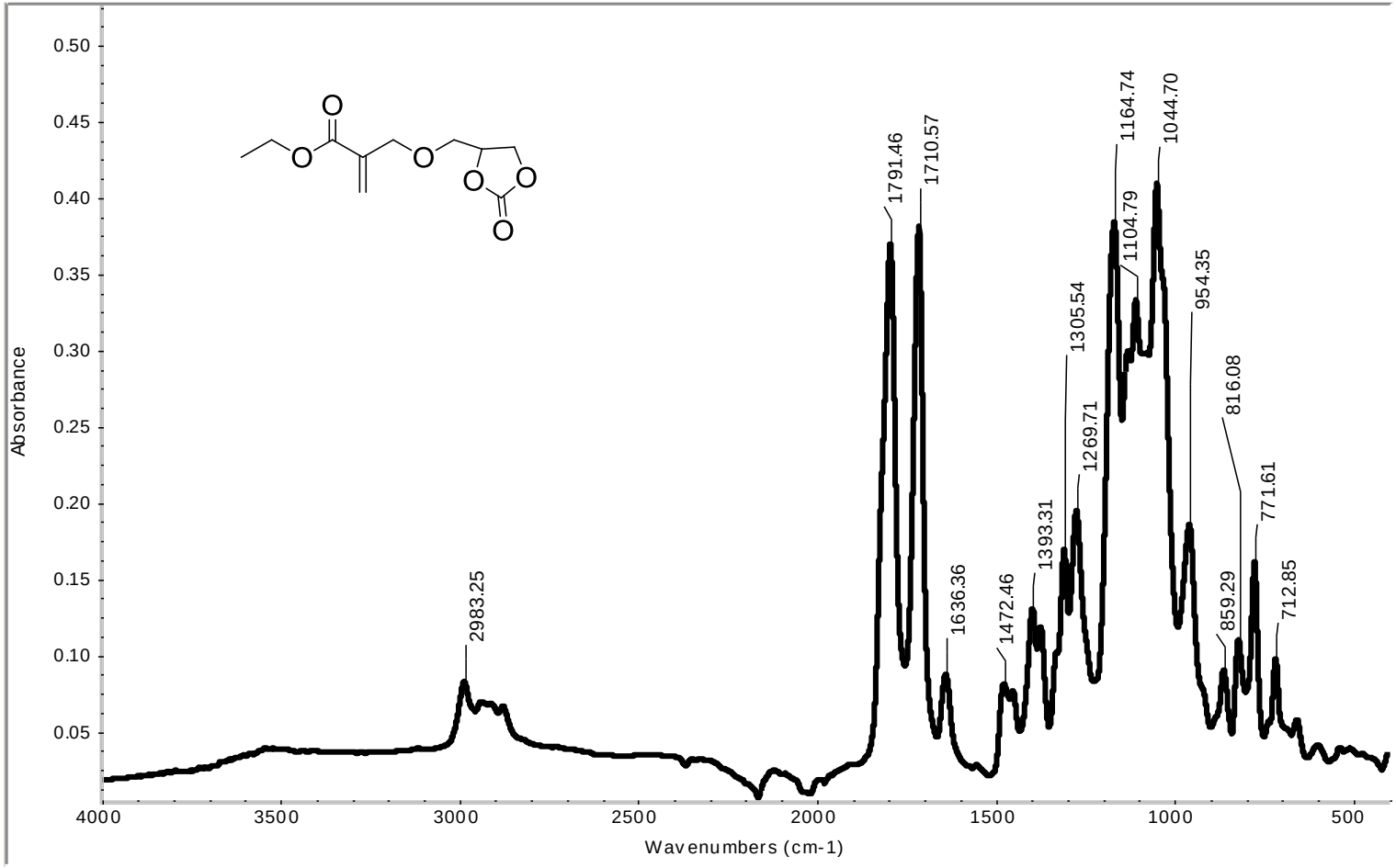

Figure A.28. FTIR spectra of monomer **A6**.

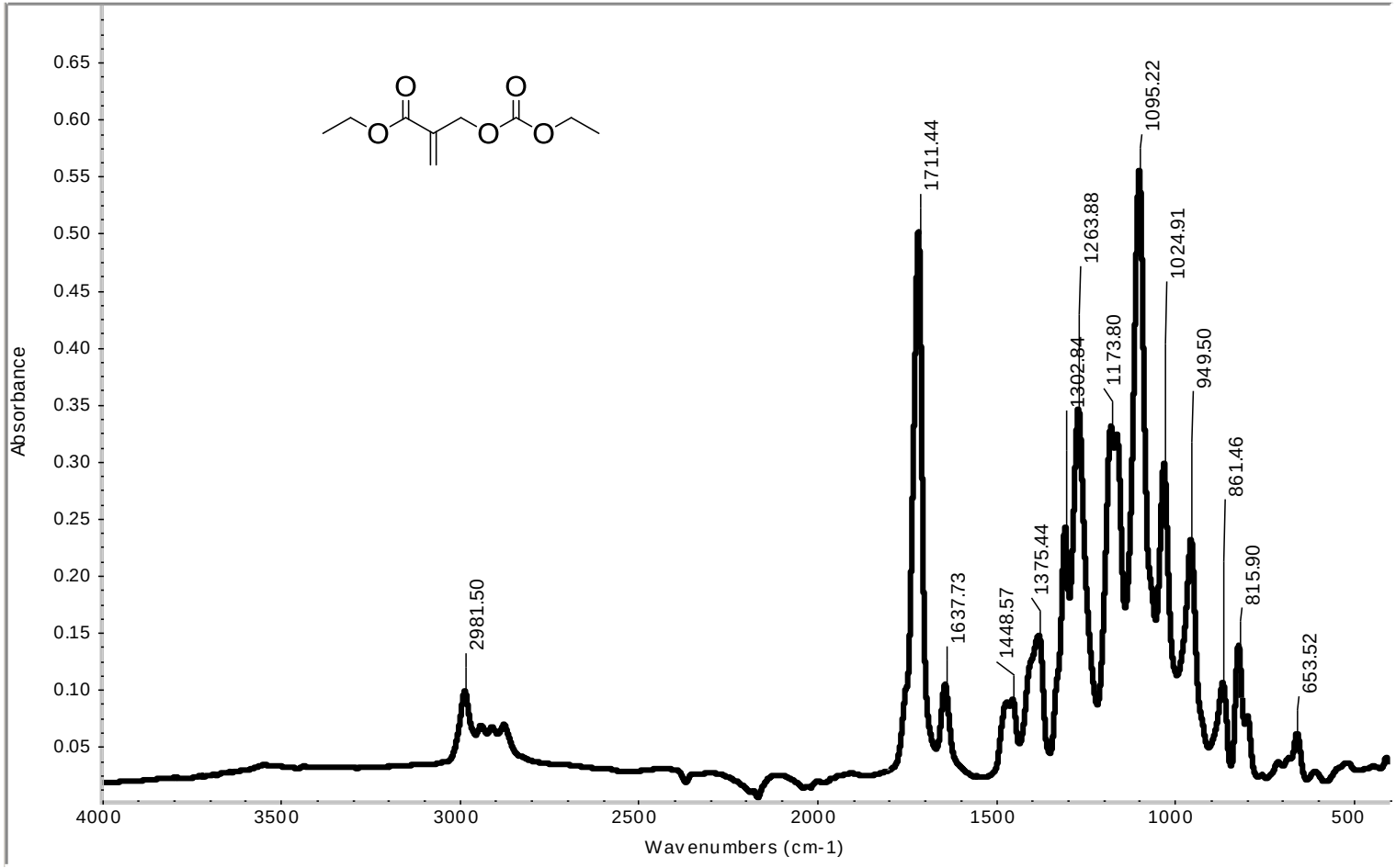

Figure A.29. FTIR spectra of monomer **A8**.

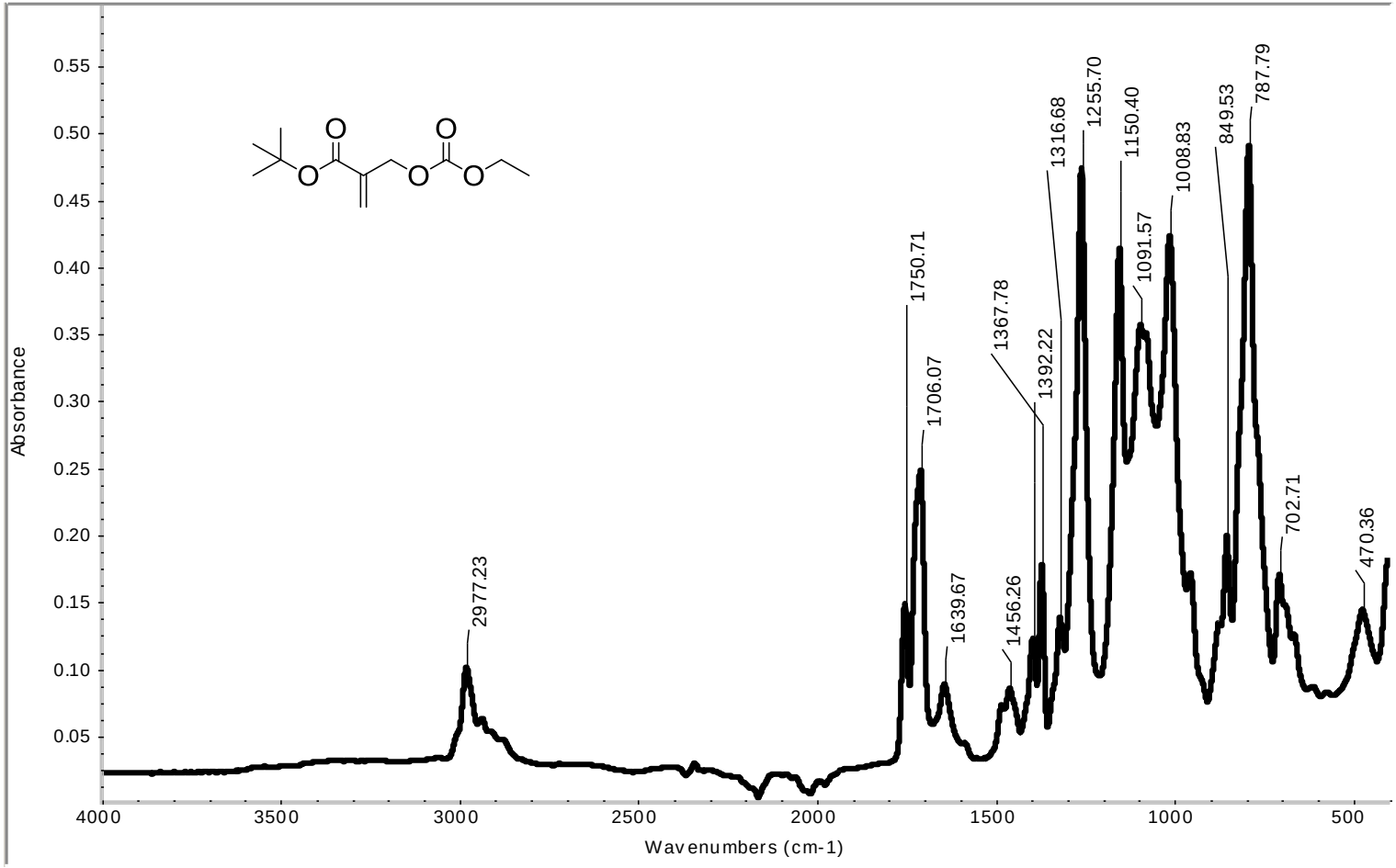

Figure A.30. FTIR spectra of monomer **A9**.

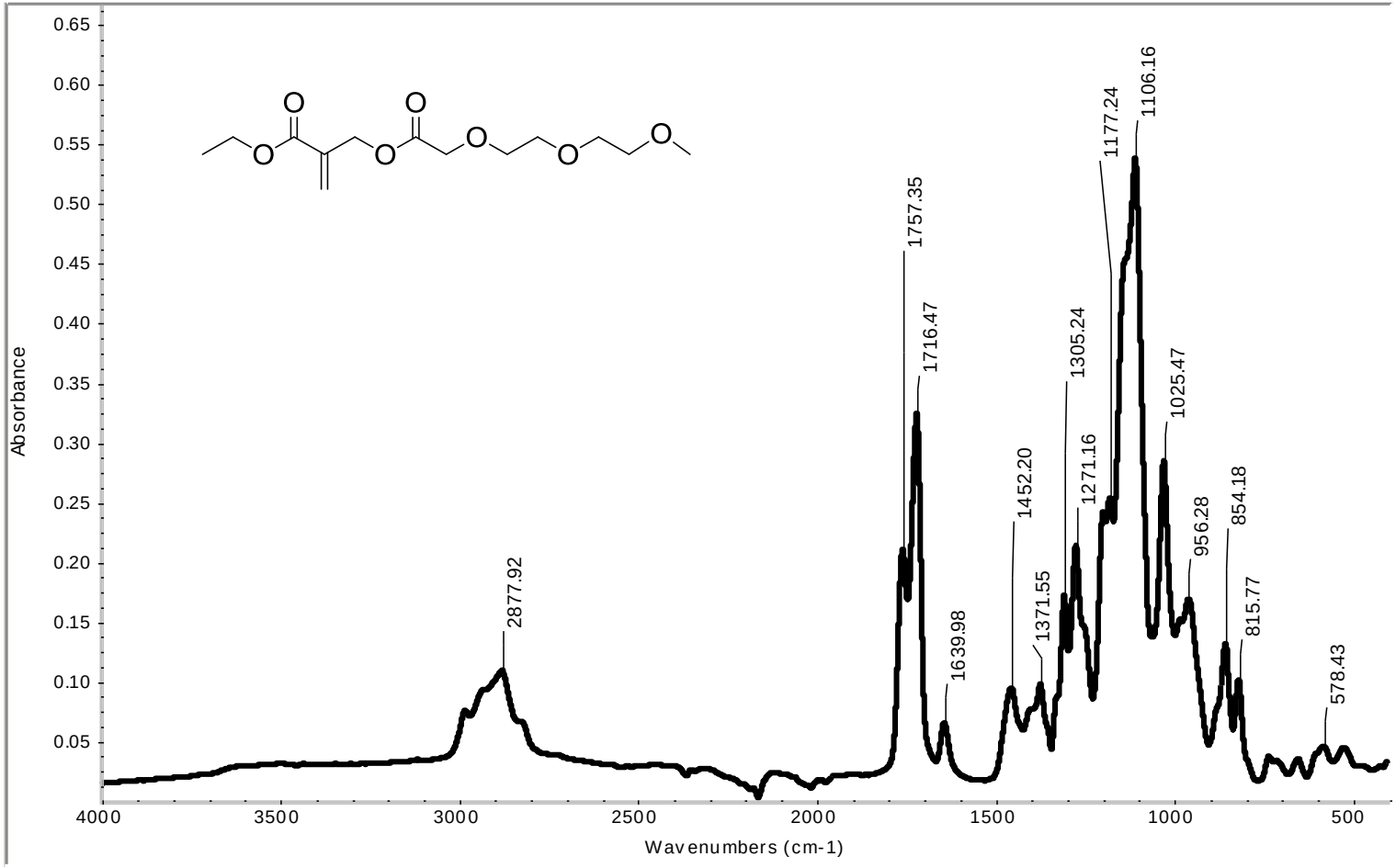

Figure A.31. FTIR spectra of monomer **A10**.

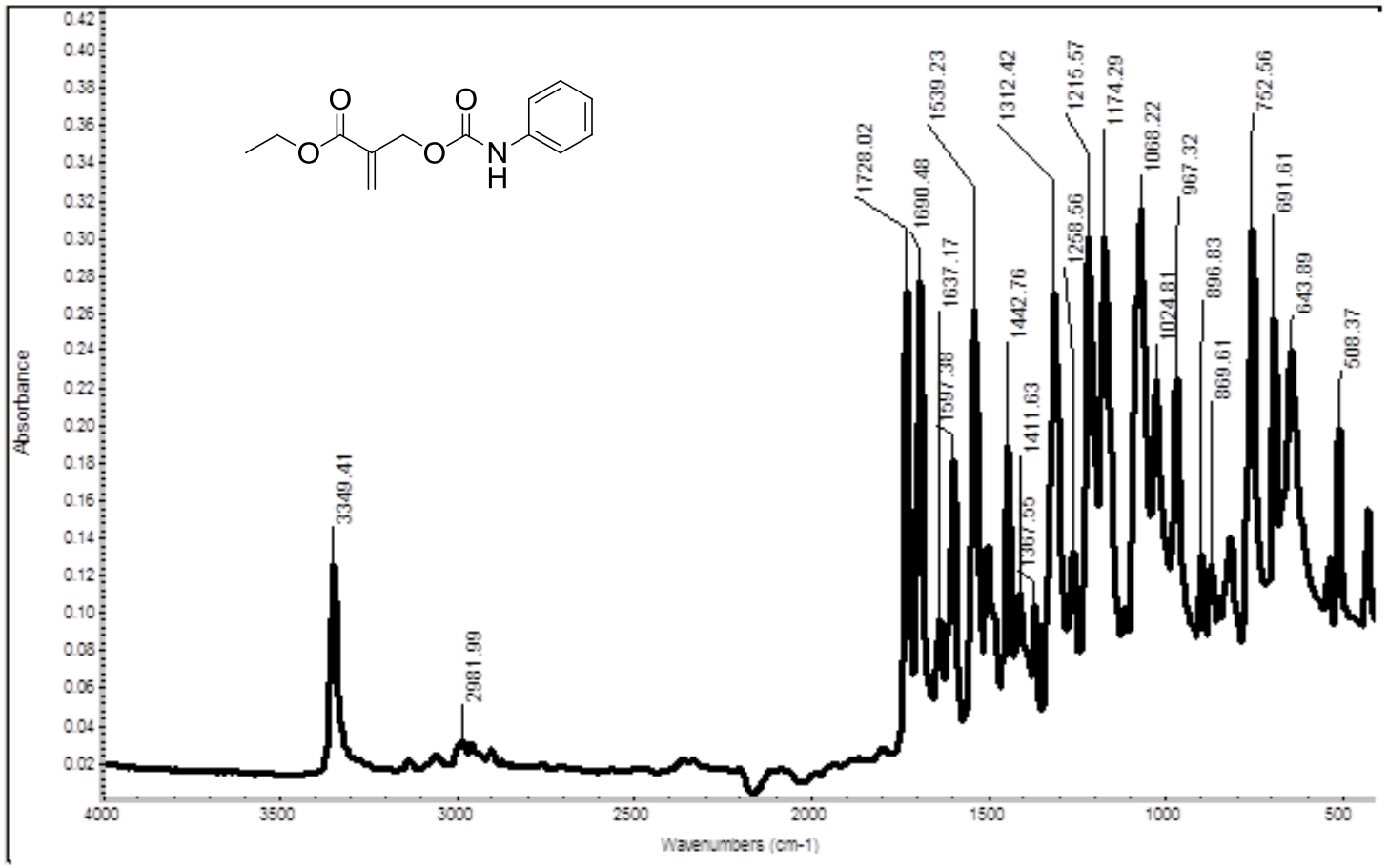

Figure A.32. FTIR spectra of monomer **A13**.

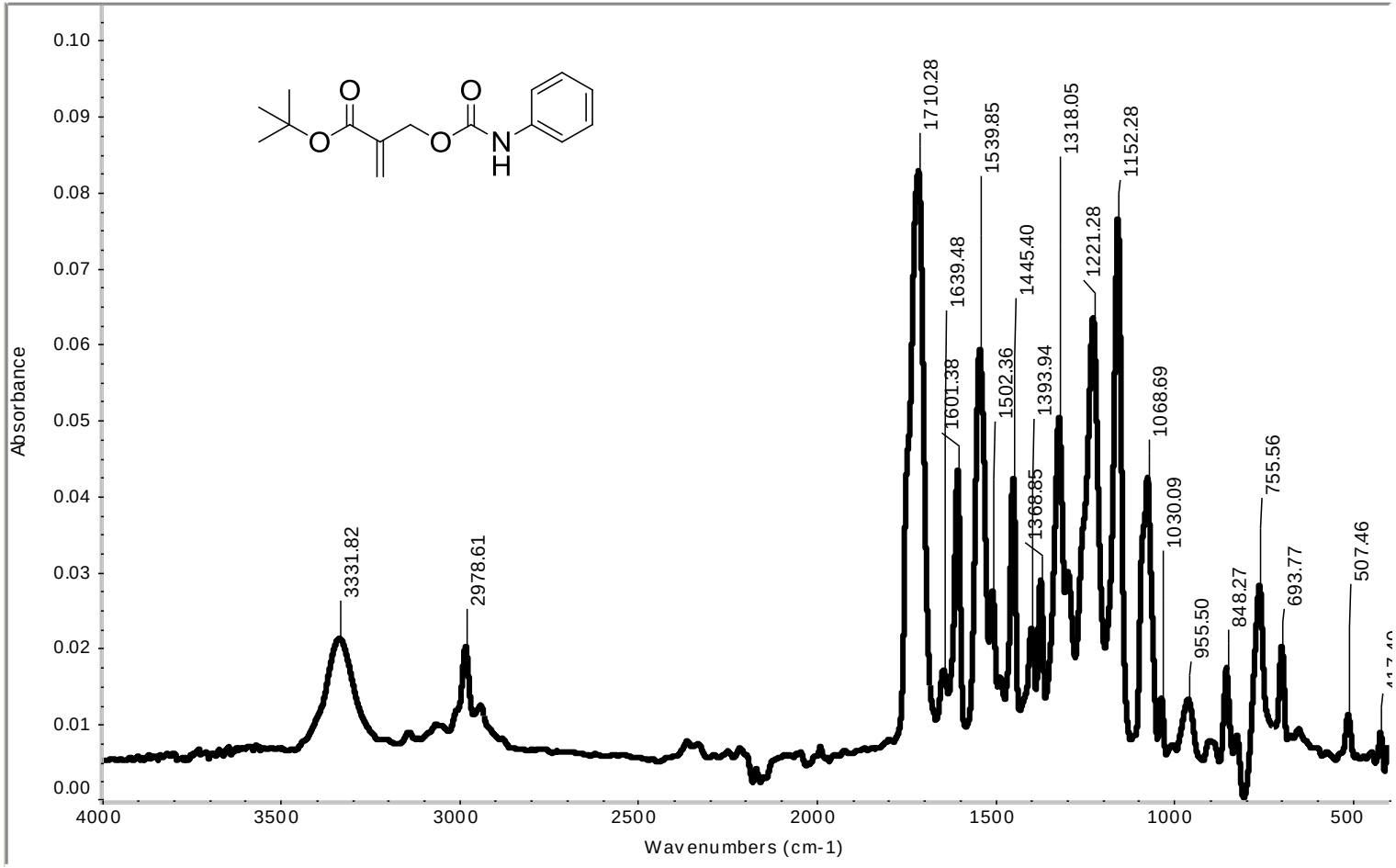

Figure A.33. FTIR spectra of monomer **A14**.

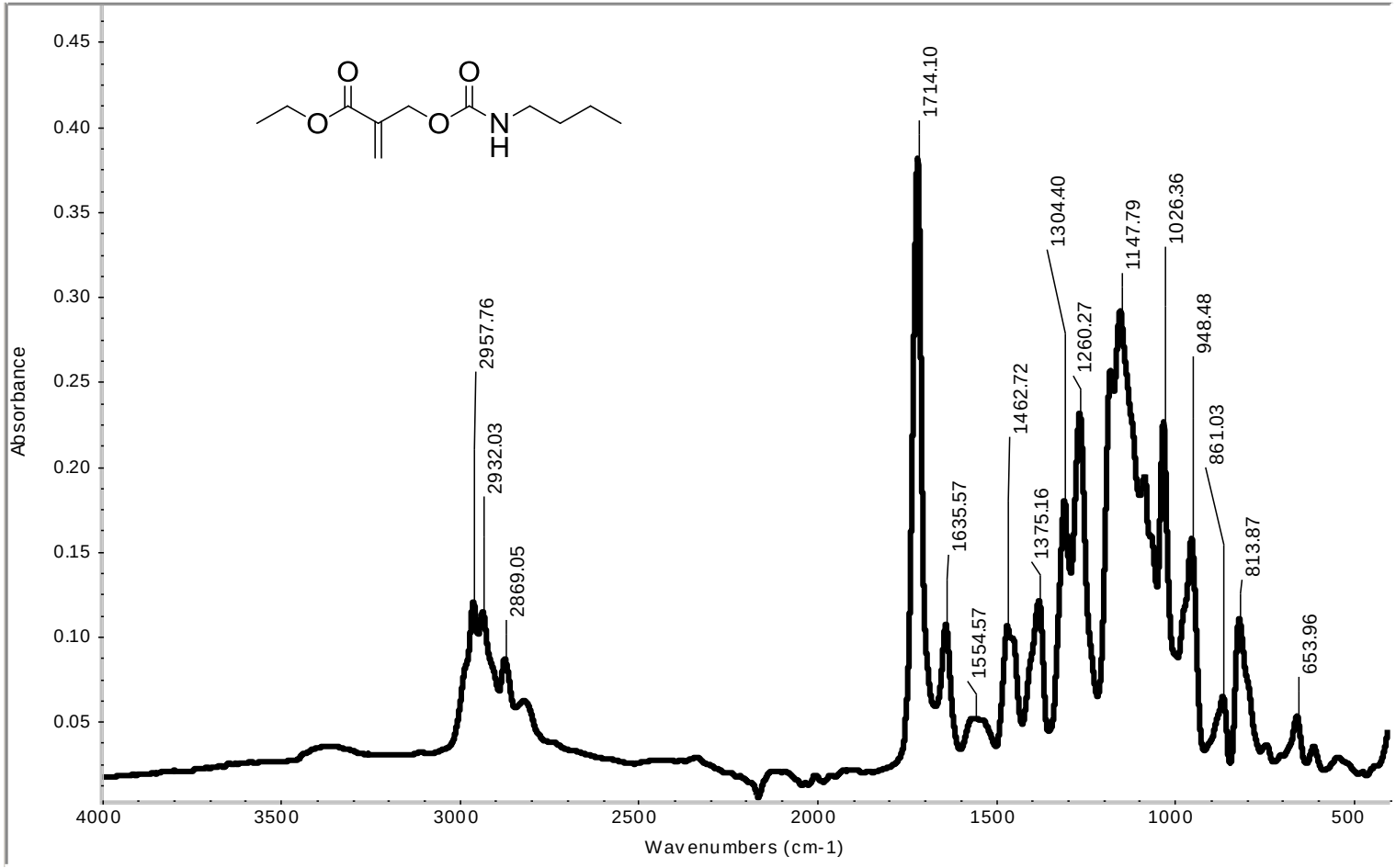

Figure A.34. FTIR spectra of monomer **A15**.

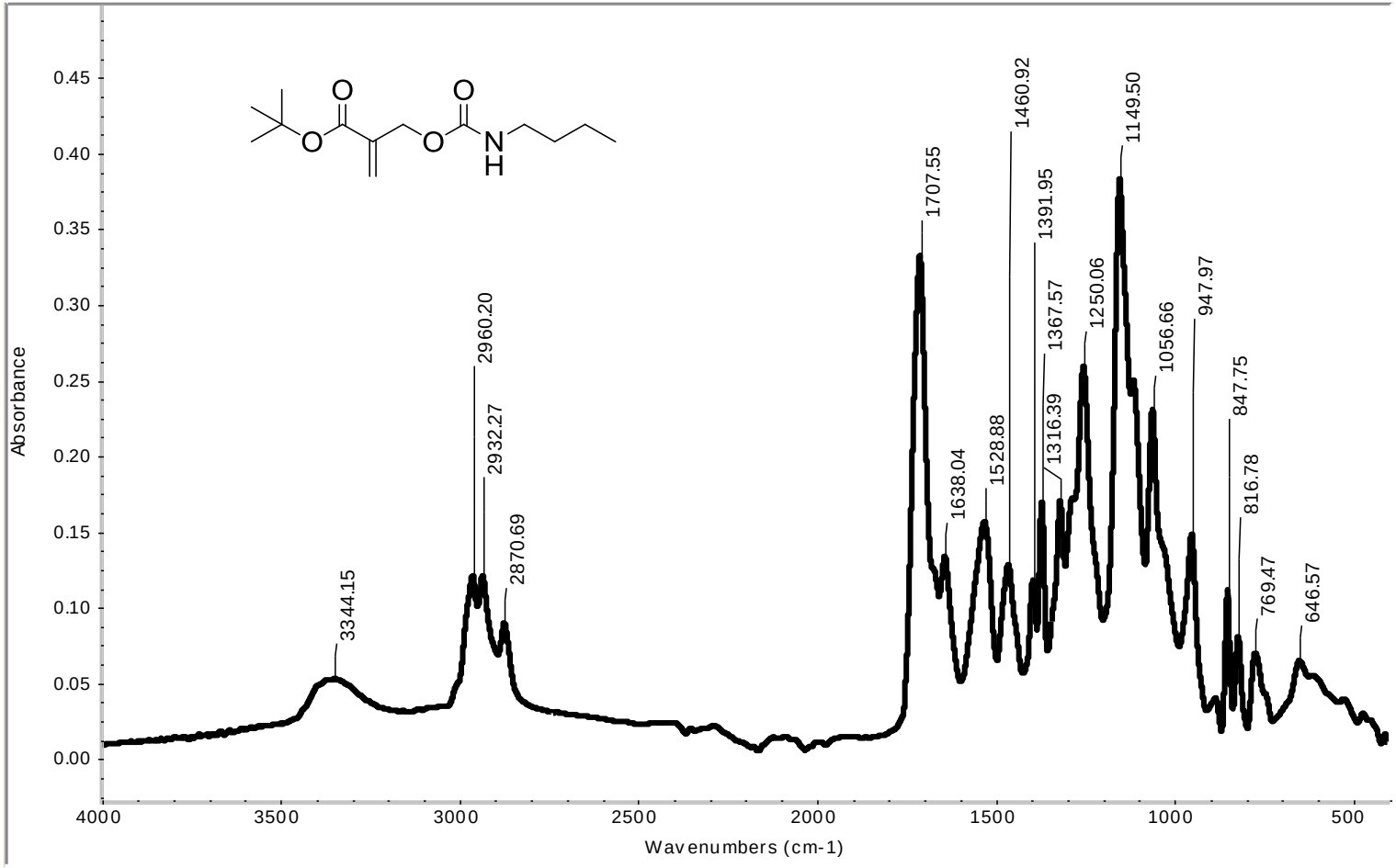

Figure A.35. FTIR spectra of monomer **A16**.

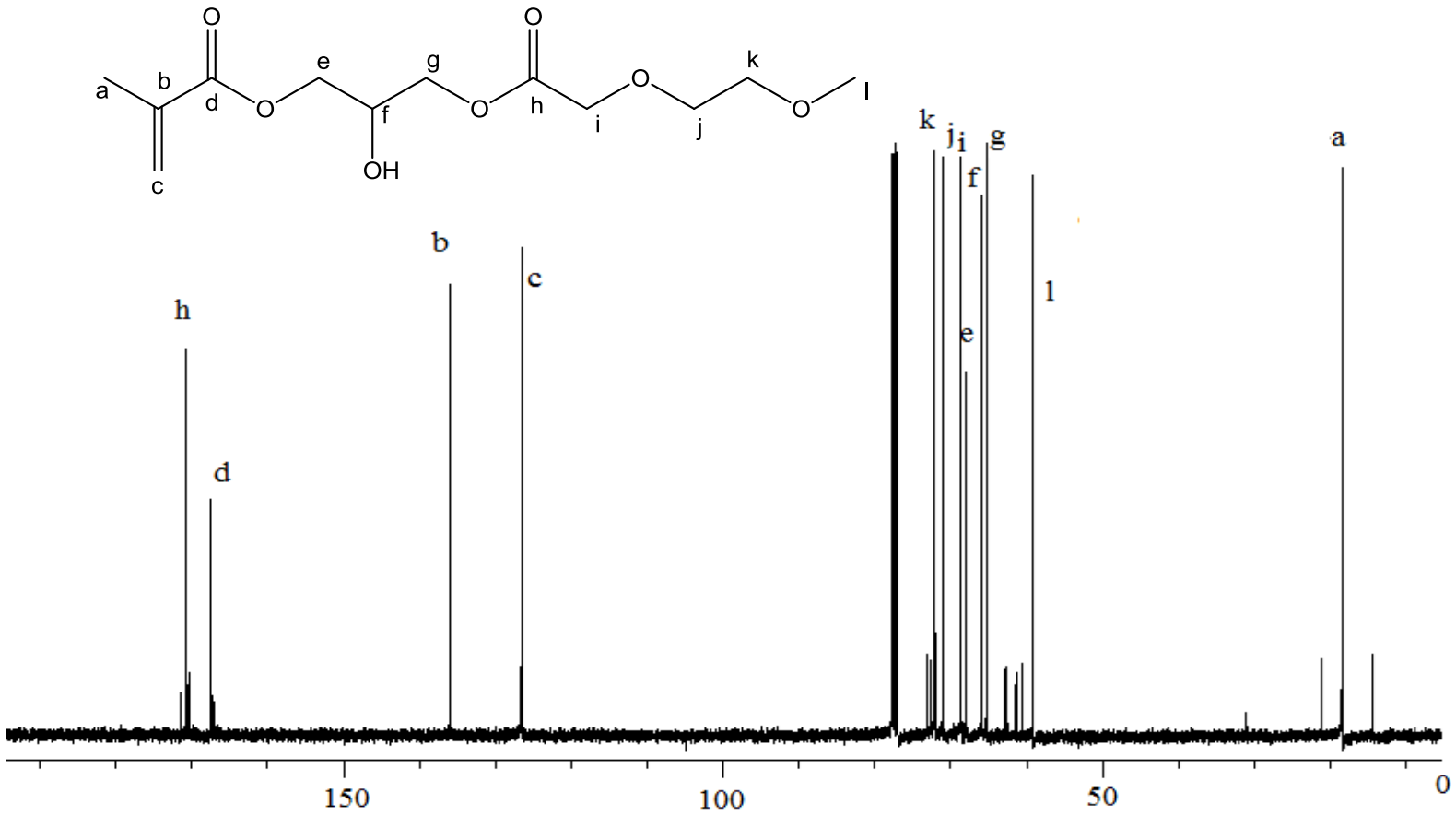

Figure A.36. ^{13}C-NMR spectra of monomer **D1**.

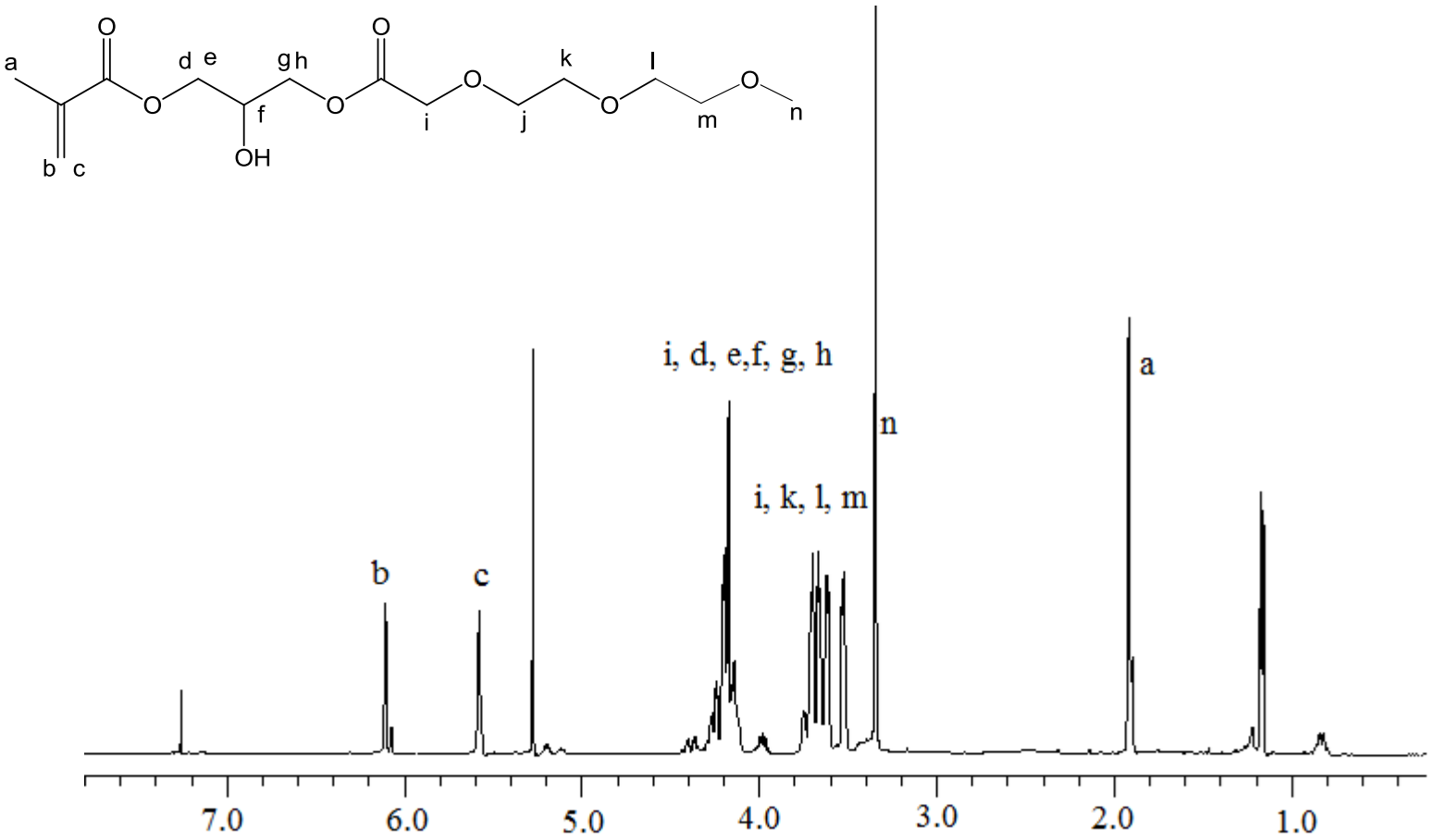

Figure A.37. ^{1}H-NMR spectra of monomer **D2**.

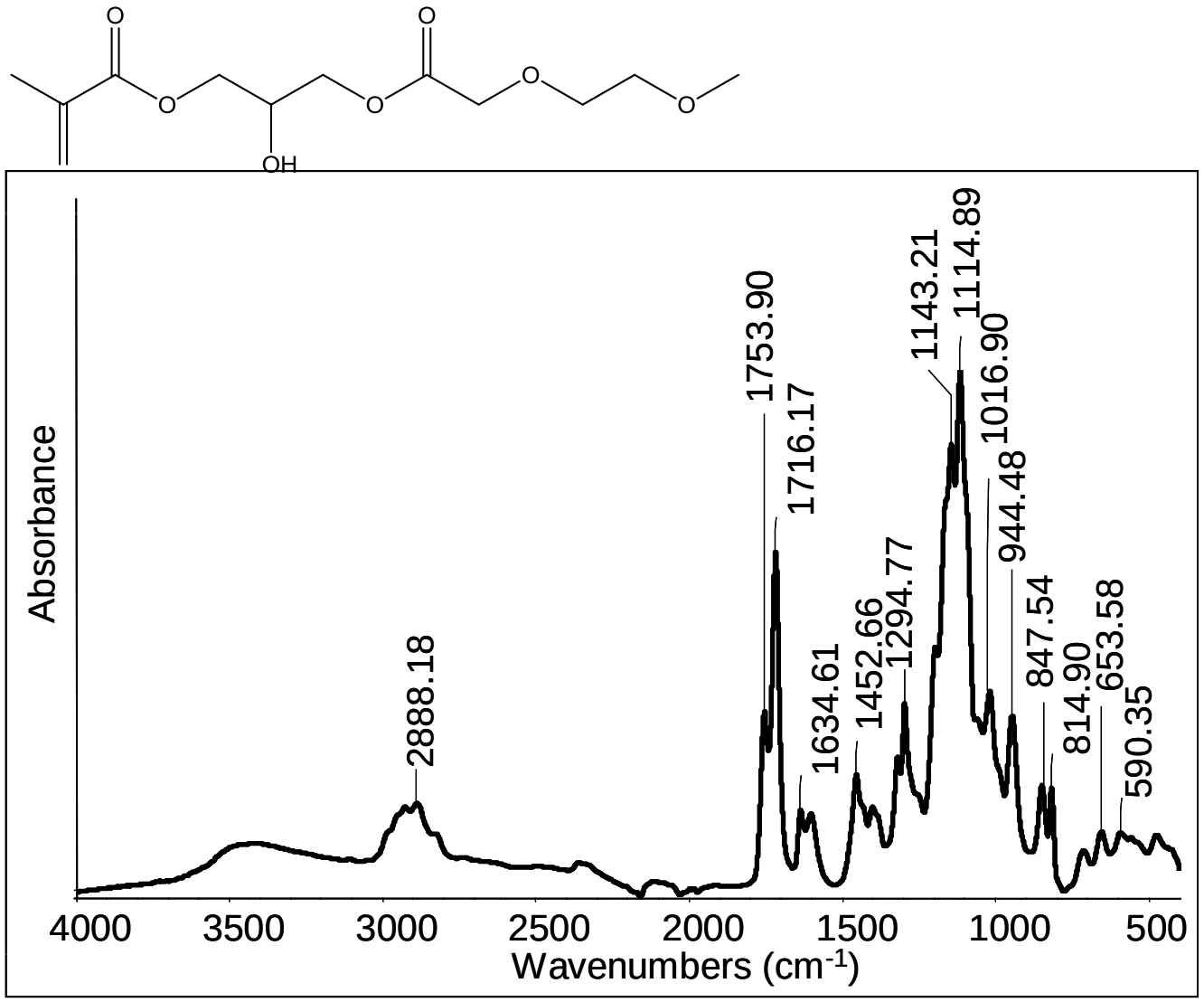

Figure A.38. FTIR spectra of monomer **D1**.

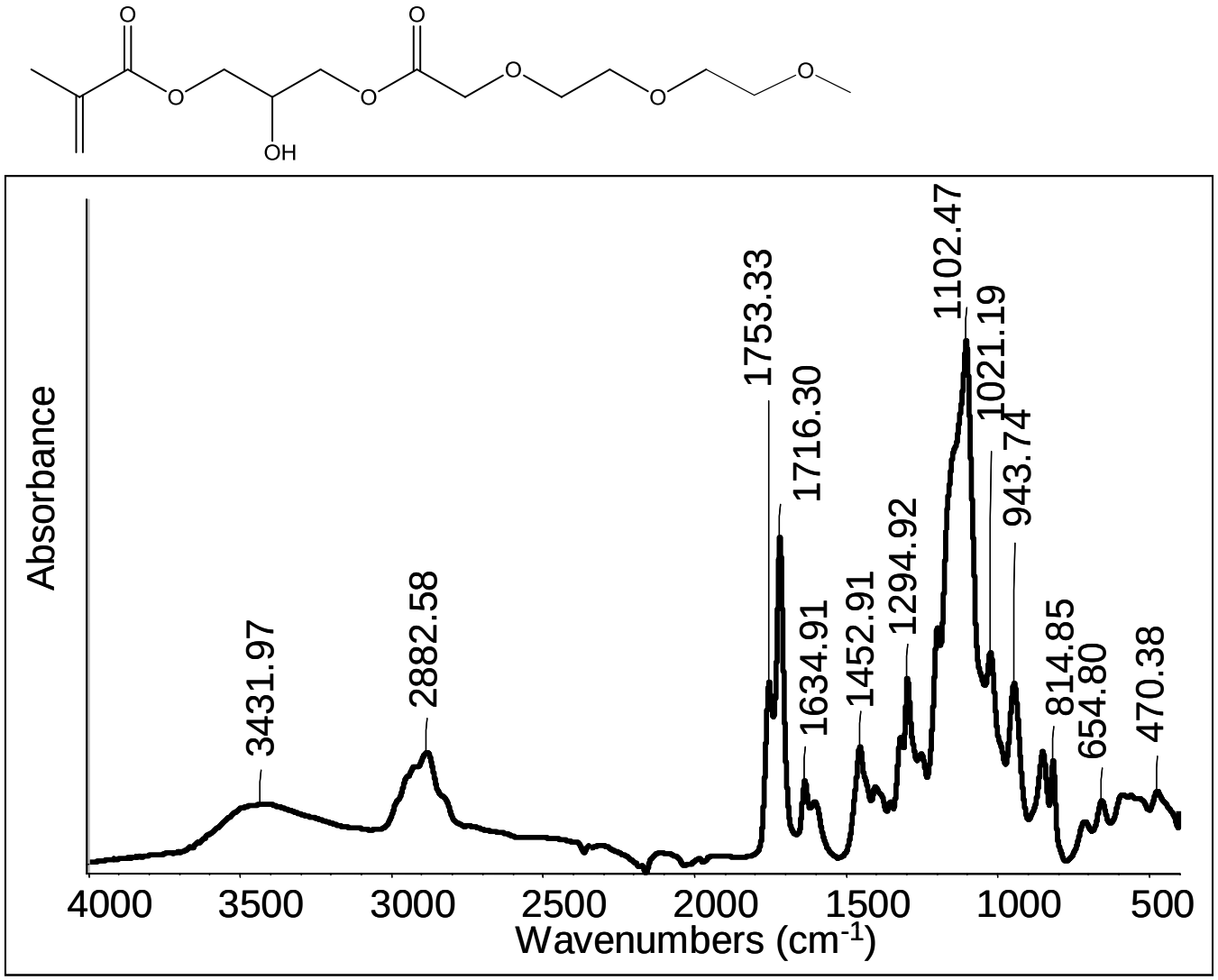

Figure A.39. FTIR spectra of monomer **D2**.

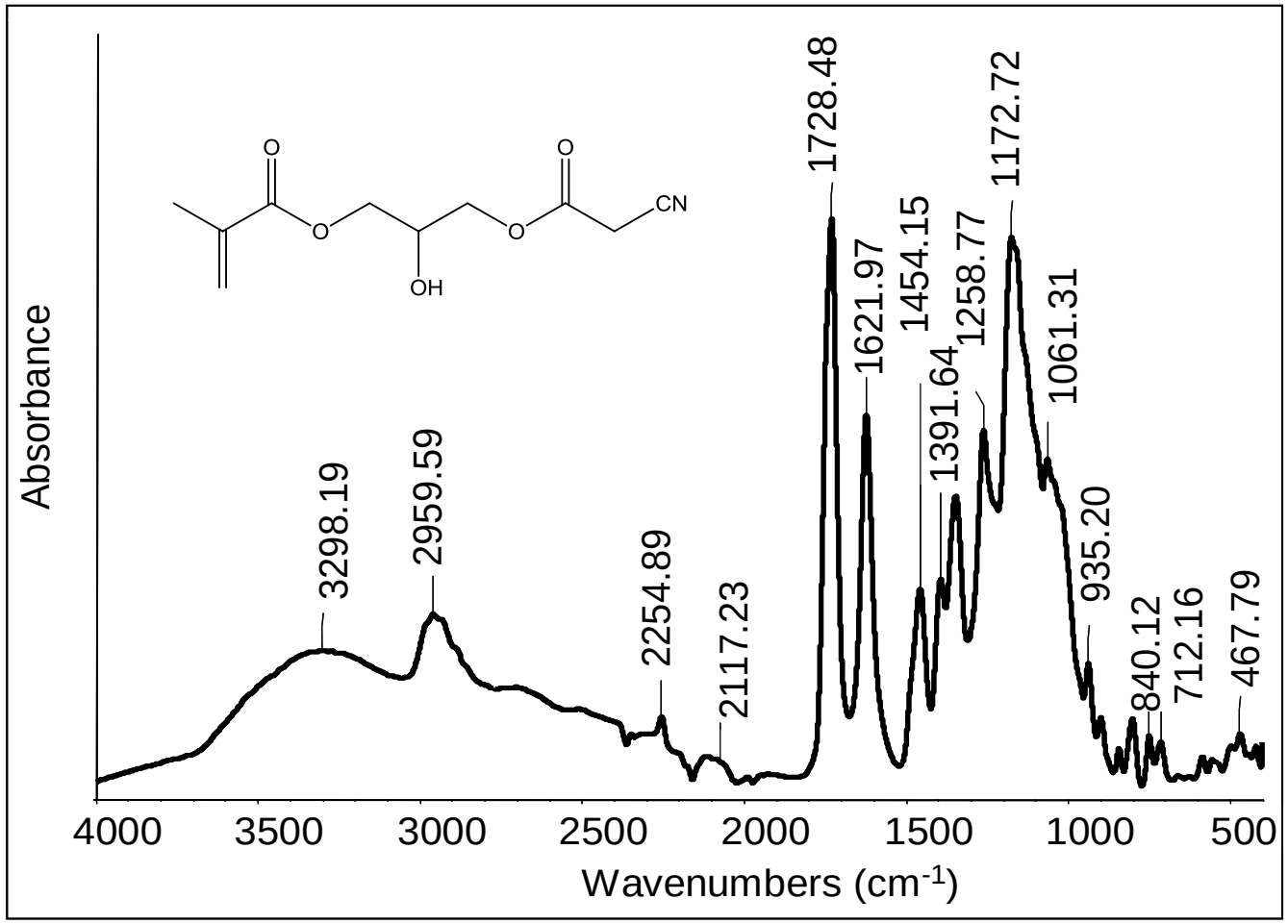

Figure A.40. FTIR spectra of monomer **D3**.

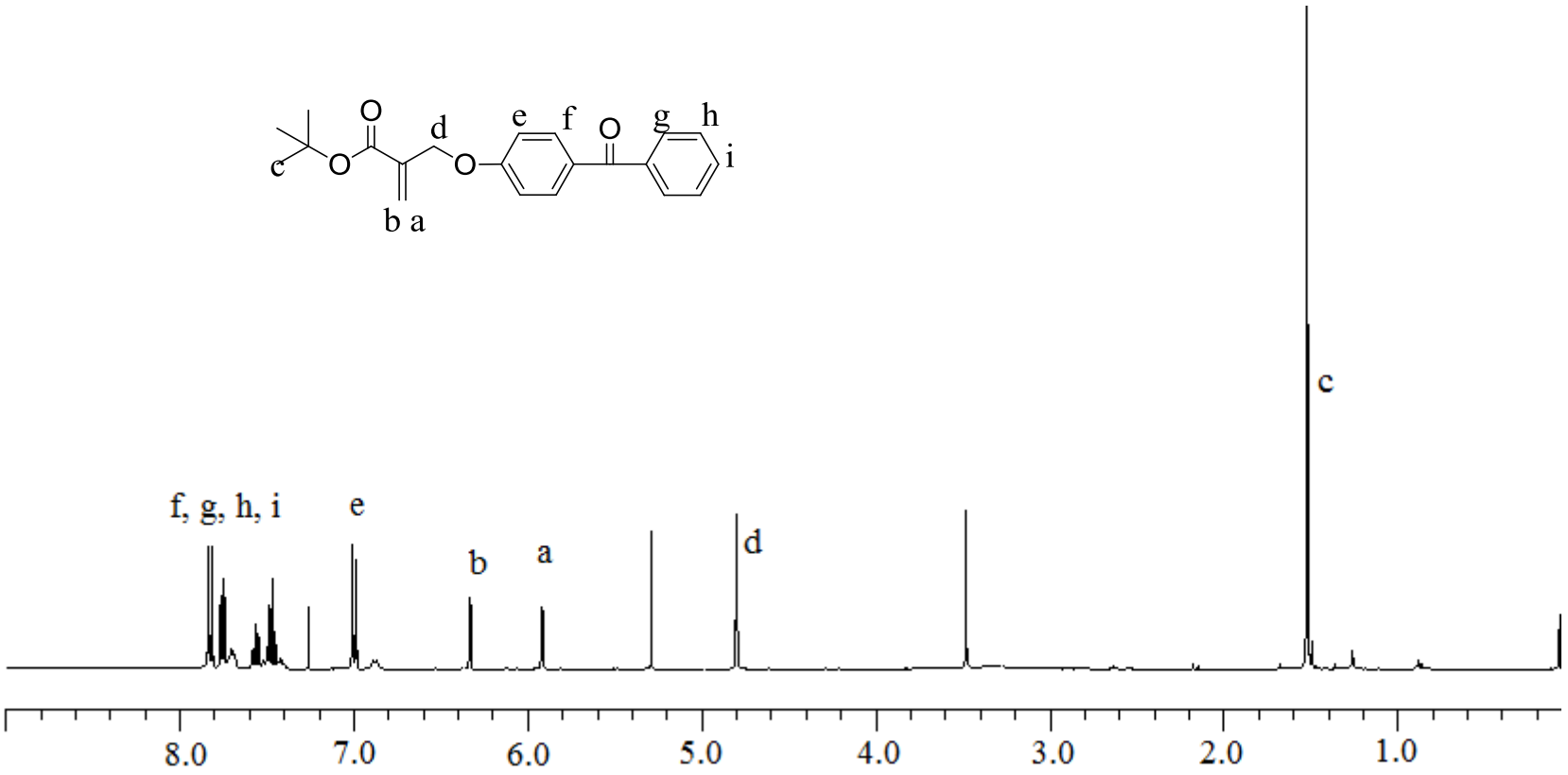

Figure A.41. ^{1}H-NMR spectra of monomer **E1**.

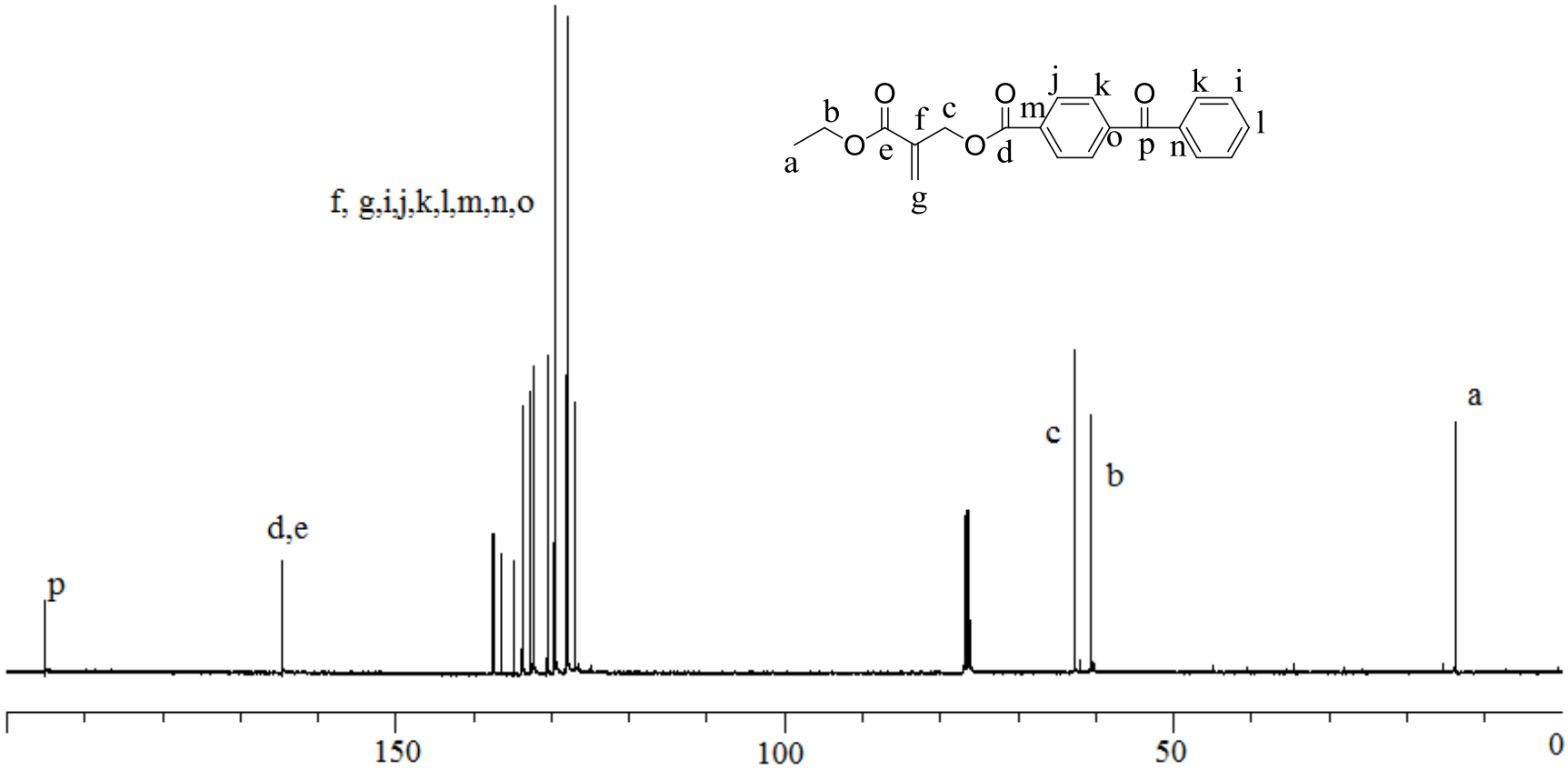

Figure A.42. ^{13}C-NMR spectra of monomer **E1**.

REFERENCES

1. Moad, G. and D. H. Solomon, *The Chemistry of Free Radical Polymerization,* Pergamon, Oxford, 1995.

2. Matyjaszewski, K., S. G. Gaynor, C. D. Craver, and C. E. Carraher, Jr., *Applied Polymer Science,* Pergamon Press, Oxford, 2000, p. 929.

3. Moad, G. and D. H. Solomon, *The Chemistry of Free Radical Polymerization,* Pergamon, Oxford, 1995.

4. Atkins, P. and J. De Paula, *Atkins' Physical Chemistry,* 8th Edition, Oxford University Press, New York, 2006.

5. Beuermann, S. and M. Buback, "Rate Coefficients of Free Radical Polymerization Deduced from Pulsed Laser Experiments", *Progress in Polymer Science,*Vol. 27, pp. 191-254, 2002.

6. Kloosterboer, J. G., "Network Formation by Chain Crosslinking Photopolymerization and Its Applications in Electronics", *Advanced Polymer Science,* Vol. 84, pp. 1-61, 1988.

7. Decker, C., "Photoinitiated Crosslinking Polymerization", *Progress in Polymer Science,* Vol. 21, pp. 593-650, 1996.

8. Anseth, K. S., S. M. Newman and C. N. Bowman, "Polymeric Dental Composites: Properties and Reaction Behavior of Multimethacrylate Dental Restorations", *Advances in Polymer Science,* Vol. 122, pp. 177-217, 1995.

9. Decker, C. and Elzaouk, B., "Laser-Induced Crosslinking Polymerization of Acrylic Photoresists", *Journal of Applied Polymer Science,* Vol. 65, pp. 833-844, 1997.

10. Coleman, M. M., K. H. Lee, D. J. Skrovanek and P. C. Painter, "Hydrogen Bonding in Polymers. 4. Infrared Temperature Studies of a Simple Polyurethane", *Macromolecules*, Vol. 19, pp. 2149-2157, 1986.

11. George Odian, "*Principles of Polymerization*", 4th Edition, Wiley Intersinece, New-York, 2004.

12. Andrzejewska E., "Photopolymerization Kinetics of Multifunctional Monomers", *Progress in Polymer Science*, Vol. 26, pp. 605-665, 2001.

13. Kerbouc'h, P., P. Lebaudy, L. Lecamp and C. Bunel, "Numerical Simulation to Correlate Photopolymerization Kinetics Monitoring by RT-NIR Spectroscopy and Photocalorimetry",*Thermochimica Acta*, Vol. 410, pp. 73-78, 2004.

14. Kloosterboer, J.G. and G.F.C.M. Lijten, "Thermal and Mechanical Analysis of a Photopolymerization Process", *Polymer*, Vol. 28, pp. 1149-1155, 1987.

15. Lecamp, L., B. Youssef and C. Bunel, "Photoinitiated Polymerization of a Dimethacrylate Oligomer: 1. Influence of Photoinitiator Concentration, Temperature and Light Intensity", *Polymer*, Vol. 38 pp. 6089-6096, 1997.

16. Zhou, H., Q. Li, T. Y. Lee, C. A. Guymon, E. S. Jonsson and C. E. Hoyle, "Photopolymerization of Acid Containing Monomers: Real-Time Monitoring of Polymerization Rates", *Macromolecules*, Vol. 39, pp. 8269-8273, 2006.

17. Scherzer, T. and U. Decker, "Real-Time FTIR-ATR Spectroscopy to Study the Kinetics of UltraFast Photopolymerization Reactions Induced by Monochromatic UV Light", *Vibrational Spectroscopy*, Vol. 19, pp. 385-398, 1999.

18. Scherzer, T. and U. Decker, "The Effect of Temperature on the Kinetics of Diacrylate Photopolymerizations Studied by Real-Time FTIR Spectroscopy", *Polymer*, Vol. 41, pp. 7681-7690, 2000.

19. Zhou, H., Q. Li, J. Shin and C. E. Hoyle, "Effects of Monomer Functionality and Hydrogen Bonding on the Polymerization Kinetics and Properties of Thiol−Ene Networks", *Macromolecules*, , Vol. 42, pp. 2994-2999, 2009.

20. Yagci, Y., S. Jockusch and N. J. Turro, "Photoinitiated Polymerization: Advances, Challenges, and Opportunities", *Macromolecules*, Vol. 43, pp. 6245-6260, 2010.

21. Davidson, R. S., "The Chemistry of Photoinitiators-Some Recent Developments", *Journal of Photochemistry and Photobiology A: Chemistry*, Vol.73, pp. 81-96, 1993.

22. Ajayaghosh, A., "Macrophotoinitiator Containing Pendent Xanthate Chromophore: Photopolymerization of Methyl methacrylate and Evaluation of Kinetic Parameters", *Polymer*, Vol. 36, pp. 2049-2053, 1995.

23. Angiolini, L., D. Caretti, C. Carlini, E. Corelli and E. Salatelli, "Polymeric Photoinitiators Having Benzoin Methylether Moieties Connected to the Main Chain Through the Benzyl Aromatic Ring and Their Activity for Ultraviolet-Curable Coatings", *Polymer*, Vol. 40, pp. 7197-7207, 1999.

24. Corrales, T., F. Catalina, C. Peinado and N. S. Allen, "Free Radical Macrophotoinitiators: an Overview on Recent Advances", *Journal of Photochemistry and Photobiology A: Chemistry* Vol. 159, pp. 103–114, 2003.

25. Degirmenci, M., G. Hizal and Y. Yagci, "Synthesis and Characterization of Macrophotoinitiators of Poly(ε-caprolactone) and Their Use in Block Copolymerization", *Macromolecules*, Vol. 35, pp. 8265–8270, 2002.

26. Temel, G., B. Aydogan, N., Arsu and Y. Yagci, "Synthesis and Characterization of One-Component Polymeric Photoinitiator by Simultaneous Double Click Reactions and Its Use in Photoinduced Free Radical Polymerization", *Macromolecules*, Vol. 42, pp. 6098-6106, 2009.

27. Wei, J. and F. Liu, "Novel Highly Efficient Macrophotoinitiator Comprising Benzophenone, Coinitiator Amine, and Thio Moieties for Photopolymerization", *Macromolecules*, Vol. 42, pp. 5486-5491, 2009

28. Arsu, N., I. Reetz, Y. Yagci and M. K. Mishra, Chapter 8. *In Handbook of Vinyl Polymers: Radical Polymerization, Process, and Technology* , 2nd Eddition., Mishra, M. K., Yagci, Y., Eds.; CRC Press: Boca Raton, FL, pp. 141-204, 2009.

29. Dietliker, K. In Chemistry & Technology of UV & EB Formulation for Coatings, Inks, and Paints, SITATechnology Ltd.: London, Vol. III, pp. 76-78, 1991.

30. Fouassier, J. P., *In Photoinitiation, Photopolymerization, and Photocuring: Fundamentals and Applications*, Hanser: Munich, pp 1-7, 1995.

31. Pappas, S. P. *In UV Curing: Science and Technology*,Technology Marketing Corporation: Norwalk, CT, pp. 2-13, 1987.

32. Carlini, C. and L. Angiolini, "Polymers as Free Radical Photoinitiators", *Synthesis and Photosynthesis Advances in Polymer Science*, Vol. 123, pp. 127-214, 1995.

33. Angiolini, L., D. Caretti and E. Salatelli, "Synthesis and Photoinitiation Activity of Radical Polymeric Photoinitiators Bearing Side-Chain Camphorquinone Moieties", *Macrmolecular Chemistry and Physics*, Vol. 201, pp. 2646-2653, 2000.

34. Angiolini, L., D. Caretti, C. Carlini, E. Corelli and E. Salatelli "Polymeric Photoinitiators Having Benzoin Methylether Moieties Connected to the Main Chain Through the Benzyl Aromatic Ring and Their Activity for Ultraviolet-Curable Coatings", *Polymer*, Vol. 40, pp. 7197-7207, 1999.

35. Angiolini, L., D. Caretti, C. Carlini and E. Corelli "Polymeric Photoinitiators Having Benzoin Methyl Ether Moieties Connected to the Main Chain by the Benzoyl Group and Their Activity for Ultra-Violet Curable Coatings", *Polymer* Vol. 35, pp. 5413-5421, 1994.

36. Wei J., Ho. Wang, X. Jiang and J. Yin "Novel Photosensitive Thio-Containing Polyurethane as Macrophotoinitiator Comprising Side-Chain Benzophenone and Co-Initiator Amine for Photopolymerization", *Macromolecules*, 40, pp. 2344-2351, 2007.

37. Wang, H., J. Wei, X. Jiang and J. Yin, "Highly efficient sulfur-containing polymeric photoinitiators bearing side-chain benzophenone and coinitiator amine for photopolymerization", *Journal of Photochemistry and Photobiology A: Chemistry*, Vol. 186, pp. 106-114, 2007.

38. Chen Y., J. Loccufier, L. Vanmaele, E. Barriau and H. Frey "Novel Multifunctional Polymeric Photoinitiators and Photo-Coinitiators Derived from Hyperbranched Polyglycerol", *Macromolecular Chemistry and Physics*, Vol. 208, pp. 1694-1706, 2007.

39. Wei J., X. S. Jiang and H. Y. Wang, "Effect of the Structure of Photosensitive Groups Contained in Novel PU-Type Polymeric Benzophenone Photoinitiators on Photopolymerization", *Macromolecular Chemistry and Physics*, Vol. 208, pp. 2303-2311, 2007.

40. Wei, J., H. Wang, X. Jiang and J. Yin, "Study of Novel PU-Type Polymeric Photoinitiators Comprising of Side-Chain Benzophenone and Coinitiator Amine: Effect of Macromolecular Structure on Photopolymerization", *Macromolecular Chemistry and Physics*, Vol. 208, pp. 287-294, 2007.

41. Wang H., J. Wei, X. Jian and J. Yin, "Novel Chemical-Bonded Polymerizable Sulfur-Containing Photoinitiators Comprising the Structure of Planar *N*-Phenylmaleimide and Benzophenone for Photopolymerization", *Polymer*, Vol. 47, pp. 4967-4975, 2006.

42. X. Jiang and J. Yin, "Polymeric Photoinitiator Containing In-Chain Thioxanthone and Coinitiator Amines", *Macromolecular Rapid Communications*, Vol. 25, pp. 748-752, 2004.

43. Angiolini, L., D. Caretti and E. Salatelli "Synthesis and Photoinitiation Activity of Radical Polymeric Photoinitiators Bearing Side-Chain Camphorquinone Moieties", *Macromolecular Chemistry and Physics*, Vol. 201, pp. 2646-2653, 2000.

44. Kilambi, H., E. R. Beckel, K. A. Berchtold, J. W. Stansbury and N. C. Bowman, "Influence of Molecular Dipole on Monoacrylate Monomer Reactivity", *Polymer*, Vol. 46, pp. 4735-4742, 2005.

45. Lu, H., J. W. Stansbury and C. N. Bowman ,"Impact of Curing Protocol on Conversion and Shrinkage Stress", *Journal of Dental Research*, Vol. 84, pp. 822-826, 2005.

46. Studer K., C. Decker, E. Beck and R. Schwalm, " Overcoming Oxygen Inhibition in UV-Curing of Acrylate Coatings by Carbon Dioxide Inerting, Part I", *Progress in Organic Coatings*, Vol. 48, pp. 92-100, 2003.

47. Lee, T. Y., C. A. Guymon, E. S. Jonsson and C. E. Hoyle, "The Effect of Monomer Structure on Oxygen Inhibition of (meth)acrylates Photopolymerization", *Polymer*, Vol. 45, pp. 6155-6162, 2004.

48. Ruiz, C. S. B., L. D. B. Machado, J. E. Volponi and E. S. Pino, "Oxygen Inhibition and Coating Thickness Effects on UV Radiation Curing of Weatherfast Clearcoats Studied by Photo-DSC", *Journal of Thermal Analysis and Calorimetry*, Vol. 75, pp. 507-512, 2004.

49. Young, J. S., A. R. Kannurpatti and C. N. Bowman, "Effect of Comonomer Concentration and Functionality on Photopolymerization Rates, Mechanical Properties and Heterogeneity of the Polymer", *Macromolecular Chemistry and Physics*, Vol. 199, pp. 1043-1049, 1998.

50. Moussa, K. and C. Decker, "Light-Induced Polymerization of New Highly Reactive Acrylic Monomers", *Journal of Polymer Science: Part A: Polymer Chemistry,* Vol. 31 pp. 2197-2203, 1993.

51. Kilambi, H., S. K. Reddy, L. Schneidewind, J. W. Stansbury and N. C. Bowman, " Influence of the Secondary Functionality on the Radical-Vinyl Chemistry of Highly Reactive Monoacrylates", *Journal of Polymer Science: Part A: Polymer Chemistry*, Vol. 47, pp. 4859-4870, 2009.

52. Lu, H., J. W. Stansbury, J. Nie, K. A. Berchtold and C. N. Bowman, "Development of Highly Reactive Mono-(meth)acrylates as Reactive Diluents for Dimethacrylate-Based Dental Resin Systems", *Biomaterials*, Vol. 26, pp. 1329-1336, 2005.

53. Berchtold, K. A., J. Nie, J. W. Stansbury, B. Hacioglu, E. R. Beckel and N. C. Bowman, "Novel Monovinyl Methacrylic Monomers Containing Secondary Functionality for Ultrarapid Polymerization: Steady-State Evaluation", *Macromolecules*, Vol. 37, pp. 3165-3179, 2004.

54. Beckel, E. R., J. W. Stansbury and N. C. Bowman, "Evaluation of a Potential Ionic Contribution to the Polymerization of Highly Reactive (Meth)acrylate Monomers", *Macromolecules*, Vol. 38, pp. 9474-9481, 2005.

55. Beckel, E. R., J. Nie, J. W. Stansbury and N. C. Bowman, "Effect of Aryl Substituents on the Reactivity of Phenyl Carbamate Acrylate Monomers", *Macromolecules*, Vol. 37, pp. 4062-4069, 2004.

56. Jansen, J. F. G. A., A. A. Dias, M. Dorschu and B. Coussens, "Fast Monomers: Factors Affecting the Inherent Reactivity of Acrylate Monomers in Photoinitiated Acrylate Polymerization", *Macromolecules*, Vol. 36, pp. 3861-3873, 2003.

57. Jansen, J. F. G. A., A. A. Dias, M. Dorschu and B. Coussens "Effect of Dipole Moment on the Maximum Rate of Photoinitiated Acrylate Polymerizations", *Macromolecules*, Vol. 35, pp. 7529-7531, 2002.

58. Deepak, V. D., J. Rajan, and S. K. Asha, "Hydrogen Bonding and Rate Enhancement in the Photoinduced Polymerization of Telechelic Urethane Methacrylates Based on a Cycloaliphatic System: Tricyclodecane dimethanol", *Journal of Polymer Science: Part A: Polymer Chemistry*, Vol. 44, pp. 4384-4395, 2006.

59. Berchtold, K. A., J. Nie, J. W. Stansbury, and C. N. Bowman, "Reactivity of Monovinyl (Meth)acrylates Containing Cyclic Carbonates", *Macromolecules*, Vol. 41 pp. 9035-9043, 2008.

60. Andrzejewska, E. and M. Andrzejesky, "Polymerization Kinetics of Photocurable Acrylic Resins", *Journal of Polymer Science: Part A: Polymer Chemistry*, Vol. 36, pp. 665-673, 1998.

61. Lee, T. Y., T. M. Roper, S. Jonsson, C. A. Guymon and C. E. Hoyle, "Influence of Hydrogen Bonding on Photopolymerization Rate of Hydroxyalkyl Acrylates", *Macromolecules*, Vol. 37, pp. 3659–3665, 2004.

62. Jariwala, P. C. and Mathias, L. J., "Syntheses, Polymerization, and Characterization of Novel Semifluorinated Methacrylates, Including Novel Liquid Crystalline Materials", *Macromolecules*, Vol. 26, pp. 5129–5136, 1993.

63. Avci, D., S. H. Kusefoglu, R. D. Thompson, and L. J. Mathias, "Ester Derivatives of α-(Hydroxymethy1)acrylates: Itaconate Isomers Giving High Molecular Weight Homopolymers", *Macromolecules*, Vol. 27, pp. 1981–1982, 1994.

64. Mathias, L. J., K.Thigpen and D. Avci, "Superfast Methacrylate Photomonomers: Ester Derivatives of Ethyl α -Hydroxymethacrylates", *Macromolecules*, Vol. 28, pp. 8872–8874, 1995.

65. Thompson, R. D., T. B. Barclay, K. R. Basu and L. J. Mathias, "Facile Synthesis and Polymerization of Ether Substituted Methacrylates", *Polymer Journal*, Vol. 27, pp. 325–338, 1995.

66. Avci, D. and A. Z. Albayrak, "Synthesis and Copolymerization of New Phosphorus-Containing Acrylates", *Journal of Polymer Science: Part A: Polymer Chemistry*, Vol. 41, pp. 2207–2217, 2003.

67. Avci, D. and L. J. Mathias, "Synthesis and Polymerization of Phosphorus-Containing Acrylates", *Journal of Polymer Science: Part A: Polymer Chemistry*, Vol. 40, pp. 3221–3231, 2002.

68. Avci, D., and Mathias, L. J. , "Synthesis and Photopolymerizations of New Hydroxyl-Containing Dimethacrylate Crosslinkers", *Polymer*, Vol. 45, pp. 1763–1769, 2004.

69. Avci, D. and S. H Kusefoglu, "Functionalization and Crosslinking Reactions of Ethyl-α-hydroxymethylacrylate", *Journal of Polymer Science: Part A: Polymer Chemistry*, Vol. 31, pp. 2941–2949, 1993

70. Yamada, B. and S. Kobatake, "Radical Polymerization, co-Polymerization, and Chain Transfer of α-Substituted Acrylic Esters", *Progress in Polymer Science*, Vol. 19, pp. 1089-1131, 1994.

71. Warren, S. C. and L. J. Mathias, "Synthesis and Polymerization of Ethyl α-Chloromethylacrylate and Related Derivatives", *Journal of Polymer Science: Part A: Polymer Chemistry*, Vol. 28, pp. 1637–1648, 1990.

72. Mathias, L. J., M. R.Warren and S. Huang, "tert-Butyl α-(Hydroxymethy1)acrylate and Its Ether Dimer: Multifunctional Monomers Giving Polymers with Easily Cleaved Ester Groups", *Macromolecules*, Vol. 24, pp. 2036–2042, 1991.

73. Anseth, K. S., C. M. Wang, and C. N. Bowman, "Kinetic Evidence of Reaction Diffusion during the Polymerization of Multi(meth)acrylate Monomers", *Macromolecules*, Vol. 27, pp. 650–655, 1994.

74. Brandrup, J., E. H. Immergut and E. A. Grulke, *Polymer Handbook*, 4th Eddition, Wiley-Interscience: Hoboken, NJ, 1999.

75. Spartan version 4.0, 1995, Wavefunction, Inc.; Irvine, CA.

76. D'alelio, G. F. and T. Huemmer "Preparation and Polymerization of Some Vinyl Monomers Containing the 2-oxo-1,3-dioxolane group", *Journal of Polymer Science: Part A: Polymer Chemistry*, Vol. 5, pp. 307–321, 1967.

77. Burton, B. L. In Proceedings of Epoxy Resin Formulators' Meeting of the Society of the Plastics Industry, Baltimore, MD, July, 2001.

78. Barner-Kowollik, C. P. Vana, and T. P. Davis, *In Handbook of Radical Polymerization*, Matyjaszewski, K.; Davis, T. P., Eds.; Wiley: New York, Chapter 4, pp. 197–198, 2002.

79. Davis, T. P., J. P. A. Heuts, Barner-Kowollik, S. Harrisson, D. A Morrison, L. H. Yee, H. M. Kapfenstein and M. L. Coote, *Macromolecular Symposia* 2002, 182, 131–148.

80. Morrison, D. A. and T. P. Davis, "Studies On The Propagation Reaction In The Free Radical Polymerization of Ethyl α-Hydroxymethacrylate", *Macromolecular Chemistry and Physics,* Vol. 201, pp. 2128-2137, 2000.

81. Kilambi, H., J. W. Stansbury, and C. N. Bowman, "Deconvoluting the Impact of Intermolecular and Intramolecular Interactions on the Polymerization Kinetics of Ultrarapid Mono(meth)acrylates", *Macromolecules*, Vol. 40, pp. 47–54, 2007.

82. Sato, T. I. Kamiya, H. Tanaka and T. Ota, "Radical Polymerization of Ethyl α-Benzoyloxymethylacrylate in Benzene", *European Polymer Journal*, Vol. 27, pp. 1087–1092, 1991.

83. Yamada, B., M. Satake, and T. Otsu, "Role of Bulky α-substituent in Free-Radical Polymerization and Copolymerization of methyl α-(alkoxymethyl)acrylates", *Makromolecular Chemistry and Physics*, Vol. 192, pp. 2713–2722, 1991.

84. Vaidya, R. A. and L. J. Mathias, "On Prediction Free Radical Polymerization of Allyl Monomers. MINDOM and ^{13}C NMR Results", *Journal of Polymer Science: Polymer Symposium*, Vol. 74, pp. 243–251, 1986.

85. Kodaira, T., T. Fujisawa, Q.-Q. Liu and M. Urushisaki, "Cyclopolymerization. 22. Radical Polymerization of *N*-Methyl-*N*-allyl-2-(methoxycarbonyl) allylamine: Design of Unconjugated Dienes with High Polymerizability and High Cyclization Tendency Using Functional Groups of Low Polymerizabilities", *Macromolecules*, Vol. 29, pp. 484–485, 1996.

86. Buback, M., R.G. Gilbert, R.A. Hutchinson, B. Klumperman, F.D. Kuchta and B.G. Manders, O'Driscoll, K.F., Russell, G.T., and Schweer, J., "Critically Evaluated Rate Coefficients for Free-Radical Polymerization, 1 Propagation Rate Coefficient for Styrene", *Macromolecular Chemistry Physics*, Vol. 196, pp. 3267-80, 1995.

87. Yamada B., M. Azukizawa, H. Yamazoe, D. J. T. Hill and P. J. Pomery, "Free Radical Polymerization of Cyclohexyl Acrylate Involving Interconversion Between Propagating and Mid-Chain Radicals", *Polymer*, Vol. 41 pp. 5611-5618, 2000.

88. Kobatake, S. and B. Yamada, "Severely Hindered Propagation and Termination Allowing Radical Polymerization of a-Substituted Acrylate Bearing a Bis(carbomethoxy)ethyl Group", *Macromolecules*, Vol. 28, pp. 4047-4054, 1995.

89. Gaussian 03. Revision D.01; Frisch, M. J. T., G. W. Schlegel, H. B. Scuseria, G. E. Robb, M. A. Cheeseman, J. R. Montgomery Jr., J. A. Vreven, T. Kudin, K. N. Burant, J. C. Millam, J. M. Iyengar, S. S. Tomasi, J. Barone, V. Mennucci, B. Cossi, M. Scalmani, G. Rega, N. Petersson, G. A. Nakatsuji, H. Hada, M. Ehara, M. Toyota, K. Fukuda, R. Hasegawa, J. Ishida, M. Nakajima, T.Honda, Y. Kitao, O. Nakai, H. Klene, M. Li, X. Knox, J. E. Hratchian, H. P. Cross, J. B. Bakken, V. Adamo, C. Jaramillo, J. Gomperts, R. Stratmann, R. E. Yazyev, O. Austin, A. J. Cammi, R. Pomelli, C. Ochterski, J. W. Ayala, P. Y. Morokuma, K. Voth, G. A. Salvador, P. Dannenberg, J. J. Zakrzewski, V. G. Dapprich, S. Daniels, A. D. Strain, M. C. Farkas, O. Malick, D. K. Rabuck, A. D. Raghavachari, K. Foresman, J. B. Ortiz, J. V. Cui, Q. Baboul, A. G. Clifford, S. Cioslowski, J. Stefanov, B. B. Liu, G. Liashenko, A. Piskorz, P. Komaromi, I. Martin, R. L. Fox, D. J. Keith, T. Al-Laham, M. A. Peng, C. Y. Nanayakkara, A. Challacombe, M. Gill, P. M. W. Johnson, B. Chen, W. Wong, M. W. Gonzalez, C. and Pople, J. A. Gaussian. Inc.: Wallingford CT, 2004. Gaussian 03. Revision D.01. Gaussian. Inc.. Wallingford CT, 2004.

90. Gaussian 09. Revision D.01; Frisch, M. J. T., G. W. Schlegel, H. B. Scuseria, G. E. Robb, M. A. Cheeseman, J. R. Montgomery Jr., J. A. Vreven, T. Kudin, K. N. Burant, J. C. Millam, J. M. Iyengar, S. S. Tomasi, J. Barone, V. Mennucci, B. Cossi, M. Scalmani, G. Rega, N. Petersson, G. A. Nakatsuji, H. Hada, M. Ehara, M. Toyota, K. Fukuda, R. Hasegawa, J. Ishida, M. Nakajima, T.Honda, Y. Kitao, O. Nakai, H. Klene, M. Li, X. Knox, J. E. Hratchian, H. P. Cross, J. B. Bakken, V. Adamo, C. Jaramillo, J. Gomperts, R. Stratmann, R. E. Yazyev, O. Austin, A. J. Cammi, R. Pomelli, C. Ochterski, J. W. Ayala, P. Y. Morokuma, K. Voth, G. A. Salvador, P. Dannenberg, J. J. Zakrzewski, V. G. Dapprich, S. Daniels, A. D. Strain, M. C. Farkas, O. Malick, D. K. Rabuck, A. D. Raghavachari, K. Foresman, J. B. Ortiz, J. V. Cui, Q. Baboul, A. G. Clifford, S. Cioslowski, J. Stefanov, B. B. Liu, G. Liashenko, A. Piskorz, P. Komaromi, I. Martin, R. L. Fox, D. J. Keith, T. Al-Laham, M. A. Peng, C. Y. Nanayakkara, A. Challacombe, M. Gill, P. M. W. Johnson, B.

Chen, W. Wong, M. W. Gonzalez, C. and Pople, J. A. Gaussian. Inc.: Wallingford CT, 2004. Gaussian 03. Revision D.01. Gaussian. Inc.. Wallingford CT, 2009.

91. Zhao, Y. and D. G. Truhlar, "The M06 Suite of Density Functionals for Main Group Thermochemistry, Thermochemical Kinetics, Noncovalent Interactions, Excited States, and Transition Elements: Two New Functionals and Systematic Testing of Four M06-Class Functionals and 12 Other Functionals", *Theoretical Chemistry Accounts*, Vol. 120, pp. 215-241, 2008.

92. Zhao, Y., N. E. Schultz and D. G.Truhlar, "Design of Density Functionals by Combining the Method of Constraint Satisfaction with Parametrization for Thermochemistry, Thermochemical Kinetics, and Noncovalent Interactions", *Journal of Chemical Theory and Computation*, Vol. 2, pp. 364-382, 2006.

93. Zhoa Y and D. G. Thruhlar "Hybrid Meta Density Functional Theory Methods for Thermochemistry, Thermochemical Kinetics, and Noncovalent Interactions: The MPW1B95 and MPWB1K Models and Comparative Assessments for Hydrogen Bonding and van der Waals Interactions", *Journal of Physical Chemistry A*, Vol. 108, pp. 6908-6918, 2004.

94. Atkins, P. W. and J. De Paula, *Atkins' physical chemistry*, 8th Eddition, Oxford ; New York: Oxford University Press, 2006.

95. Liptak M. D., K. C.Gross, P. G. Seybold, S. Feldgus and G. C. Shields "Absolute pKa Determinations for Substituted Phenols", *Journal of American Chemical Society*, Vol. 124, pp. 6421–6427, 2002.

96 . Reed, E.A., L.A. Curtiss and F.Weinhold, "Intermolecular Interactions from a Natural Bond Orbital, Donor-Acceptor Viewpoint", *Chemical Reviews*, Vol. 88, pp. 899-926, 1988.

97. Tomasi, J., B. Mennucci and E. Cances, "The IEF Version of the PCM Solvation Method: an Overview of a New Method Addressed to Study Molecular Solutes at the QM ab Initio Level", *Journal of Molecular Structure-Theochem*, Vol. 464, pp. 211-226, 1999.

98. Cances, E., B. Mennucci and J. Tomasi, "A New Integral Equation Formalism for the Polarizable Continuum Model: Theoretical Background and Applications to Isotropic and Anisotropic Dielectrics", *Journal of Chemical Physics*, Vol. 107, pp. 3032-3041, 1997.

99. Mennucci, B. and J.Tomasi, "Continuum solvation models: A New Approach to the Problem of Solute's Charge Distribution and Cavity Boundaries", *Journal of Chemical Physics*, Vol. 106, pp. 5151-5158, 1997.

100. Mennucci, B., E. Cances and J. Tomasi, "Evaluation of Solvent Effects in Isotropic and Anisotropic Dielectrics and in Ionic Solutions with a Unified Integral Equation Method: Theoretical Bases, Computational Implementation, and Numerical Applications", *Journal of Physical Chemistry B*, Vol. 101, pp. 10506-10517, 1997.

101. Barone V. and M. Cossi "Quantum Calculation of Molecular Energies and Energy Gradients in Solution by a Conductor Solvent Model", *Journal of Physical Chemistry A*, Vol. 102, pp. 1995-2001, 1998.

102. Degirmenci, I., T. F. Ozaltin, O. Karahan, V.Van Speybroeck, M. Waroquier and V. Aviyente, "Origins of the Solvent Effect on the Propagation Kinetics of Acrylic Acid and Methacrylic Acid", accepted to *Journal of Polymer Science Part A: Polymer Chemistry*, 2013.

103. Smith, T. J., B. S. Shemper, J. S. Nobles, A.M. Casanova, C. Ott and L. J. Mathias, "Crosslinking Kinetics of Methyl and Ethyl (a-hydroxymethyl)acrylates: Effect of Crosslinker Type and Functionality", *Polymer*, Vol. 44, pp. 6211-6216, 2003.

104. Gunaydin, H., S. Salman, N. S. Tuzun, D. Avci and Aviyente, V., "Modeling the Free Radical Polymerization of Acrylates", *International Journal of Quantum Chemistry*, Vol. 103, pp. 176-189, 2005.

105. Degirmenci, I., V. Aviyente, V. Van Speybroeck and M.Waroquier, "DFT Study on the Propagation Kinetics of Free-Radical Polymerization of alpha-Substituted Acrylates", *Macromolecules*, Vol. 42, pp. 3033-3041, 2009.

106. Karahan O., D. Avci and V. Aviyente "Structure–Reactivity Relationships of Alkyl α-Hydroxymethacrylate Derivatives", *Journal of Polymer Science Part A: Polymer Chemistry*, Vol. 49, pp. 3058-3068, 2011.

107. Thiery, M.M. and C. Rerat, "High Pressure Solid Phases of Benzene. III. Molecular Packing Analysis of the Crystalline Structures of C_6H_6", *Journal of Chemical Physics*, Vol. 104, pp. 9079-9089, 1996.

108. Errington, J. R. and A.Z. Panagiotopoulos, "New Intermolecular Potential Models for Benzene and Cyclohexane", *Journal of Chemical Physics*, Vol. 111, pp. 9731-9738, 1999.

109. Spirko, V., O. Engkvist, P. Soldan, H.L. Selzle, E.W. Schlag and P. Hobza, "Structure and Vibrational Dynamics of the Benzene Dimer", *Journal of Chemical Physics*, Vol. 111, pp. 572-582, 1999.

110. Gonzales, C. and E.C. Lim, "A Quantum Chemistry Study of the van der Waals Dimers of Benzene, Naphthalene, and Anthracene: Crossed (D_{2d}) and Parallel-Displaced (C_{2h}) Dimers of Very Similar Energies in the Linear Polyacenes", *Journal of Physical Chemistry A*, Vol. 104, pp. 2953-2957, 2000.

111. Kim, K. S., P. Tarakeshwar, and J. Y. Lee, "Molecular Clusters of π-Systems: Theoretical Studies of Structures, Spectra, and Origin of Interaction Energies", *Chemical Reviews*, Vol. 100, pp. 4145-4185, 2000.

112. Tsuzuki D., K. Honda and R. Azumi, "Model Chemistry Calculations of Thiophene Dimer Interactions: Origin of π-stacking", *Journal of American Chemical Society*, Vol. 124, pp. 12200-12209, 2002.

113. Mignon, P., S. Loverix, F. D. Proft and P. Geerlings, "Influence of Stacking on Hydrogen Bonding: Quantum Chemical Study on Pyridine-Benzene Model Complexes", *Journal of Physical Chemistry A*,Vol. 108, pp. 6038-6044, 2004.

114. Jurecka, P. and P. Hobza, "True Stabilization Energies for the Optimal Planar Hydrogen-Bonded and Stacked Structures of GuanineâââCytosine, AdenineâââThymine, and Their 9- and 1-Methyl Derivatives: Complete Basis Set Calculations at the MP2 and CCSD(T) Levels and Comparison with Experiment", *Journal of American Chemical Sociecty*, Vol. 125, pp. 15608-15613, 2003.

115. Sponer, J., H. A. Gabb, J. Leszczynski and P. Hobza, "Base-Base and Deoxyribose-Base Stacking Interactions in B-DNA and Z-DNA: A Quantum-Chemical Study", *Biophysical Journal*, Vol. 73, pp. 76-87, 1997.

116. Reha, D., M. Kabelac, F. Ryjacek, J. Sponer, J. E. Sponer, M. Elstner, S. Suhai and P. Hobza, "Intercalators. 1. Nature of Stacking Interactions between Intercalators (Ethidium, Daunomycin, Ellipticine, and 4',6-Diaminide-2-phenylindole) and DNA Base Pairs. Ab Initio Quantum Chemical, Density Functional Theory, and Empirical Potential Study", *Journal of American Chemical Society*, Vol. 124, pp. 3366-3376, 2002.

117. Gu, J., J. Wangb, J. Leszczynski, Y. Xie and H.F. Schaefer, "To Stack or not to Stack: Performance of a New Density Functional for the Uracil and Thymine Dimers", *Chemical Physics Letters*, Vol. 459, pp. 164–166, 2008.

118. Guerra F. C., T. van der Wijst, J. Poater, M. Swart and F.M. Bickelhaupt, "Adenine Versus Guanine Quartets in Aqueous Solution: Dispersion-Corrected DFT Study on

the Differences in *p*-Stacking and Hydrogen-Bonding Behavior", *Theoretical Chemistry Accounts*; Vol. 125, pp. 245-252, 2010.

119. Lozynski M., D. Rusinska-Roszak and H. G. Mack, "Hydrogen Bonding and Density Functional Calculations: The B3LYP Approach as the Shortest Way to MP2 Re-sults", *Journal of Physical Chemistry A*, Vol. 102, pp. 2899-2903, 1998.

120. Swart, M., T. van der Wijst, F. C. Guerra and F. M. Bickelhaupt, "π-π Stacking Tackled with Density Functional Theory", *Journal of Molecular Modeling*, Vol. 13, pp. 1245–1257, 2007.

121. Satoh, K.. and M. Kamigatio, "Stereospecific Living Radical Polymerization: Dual Control of Chain Length and Tacticity for Precision Polymer Synthesis",*Chemical Reviews*, Vol. 109, pp. 5120-56, 2009.

122. Degirmenci, I., D. Avci, V. Aviyente, K. Van Cauter, V. Van Speybroeck and M. Waroquier, "Density Functional Theory Study of Free-Radical Polymerization of Acrylates and Methacrylates: Structure-Reactivity Relationship", *Macromolecules*, Vol. 40, pp. 9590-9602, 2007.

123. Karahan, O., V. Aviyente, D. Avci, H. Zijlstra and F. M. Bickelhaupt, "A Computational Study on the Reactivity Enhancement in the Free Radical Polymerization of Alkyl α-Hydroxymethacrylate and Acrylate Derivatives", *Journal of Polymer Science Part A: Polymer Chemistry*, Vol.51, pp. 880-889, 2013.

124. Furuncuoglu, T., I. Ugur, I. Degirmenci and V. Aviyente, "Role of Chain Transfer Agents in Free Radical Polymerization Kinetics", *Macromolecules*, Vol. 43, pp. 1823-1835, 2010.

125. Degirmenci, I., S. Eren, V. Aviyente, B. De Sterck, K. Hemelsoet, V. Van Speybroeck and M.Waroquier, "Modeling the Solvent Effect on the Tacticity in the

Free Radical Polymerization of Methyl Methacrylate", *Macromolecules*, Vol. 43, pp. 5602-5610, 2010.

126. Karahan, O., M. Isik, G. Cifci, I. Ugur, D. Avci and V. Aviyente, " Cyclization Tendencies in the Free Radical Polymerization of Allyl Acrylate Derivatives: A Computational Study", *Journal of Polymer Science Part A: Polymer Chemistry*, Vol. 49, pp. 2474–2483, 2011.

127. Ozaltin, T. F., I. Degirmenci, V. Aviyente, C. Atilgan, B. De Sterck, V. Van Speybroeck and M. Waroquier, "Controlling the Tacticity in the Polymerization of N-isopropylacrylamide: A Computational Study", *Polymer*, Vol. 52, pp. 5503-5512, 2011.

128. Dogan B., S. Catak, V. Van Speybroeck, M.Waroquier and V. Aviyente, "Free Radical Polymerization of Ethyl Methacrylate and Ethyl α-hydroxy methacrylate: A Computational Approach to the Propagation Kinetics", *Polymer*, Vol. 53, pp. 3211-3219, 2012.

129 . Alfrey T. and C.C. Price, "Relative reactivities in Vinyl Copolymerization", *Journal of Polymer Science*, Vol. 2, pp. 101-106, 1947.

130 . Zhan C., D. A. Dixon, "A Density Functional Theory Approach to the Development of Q-e Parameters for the Prediction of Reactivity in Free-Radical Copolymerizations ", *Journal of Phyical Chemistry A*, Vol. 106, pp. 10311-10325, 2002.

131. Yu X., W. Liu, F. Liu and X. Wang, "DFT-Based Theoretical QSPR Models of *Q-e* Parameters for the Prediction of Reactivity in Free-Radical Copolymerizations", *Journal of Molecular Modeling*, Vol. 14, pp. 1065-1070, 2008.

132. Yu X., X. Wang and B. Li, "Prediction of the Q-e Parameters from Radical Structures", *Colloid Polymer Science*, Vol. 288, pp. 951-958, 2010.

133. Guillaneuf Y., D. Gigmes, S. R. A. Marque, P. Astolfi, L. Greci, P. Tordo and D. Bertin "First Effective Nitroxide-Mediated Polymerization of Methyl Methacrylate", *Macromolecules*, Vol. 40, pp. 3108-3114, 2007.

134 . Hodgson J. L., C. Y. Lin, M. L. Coote, S. R. A. Marque and K. Matyjaszewski, "Linear Free-Energy Relationships for the Alkyl Radical Affinities of Nitroxides: A Theoretical Study", *Macromolecules*, Vol. 43, pp. 3728-3743, 2010.

135. Lin CY, S. R. A. Marque, K. Matyjaszewski and M. L. Coote "Linear-Free Energy Relationships for Modeling Structure–Reactivity Trends in Controlled Radical Polymerization", *Macromolecules*, Vol. 44, pp. 7568-7583, 2011.

136. Morrill J. A., J. H. Biggs, C. N. Bowman and J. W. Stansbury, "Development of Quantitative Structure–Activity Relationships for Explanatory Modeling of Fast Reacting (meth)acrylate Monomers Bearing Novel Functionality", *Journal of Molecular Graphics Modelling*, Vol. 29, pp. 763-772, 2011.

137. Mathias L. J, S. H. Kusefoglu, A. O. Kress, S. Lee and C.W. Dickerson and S. F. Thames "New Acrylate-Containing Dimers and Oligomers for Crosslinking Vinyl Polymers", *Polymer News*, Vol. 17, pp. 36–42, 1992.

138 . Avci D. and L. J. Mathias "Synthesis and Cyclopolymerization of Novel allyl-Acrylate Quaternary Ammonium Salts", *Journal of Polymer Science Part A: Polymer Chemistry*, Vol. 37, pp. 901–907, 1999.

139. Navidi, W., *Statistics for Engineers and Scientists*, New York: MvGraw-Hill, 2008.

140. Yeniad, B., A. Z. Albayrak, N. C. Olcum, and D. Avci, "Synthesis and Photopolymerizations of New Phosphonated Monomers for Dental Applications", *Journal of Polymer Science Part A: Polymer Chemistry*, Vol. 46, pp. 2290–2299, 2008.

141 . Sahin, G., D. Avci, O. Karahan, and N. Moszner, "Synthesis and Photopolymerizations of New Phosphonated Methacrylates from Alkyl α-Hydroxymethacrylates and Glycidyl Methacrylate", *Journal of Applied Polymer Science*, Vol. 114, pp. 97–106, 2009.

142. Naoki, Y., Y. Junji and Y. Motoyoshi, Jpn. Kokai Tokkyo Koho, JP 58098313, 1983.

143. Khalafi-Nezhad, A., M. N. Soltani Rad and A. Khoshnood, "An Efficient Method for the Chemoselective Preparation of Benzoylated 1, 2-diols from Epoxides", *Synthesis*, Vol. 16, pp. 2552–2558, 2003.

144. Van Den Bergen, H. and J. C. Vanovervelt, WO 01/74826 A1, 2001.

145. Tamareselvy, K. and F. A. Rueggeberg, "Synthesis and Characterization of a Monofunctional Analog to BIS-GMA: A Dental Monomer", *Journal of Applied Polymer Science*, Vol. 57, pp. 705–716, 1995.

146. Davy, K. W. M., S. Kalachandra, M. S. Pandain and M. Braden, "Relationship Between Composite Matrix Molecular Structure and Properties", *Biomaterials*, Vol. 19, pp. 2007–2014, 1998.

147. Liu, Y.H., Q. S. Liu, and Z. H. Zhang, "Amberlyst-15 as a New and Reusable Catalyst for Regioselective Ring-Opening Reactions of Epoxides to β-alkoxy Alcohols", *Journal of Molecular Catalysis A:Chemical*, Vol. 296, pp. 42–46, 2008

148. Olszewski-Ortar, A., P. Gros, and Y. Fort, "Selective Ring-Opening of ω-epoxyalkyl (meth)acrylates. An Efficient Access to Bifunctional Monomers", *Tetrahedron Letters*, Vol. 38, pp. 8699–8702, 1997.

149. Caubere, P.; Fort, Y., Ortar, A. (Atochem Invs). U.S. Patent 5.283.360, 1994.

150. Price, D., L. K. Cunliffe, K. J. Bullet, T. R. Hull, G. J. Milnes, J. R. Ebdon, J. B. Hunt and P. Joseph, "Thermal Behavior of Covalently Bonded Phosphonate Flame-Retarded poly(methyl methacrylate) Systems", *Polymer for Advanced Technologies*, Vol. 19, pp.710–723, 2008.

151. Avci, D. and L. J. Mathias, "Synthesis and Photopolymerizations of New Hydroxyl-Containing Dimethacrylate Crosslinkers", *Polymer*, Vol. 45, pp.1763–1769, 2004.

152. Vaidya, R. A. and L. J. Mathias, "On Prediction Free Radical Polymerization of Allyl Monomers. MINDOM and ^{13}C NMR Results", *Journal of Polymer Science: Polymer Symposium*, Vol. 74, pp. 243–251, 1986.

153. Kodaira, T., T. Fujisawa, Q.-Q. Liu and M. Urushisaki, "Cyclopolymerization. 22. Radical Polymerization of *N*-Methyl-*N*-allyl-2-(methoxycarbonyl) Allylamine: Design of Unconjugated Dienes with High Polymerizability and High Cyclization Tendency Using Functional Groups of Low Polymerizabilities", *Macromolecules*, Vol. 29, pp. 484–485, 1996.

154. Carlini C., L. Angiolini D. Careiti and E. Corelli, "Recent Advances on Photosensitive Polymers: Polymeric Photoinitiators", *Polymers for Advanced Technologies*, Vol. 7, pp.379-384, 1996.

155. Yagci Y., S. Jockush and N. J. Turro, "Photoinitiated Polymerization: Advances, Challenges, and Opportunities", *Macromolecules*, Vol. 43, pp. 6245-6260, 2010.

156. Angiolini, L., D. Caretti and E. Salatelli, "Synthesis and Photoinitiation Activity of Radical Polymeric Photoinitiators Bearing Side-Chain Camphorquinone Moieties", *Macromolecular Chemistry and Physics* ,Vol. 201, pp. 2646-2653, 2000.

157. Corrales T, F. Catalina, C. Peinado, N. S. Allen, A. M. Rufs, C. Bueno and M. V. Encinas, "Photochemical Study and Photoinitiation Activity of Macroinitiators Based on Thioxanthone", *Polymer*, Vol. 43, pp.4591–4597, 2002.

158. Jiang X. and J. Yin "Polymeric Photoinitiator Containing In-Chain Thioxanthone and Coinitiator Amines", *Macromolecular Rapid Communications*, Vol. 25, pp. 748-752, 2004.

159. Angiolini L., D. Caretti, C. Carlini, E. Corelli and E. Salatelli "Polymeric Photoinitiators Having Benzoin Methylether Moieties Connected to the Main Chain Through the Benzyl Aromatic Ring and Their Activity for Ultraviolet-Curable Coatings", *Polymer*, Vol. 40, pp.7197–7207, 1999.

160. Castelvetro V., M. Molesti and P. Rolla "UV-Curing of Acrylic Formulations by Means of Polymeric Photoinitiators with the Active 2,6-dimethylbenzoylphosphine Oxide Moieties Pendant from a Tetramethylene Side Chain, *Macromolecular Chemistry and Physics*, Vol. 203, pp. 1486–1496, 2002.

161. Allonas X., J. P. Fouassier, L. Angiolini and D. Caretti , "Excited-State Properties of Camphorquinone Based Monomeric and Polymeric Photoinitiators", *Helvetica Chimica Acta*,Vol. 84, pp. 2577, 2001.

162. Wei, J., H. Y. Wang, X. S. Jiang and J. Yin, "Novel Photosensitive Thio-Containing Polyurethane as Macrophotoinitiator Comprising Side-Chain Benzophenone and Co-Initiator Amine for Photopolymerization", *Macromolecules*, Vol. 40, pp. 2344–2351, 2007.

163. Wang, H., J. Wei, X.. Jiang and J. Yin "Highly Efficient Sulfur-Containing Polymeric Photoinitiators Bearing Side-Chain Benzophenone and Coinitiator Amine for Photopolymerization", *Journal of Photochemistry and Photobiology A: Chemistry*, Vol. 186, pp. 106-114, 2007.

164. Chen, Y., J. Loccufier, L. Vanmaele, E. Barriau and H. Frey, "Novel Multifunctional Photoinitiators and Photo-Coinitiators Derived from Hyperbranched Polyglycerol", *Macromolecular Chemistry Physics*, Vol. 208, 1694-1706, 2007.

165. Wei, J., H. Y. Wang and X. S. Jiang, "Effect of the Structure of Photosensitive Groups Contained in Novel PU-Type Polymeric Benzophenone Photoinitiators on Photopolymerization", *Macromolecular Chemistry and Physics*, Vol. 208, pp. 2303–2311, 2007.

166. Wei, J., H. Y Wang,. X. S. Jiang and J. Yin, "Study of Novel PU-Type Polymeric Photoinitiators Comprising of Side-Chain Benzophenone and Coinitiator Amine: Effect of Macromolecular Structure on Photopolymerization", *Macromolecular Chemistry and Physics*, Vol. 208, pp. 287–294, 2007.

167. Nayak B. R. and L. J. Mathias, "A novel Photoinimer for the Polymerization of Acrylates and Methacrylates", *Journal of Polymer Science Part A: Polymer Chemistry*, Vol. 43, pp. 5661-5670, 2005.

168. Wang, H. Y., J. Wei, X.S. Jiang and J. Yin, "Novel Chemical-Bonded Polymerizable Sulfur-Containing Photoinitiators Comprising the Structure of Planar N-phenylmaleimide and Benzophenone for Photopolymerization", *Polymer*, Vol. 47, pp. 4967-4975, 2006.

169. Wen, Y., X. Jiang, R. Liu and J. Yin, "Amphiphilic Polymeric Michler's Ketone (MK) Photoinitiators (APMKs) Containing PEO Chain and Coinitiator Amine", *Polymers for Advanced Technologies*, Vol. 22, pp. 598-604, 2011.

170. Liska, R. J., "Photoinitiators with Functional groups. V. New Water-Soluble Photoinitiators Containing Carbohydrate Residues and Copolymerizable Derivatives Thereof", *Journal of Polymer Science Part A: Polymer Chemistry*, Vol. 40, pp. 1504-1518, 2002.

171. Jiang X, X. Luo and J. Yin, "Photoinitiators Containing in-Chain Benzophenone and Coinitiators Amine: Effect of the Structure of Coinitiator Amine on Photopolymerization", *Journal of Photochemistry and Photobiology A: Chemistry* Vol. 174, pp. 165–170, 2005.

172. Wei J., L. Rong and R, F. Liu, "Effect of Photosensitive Groups on the Photoefficiency of Polymeric Photoinitiators", *Journal of Polymer Research,* Vol. 18, pp.1001–1008, 2011.

173. Wang Y., X. Jiang and J. Yin "Novel Polymeric Photoinitiators Comprising of Side-Chain Benzophenone and Coinitiator amine: Photochemical and Photopolymerization Behaviors", *European Polymer Journal*, Vol. 45, pp. 437–447, 2009.

174. Xie H., L. Hu and W. Shi, "Synthesis and Photoinitiating Activity Study of Polymeric Photoinitiators Bearing BP moiety Based on Hyperbranched Poly(ester-amine) via Thiol-ene click Reaction", *Journal of Applied Polymer Science*, Vol. 123, pp. 1494–1501, 2012.

175. Heatley, F., P. A. Lovell and J. McDonald "NMR Studies of Free Radical Polymerization and Copolymerization of Monomers and Polymers Containing Allyl Groups", *European Polymer Journals*, Vol. 29, pp. 255-268, 1993.

176. Odian, G., *Principles of Polymerization*, 2nd Edition, Wiley-Interscience, New-York, p. 250, 1981.

177. Ranby, B. *Journal of Applied Polymer Science, Applied Polymer Symposium.*,26, p. 327, 1975.

178. Vardareli,T. K., S. Keskin and A.Usanmaz, "Synthesis and Characterization of Poly(allyl methacrylate) Obtained by Free Radical Initiator", *Journal of Macromolecular Science, Part A: Pure and Applied Chemistry*, Vol. 45, pp. 302-311, 2008.

179. Matsumoto, A., H. Ishido, M. Oiwa and K. Urushido, "Polymerization of Allyl Esters of Unsaturated Acids. IX. Controlled Ring Closure in the Radical

Cyclopolymerization of Allyl Methacrylate", *Journal of Polymer Science Part A: Polym Chem.*, Vol. 20, pp. 3207-3217, 1982.

180. Karahan, O. and D. Avci, unpublished results.

181. Thompson, R. D., W. L. Jarrett, and L. J. Mathias, "Unusually Facile Cyclopolymerization of a New Allyl Ether Substituted Acrylate and Confirmation of Repeat Unit Structure by INADEQUATE NMR", *Macromolecules*, Vol. 25, pp. 6455-6459, 1992.

182. Mulliken, R.S. "Electronic Population Analysis on LCAO-MO Molecular Wave Functions. I", *Journal of Chemical physics*, Vol. 23, pp. 1833-1840, 1955**.**

183. Parr, R. G. and W. Yang, "*Density Functional Theory of Atoms and Molecules*", Oxford University Press: New York, 1989.

184. Parr, R. G. and W. Yang, "Density-Functional Theory of the Electronic Structure of Molecules", *Annual Review of Physical Chemistry* , Vol. 46, 701-728, 1995.

185. Kohn, W., A. D. Becke and R. G. Parr, "Density Functional Theory of Electronic Structure", *Journal of Physical Chemistry*, Vol. 100, pp. 12974-12980, 1996.

186. Geerlings, P., F. De Proft and W. Langenaeker, "Density Functional Theory : a source of chemical concepts and a cost-effective methodology for their calculation", *Invited contribution to Advances in Quantum Chemistry,* Vol. 33, pp. 303-328, 1999.

187. Chermette, H. "Chemical Reactivity Indexes in Density Functional Theory", *Journal of Computational Chemistry*, Vol. 20, pp. 129-154, 1999.

188. Geerlings, P., F. De Proft and W. Langenaeker, "Conceptual Density Functional Theory", *Chemical Reviews,* Vol. 103, pp. 1793-1874, 2003.

189. Ayers, P. W., J. S. M. Anderson and L. J. Bartolotti, "Perturbative Perspectives on the Chemical Reaction Prediction Problem", *International Journal of Quantum Chemistry*, Vol. 101, pp. 520-534, 2005.

190. Geerlings, P. and F. De Proft, "Conceptual DFT: the Chemical Relevance of Higher Response Functions", *Physical Chemistry Chemical Physics*, Vol. 10, pp. 3028-3042, 2008.

191. Parr, R. G. and W. T. Yang, "Density Functional Approach to the Frontier-Electron Theory of Chemical Reactivity", *Journal of American Chemical Society*, Vol. 106, pp. 4049-4050, 1984.

192. Ayers, P. W. and M. Levy, "Perspective on Density Functional Approach to the Frontier-Electron Theory of Chemical Reactivity", *Theoretical Chemistry Accounts.*, Vol. 103, pp. 353-360, 2000.

193. Perdew, J. P., R. G. Parr and M. Levy, "Density-Functional Theory for Fractional Particle Number: Derivative Discontinuities of the Energy", *Physical. Re*views *Letters*, Vol. 49, pp. 1691-1694, 1982.

194. Tüzün, N. S. and V. Aviyente, "Modeling the Cyclopolymerization of Diallyl Ether and Methyl α-[(allyloxy)methyl]acrylate", *Inernational. Journal of Quantum Chemistry*, Vol. 107, pp. 894-906, 2007.

195. Uğur, I., F. De Vleeschouwer, N. Tüzün, V., V. Aviyente, P. Geerlings, S. Liu, P. W. Ayers and F. De Proft, "Cyclopolymerization Reactions of Diallyl Monomers: Exploring Electronic and Steric Effects Using DFT Reactivity Indices", *Journal of Phyical Chemistry A*, , Vol. 113, pp. 8704–8711, 2009.

196. Tüzün, N. S., V. Aviyente, D. Avci and N. Ince, "A Computational Approach to the Polymerizabilities of Diallylamines", *Journal of Molecular Modeling*, Vol. 7, pp. 257-264, 2001.

197. Tüzün, N. S., V. Aviyente and K. N. Houk, "Theoretical Study of Factors Controlling Rates of Cyclization of Radical Intermediates from Diallylamine and Diallylammonium monomers in Radical Polymerizations", *The Journal of Organic Chemistry*, Vol. 67, pp. 5068-5075, 2002.

198. Tüzün, N. S.; Aviyente, V. "A Computational Study on the Substituent Effect of Diallylamine Monomers in Their Cyclopolymerization Reactions", *Journal of Physical Chemistry A*, Vol. 106, pp. 8184-8190, 2002.

199. Tüzün, N. S., V. Aviyente and K.N. Houk, "A Theoretical Study on the Mechanism of the Cyclopolymerization of Diallyl Monomers", *The Journal of Organic Chemistry*, Vol. 68, pp. 6369-6374, 2003.

200. Butler, G. B. and M. A. Raymond, "Further Evidence for Nonconjugated Chromophoric Interactions in Certain Polyenes[1,2]", *The Journal of Organic Chemistry*, Vol. 30, pp. 2410-2414, 1965.

201. Butler, G. B., Cyclopolymerization and Cyclocopolymerization, *Accounts of Chemical Research*, Vol. 15, pp. 370-378, 1982.

202. Butler, G. B. and Marcel Dekker, *Cyclopolymerization and Cyclocopolymerization*, Inc, New York, 1992.

203. Capon, B. and C.W. Rees, Functional Theory of Atoms and Molecules, Oxford University Press: New York, 1989.

204. Hammond, G. S., "A correlation of reaction rates", *Journal of American Chemical Society*, Vol. 77, pp.334-338, 1955.

205. Gray, T. F. and G. B. Butler, "The Fundamental Basis for Cyclopolymerization. X. A Systematic Study of the Cyclopolymerization of Methacrylic Anhydride" , *Journal of Macromolecular Science: Part A-Chemistry*, Vol. 9, pp. 45-82, 1975.

206. Kirsh, Y. E., Water-soluble poly-N-vinylamides : Synthesis and Physico-Chemical Properties, Chichester ; New York: Wiley, 1998.

207. Tripathy, S. K., J. Kumar and H. S. Nalwa, "Handbook of Polyelectrolytes and Their Applications. Vol. 3. Applications of Polyelectrolytes and Theoretical Models", Stevenson Ranch, Calif.: American Scientific, 2002.

208. Beuermann, S., "Solvent Influence on Propagation Kinetics in Radical Polymerizations Studied by Pulsed Laser Initiated Polymerizations", *Macromolecular Rapid Communications*, Vol. 30, pp. 1066-1088, 2009.

209. ODriscoll, K. F., M. L. Monteiro and B. Klumperman, "The Effect of Benzyl Alcohol on Pulsed Laser Polymerization of Styrene and Methylmethacrylate", *Journal of Polymer Science Part A-Polymer Chemistry*, Vol. 35, pp. 515-520, 1997.

210. Zammit, M. D., T. P.Davis, G. D. Willett and K. F. ODriscoll, "The Effect of Solvent on the Home-Propagation Rate Coefficients of Styrene and Methyl Methacrylate", *Journal of Polymer Science Part A-Polymer Chemistry,* Vol. 35, pp. 2311-2321, 1997.

211. Harrisson, S., C. Barner-Kowollik, T. P. Davis, R. Evans, E. Rizzardo, M. Stenzel and M. Yin, "Remarkable Solvent Effects of Oxygen- and Sulfur-Containing Compounds on the Propagation Rate of Methyl Methacrylate", *Zeitschrift Fur Physikalische Chemie-International Journal of Research in Physical Chemistry & Chemical Physics*, Vol. 219, pp. 267-281, 2005.

212. Beuermann, S., M. Buback and G. T. Russell, "Rate of Propagation in Free-Radical Polymerization of Methyl-Methacrylate in Solution", *Macromolecular Rapid Communications*, Vol. 15, pp. 647-653, 1994.

213. Beuermann, S., D. A. Paquet, J. H. McMinn and R. A. Hutchinson, "Propagation Kinetics of Methacrylic Acid Studied by Pulsed-Laser Polymerization", *Macromolecules*, Vol. 30, pp. 194-197, 1997.

214. Davis, T. P., K. F. Odriscoll, M. C. Piton and M. A. Winnik, , "Determination of Propagation Rate Constants Using a Pulsed Laser Technique", *Macromolecules*, Vol. 22, pp. 2785-2788, 1989.

215. Hutchinson, R. A., J. R. Richards and M. T. Aronson, "Determination of Propagation Rate Coefficients by Pulsed-Laser Polymerization for Systems with Rapid Chain Growth - Vinyl-Acetate", *Macromolecules*, Vol. 27, pp. 4530-4537, 1994.

216. Kuchta, F. D., A. M. van Herk and A. L. German, "Propagation Kinetics of Acrylic and Methacrylic Acid in Water and Organic Solvents Studied by Pulsed-Laser Polymerization", *Macromolecules*, Vol. 33, pp. 3641-3649, 2000.

217. Lyons, R. A., J. Hutovic, M. C. Piton, D. I. Christie, P. A. Clay, B. G. Manders, S. H. Kable and R. G. Gilbert, "Pulsed-Laser Polymerization Measurements of the Propagation Rate Coefficient for Butyl Acrylate", *Macromolecules*, Vol. 29, pp. 1918-1927, 1996.

218. Morrison, B. R., M. C. Piton, M. A. Winnik, R. G. Gilbert and D. H. Napper, "Solvent Effects on the Propagation Rate Coefficient for Free-Radical Polymerization", *Macromolecules*, Vol. 26, pp. 4368-4372, 1993.

219. Ganachaud, F., R. Balic, M. J. Monteiro and R. G. Gilbert, "Propagation Rate Coefficient of poly(N-isopropylacrylamide) in Water Below its Lower Critical Solution Temperature", *Macromolecules*, Vol. 33, pp. 8589-8596, 2000.

220. Lin, H. R., "Solution Polymerization of Acrylamide Using Potassium Persulfate as an Initiator: Kinetic Studies, Temperature and pH Dependence", *European Polymer Journal*, Vol. 37, pp. 1507-1510, 2001.

221. Pascal, P., M. A. Winnik, D. H. Napper and R. G. Gilbert, "Pulsed-Laser Study of the Propagation Kinetics of Acrylamide and Its Derivatives in Water", *Macromolecules*, Vol. 26, pp. 4572-4576, 1993.

222. Seabrook, S. A., M. P. Tonge and R. G. Gilbert, "Pulsed Laser Polymerization Study of the Propagation Kinetics of Acrylamide in Water", *Journal of Polymer Science Part A-Polymer Chemistry*, Vol. 43, pp. 1357-1368, 2005.

223. Beuermann, S., M. Buback, P. Hesse, F. D. Kuchta, I. Lacik and A. M. Van Herk, "Critically Evaluated Rate Coefficients for Free-Radical Polymerization. Part 6: Propagation Rate Coefficient of Methacrylic Acid in Aqueous Solution", *Pure and Applied Chemistry*, Vol. 79, pp. 1463-1469, 2007.

224. Beuermann, S., M. Buback, P. Hesse, S. Kukuckova and I. Lacik, "Propagation Kinetics of Free-Radical Methacrylic Acid Polymerization in Aqueous Solution. The Effect of Concentration and Degree of Ionization", *Macromolecular Symposia*, Vol. 248, pp. 23-32, 2007.

225. Beuermann, S., M. Buback, P. Hesse, S. Kukuckova and I. Lacik, "Propagation Rate Coefficient of non-ionized Methacrylic Acid Radical Polymerization in Aqueous Solution. The Effect of Monomer Conversion", *Macromolecular Symposia*, Vol. 248, pp. 41-49, 2007.

226. Beuermann, S., M. Buback, P. Hesse and I. Lacik, "Free-Radical Propagation Rate Coefficient of Nonionized Methacrylic Acid in Aqueous Solution from Low Monomer Concentrations to Bulk Polymerization", *Macromolecules*, Vol. 39, pp. 184-193, 2006.

227. Lacik, I., S., Beuermann and M. Buback, "Aqueous Phase Size-Exclusion-Chromatography Used for PLP-SEC Studies into Free-Radical Propagation Rate of Acrylic Acid in Aqueous Solution", *Macromolecules*, Vol. 34, pp. 6224-6228, 2001.

228. Lacik, I., S. Beuermann and M. Buback, "PLP-SEC Study into Free-Radical Propagation Rate of nonionized Acrylic Acid in Aqueous Solution", *Macromolecules*, Vol. 36, pp. 9355-9363, 2003.

229. Lacik, I., S. Beuermann and M. Buback, "PLP-SEC Study into the Free-Radical Propagation Rate Coefficients of Partially and Fully Ionized Acrylic Acid in Aqueous Solution", *Macromolecular Chemistry and Physics*, Vol. 205, pp. 1080-1087, 2004.

230. Chapiro, A., "Auto-Acceleration in Free-Radical Polymerizations Caused by Oriented Monomer-Polymer Association Complexes", *Pure and Applied Chemistry*, Vol. 53, pp. 643-655, 1981.

231. Chapiro, A. and J. Dulieu, "Influence of Solvents on Molecular Associations and on Radiation Initiated Polymerization of Acrylic-Acid", *European Polymer Journal*, Vol. 13, pp. 563-577, 1977.

232. Gromov, V. F., N. I. Galperina, T. O. Osmanov, P. M. Khomikovskii and A. D. Abkin, "Effect of Solvent on Chain Propagation and Termination Reaction-Rates in Radical Polymerization", *European Polymer Journal*, Vol. 16, pp. 529-535, 1980.

233. Plochocka, K., "Effect of the Reaction Medium on Radical Copolymerization", *Journal of Macromolecular Science-Reviews in Macromolecular Chemistry and Physics*, Vol. C20, pp. 67-148, 1981.

234. Buback, M., P. Hesse, R. A. Hutchinson, P. Kasak, I. Lacik, M. Stach and I. Utz, "Kinetics and Modeling of Free-Radical Batch Polymerization of Nonionized Methacrylic Acid in Aqueous Solution", *Industrial & Engineering Chemistry Research*, Vol. 47, pp. 8197-8204, 2008.

235. Stach, M., I. Lacik, D. Chorvat, M. Buback, P. Hesse, R. A. Hutchinson and L. Tang, "Propagation Rate Coefficient for Radical Polymerization of N-vinyl Pyrrolidone in

Aqueous Solution Obtained by PLP-SEC", *Macromolecules*, Vol. 41, pp. 5174-5185, 2008.

236. Buback, M., "Propagation Kinetics in Radical Polymerization Studied via Pulsed Laser Techniques", *Macromolecular Symposia*, Vol. 275–276, pp. 90-101, 2009.

237. Dossi, M., G. Storti and D. Moscatelli, "Initiation Kinetics in Free-Radical Polymerization: Prediction of Thermodynamic and Kinetic Parameters Based on ab initio Calculations", *Macromolecular Theory and Simulations*, Vol. 19, pp. 170-178, 2010.

238. Gomez-Balderas, R., M. L. Coote, D. J. Henry, H. Fischer and L. Radom, "What is the Origin of the Contrathermodynamic Behavior in Methyl Radical Addition to Alkynes versus Alkenes?", *Journal of Physical Chemistry A*, Vol. 107, pp. 6082-6090, 2003.

239. Gomez-Balderas, R., M. L. Coote, D. J. Henry and L. Radom, "Reliable Theoretical Procedures for Calculating the Rate of Methyl Radical Addition to Carbon-Carbon Double and Triple Bonds", *Journal of Physical Chemistry A*, Vol. 108, pp. 2874-2883, 2004.

240. Henry, D. J., M. L. Coote, R. Gomez-Balderas and L. Radom, "Comparison of the Kinetics and Thermodynamics for Methyl Radical Addition to C=C, C=O, and C=S Double Bonds", *Journal of the American Chemical Society*, Vol. 126, pp. 1732-1740, 2004.

241. Heuts, J. P. A., R. G. Gilbert and I. A. Maxwell, , "Penultimate Unit Effect in Free-Radical Copolymerization", *Macromolecules*, Vol. 30, pp. 726-736, 1997.

242. Heuts, J. P. A., R. G. Gilbert and L. Radom, "A Priori Prediction of Propagation Rate Coefficients in Free-Radical Polymerizations: Propagation of Ethylene", *Macromolecules*, Vol. 28, pp. 8771-8781, 1995.

243. Heuts, J. P. A., R. G. Gilbert and L. Radom, "Determination of Arrhenius Parameters for Propagation in Free-Radical Polymerizations: An assessment of Ab Initio Procedures", *Journal of Physical Chemistry*, Vol. 100, pp. 18997-19006, 1996.

244. Huang, D. M., M. J. Monteiro and R. G. Gilbert, "A Theoretical Study of Propagation Rate Coefficients for Methacrylonitrile and Acrylonitrile", *Macromolecules*, Vol. 31, pp. 5175-5187, 1998.

245. Izgorodina, E. I. and M. L. Coote, "Accurate Ab Initio Prediction of Propagation Rate Coefficients in Free-Radical Polymerization: Acrylonitrile and Vinyl Chloride", *Chemical Physics*, Vol. 324, pp. 96-110, 2006.

246. Lin, C. Y., E. I. Izgorodina and M. L. Coote, "First Principles Prediction of The Propagation Rate Coefficients of Acrylic and Vinyl Esters: Are We There Yet?", *Macromolecules*, Vol. 43, pp. 553-560, 2010.

247. Moscatelli, D., M. Dossi, C. Cavallotti and G. Storti, "Ab Initio Calculation of the Propagation Kinetics in Free Radical Polymerization: Chain Length and Penultimate Effects", *Macromolecular Symposia*, Vol. 259, pp. 337-347, 2007.

248. Moscatelli, D., M. Dossi, C. Cavallotti and G. Storti, "Density Functional Theory Study of Addition Reactions of Carbon-Centered Radicals to Alkenes", *Journal of Physical Chemistry A*, Vol. 115, pp. 52-62, 2011.

249. Van Cauter, K., K. Hemelsoet, V. Van Speybroeck, M. F. Reyniers and M. Waroquier, , "Comparative Study of Kinetics and Reactivity Indices of Free Radical Polymerization Reactions", *International Journal of Quantum Chemistry*, Vol. 102, pp. 454-460, 2005.

250. Van Cauter, K., V. Van Speybroeck, P. Vansteenkiste, M. F. Reyniers and M. Waroquier, "Ab Initio Study of Free-Radical Polymerization: Polyethylene Propagation Kinetics", *Chemphyschem*, Vol. 7, pp. 131-140, 2006.

251. Van Cauter, K., V. Van Speybroeck and M. Waroquier, "Ab Initio Study of Poly(vinyl chloride) Propagation Kinetics: Head-to-Head versus Head-to-Tail Additions", *Chemphyschem*, Vol. 8, pp. 541-552, 2007.

252. Wong, M. W. and L. Radom, "Radical-Addition to Alkenes - an Assessment of Theoretical Procedures", *Journal of Physical Chemistry*, Vol. 99, pp. 8582-8588, 1995.

253. Wong, M. W. and L. Radom, "Radical Addition to Alkenes: Further Assessment of Theoretical Procedures", *Journal of Physical Chemistry A*, Vol. 102, pp. 2237-2245, 1998.

254. Dossi, M., K. Liang, R. A. Hutchinson and D. Moscatelli, "Investigation of Free-Radical Copolymerization Propagation Kinetics of Vinyl Acetate and Methyl Methacrylate", *Journal of Physical Chemistry B*, Vol. 114, pp. 4213-4222, 2010.

255. Dossi, M., G. Storti and D. Moscatelli, "Quantum Chemistry: A Powerful Tool in Polymer Reaction Engineering", *Polymer Reaction Engineering - 10th International Workshop*, Vol. 302, pp. 16-25, 2011.

256. Moscatelli, D., C. Cavallotti and M. Morbidelli, "Prediction of Molecular Weight Distributions Based on Ab initio Calculations: Application to the High Temperature Styrene Polymerization", *Macromolecules*, Vol. 39, pp. 9641-9653, 2006.

257. Salman, S., A. Z. Albayrak, D. Avci and V.Aviyente, "Synthesis and Modeling of New Phosphorus-Containing Acrylates", *Journal of Polymer Science Part a-Polymer Chemistry*, Vol. 43, pp. 2574-2583, 2005.

258. Yu, X. R., J. Pfaendtner and L. J. Broadbelt, "Ab Initio Study of Acrylate Polymerization Reactions: Methyl methacrylate and Methyl Acrylate Propagation", *Journal of Physical Chemistry A*, Vol. 112, pp. 6772-6782, 2008.

259. Thickett, S. C. and R. G. Gilbert, "Propagation Rate Coefficient of Acrylic Acid: Theoretical Investigation of the Solvent Effect", *Polymer*, Vol. 45, pp. 6993-6999, 2004.

260. De Sterck, B., R.Vaneerdeweg, F. Du Prez, M. Waroquier and V. Van Speybroeck, "Solvent Effects on Free Radical Polymerization Reactions: The Influence of Water on the Propagation Rate of Acrylamide and Methacrylamide", *Macromolecules*, Vol. 43, pp. 827-836, 2010.

261. Yu, X. R., Levine, S. E. and L. J. Broadbelt, "Kinetic Study of the Copolymerization of Methyl Methacrylate and Methyl Acrylate Using Quantum Chemistry", *Macromolecules*, Vol. 41, pp. 8242-8251, 2008.

262. Smith, D. M., R. G. Lehmann, R. Narayan, G. E. Kozerski and J. R. Miller, "Fate and effects of silicons polymer during the composting process", *Compost Science & Utilization*, Vol. 6, pp. 6-12, 1998.

263. Deglmann, P., I. Muller, F. Becker, A. Schafer, K. D. Hungenberg and H. Weiss, "Prediction of Propagation Rate Coefficients in Free Radical Solution Polymerization Based on Accurate Quantum Chemical Methods: Vinylic and Related Monomers, Including Acrylates and Acrylic Acid", *Macromolecular Reaction Engineering*, Vol. 3, pp. 496-515, 2009.

264. Coote, M. L., "Quantum-Chemical Modeling of Free-Radical Polymerization", *Macromolecular Theory and Simulations*, Vol. 18, pp. 388-400, 2009.

265. Henry, D. J., M. B. Sullivan and L. Radom, "G3-RAD and G3X-RAD: Modified Gaussian-3 (G3) and Gaussian-3X (G3X) Procedures for Radical Thermochemistry", *Journal of Chemical Physics*, Vol. 118, pp. 4849-4860, 2003.

266. Klamt, A., COSMO-RS : from Quantum Chemistry to Fluid Phase Thermodynamics and Drug Design, Amsterdam ; Oxford: Elsevier, 2005.

267. Klamt, A., "Conductor-Like Screening Model for Real Solvents - a New Approach to the Quantitative Calculation of Solvation Phenomena", *Journal of Physical Chemistry*, Vol. 99, pp. 2224-2235, 1995.

268. Klamt, A., V. Jonas, T. Burger and J. C. W. Lohrenz, "Refinement and Parametrization of COSMO-RS", *Journal of Physical Chemistry A*, Vol. 102, pp. 5074-5085, 1998.

269. Kamerlin, S. C. L., M. Haranczyk and A. Warshel, "Are Mixed Explicit/implicit Solvation Models Reliable for Studying Phosphate Hydrolysis? A Comparative Study of Continuum, Explicit and Mixed Solvation Models", *Chemphyschem*, Vol. 10, pp. 1125-1134, 2009.

270. Pilling, M. J. and P. W. Seakins, *Reaction kinetics*, Oxford: Oxford University Press, 1995.

271. Coote, M. L., T. P. Davis and L. Radom, "Conformational Dependence of the Penultimate Unit Effect in Free-Radical Copolymerization", *Macromolecules*, Vol. 32, pp. 5270-5276, 1999.

272. Louwen, J. N. P., C. E. V. Lenthe, ADF2008.01 COSMO-RS, SCM. Theoretical Chemistry: Vrije Universiteit: Amsterdam, The Netherlands, 2008.

273. Zhao, Y. and D. G. Truhlar, "Hybrid Meta Density Functional Theory Methods for Thermochemistry, Thermochemical Kinetics, and noncovalent Interactions: The MPW1B95 and MPWB1K Models and Comparative Assessments for Hydrogen

Bonding and van der Waals Interactions", *Journal of Physical Chemistry A*, Vol. 108, pp. 6908-6918, 2004.

274. Black, G. and J. M. Simmie, "Barrier Heights for H-Atom Abstraction by H(O)over dot(2) from n-Butanol-A Simple Yet Exacting Test for Model Chemistries?", *Journal of Computational Chemistry*, Vol. 31, pp. 1236-1248, 2010.

275. Galano, A., "On the Direct Scavenging Activity of Melatonin Towards Hydroxyl and a Series of Peroxyl Radicals", *Physical Chemistry Chemical Physics*, Vol. 13, pp. 7147-7157, 2011.

276. Galano, A. and J. R. Alvarez-Idaboy, "Guanosine plus OH Radical Reaction in Aqueous Solution: A Reinterpretation of the UV-vis Data Based on Thermodynamic and Kinetic Calculations", *Organic Letters*, Vol. 11, pp. 5114-5117, 2009.

277. Galano, A., N. A. Macias-Ruvalcaba, O. N. M. Campos, and J. Pedraza-Chaverri, "Mechanism of the OH Radical Scavenging Activity of Nordihydroguaiaretic Acid: A Combined Theoretical and Experimental Study", *Journal of Physical Chemistry B*, Vol. 114, pp. 6625-6635, 2010.

278. Gao, T. T., J. M. Andino and J. R. Alvarez-Idaboy, "Computational and Experimental Study of the Interactions Between Ionic Liquids and Volatile Organic Compounds", *Physical Chemistry Chemical Physics*, Vol. 12, pp. 9830-9838, 2010.

279. Iuga, C., J. R. Alvarez-Idaboy and A. Vivier-Bunge, "Mechanism and Kinetics of the Water-Assisted Formic Acid plus OH Reaction under Tropospheric Conditions", *Journal of Physical Chemistry A*, Vol. 115, pp. 5138-5146, 2011.

280. Leon-Carmona, J. R. and A. Galano, "Is Caffeine a Good Scavenger of Oxygenated Free Radicals?", *Journal of Physical Chemistry B*, Vol. 115, pp. 4538-4546, 2011.

281. Perez-Gonzalez, A. and A. Galano, "OH Radical Scavenging Activity of Edaravone: Mechanism and Kinetics", *Journal of Physical Chemistry B*, Vol. 115, pp. 1306-1314, 2011.

282. Vega-Rodriguez, A. and J. R. Alvarez-Idaboy, "Quantum Chemistry and TST Study of the Mechanisms and Branching Ratios for the Reactions of OH with Unsaturated Aldehydes", *Physical Chemistry Chemical Physics*, Vol. 11, pp. 7649-7658, 2009.

283. Velez, E., J. Quijano, R. Notario, E. Pabon, J. Murillo, J. Leal, E. Zapata and G. Alarcon, "A Computational Study of Stereospecifity in the Thermal Elimination Reaction of Menthyl Benzoate in the Gas Phase", *Journal of Physical Organic Chemistry*, Vol. 22, pp. 971-977, 2009.

284. Zavala-Oseguera, C., J. R. Alvarez-Idaboy, G. Merino and A. Galano, "OH Radical Gas Phase Reactions with Aliphatic Ethers: A Variational Transition State Theory Study", *Journal of Physical Chemistry A*, Vol. 113, pp. 13913-13920, 2009.

285. Zhao, Y. and D. G. Truhlar, "Density Functionals for Noncovalent Interaction Energies of Biological Importance", *Journal of Chemical Theory and Computation*, Vol. 3, pp. 289-300, 2007.

286. McQuarrie, D. A. and J. D. Simon, *Physical chemistry : A Molecular Approach*, Sausalito, Calif.: University Science Books, 1997.

287. De Sterck, B., V. Van Speybroeck, S. Mangelinckx, G. Verniest, N. De Kimpe and M. Waroquier, "Theoretical Study on the Structural Properties of Various Solvated Metalated 3-Halo-1-azaallylic Anions", *Journal of Physical Chemistry A*, Vol. 113, pp. 6375-6380, 2009.

288. Kelly, C. P., C. J. Cramer and D. G. Truhlar, "SM6: A Density Functional Theory Continuum Solvation Model for Calculating Aqueous Solvation Free Energies of

Neutrals, Ions, and Solute-Water Clusters", *Journal of Chemical Theory and Computation*, Vol. 1, pp. 1133-1152, 2005.

289. Kelly, C. P., C. J. Cramer and D. G. Truhlar, "Adding Explicit Solvent Molecules to Continuum Solvent Calculations for the Calculation of Aqueous Acid Dissociation Constants", *Journal of Physical Chemistry A*, Vol. 110, pp. 2493-2499, 2006.

290. Van Speybroeck, V., K. Moonen, K. Hemelsoet, C. V. Stevens and M. Waroquier, "Unexpected Four-Membered Over Six-Membered Ring Formation During the Synthesis of Azaheterocyclic Phosphonates: Experimental and Theoretical Evaluation", *Journal of the American Chemical Society*, Vol. 128, pp. 8468-8478, 2006.

291. Theodorou, D. N. and U. W. Suter, "Detailed Molecular-Structure of a Vinyl Polymer Glass", *Macromolecules*, Vol. 18, pp. 1467-1478, 1985.

292. Sun, H., "COMPASS: An Ab Initio Force-Field Optimized for Condensed-Phase Applications - Overview with Details on Alkane and Benzene Compounds", *Journal of Physical Chemistry B*, Vol. 102, pp. 7338-7364, 1998.

293. Andersen, H. C., "Molecular-Dynamics Simulations at Constant Pressure and-or Temperature", *Journal of Chemical Physics*, Vol. 72, pp. 2384-2393, 1980.